

eman ta zabal zazu



Universidad  
del País Vasco

Euskal Herriko  
Unibertsitatea

***Synthesis and Characterization of  
Polymers Containing Monomers from  
PET Waste Obtained by Organocatalysis.***

Ph.D. Thesis presented by

**Irma Flores Cerón**

Polymer Science and Technology Department  
Faculty of Chemistry  
Donostia-San Sebastián, Junio 2019

eman ta zabal zazu



Universidad  
del País Vasco

Euskal Herriko  
Unibertsitatea

**POLYMAT**

***Synthesis and Characterization of  
Polymers Containing Monomers from  
PET Waste Obtained by Organocatalysis.***

Ph.D. Thesis presented by

**Irma Flores Cerón**

Under the supervision of:

Prof. Alejandro Jesús Müller Sánchez

Prof. Haritz Sardon Muguruza

Polymer Science and Technology Department

Faculty of Chemistry

Donostia-San Sebastián, Junio 2019

## **Dedicatoria**

A Dios por nunca dejarme sola, al amor que en todas sus formas de expresión siempre ha estado conmigo y a mi familia por ser mi soporte siempre.

En especial a mi mamá, papá, hermana y abuela (Irma, Carlos, Karla y Juliana) por apoyarme siempre en todo, por enseñarme que debo ser fuerte siempre sin importar que tan grande sea la adversidad, por ser mi fortaleza al estar tan lejos de casa y porque a pesar de todos los momentos difíciles que hemos vivido en estos últimos años, siempre nos hemos mantenido unidos.

A mi primo Irving, a mi tío Venicio y a mi tío Alfredo, cuya muerte dejó un gran vacío en mí, pero también me enseñó que la vida cambia con cada respiro que damos, que debemos sonreír siempre sin importar las adversidades y sobre todo que la vida es un regalo que debemos apreciar cada día.

## Agradecimientos

Gracias a mis directores de Tesis: Prof. Alejandro Müller y Prof. Haritz Sardon, por haberme aceptado ambos en sus grupos de investigación, por enseñarme tantas cosas desconocidas para mí, por tener paciencia en la escritura de mis papers, por haberme dedicado tiempo durante estos casi cuatro años para el desarrollo de esta tesis y por haber hecho de mi una mejor persona y profesionalista.

De forma particular quiero decir gracias al Prof. Alejandro Müller por haber dicho que sí a mi petición de hacer el doctorado con él y por los consejos que me dio durante estos años, los cuáles me serán útiles siempre. Fue muy grato trabajar con usted y me llevo una gran experiencia personal y profesional.

Quiero agradecer también al Prof. Haritz Sardon, por haber querido trabajar conmigo sin conocerme de nada, por tener la paciencia para enseñarme a sintetizar mil muestras, por soportar las lagrimas que de vez en cuando me salían y por apoyarme siempre, tanto en el ámbito profesional, como en el personal.

Gracias también al Prof. David Mecerreyes, quien a pesar de no ser mi director de tesis, siempre estuvo pendiente de mi trabajo y dándome consejos para mejorarlo. Gracias por estar siempre también pendiente de mi persona y ser tan amable conmigo.

Por la grata estancia que tuve en la UPC en Barcelona quiero agradecer al Prof. Sebastián Muñoz y al Dr. Antxon Martínez de Ilarduya, hicieron que la estancia fuera fructífera y enriquecedora para mi trabajo, gracias por su amabilidad y aportaciones a esta tesis.

Por otro lado quiero agradecer a los profesores Agustín Etxeberria y Lourdes Irusta por sus aportaciones durante el desarrollo de este trabajo y por el tiempo que compartimos hablando de mil cosas.

A lo largo de esta tesis conocí a muchas personas que de una u otra forma me apoyaron durante todo este tiempo, quiero agradecerles toda la amabilidad que tuvieron conmigo, por tratarme siempre bien, por contestar a todas mis dudas pero sobre todo por estar dispuestos siempre a ayudarme cuando lo he necesitado. Gracias:

Antxon Santamaría, Sofía Guezala, Alba González, Itxaso Calafel, Inés Plaza, Agurtzane Mugica y Manoli Zubitur.

Quiero agradecer a mi familia en México (los 23 yo incluida): Carlos, Irma, Karla, Juliana, tía Ana, tío Pancho, Rigo, Paco, Maribel, Tía Silvia, Héctor, Víctor, Lalito, Claudia, Don Melchor, Nohemí, Ximenita, Venicio, María, Mónica y a los dos que ya no están con nosotros (Irving y tío Venicio). Por ser una familia que se apoya entre unos y otros cuando más lo necesitamos, no somos una familia perfecta pero somos una familia capaz de superar todas las tristezas y dificultades que se nos presentan. Y finalmente a mi ti Mateo por estar siempre pendiente de mí.

A mis amigos en México que siempre están conmigo a donde sea que vaya, gracias: Roman, Gustavo, Daniel, Carlitos, Genaro, Fernando, Carmen, Isabel, Marilyn y Javier.

A mis amigos y compañeros de trabajo en México por estar siempre pendientes de mí: Susi, Base, Miss Juanita, Miss Lupita, Miss Anita y Prof. Filemón.

A las personas que conocí en México en mis inicios con la ciencia y que siempre me alentaron a seguir con los estudios de posgrado: Dr. Alex Valádez, Dr. Francis Avilés, Dr. Luis Héctor, Dr. Jorge Zuno, Carlitos, Miguel y Fernando.

A mis compañeros de piso en San Sebastián, Asier (mi vecino de habitación) y Naroa, gracias por ser unos buenos compañeros de piso, por los buenos momentos que compartimos, las cenas insanas, las fugas de agua y huecos en el techo, por los recuerdos de las fiestas en casa y el vecino incomodo del 3er piso, jajaja. También quiero dar las gracias a mi compañera de piso temporal, Estefanía, fue poco el tiempo que vivimos juntas pero con gratos recuerdos.

Gracias a Rafael y Puy, por abrirme las puertas de su casa y recibirme siempre amablemente, me quedo con todos los gratos momentos que compartí con ustedes (cosechar peras mil me encanto, jijiji).

A mis compañeras de piso en Barcelona, Gala y Begoña, gracias por esos buenos momentos, pláticas nocturnas, fiestas y por enseñarme ese mundo del cine con todas sus peculiaridades.

Por último pero no menos importantes quiero agradecer a todas las personas de mil nacionalidades, con las que conviví durante el doctorado ya sea en los grupos de investigación, en el laboratorio, en las fiestas, en la oficina o en la universidad; gracias por aportar un recuerdo a mi memoria.

Gracias a: Andrea, Nerea, Idoia, Maryam, Eider, Jon, Ester, Ricardo, Jorge Luis, Nicolás, Borja, Ainara, Leire, June, Oihane, Ana, Jaime, Coralie, Amaury, Nicola, Andere, Leire Meabe, Iñaki, Ester Udabe, Elena, Noe, Naroa, Nerea Casado, Asier, Antonio, Sara, Álvaro, Fermín, Marine, Luca, Mehmet, Daniele, Maitane, Sil, Stefano, Giulia, Bertha y Noushin.

En especial quiero agradecer a Nerea, Idoia, Jon, Eider, Maryam y Ester por brindarme su apoyo y ayuda en los momentos más difíciles que viví estando aquí y también por regalarme momentos felices, ahora sé que todo se reduce a un "It's ok", jajaja. Me llevo su amistad en mi corazón por siempre.

Gracias Maryam por enseñarme que la amistad no tiene fronteras de nacionalidad, idioma o religión, pues a pesar, de que tú hablas persa y yo español hicimos una amistad muy bonita, que sé, durará forever. Thank you for all my beautiful friend.

Empecé el doctorado con algunos de ustedes: Coralie, Amaury, Andere, Leire Meabe, Iñaki, Noe y Naroa, nos vimos crecer, frustrarnos y alegrarnos de nuestros logros, me quedo con todos esos recuerdos.

Eider y Elena, a veces olvido que son tan jóvenes, jijiji. Gracias por compartir unos viajes conmigo que jamás olvidare.

Gracias a todas las personas que olvidé mencionar pero que de un modo u otro formaron parte de mi vida durante estos casi cuatro años en Donostia-San Sebastián.

**Gracias mil millones a todos y a todas...**

---

**Index**

<b>List of Abbreviations</b> .....	iii
<b>Chapter 1 Introduction</b>	
1.1 General Introduction.....	2
1.2 Objectives.....	5
1.3 Structure of the thesis.....	6
1.4 References.....	8
<b>Chapter 2 Experimental Part</b>	
2.1 Materials .....	17
2.2 Synthesis of Polymers.....	18
2.3 Characterization Techniques.....	26
2.4 Theoretical Concepts of Thermal Characterization of Polymers.....	36
2.5 References.....	47
<b>Chapter 3 Screening of Different Organocatalysts for the Sustainable Synthesis of PET</b>	
3.1 Abstract .....	51
3.2 Introduction.....	52
3.3 Results and Discussion.....	54
3.4 Conclusions.....	64
3.5 References.....	65
<b>Chapter 4 PET-<i>ran</i>-PLA partially degradable random copolymers prepared by organocatalysis: Effect of PLA incorporation on crystallization and morphology</b>	
4.1 Abstract .....	71
4.2 Introduction.....	72
4.3 Results and Discussion.....	74
4.4 Conclusions.....	98
4.5 References.....	99

---

<b>Chapter 5 Organocatalyzed Polymerization of PET-<i>b</i>-Polyether Copolymers</b>	
5.1 Abstract .....	106
5.2 Introduction.....	107
5.3 Results and Discussion.....	109
5.4 Conclusions.....	141
5.5 References.....	142
<b>Chapter 6 Synthesis of Aromatic–Aliphatic Polyesters by Enzymatic Ring Opening Polymerization of Cyclic Oligoesters and their Cyclodepolymerization for a Circular Economy</b>	
6.1 Abstract .....	148
6.2 Introduction.....	149
6.3 Results and Discussion.....	151
6.4 Conclusions.....	158
6.5 References.....	159
<b>Chapter 7 Triblock Copolymers using PHF or PHT with L-lactide: Synthesis and Characterization</b>	
7.1 Abstract .....	164
7.2 Introduction.....	165
7.3 Results and Discussion.....	167
7.4 Conclusions.....	189
7.5 References.....	190
<b>Chapter 8 Conclusions.....</b>	<b>195</b>
<b>Annexes</b>	
Annex A.....	198
Annex B.....	203
Annex C.....	212
Annex D.....	221
Annex E.....	231
<b>Publications made during the PhD Period.....</b>	<b>240</b>
<b>Resumen.....</b>	<b>241</b>

## List of Abbreviations

<b>AFM</b>	Atomic Force Microscopy
<b>BA</b>	Benzoic acid
<b>BAIL</b>	1-(4-sulfobutyl)-3-methylimidazolium hydrogen sulfate
<b>CAL B</b>	<i>Candida antarctica</i> lipase B
<b>CDP</b>	Cyclodepolymerization
<b>c(HF)</b>	Cyclic oligomers of hexamethylene furanoate
<b>c(HT)</b>	Cyclic oligomers of hexamethylene terephthalate
<b>CHCl<sub>3</sub></b>	Chloroform
<b>CH<sub>3</sub>OH</b>	Methanol
<b>HDC</b>	High dilution condensation
<b>Đ</b>	Polydispersity index
<b>DBU</b>	1,8-Diazabicyclo[5.4.0]undec-7-ene
<b>DBU:BA</b>	Ionic salt of 1,8-Diazabicyclo[5.4.0]undec-7-ene with Benzoic acid
<b>DCM</b>	Dichloromethane
<b>DMF</b>	Dimethyl furanoate
<b>DMT</b>	Dimethyl terephthalate
<b>DMAP</b>	4-Dimethylaminopyridine
<b>DMTA</b>	Dynamic Mechanical Thermal Analysis
<b>DSC</b>	Differential Scanning Calorimetry
<b>ED-ROP</b>	Entropically driven ring-opening polymerization
<b>EG</b>	Ethylene glycol
<b>EU28+NO/CH</b>	European Union 28 countries + Norway + Switzerland
<b>FDCA</b>	2,5-furandicarboxylic acid
<b>FTIR</b>	Fourier-Transform Infrared
<b>G</b>	Growth rate
<b>HD</b>	1,6 hexanediol
<b>HDC</b>	High dilution condensation
<b>HPLC</b>	High –Performance Liquid Chromatography
<b>I.V.</b>	Intrinsic viscosity
<b>K<sup>1/n</sup></b>	Isothermal crystallization rate constant
<b>K<sub>g</sub><sup>r</sup></b>	Total energy barrier for the overall crystallization
<b>MALDI-TOF</b>	Matrix-Assisted Laser Desorption/Ionization Time of Flight
<b>M<sub>n</sub></b>	Number Average Molecular Weight
<b>MSA</b>	Methanesulfonic acid
<b>M<sub>w</sub></b>	Weight Average Molecular Weight
<b>NMR</b>	Nuclear Magnetic Resonance
<b>Ñ</b>	Nucleation rate
<b>n</b>	Avrami index
<b>PBT</b>	Poly (butylene terephthalate)
<b>PEG</b>	Poly (ethylene glycol)
<b>PEO</b>	Poly (ethylene oxide)
<b>PET</b>	Poly (ethylene terephthalate)
<b>PG</b>	Propanediol
<b>PHF</b>	Poly(hexamethylene furanoate)
<b>PHT</b>	Poly(hexamethylene terephthalate)
<b>PLA</b>	Poly (lactic acid)
<b>PLOM</b>	Polarized Light Optical Microscopy
<b>Poly (1,6 HD)</b>	Poly (1,6 hexanediol)
<b>Poly (1,8 HD)</b>	Poly (1,8 octanediol)

<b>Poly (1,12 HD)</b>	Poly (1,12 dodecanediol)
<b>p-TSA</b>	p-toluenesulfonic acid monohydrate
<b>ROP</b>	Ring Opening Polymerization
<b>SAXS</b>	Small-Angle X-ray Scattering
<b>SEC</b>	Size Exclusion Chromatography
<b>TAI</b>	Trichloroacetyl isocyanate
<b>TBD</b>	1,5,7-triazabicyclo[4.4.0]dec-5-ene
<b>TBD:MSA</b>	Ionic salt of 1,5,7-triazabicyclo[4.4.0]dec-5-ene with Methanesulfonic acid
$T_c$	Crystallization temperature
$T_{cc}$	Cold crystallization temperature
<b>TFA</b>	Trifluoroacetic acid
$T_g$	Glass transition temperature
<b>TGA</b>	Thermogravimetric Analysis
<b>THF</b>	Tetrahydrofuran
<b>TiBut</b>	Titanium (IV) butoxide
$T_m$	Melting temperature
$T_m^0$	Melting temperature in equilibrium
<b>TMS</b>	Tetramethylsilane
<b>WAXS</b>	Wide-Angle X-ray Scattering
$X_c$	Degree of crystallinity
$\eta$	Degree of randomness
$\Delta H_m$	Latent heat of fusion
$\Delta H_c$	Latent heat of crystallization
$\Delta H_{cc}$	Latent heat of cold crystallization
$\tau_{50\%}$	Half-crystallization time
$\chi$	Interaction parameter
$\delta_1$	Solubility parameter of solvent
$\delta_2$	Solubility parameter of solute
$\Delta\delta$	Solubility parameter difference

# Chapter 1

---

---

## *Introduction*

1.1 General Introduction.....	2
1.2 Objectives.....	5
1.3 Structure of the Thesis.....	6
1.4 References.....	8

## 1.1 General Introduction

The irruption of plastics in the world has meant a revolution in all economic sectors. Additionally, the contribution of polymers on technological development is undoubted. The importance of polymers lies especially in the variety of utilities that humans can give to these materials. The great versatility of polymers have allowed to generate products with a certain simplicity such as plastic bags to products with a high complexity of development, such as those used in medical applications, aeronautics and construction, among others. <sup>1</sup> A clear example of the above is shown Figure 1.1, which presents the percentage of plastics (with respect to the total of plastics required for their transformation) used in each sector for the manufacture of products in Europe (EU28+NO/CH).



**Figure 1.1.** Distribution of European (EU28+NO/CH) plastics converter by segment in 2016. Source: Plastics Europe Market Research Group (PEMRG) and Conversio Market & Strategy GmbH.

Man-made polymeric materials have been under study since the middle of the nineteenth century, the so-called synthetic polymers (synthesized in the laboratories). <sup>2,3</sup> As a consequence of the above, polymers are present in many foods or raw materials that we consume, but also in textiles, in electricity or materials used for construction. Polyurethanes and other everyday materials such as polystyrene,

polyethylene, polypropylene or polyesters are used for different reasons because they provide different and specific properties for each necessity. So, depending on each polymer, its applications will be different and will be based on the required characteristics of the final product (Figure 1.2).



**Figure 1.2.** European (EU28+NO/CH) plastics converter demand by polymer types in 2016. Source: Plastics Europe Market Research Group (PEMRG) and Conversio Market & Strategy GmbH.

So undeniable there is a need for polymers in our daily lives that only in 2016 accounted for nearly 336 million tons worldwide. <sup>1</sup> Reports of this same year indicated that after China, Europe is the second region with the highest production of plastic materials; in 2016 Europe produced 60 million tons of polymeric materials. <sup>1</sup>

However, despite all the advantages that polymer materials provide, it is a reality that one of the biggest environmental problems that exist in the world is related to contamination by plastics. <sup>4,5</sup> In this sense, solutions must be taken to tackle environmental problems caused by plastics.

Several areas of research have been developed over the last few years. <sup>6</sup> One of them is the development of biodegradable polymers from renewable raw materials, derived from plants and bacteria such poly (lactic acid) PLA or Poly (hydroxybutyrate) PHB. <sup>7-9</sup> Besides being derived from biomass, these plastics are also compostable; meaning that they decompose biologically by the action of microorganisms and end up returning to the earth in the form of simple products that can be reused by living organisms. Therefore, the production of this type of polymers shows a tendency to

increase in the future but to date they account to less than 1 % of total plastic production.<sup>10</sup>

One of the great challenges for the science and technology of polymers in the attempt to reduce pollution to the environment is to generate materials that fulfill the function for which they are designed, without generating any residue in the environment. In this sense, an area of research is dedicated to the synthesis of copolymers made by combining non-biodegradable polymers with biodegradable polymers, with the intention of producing polymers whose composition and structure, allows to preserve the good mechanical, thermal properties, etc., in the materials. But at the same time also allows the degradability of these by various environmental factors.<sup>11-16</sup>

One of the polymers with wide applications and, therefore, one of those that generates a large amount of non-biodegradable waste is polyethylene terephthalate (PET).<sup>1,17</sup> This material has been the subject of multiple studies with the intention of copolymerizing it with other polymers that can give it a certain degree of degradability but that do not diminish the good properties that characterize it. Some copolymers that have been investigated are: PET-PLA, PET-co-alkylene succinates, PET-co-alkylene dicarboxylates, PET-co-Poly (ethyleneglycol), among others.<sup>11,18-26</sup>

In the plastics manufacturing process the use of catalysts is an essential factor to generate materials with the quality required for each use (high molecular weights, coloration, thermal properties, among others).<sup>27</sup> In spite of promoting in a very effective way the polymerization of diverse materials, the classic catalysts used, have environmental disadvantages such as: being non-biodegradable compounds, being made of metals and having a certain degree of toxicity.<sup>28</sup> The above, together with the fact that final products tend to have catalyst residues in their composition, makes it necessary to develop new catalysts that become more environmentally friendly (less toxic, easier to remove from final products and preferably biodegradable).

In response to the above, organocatalysis<sup>28-32</sup> and enzymes<sup>33-37</sup> have emerged as an alternative to conventional organometallic catalyst because of their low or no toxicity in comparison to organometallic counterparts. Therefore, it is believed that the use of these two families of catalysts (organocatalysts and enzymes) is a more sustainable alternative in comparison to the current catalysts employed in the plastic

manufacturing process. Current investigations have shown that the use of organocatalysis<sup>29,38-47</sup> or enzymes<sup>33-37,48-51</sup> can mediate the polymerization of a large variety of homopolymers and copolymers demonstrating their feasibility for polymerizations.

## 1.2 Objectives

Considering the background presented above, in this work, all possible factors that will help to increase the degree of sustainability in the synthesis of polyesters is considered. The first part of the thesis focuses on the sustainable synthesis of PET, the largest produced polyester by far which account to near 30-40 million tons per year, using step-growth polymerization methods.<sup>52</sup> In order to make the synthesis of PET more sustainable and to reduce the impact of organometallic catalysts in the environment, first the organocatalyzed synthesis of PET using dimethyl terephthalate (DMT) as a monomer (material that can be obtained from the chemical recycling of PET waste)<sup>53-55</sup> was investigated. The results demonstrate the feasibility of organocatalysts to polymerize PET.

After demonstrating the organocatalyzed polymerization of PET, the copolymerization of PET with PLLA was studied. The impact of the presence of different PLLA contents in the degradability and in the properties of PET was analyzed. While it was found that the copolymerization of PET with PLLA could be of great interest due to the combination of properties from both homopolymers, the obtained molecular weights were relatively modest due to the degradation of PLLA during the harsh polymerization conditions.

Therefore, the copolymerization of PET with low molecular weight semi-crystalline polyethers was investigated. These new copolymers were fully characterized and showed the ability to produce multiblock copolymers with double crystallinity. The double crystallinity was studied in detail and the effect of different polyether compositions in the crystallization was deeply investigated.

The second part of the thesis was focused on the synthesis of PET like materials by ring opening polymerization using enzymes. It showed the ability to produce macrocycles in excellent yields using DMT as monomer in the presence of enzymes, to

subsequently make polyesters. These enzymes not only favored the ROP of macrocycles but also showed that tuning the reactions conditions were able to promote the recycling by cyclodepolymerization (CDP) of polyesters formed from macrocycles, which could be an effective way to reduce the impact of plastics on the environment.<sup>56,57</sup> It was also demonstrated that this process could be implemented with monomers derived from biomass such as dimethyl furanoate (DMF).<sup>51,58</sup> The study showed that the properties of the materials obtained were very similar to those synthesized with DMT. These results indicate that both monomers (DMT and DMF) despite coming from different sources are able to generate polymers with similar properties suggesting that DMF could be a good sustainable alternative for DMT.

In order to further exploit the potential of ROP the synthesis of triblock copolymers was explored, first the linear polyesters were obtained by ROP from macrocycles and subsequently were copolymerized with PLA (obtained by ROP of lactide during the copolymerization). The results show that using ROP approach well-defined triblock copolymers could be obtained, the effect of PLA on the thermal properties of the copolymers was studied.

This work is focused on synthesizing polymers from monomers derived from PET waste and biomass, showing the feasibility of using organic catalysts and enzymes (metal free catalysts) and the subsequent characterization of the obtained materials in order to understand their structure and properties.

The above with the intention of serving as a base study for future research focused on improving sustainability in the various synthetic routes for obtaining polymers and with this help to reduce the environmental footprint left by the manufacturing processes of plastics.

### **1.3 Structure of the Thesis**

The PhD work has been divided into eight chapters. In chapter 1, a general introduction is presented, which describes the origin of this work and refers to everything related to this topic and that has been reported in the literature. In the same chapter the objectives of the thesis are presented.

In chapter 2 the synthesis of each of the polymers made in this work is described; as well as the characterization techniques used for the study of these polymers. In this chapter also some concepts related to the synthesis of polymers and to the study of morphology and crystallization of materials have been written, with the intention of a better understanding of some concepts used throughout the thesis.

In Chapter 3 a screening of different organocatalysts to polymerize PET and the respective characterization of the materials obtained is reported. The study focuses on the use of a monomer that can be derived from the chemical recycling of PET (dimethyl terephthalate, DMT) for the synthesis of the different polymers using various organocatalysts to find an organic catalyst with an effective catalytic activity to promote the polymerization of this polyester.

Chapter 4 explains the synthesis and characterization of PET-*ran*-PLA copolymers and the effect of PLA on the morphology and crystallization of PET. The effect of different PLA ratios in the thermal properties as well as in the hydrolytic degradation has been investigated.

In order to expand the studies related to the copolymerization in chapter 5, the synthesis of PET-*b*-Polyether multiblock copolymers and the effect that polyether causes on the thermal properties of PET and vice versa are described.

Chapter 6 describes the synthesis of cyclic oligoesters using DMT and their subsequent polymerization to linear polymers and finally the cyclodepolymerization of these linear polymers are shown; as well as the thermal characterization of the obtained polymers. The synthesis of cyclic oligoesters using a monomer derived from biomass such as DMF was also investigated.

The synthesis of triblock copolymers derived from L-lactide with PHT or PHF and their respective characterization are reported in Chapter 7.

Chapter 8 summarizes the main accomplishments and challenges of this work.

Attached is also a section of annexes that complements what is shown in chapters 3 to 7. Finally, a list of publications and a summary of the content of this thesis are also included.

## 1.4 References

- (1) Plastics -the Facts 2017  
[https://www.plasticseurope.org/application/files/5715/1717/4180/Plastics\\_the\\_facts\\_2017\\_FINAL\\_for\\_website\\_one\\_page.pdf](https://www.plasticseurope.org/application/files/5715/1717/4180/Plastics_the_facts_2017_FINAL_for_website_one_page.pdf) (accessed Feb 23, 2019).
- (2) Namazi, H. Polymers in Our Daily Life. *BioImpacts* **2017**, *7* (2), 73–74.  
<https://doi.org/10.15171/bi.2017.09>.
- (3) Hasirci, V.; Yilgor, P.; Endogan, T.; Eke, G.; Hasirci, N. Polymer Fundamentals: Polymer Synthesis. In *Comprehensive Biomaterials*; Elsevier, 2011; pp 349–371.  
<https://doi.org/10.1016/B978-0-08-055294-1.00034-9>.
- (4) Ojeda, T. Polymers and the Environment. In *Polymer Science*; Ylmaz, F., Ed.; InTech, 2013. <https://doi.org/10.5772/51057>.
- (5) Geyer, R.; Jambeck, J. R.; Law, K. L. Production, Use, and Fate of All Plastics Ever Made. *Science Advances* **2017**, *3* (7), e1700782.  
<https://doi.org/10.1126/sciadv.1700782>.
- (6) Zhang, X.; Fevre, M.; Jones, G. O.; Waymouth, R. M. Catalysis as an Enabling Science for Sustainable Polymers. *Chemical Reviews* **2018**, *118* (2), 839–885.  
<https://doi.org/10.1021/acs.chemrev.7b00329>.
- (7) Amass, W.; Amass, A.; Tighe, B. A Review of Biodegradable Polymers: Uses, Current Developments in the Synthesis and Characterization of Biodegradable Polyesters, Blends of Biodegradable Polymers and Recent Advances in Biodegradation Studies. *Polymer International* **1998**, *47* (2), 89–144.  
[https://doi.org/10.1002/\(SICI\)1097-0126\(199810\)47:2<89::AID-PI86>3.0.CO;2-F](https://doi.org/10.1002/(SICI)1097-0126(199810)47:2<89::AID-PI86>3.0.CO;2-F).
- (8) Aeschelmann, F.; Carus, M. Biobased Building Blocks and Polymers in the World: Capacities, Production, and Applications—Status Quo and Trends Towards 2020. *Industrial Biotechnology* **2015**, *11* (3), 154–159.  
<https://doi.org/10.1089/ind.2015.28999.fae>.
- (9) Williams, C.; Hillmyer, M. Polymers from Renewable Resources: A Perspective for a Special Issue of Polymer Reviews. *Polymer Reviews* **2008**, *48* (1), 1–10.  
<https://doi.org/10.1080/15583720701834133>.
- (10) Rosenheim, H.; De, I.; Hyvedemm, S. Bioplastics Market Data 2017. **2017**, *4*.

- 
- (11) Sousa, A. F.; Vilela, C.; Matos, M.; Freire, C. S. R.; Silvestre, A. J. D.; Coelho, J. F. J. Polyethylene Terephthalate: Copolyesters, Composites, and Renewable Alternatives. In *Poly(Ethylene Terephthalate) Based Blends, Composites and Nanocomposites*; Elsevier, 2015; pp 113–141. <https://doi.org/10.1016/B978-0-323-31306-3.00007-5>.
- (12) Lambert, S.; Wagner, M. Environmental Performance of Bio-Based and Biodegradable Plastics: The Road Ahead. *Chemical Society Reviews* **2017**, *46* (22), 6855–6871. <https://doi.org/10.1039/C7CS00149E>.
- (13) Gilding, D. K.; Reed, A. M. Biodegradable Polymers for Use in Surgery—Poly(Ethylene Oxide) Poly(Ethylene Terephthalate) (PEO/PET) Copolymers: 1. *Polymer* **1979**, *20* (12), 1454–1458. [https://doi.org/10.1016/0032-3861\(79\)90008-9](https://doi.org/10.1016/0032-3861(79)90008-9).
- (14) Deschamps, A. A.; Grijpma, D. W.; Feijen, J. Poly(Ethylene Oxide)/Poly(Butylene Terephthalate) Segmented Block Copolymers: The Effect of Copolymer Composition on Physical Properties and Degradation Behavior. *Polymer* **2001**, *42* (23), 9335–9345. [https://doi.org/10.1016/S0032-3861\(01\)00453-0](https://doi.org/10.1016/S0032-3861(01)00453-0).
- (15) Arkatkar, A.; Arutchelvi, J.; Sudhakar, M.; Bhaduri, S.; Uppara, P. V.; Doble, M. Approaches to Enhance the Biodegradation of Polyolefins. *The Open Environmental Engineering Journal* **2009**, *2* (1), 68–80. <https://doi.org/10.2174/1874829500902010068>.
- (16) Acik, G.; Altinkok, C.; Tasdelen, M. A. Synthesis and Characterization of Polypropylene- Graft -Poly( L -Lactide) Copolymers by CuAAC Click Chemistry. *Journal of Polymer Science Part A: Polymer Chemistry* **2018**, *56* (22), 2595–2601. <https://doi.org/10.1002/pola.29241>.
- (17) National Association for PET Container Resources. *Report on Postconsumer PET Container Recycling Activity in 2016; 2017*.
- (18) Tan, L. C.; Zhou, W. H.; Huang, Y. L.; Chen, Y. W. Sequential Structure, Crystallization, and Properties of Biodegradable Poly(Ethylene Terephthalate-Co-Ethylene Oxide-Co-Lactide) Copolyester. *Journal of Macromolecular Science, Part B* **2014**, *53* (7), 1231–1243. <https://doi.org/10.1080/00222348.2014.901870>.

- (19) Rwei, S. P.; Lin, W. P.; Wang, J. F. Synthesis and Characterization of Biodegradable and Weather-Durable PET/PEG/NDC Copolymers. *Colloid and Polymer Science* **2012**, *290* (14), 1381–1392. <https://doi.org/10.1007/s00396-012-2662-6>.
- (20) Qian, Z.; Li, S.; He, Y.; Liu, X. Synthesis and in Vitro Degradation Study of Poly(Ethylene Terephthalate)/Poly(Ethylene Glycol) (PET/PEG) Multiblock Copolymer. *Polymer Degradation and Stability* **2004**, *83* (1), 93–100. [https://doi.org/10.1016/S0141-3910\(03\)00229-5](https://doi.org/10.1016/S0141-3910(03)00229-5).
- (21) Olewnik, E.; Czerwiński, W.; Nowaczyk, J.; Sepulchre, M.-O.; Tessier, M.; Salhi, S.; Fradet, A. Synthesis and Structural Study of Copolymers of L-Lactic Acid and Bis(2-Hydroxyethyl Terephthalate). *European Polymer Journal* **2007**, *43* (3), 1009–1019. <https://doi.org/10.1016/j.eurpolymj.2006.11.025>.
- (22) Namkajorn, M.; Petchsuk, A.; Opaprakasit, M.; Opaprakasit, P. Synthesis and Characterizations of Degradable Aliphatic-Aromatic Copolyesters from Lactic Acid, Dimethyl Terephthalate and Diol: Effects of Diol Type and Monomer Feed Ratio. *Express Polymer Letters* **2010**, *4* (7), 415–422. <https://doi.org/10.3144/expresspolymlett.2010.52>.
- (23) Kumar, K. S.; Selvaraj, V.; Alagar, M. Synthesis of PET-PLA/Drug Nanoparticles and Their Effect with Gold Nanoparticles for Controlled Drug Release in Cancer Chemotherapy. *Research Letters in Nanotechnology* **2008**, *2008*, 1–4. <https://doi.org/10.1155/2008/389512>.
- (24) Chun, B. C.; Cha, S. H.; Chung, Y.-C.; Cho, J. W. Enhanced Dynamic Mechanical and Shape-Memory Properties of a Poly(Ethylene Terephthalate)-Poly(Ethylene Glycol) Copolymer Crosslinked by Maleic Anhydride. *Journal of Applied Polymer Science* **2002**, *83* (1), 27–37. <https://doi.org/10.1002/app.2228>.
- (25) Buasri, A.; Juengrungchaiwattana, S. Preparation and Characterization of PET-PLA Copolyester from Waste PET and Lactic Acid (LA). *Chiang Mai J. Sci.* **2011**, *38*, 619–624.
- (26) Ben Gara, M.; Kammoun, W.; Delaite, C. Synthesis and Characterization of Aliphatic-Aromatic Copolyesters PET-PLA from PET Waste and Lactide. *Journal of New Technology and Materials* **2016**, *6* (1), 42–48. <https://doi.org/10.12816/0043923>.

- (27) *Metal Catalysts in Olefin Polymerization*; Guan, Z., Carnahan, E. M., Eds.; Topics in organometallic chemistry; Springer-Verlag: Berlin, 2009.
- (28) Shaikh, I. R. Organocatalysis: Key Trends in Green Synthetic Chemistry, Challenges, Scope towards Heterogenization, and Importance from Research and Industrial Point of View. *Journal of Catalysts* **2014**, *2014*, 1–35. <https://doi.org/10.1155/2014/402860>.
- (29) Ottou, W. N.; Sardon, H.; Mecerreyes, D.; Vignolle, J.; Taton, D. Update and Challenges in Organo-Mediated Polymerization Reactions. *Progress in Polymer Science* **2016**, *56*, 64–115. <https://doi.org/10.1016/j.progpolymsci.2015.12.001>.
- (30) MacMillan, D. W. C. The Advent and Development of Organocatalysis. *Nature* **2008**, *455* (7211), 304–308. <https://doi.org/10.1038/nature07367>.
- (31) Dalko, P. I.; Moisan, L. In the Golden Age of Organocatalysis. *Angewandte Chemie International Edition* **2004**, *43* (39), 5138–5175. <https://doi.org/10.1002/anie.200400650>.
- (32) Bertelsen, S.; Jørgensen, K. A. Organocatalysis—after the Gold Rush. *Chemical Society Reviews* **2009**, *38* (8), 2178. <https://doi.org/10.1039/b903816g>.
- (33) Uyama, H.; Kobayashi, S. Enzyme-Catalyzed Polymerization to Functional Polymers. **2002**, *11*.
- (34) Shoda, S.; Uyama, H.; Kadokawa, J.; Kimura, S.; Kobayashi, S. Enzymes as Green Catalysts for Precision Macromolecular Synthesis. *Chemical Reviews* **2016**, *116* (4), 2307–2413. <https://doi.org/10.1021/acs.chemrev.5b00472>.
- (35) Sheldon, R. A.; Woodley, J. M. Role of Biocatalysis in Sustainable Chemistry. *Chemical Reviews* **2018**, *118* (2), 801–838. <https://doi.org/10.1021/acs.chemrev.7b00203>.
- (36) Kobayashi, S.; Uyama, H.; Kimura, S. Enzymatic Polymerization. *Chemical Reviews* **2001**, *101* (12), 3793–3818. <https://doi.org/10.1021/cr990121l>.
- (37) Kobayashi, S. Enzymatic Polymerization: A New Method of Polymer Synthesis. *Journal of Polymer Science Part A: Polymer Chemistry* **1999**, *37* (16), 3041–3056. [https://doi.org/10.1002/\(SICI\)1099-0518\(19990815\)37:16<3041::AID-POLA1>3.0.CO;2-V](https://doi.org/10.1002/(SICI)1099-0518(19990815)37:16<3041::AID-POLA1>3.0.CO;2-V).

- (38) Simón, L.; Goodman, J. M. The Mechanism of TBD-Catalyzed Ring-Opening Polymerization of Cyclic Esters. *The Journal of Organic Chemistry* **2007**, *72* (25), 9656–9662. <https://doi.org/10.1021/jo702088c>.
- (39) Sardon, H.; Pascual, A.; Mecerreyes, D.; Taton, D.; Cramail, H.; Hedrick, J. L. Synthesis of Polyurethanes Using Organocatalysis: A Perspective. *Macromolecules* **2015**, *48* (10), 3153–3165. <https://doi.org/10.1021/acs.macromol.5b00384>.
- (40) Qin, Y.; Zhu, L.; Luo, S. Organocatalysis in Inert C–H Bond Functionalization. *Chemical Reviews* **2017**, *117* (13), 9433–9520. <https://doi.org/10.1021/acs.chemrev.6b00657>.
- (41) Pinaud, J.; Tang, R.; Gimello, O.; Robin, J.-J. Organocatalyzed Ring-Opening Polymerization of Cyclic Butylene Terephthalate Oligomers. *Journal of Polymer Science Part A: Polymer Chemistry* **2017**, *55* (9), 1611–1619. <https://doi.org/10.1002/pola.28534>.
- (42) Mezzasalma, L.; Dove, A. P.; Coulembier, O. Organocatalytic Ring-Opening Polymerization of L-Lactide in Bulk: A Long Standing Challenge. *European Polymer Journal* **2017**, *95*, 628–634. <https://doi.org/10.1016/j.eurpolymj.2017.05.013>.
- (43) Kadota, J.; Pavlović, D.; Hirano, H.; Okada, A.; Agari, Y.; Bibal, B.; Deffieux, A.; Peruch, F. Controlled Bulk Polymerization of L-Lactide and Lactones by Dual Activation with Organo-Catalytic Systems. *RSC Advances* **2014**, *4* (28), 14725. <https://doi.org/10.1039/c4ra01239a>.
- (44) García-Argüelles, S.; García, C.; Serrano, M. C.; Gutiérrez, M. C.; Ferrer, M. L.; del Monte, F. Near-to-Eutectic Mixtures as Bifunctional Catalysts in the Low-Temperature-Ring-Opening-Polymerization of  $\epsilon$ -Caprolactone. *Green Chem.* **2015**, *17* (6), 3632–3643. <https://doi.org/10.1039/C5GC00348B>.
- (45) Dove, A.; Sardon, H.; Stefan, N. *Organic Catalysis for Polymerisation*; Polymer Chemistry; 2018.
- (46) Bossion, A.; Heifferon, K. V.; Meabe, L.; Zivic, N.; Taton, D.; Hedrick, J. L.; Long, T. E.; Sardon, H. Opportunities for Organocatalysis in Polymer Synthesis via Step-Growth Methods. *Progress in Polymer Science* **2019**, *90*, 164–210. <https://doi.org/10.1016/j.progpolymsci.2018.11.003>.
- (47) Basterretxea, A.; Gabirondo, E.; Jehanno, C.; Zhu, H.; Flores, I.; Müller, A. J.; Etxeberria, A.; Mecerreyes, D.; Coulembier, O.; Sardon, H. Polyether Synthesis by

- Bulk Self-Condensation of Diols Catalyzed by Non-Eutectic Acid–Base Organocatalysts. *ACS Sustainable Chemistry & Engineering* **2019**, *7* (4), 4103–4111. <https://doi.org/10.1021/acssuschemeng.8b05609>.
- (48) Joo, H.; Yoo, Y. J.; Dordick, J. S. Polymers from Biocatalysts. *Korean J. Chem. Eng.* **1998**, *15* (4), 13.
- (49) Jiang, Y.; Woortman, A. J. J.; Alberda van Ekenstein, G. O. R.; Loos, K. A Biocatalytic Approach towards Sustainable Furanic–Aliphatic Polyesters. *Polymer Chemistry* **2015**, *6* (29), 5198–5211. <https://doi.org/10.1039/C5PY00629E>.
- (50) Jiang, Y.; Loos, K. Enzymatic Synthesis of Biobased Polyesters and Polyamides. *Polymers* **2016**, *8* (7), 243. <https://doi.org/10.3390/polym8070243>.
- (51) Cruz-Izquierdo, Á.; van den Broek, L. A. M.; Serra, J. L.; Llama, M. J.; Boeriu, C. G. Lipase-Catalyzed Synthesis of Oligoesters of 2,5-Furandicarboxylic Acid with Aliphatic Diols. *Pure and Applied Chemistry* **2015**, *87* (1), 59–69. <https://doi.org/10.1515/pac-2014-1003>.
- (52) Polyethylene Terephthalate (PET): Production, Price, Market and its Properties <https://www.plasticsinsight.com/resin-intelligence/resin-prices/polyethylene-terephthalate/> (accessed Apr 9, 2019).
- (53) Sinha, V.; Patel, M. R.; Patel, J. V. Pet Waste Management by Chemical Recycling: A Review. *Journal of Polymers and the Environment* **2010**, *18* (1), 8–25. <https://doi.org/10.1007/s10924-008-0106-7>.
- (54) Sharma, V.; Parashar, P.; Srivastava, P.; kumar, S.; Agarwal, D. D.; Richharia, N. Recycling of Waste PET-Bottles Using Dimethyl Sulfoxide and Hydrotalcite Catalyst. *Journal of Applied Polymer Science* **2013**, *129* (3), 1513–1519. <https://doi.org/10.1002/app.38829>.
- (55) Al-Sabagh, A. M.; Yehia, F. Z.; Eshaq, Gh.; Rabie, A. M.; ElMetwally, A. E. Greener Routes for Recycling of Polyethylene Terephthalate. *Egyptian Journal of Petroleum* **2016**, *25* (1), 53–64. <https://doi.org/10.1016/j.ejpe.2015.03.001>.
- (56) Ben-Haida, A.; Conzatti, L.; Hodge, P.; Manzini, B.; Stagnaro, P. An Introduction to Entropically-Driven Ring-Opening Polymerizations. *Macromolecular Symposia* **2010**, *297* (1), 6–17. <https://doi.org/10.1002/masy.200900109>.

- (57) Hodge, P. Recycling of Condensation Polymers via Ring-Chain Equilibria: RECYCLING VIA RING-CHAIN EQUILIBRIA. *Polymers for Advanced Technologies* **2015**, 26 (7), 797–803. <https://doi.org/10.1002/pat.3469>.
- (58) Gandini, A.; Silvestre, A. J. D.; Neto, C. P.; Sousa, A. F.; Gomes, M. The Furan Counterpart of Poly(Ethylene Terephthalate): An Alternative Material Based on Renewable Resources. *Journal of Polymer Science Part A: Polymer Chemistry* **2009**, 47 (1), 295–298. <https://doi.org/10.1002/pola.23130>.

# Chapter 2

## *Experimental Part*

2.1 Materials.....	17
2.2 Synthesis of Polymers.....	18
2.2.1 Synthesis of PET.....	19
2.2.2 Synthesis of Random Copolymers.....	20
2.2.3 Synthesis of PET- <i>b</i> -Polyether Copolymers.....	22
2.2.4 Synthesis of Polyesters from Cyclic Oligoesters and their Cyclodepolymerization.....	22
2.2.5 Synthesis of Triblock Copolymers PLLA- <i>b</i> -PHF- <i>b</i> -PLLA and PLLA- <i>b</i> -PHT- <i>b</i> -PLLA.....	25
2.3 Characterization Techniques.....	26
2.3.1 NMR Spectroscopy.....	26
2.3.2 FTIR Spectroscopy.....	27
2.3.3 Size Exclusion Chromatography (SEC).....	27
2.3.4 Hydrolytic Degradation.....	28

---

---

2.3.5 High –Performance Liquid Chromatography (HPLC).....	28
2.3.6 Matrix-Assisted Laser Desorption/Ionization Time of Flight (MALDI-TOF).....	28
2.3.7 Intrinsic Viscosity.....	29
2.3.8 Dynamic Mechanical Thermal Analysis (DMTA).....	29
2.3.9 Differential Scanning Calorimetry (DSC).....	30
2.3.10 Flash DSC.....	34
2.3.11 Thermogravimetric Analysis (TGA).....	34
2.3.12 Simultaneous Wide-Angle and Small-Angle X-ray Scattering (SAXS/WAXS).....	34
2.3.13 Polarized Light Optical Microscopy (PLOM) and Atomic Force Microscopy (AFM).....	35
2.4 Theoretical Concepts of Thermal Characterization of Polymers.....	36
2.4.1 Crystallization in Polymers.....	37
2.4.2 Crystal Growth.....	38
2.4.3 Structure and Morphology of Polymers.....	39
2.4.4 Polymer Crystallization Theories.....	41
2.4.5 Thermal Properties of Copolymers.....	45
2.5 References.....	47

## 2.1 Materials

Dimethyl terephthalate (DMT,  $\geq 99\%$ ), ethylene glycol (EG, 99.8%), 1,3-Propanediol (PG, 98%), 1,6 hexanediol (HD, 99%), titanium (IV) butoxide (TiBut,  $\geq 99\%$ ), 1,8-Diazabicyclo[5.4.0]undec-7-ene (DBU, 98%), benzoic acid (BA, 99.5%), 1,5,7-triazabicyclo[4.4.0]dec-5-ene (TBD, 98%), p-toluenesulfonic acid monohydrate (p-TSA, 98.5%), trifluoroacetic acid (TFA, 99%), methanesulfonic acid (MSA,  $\geq 99.5\%$ ) and (3S)-*cis*-3,6-Dimethyl-1,4-dioxane-2,5-dione (L-lactide, 98%) were purchased from Sigma-Aldrich. Water was removed from the p-TSA before use. Novozyme 434 (*Candida antarctica* lipase B) was a kind gift of Novozymes. L-lactide was supplied from Futerro. 2,5-furandicarboxylic acid (FDCA, 98%) was bought with Satachem Co. 4-Dimethylaminopyridine (DMAP, 99%), Tetrahydrofuran (THF, 99.9%, Extra Dry) and Dichloromethane (DCM, 99.9%) were provided by Acros. 1-(4-sulfobutyl)-3-methylimidazolium hydrogen sulfate (BAIL, 98%) was obtained from Solvionic. Methanol (CH<sub>3</sub>OH, 99.5%), anhydrous toluene (99.8%) and chloroform (CHCl<sub>3</sub>, 99.9%) were acquired from Fisher Scientific.

The DBU:BA catalyst at molar ratio of base to acid (1:1) was prepared following the procedure reported by Coady et al.<sup>1</sup> TBD and MSA at molar ratio of base to acid (1:1), were mixed to obtain a TBD:MSA catalyst due to its ability to form PET from Bis(2-Hydroxyethyl) terephthalate.<sup>2</sup>

Dimethyl furanoate (DMF) was previously synthesized following the method reported by Gubbels et al.<sup>3</sup>

The polyether used poly (1,6 Hexanediol) [poly (1,6 HD)], was previously obtained according to the procedure reported by Andere et al.<sup>4</sup>

## 2.2 Synthesis of Polymers

Chain growth and step-growth polymerizations are two distinctive polymerization mechanisms in the production of polymers. The biggest difference between both types of polymerization is the molecular weight dependence on the extent of monomer conversion. During chain growth polymerization process, a reactive intermediate (i.e. radical, anion, cation or metallocene) forms through an initiation step. This reactive center reacts with a monomer, in a propagation step transferring the reactive center to the end of the chain. Molecular weight growth occurs through the consecutive addition of monomers until termination consumes the reactive center (Figure 2.1). The overall concentration of high molecular weight polymer chains and polymer dispersity index becomes reliant on % conversion.<sup>5</sup> In contrast, the mechanism of growth in step-growth polymerizations begins with the formation of dimers from monomers then systematically increases in size to trimers and tetramers until high molecular weights are achieved (Figure 2.1).<sup>5</sup>

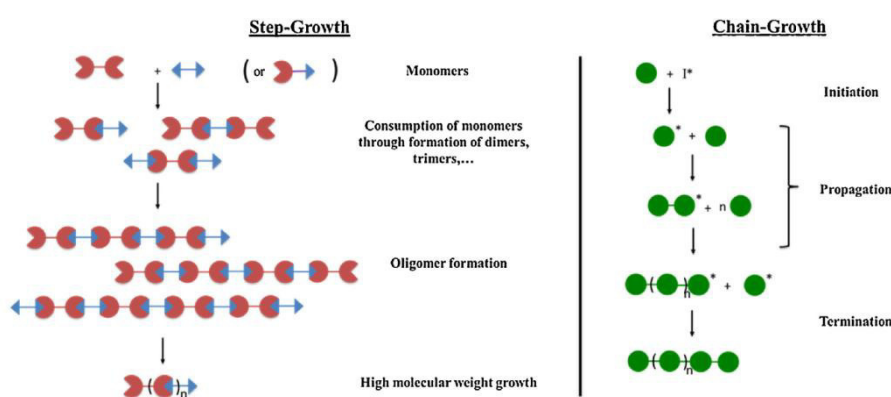
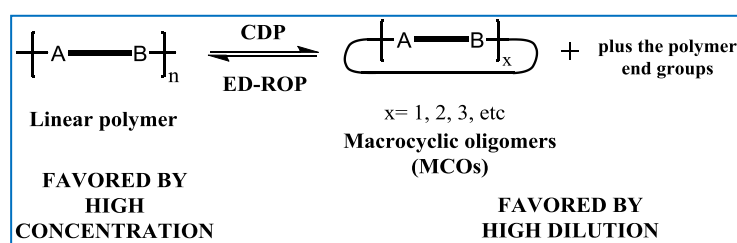


**Figure 2.1.** Illustration of mechanistic difference between step-growth polymerization and chain growth polymerization.<sup>5</sup>

Polyesters (R-COO-R') are an important class of polymeric materials. A wide range of polymerization synthetic routes to polyesters are known, including the step-growth polymerization of diacids and diols (and derivatives), the self-polycondensation of hydroxyacid, or the ring-opening polymerization (ROP) of cyclic esters. (ROP) is a type of chain-growth polymerization that allows for precise control over molecular weights and dispersity and gives access to complex structure, such as block

copolymers.<sup>5</sup> On the other hand, Entropically driven ring-opening polymerization (ED-ROP) is a ROP of individual strainless macrocycles, or homologous families of strainless macrocycles, at high concentration.<sup>6-8</sup> The reverse polymerization to the previous one is the Cyclodepolymerization (CDP), it involves taking a dilute solution, typically <3% w/v, of the appropriate polymer and establishing the RCE (Ring-chain equilibria).<sup>6</sup> Another way to obtain cyclic oligomers is the High dilution condensation (HDC), it consists of carrying out condensation reactions between the end groups of linear species at sufficiently low concentrations that intramolecular reactions are greatly favored over intermolecular reactions.<sup>6</sup> The formation of cyclic oligomers and the opening of macrocycles depend on the equilibrium conditions of the ring-chain (Scheme 2.1).



**Scheme 2.1** A generalized ring-chain equilibrium.<sup>8</sup>

In this thesis the step growth polymerization of polyesters and the ROP of polyester will be explored for the synthesis of sustainable polyesters derived from DMT monomer.

## 2.2.1 Synthesis of PET

### 2.2.1.1 Screening of Different Catalysts for PET Synthesis

The catalysts tested for PET polymerization were: TiBut, DBU:BA (1:1), DMAP, TBD, DBU, p-TSA, BAIL and TBD:MSA (1:1). PET was obtained by reacting DMT (1 equiv., 0.015 mol, 3.0 g) with EG (1.4 equiv., 0.021, 1.3 g) in the presence of 5 mol% of catalyst (with respect to DMT). The reaction was performed in a tubular Schlenk flask with glass key and equipped with a magnetic stirrer and the flask was heated in a molten salt bath. This procedure was the same for each catalyst employed.

The polymerization reaction was carried out at 200 °C for 24 h at atmospheric pressure, followed by 24 h under vacuum. During the reaction, an aliquot was taken at

different reaction times to follow the conversion by FTIR. Finally, the polymer obtained was diluted in a mixture of chloroform and trifluoroacetic acid (8:1, v/v), precipitated an excess of methanol and collected by centrifugation. Then, the material was dried under vacuum.

**PET.**  $^1\text{H}$  NMR ( $\delta$ ppm,  $\text{CDCl}_3/\text{TFA}$ , 300 MHz): 8.12 (4H, Ar-**CH**), 4.78 (4H,  $\text{COO-CH}_2\text{-CH}_2\text{-OCO}$ , internal group), 4.63 (4H,  $\text{COO-CH}_2\text{-CH}_2\text{-O-CH}_2\text{-CH}_2\text{-OCO}$ , dimer)/ (2H,  $\text{COO-CH}_2\text{-CH}_2\text{-OH}$ , end group), 4.18 (2H,  $\text{COO-CH}_2\text{-CH}_2\text{-OH}$ , end group), 4.10 (4H,  $\text{COO-CH}_2\text{-CH}_2\text{-O-CH}_2\text{-CH}_2\text{-OCO}$ , dimer) and 4.02 (3H,  $\text{COO-CH}_3$ , end group).

### 2.2.1.2 Optimized PET polymerization

Following the procedure described previously for PET synthesis, but in order to optimize the polymerization, DBU:BA (1:1) was used as catalyst in two reactions, the first reaction was carried out at 240 °C for 24 h under atmospheric pressure followed by 24 h under vacuum. The second reaction was carried out at 200 °C under atmospheric pressure for 24 h and then the temperature was increased to 250 °C and vacuum was applied for 4 h.

To complete the study, other reactions were carried out at 250 °C for 1 h under atmospheric pressure and 4 h under vacuum. In this case, the catalysts employed were: DBU:BA (1:1) and TBD:MSA (1:1). The same procedure than in the Screening of different catalysts for PET Synthesis section was applied to the purification of PET.

A complementary study has been made under the latter conditions but using 500 ppm of catalysts, being TiBut, DBU:BA and TBD:MSA. In this purpose, a stock solution (in dried THF) of 100 mg of the catalyst was realized for higher precision and the corresponding quantity of 500 ppm mol% of this solution was added to DMT and EG.

## 2.2.2 Synthesis of Random Copolymers

### 2.2.2.1 Synthesis of PLA (Poly (L-lactic acid))

PLA was synthesized in a round bottom flask equipped with a magnetic stirrer where L-lactide (50 equiv., 0.139 mol, 20 g), 1,3-Propanediol (1 equiv., 0.0028 mol,

0.21 g) as initiator and DBU:BA as catalyst (10 mol% with respect to L-lactide) were mixed in the presence of DCM [0.139 L, calculated from  $(\frac{\text{mol(L-lactide)}}{L(\text{DCM})} = 1 \text{ M})$ ] under an inert atmosphere at 25 °C for 24 h. Then benzoic acid was added to stop the reaction while stirring continued for 30 min. The polymer obtained was precipitated in excess methanol and collected by centrifugation and finally it was dried under vacuum.

**PLLA.**  $^1\text{H}$  NMR ( $\delta$ ppm,  $\text{CDCl}_3$ , 300 MHz): 5.14 (1 H, COO-**CH**CH<sub>3</sub>O, internal group), 4.33 (1 H, COO-**CH**CH<sub>3</sub>OH, end group), 1.59 (3 H, COO-**CH**CH<sub>3</sub>O, internal group), 1.47 (3 H, COO-**CH**CH<sub>3</sub>OH, end group).

#### 2.2.2.2 Synthesis of PET-*ran*-PLA Copolyesters

The bulk polymerization of each copolyester was carried out in a tubular Schlenk flask with glass key equipped with a magnetic stirrer, where DMT (1 equiv., 0.015 mol, 3.0 g) with EG (1.4 equiv., 0.021 mol, 1.3 g) in the presence of 5 mol% of catalyst (with respect to DMT) were mixed at 200 °C for 2 h at atmospheric pressure. Maintaining the reaction conditions the PLLA was added to obtain compositions from 98/02 to 28/72 PET/PLA wt%. The amounts of DMT and EG were kept constant and the amount of PLA was varied for each composition as follows (PET/PLA, g PLA): (98/02, 0.23 g), (95/05, 0.48 g), (93/07, 0.62), (92/08, 0.69 g), (91/09, 0.72 g), (90/10, 0.77 g), (82/18, 1.86 g), (48/52, 2.17 g) and (28/72, 5.79 g). All components were mixed for 4 h and then vacuum was applied for 24 h. The same procedure was followed in the synthesis of each one of the copolyesters.

Each copolymer obtained was diluted in a mixture of chloroform ( $\text{CHCl}_3$ ) and trifluoroacetic acid (TFA) (8:1, v/v), precipitated in excess methanol and separated from impurities by centrifugation and then the material was dried under vacuum.

**PET-*ran*-PLA.**  $^1\text{H}$  NMR ( $\delta$ ppm,  $\text{CDCl}_3/\text{TFA}$ , 300 MHz): 5.43 (Link *Terephthalate-Lactide*, Ar-COO-**CH**CH<sub>3</sub>CO), 4.66 (Link *Terephthalate-Ethylene glycol-Lactide*, Ar-COO-**CH**<sub>2</sub>-**CH**<sub>2</sub>-OCOCHCH<sub>3</sub>-O), 1.69 (Link *Terephthalate-Lactide*, Ar-COO-**CH**CH<sub>3</sub>CO).

### 2.2.3 Synthesis of PET-*b*-Polyether Copolymers

The synthesis of each one of the copolymers was carried out in a tubular Schlenk flask with glass key equipped with a magnetic stirrer, where DMT (1 equiv., 0.015 mol, 3.0 g) with EG (1.4 equiv., 0.021 mol, 1.3 g) in the presence of the catalyst DBU:BA (5 mol% with respect to DMT) were mixed at 250 °C for 1.5 h at atmospheric pressure. Maintaining the reaction conditions the Polyether was added to obtain copolymers of PET-*b*-Polyether with different compositions PET/Polyether wt%. To do the above, the amounts of DMT and EG were kept constant and the amount of Polyether was varied for each composition as follows [PET/Polyether, g Polyether]: for PET/Poly (1,6 HD), (68/32, 0.48 g), (64/36, 1.08 g), (61/39, 1.86) and (34/66, 4.34 g). The components were mixed for 1.75 h and then vacuum was applied for 4 h. The same procedure was followed in the synthesis of each one of the copolymers.

Each polymer obtained was diluted in a mixture of chloroform (CHCl<sub>3</sub>) and Trifluoroacetic acid (TFA) (8:1, v/v), precipitated in excess methanol and separated from impurities by centrifugation; finally the material was dried under vacuum.

**PET-*b*-Polyether.** <sup>13</sup>C NMR (δppm, CDCl<sub>3</sub>/TFA, 300 MHz): 134.77 (Polyether-*Terephthalate*-Ethylene glycol, O-[CH<sub>2</sub>]<sub>6</sub>-COO-**CH**-Ar-CH-COO-[CH<sub>2</sub>]<sub>2</sub>-O-), 134.55 (Dyad Polyether-*Terephthalate*-Polyether, O-[CH<sub>2</sub>]<sub>6</sub>-COO-**CH**-Ar-**CH**-COO-[CH<sub>2</sub>]<sub>6</sub>-O-), 134.19 (Dyad Ethylene glycol-*Terephthalate*-Ethylene glycol, O-[CH<sub>2</sub>]<sub>2</sub>-COO-**CH**-Ar-**CH**-COO-[CH<sub>2</sub>]<sub>2</sub>-O-), 133.97 (Ethylene glycol-*Terephthalate*-Polyether, O-[CH<sub>2</sub>]<sub>6</sub>-COO-CH-Ar-**CH**-COO-[CH<sub>2</sub>]<sub>2</sub>-O).

### 2.2.4 Synthesis of Polyesters from Cyclic Oligoesters and their Cyclodepolymerization

2.2.4.1 Synthesis of hexamethylene terephthalate and hexamethylene furanoate cyclic oligomers c(HT)<sub>x</sub>, c(HF)<sub>x</sub> by enzymatic cyclization.

c(HT)<sub>x</sub> and c(HF)<sub>x</sub> were synthesized by enzymatic cyclization using the procedure reported by Sugihara et al. for the synthesis of aliphatic oligoesters.<sup>9</sup> For the case of c(HT)<sub>x</sub> cycles, 1,6-hexanediol (1.02 equiv., 0.0105 mol, 1.24 g), dimethyl terephthalate (1 equiv., 0.0102 mol, 2 g) and toluene ( $\frac{g(DMT)}{mL(toluene)} = 0.0029$ ), were

placed in a round bottom flask equipped with a nitrogen inlet, a condensation outlet and a magnetic stirrer, and immersed in a thermostated oil bath heated at 90 °C. Then immobilized lipase CAL B (100 wt.-% with respect to: g of HD + g of DMT, 3.24 g) was added. This enzyme was previously dried under vacuum for 24 hours at 50 °C. One aliquot was extracted at different reaction times (7 hours, 1 day, 2 days, 3 days, 4 days, 7 days) and, after removing the enzymes using a membrane syringe filter, were characterized by  $^1\text{H}$  NMR and HPLC. Finally the solution reaction was diluted with 1 ml of chloroform per 3.4 ml of solution, filtrated with a filter plate and evaporated to dryness under reduced pressure. The cyclic oligoesters, recovered as white products, were placed in a vacuum desiccator and used without further purification for all analysis and posterior enzymatic polymerization.

To synthesize cycles of  $c(\text{HF})_x$  the previous procedure was followed, using: , 1,6-hexanediol (1.02 equiv., 0.0110 mol, 1.30 g), dimethyl furanoate (1 equiv., 0.0108 mol, 2 g) and toluene ( $\frac{g(\text{DMF})}{\text{mL}(\text{toluene})} = 0.0029$ ), CAL B (100 wt.-%, 3.30 g). Control test without enzymes were essayed under same experimental conditions.

$c(\text{HT})_x$ .  $^1\text{H}$  NMR ( $\delta\text{ppm}$  ,  $\text{CDCl}_3$ , 300.1 MHz): 8.08-7.87 (4H, Ar-**CH**), 4.38 (4H, **OCH<sub>2</sub>**), 1.84 (4H, **OCH<sub>2</sub>CH<sub>2</sub>**), 1.63-1.54 (4H, **OCH<sub>2</sub>CH<sub>2</sub>CH<sub>2</sub>**).

$c(\text{HF})_x$ .  $^1\text{H}$  NMR ( $\delta\text{ppm}$  ,  $\text{CDCl}_3$ , 300.1 MHz): 7.19-7.18 (2H, Ar-**CH**), 4.34 (4H, **OCH<sub>2</sub>**), 1.81 (4H, **OCH<sub>2</sub>CH<sub>2</sub>**), 1.57-1.50 (4H, **OCH<sub>2</sub>CH<sub>2</sub>CH<sub>2</sub>**).

2.2.4.2 Synthesis of poly(hexamethylene terephthalate) (PHT) and poly(hexamethylene furanoate) (PHF) from  $c(\text{HT})_x$ ,  $c(\text{HF})_x$  cyclic oligomers by enzymatic polymerization.

PHT and PHF were obtained by enzymatic ROP using a slightly modified procedure of Sugihara et al.<sup>9</sup> To synthesize PHT, (1 equiv., 0.0060 mol, 1.5 g) of  $c(\text{HT})_x$ , (0.083 equiv., 0.00050 mol, 0.059 g) of 1,6-hexanediol and 1 ml of toluene (per 0.25 g of added PHF cycles) were added to a round bottom flask equipped with a magnetic stirrer, and immersed in a thermostated oil bath heated at 100 °C. Then immobilized lipase CAL B (40 wt.-% with respect to g of  $c(\text{HT})_x$ , 0.6 g) was added and maintained at this temperature for 24 h. Then chloroform was added to dilute the solid present in the reaction solution and filtrated with a filter plate and evaporated to dryness under

reduced pressure. The polymers obtained as white products were placed in a vacuum desiccator and used without further purification for GPC and NMR analysis.

With the same procedure previously described PHF was also obtained, the reagents used were: (1 equiv., 0.0063 mol, 1.5 g) of  $c(\text{HF})_x$ , (0.083 equiv., 0.00052 mol, 0.062 g) of 1,6-hexanediol and CAL B (40 wt.-%, 0.6 g). Control test without enzymes were assayed under same experimental conditions.

**PHT.**  $^1\text{H}$  NMR ( $\delta$ ppm,  $\text{CDCl}_3$ , 300.1 MHz): 8.08 (4H, Ar-**CH**), 4.36 (4H, **OCH<sub>2</sub>**), 1.83 (4H, **OCH<sub>2</sub>CH<sub>2</sub>**), 1.54 (4H, **OCH<sub>2</sub>CH<sub>2</sub>CH<sub>2</sub>**).

**PHF.**  $^1\text{H}$  NMR ( $\delta$ ppm,  $\text{CDCl}_3$ , 300.1 MHz): 7.19 (2H, Ar-**CH**), 4.34 (4H, **OCH<sub>2</sub>**), 1.79 (4H, **OCH<sub>2</sub>CH<sub>2</sub>**), 1.48 (4H, **OCH<sub>2</sub>CH<sub>2</sub>CH<sub>2</sub>**).

2.2.4.3 Synthesis of hexamethylene terephthalate and hexamethylene furanoate cyclic oligomers  $c(\text{HT})_x$ ,  $c(\text{HF})_x$  by enzymatic cyclodepolymerization.

(0.00080 mol, 0.2 g) of previously synthesized PHT and toluene ( $\frac{g(\text{PHT})}{ml(\text{Toluene})} = 0.0029$ ) were added to a round bottom flask with a magnetic stirrer and immersed in a thermostated oil bath heated at 90 °C. Then immobilized CAL B (100 wt.-%, with respect to g PHT, 0.2 g) was added and maintained at this temperature for 3 days. Then the reaction solution was diluted with 1 ml of chloroform per 3.4 ml of solution and filtrated with a filter plate and evaporated to dryness under reduced pressure. The cyclic oligoesters, recovered as a white product, were placed in a vacuum desiccator and used without further purification for all analysis.

Following the same procedure above, PHF cycles were synthesized, where (0.00084 mol, 0.2 g) of previously synthesized PHF were used, toluene ( $\frac{g(\text{PHF})}{ml(\text{Toluene})} = 0.0029$ ), CAL B (100 wt.-%, with respect to g PHF, 0.2 g). Control test without enzymes were assayed under same experimental conditions.

**$c(\text{HT})_x$ .**  $^1\text{H}$  NMR ( $\delta$ ppm,  $\text{CDCl}_3$ , 300.1 MHz): 8.09-7.85 (4H, Ar-**CH**), 4.38 (4H, **OCH<sub>2</sub>**), 1.83 (4H, **OCH<sub>2</sub>CH<sub>2</sub>**), 1.62-1.54 (4H, **OCH<sub>2</sub>CH<sub>2</sub>CH<sub>2</sub>**).

**$c(\text{HF})_x$ .**  $^1\text{H}$  NMR ( $\delta$ ppm,  $\text{CDCl}_3$ , 300.1 MHz): 7.19-7.18 (2H, Ar-**CH**), 4.34 (4H, **OCH<sub>2</sub>**), 1.81 (4H, **OCH<sub>2</sub>CH<sub>2</sub>**), 1.57-1.50 (4H, **OCH<sub>2</sub>CH<sub>2</sub>CH<sub>2</sub>**).

### 2.2.5 Synthesis of Triblock Copolymers PLLA-*b*-PHF-*b*-PLLA and PLLA-*b*-PHT-*b*-PLLA

First, telechelic oligomers of Poly(hexamethylene terephthalate) (PHT) and Poly(hexamethylene furanoate) (PHF) were synthesized following the procedure described in 2.2.4.2.

PLLA-*b*-PHF-*b*-PLLA copolymers were synthesized in a round bottom flask equipped with a magnetic stirrer, where Telechelic oligomer of PHF (1 mEq., 1.26 mmol, 300 mg) and TBD as catalyst (5 mol% with respect to L-lactide) were mixed with each one of the next amounts of L-lactide with the intention of obtaining different compositions of PHF/Lactic Acid, these amounts were: (1 mEq., 1.26 mmol, 182 mg), (2mEq., 2.52 mmol, 363 mg) and (4 mEq., 5.04 mmol, 726 mg). Then DCM [ $ml\ DCM = \frac{mmol(L-lactide)}{1\ M}$ ] was added and all components were mixed at 25 °C for 5 min. Then benzoic acid was added to stop the reaction while stirring continued for 5 min. Finally chloroform was added and then the polymer obtained was precipitated in excess methanol and collected by centrifugation and then it was dried under vacuum. NMR experiments were performed to corroborate the chemical structure and microstructure of the copolymers.

Employing the same procedure previously described PLLA-*b*-PHT-*b*-PLLA copolymers were also obtained. The reagents used were Telechelic polymer of PHT (1 mEq., 1.20 mmol, 300 mg), TBD catalyst (5 mol% with respect to L-lactide) and different amounts of L-lactide: (1 mEq., 1.20 mmol, 174 mg), (2 mEq., 2.42 mmol, 348 mg) and (4 mEq., 4.84 mmol, 697 mg).

To complement the study, reactions with a large amount of L-lactide were carried out, following the same procedure described, but with the quantities of reagents that are mentioned below, to obtain PLLA-*b*-PHF-*b*-PLLA: Telechelic polymer of PHF (1 mEq., 0.42 mmol, 100 mg), TBD (5 mol% with respect to L-lactide) and L-lactide (16 mEq., 6.72 mmol, 969 mg); for the case of PLLA-*b*-PHT-*b*-PLLA the quantities used were: Telechelic polymer of PHT (1 mEq., 0.40 mmol, 100 mg), TBD (5 mol% with respect to L-lactide) and L-lactide (16 mEq., 6.45 mmol, 930 mg).

**PLLA-*b*-PHF-*b*-PLLA:**  $^1\text{H NMR}$  (300.1 MHz,  $\text{CDCl}_3$ ,  $\delta$ ppm): 7.19 (s, ArH), 5.16 (m, CH (LA)), 4.34 (t,  $\text{OCH}_2$  (HF)), 1.79 (m,  $\text{OCH}_2\text{CH}_2$  (HF)), 1.58 (d,  $\text{CH}_3$  (LA)), 1.48 (m,

OCH<sub>2</sub>CH<sub>2</sub>CH<sub>2</sub> (HF)). <sup>13</sup>C NMR (75.5 MHz, CDCl<sub>3</sub>, δ (ppm)): 169.6 (CO (LA)), 158.1 (CO (HF)), 146.9 (ArC (HF)), 118.3 (ArCH (HF)), 69.3 (CH (LA)), 65.4 (OCH<sub>2</sub> (HF)), 28.5 (OCH<sub>2</sub>CH<sub>2</sub> (HF)), 25.5 (OCH<sub>2</sub>CH<sub>2</sub>CH<sub>2</sub> (HF)), 16.6 (CH<sub>3</sub> (LA)).

**PLLA-*b*-PHT-*b*-PLLA:** <sup>1</sup>H NMR (300.1 MHz, CDCl<sub>3</sub>, δ ppm): 8.08 (s, ArH), 5.17 (m, CH (LA)), 4.36 (t, OCH<sub>2</sub> (HT)), 1.82 (m, OCH<sub>2</sub>CH<sub>2</sub> (HT)), 1.58 (d, CH<sub>3</sub> (LA)), 1.54 (m, OCH<sub>2</sub>CH<sub>2</sub>CH<sub>2</sub> (HT)). <sup>13</sup>C NMR (75.5 MHz, CDCl<sub>3</sub>, δ (ppm)): 169.6 (CO (LA)), 165.8 (CO (HT)), 134.1 (ArC (HT)), 129.5 (ArCH (HT)), 69.0 (CH (LA)), 65.3 (OCH<sub>2</sub> (HT)), 28.6 (OCH<sub>2</sub>CH<sub>2</sub> (HT)), 25.7 (OCH<sub>2</sub>CH<sub>2</sub>CH<sub>2</sub> (HT)), 16.6 (CH<sub>3</sub> (LA)).

## 2.3 Characterization Techniques

### 2.3.1 NMR Spectroscopy

<sup>1</sup>H NMR and <sup>13</sup>C NMR spectra were recorded on a Bruker DPX300 spectrometer. For NMR analysis, polymers (PET, PET-*ran*-PLA and PET-*b*-Polyether) were dissolved in a mixture of deuterated chloroform (CDCl<sub>3</sub>) and trifluoroacetic acid (TFA) (8:1, v/v). In the case of PLA and Polyether, these were dissolved in chloroform (CDCl<sub>3</sub>), all the spectra were referenced to CDCl<sub>3</sub>. About 10 mg of sample in 0.6 mL of solvent were used for <sup>1</sup>H NMR. For <sup>13</sup>C NMR analysis, samples of 40 mg in 0.6 mL of solvent were prepared.

To analyze samples derived from HT and HF (cyclic and polymers), L-lactide and triblock copolymers (PLLA-*b*-PHF-*b*-PLLA and PLLA-*b*-PHT-*b*-PLLA), <sup>1</sup>H NMR and <sup>13</sup>C NMR spectra were recorded at 300.1 MHz on a Bruker AMX-300 NMR instrument. About 10 mg and 40 of sample for <sup>1</sup>H NMR and <sup>13</sup>C NMR respectively, were dissolved in 1 mL of deuterated chloroform containing a small amount of TMS internal reference (only for PLLA-*b*-PHF-*b*-PLLA and PLLA-*b*-PHT-*b*-PLLA, 0.7 mL of deuterated chloroform were used). Around 128 scans were collected and signal averaged with 32-K data points. For determination of polyester end-groups by <sup>1</sup>H NMR, an excess of trichloroacetyl isocyanate (TAI) (a drop) was added to the NMR tube containing 10 mg of polyester samples dissolved in 1 mL of the deuterated chloroform. The reaction with both hydroxyl and carboxyl end groups gave rise to two signals due to the imide NH

groups at around 8.5 and 10.4 ppm, respectively.<sup>10</sup> Due to partial overlapping of one of the imidic NH groups in PHT, the amount of CH<sub>2</sub>OH end groups was calculated from the <sup>1</sup>H NMR spectra of non-added TAI sample. Spectra were processed with the WINNMR Bruker program.

### 2.3.2 FTIR Spectroscopy

To analyze the samples by FTIR spectroscopy a Nicolet 6700 spectrometer (Thermo Scientific) was used with golden gate single reflection ATR with a resolution of 4 cm<sup>-1</sup>, a diamond crystal was employed.

In the case of PET samples, these were taken from the tubular Schlenk flask at different reaction times and the obtained solids were analyzed. For PET-*ran*-PLA copolymers the solids from the final products were studied.

### 2.3.3 Size Exclusion Chromatography (SEC)

To analyze PET and PET-*ran*-PLA, size exclusion chromatography was performed at 40 °C by an Agilent equipment provided with a refractive index detector and equipped with a precolumn HFIP-LG and two HFIP 804 and HFIP 803 columns from Shodex packed with polystyrene-divinylbenzene. The samples were chromatographed with a flow of 0.5 mL·min<sup>-1</sup> using 1,1,1,3,3,3-Hexafluoro-2-propanol (HFIP) as solvent.

The molecular weight of PLA was determined by SEC analysis performed at 35 °C using Tetrahydrofuran as eluent with a flow of 1 mL/min in a Waters equipment provided with an UV-visible detector and IR detector, with Styragel HR series of columns (HR6, HR4, HR2).

In the case of the polyether, was analyzed by SEC analysis (Agilent PL-GPC 50) using Shodex GPC HFIP-803 (300 x 8.0 mm), where the Chloroform was the eluent, at 50 °C and a flow rate of 1 mL/min with polystyrene standards.

Waters equipment provided with RI and UV detectors, was used to measure molecular weights of cycles and polymers (from HT and HF) and triblock copolymers (PLLA-*b*-PHF-*b*-PLLA and PLLA-*b*-PHT-*b*-PLLA). HR5E and HR2 Waters linear Styragel

columns (7.8 mm × 300 mm, pore size 103–104 Å) packed with crosslinked polystyrene and protected with a precolumn were used. For each sample, 100 µL of 0.1% (w/v) sample solution was injected and chromatographed with a flow of 0.4 mL min<sup>-1</sup>. Molar mass average and distributions were calculated against PMMA standards.

### 2.3.4 Hydrolytic Degradation

Samples of 20 mg each were dispersed in 20 mL of phosphate buffer (pH=7.4) and incubated at 37 °C (±1 °C) with stirring. At different time periods, samples of PET-*ran*-PLA copolyesters were taken out, washed and dried for later analysis by NMR.

### 2.3.5 High –Performance Liquid Chromatography (HPLC)

HPLC analysis was performed at 25 °C in a Waters apparatus equipped with a UV detector of Applied Biosystems, operating at 254 nm wavelength, and a Scharlau Science column (Si60, 5 µm; 250 × 4.6 mm). Cyclic oligomers (1 mg) were dissolved in chloroform (1 mL) and eluted with hexane/1,4-dioxane 70/30 (v/v) at a flow rate of 1.0 mL min<sup>-1</sup>.

### 2.3.6 Matrix-Assisted Laser Desorption/Ionization Time of Flight (MALDI-TOF)

(MALDI-TOF) MS spectra were recorded in a 4700 Proteomics Analyser instrument of Applied Biosystems (Proteomics Platform of Barcelona Science Park, University of Barcelona). Spectra acquisition was performed in the MS reflector positive-ion mode. About 0.1 mg of sample was dissolved in 50 µL of DCM and 2 µL of this solution were mixed with an equal volume of DCM solution of anthracene (10 mg mL<sup>-1</sup>), and the mixture left to evaporate to dryness onto the stainless steel plate of the analyser. The residue was then covered with 2 µL of a solution of 2,5-dihydroxybenzoic acid in acetonitrile/H<sub>2</sub>O (1/1) containing 0.1% TFA, and the mixture was left to dry prior to exposition to the laser beam.

### 2.3.7 Intrinsic Viscosity

The determination of the intrinsic viscosity was carried out following standard UNE-EN ISO 1628 / 5-1986 (E) in a capillary viscometer. A solution with a polymer concentration of 0.2 g/dL was prepared, the solvent used was a mixture of phenol and 1,2-dichlorobenzene (50/50 %w). The temperature of the bath to carry out the measurements was 30 °C, a capillary viscometer type Ubbelohd was used. A chronometer was used to measure the flow time, at least three measurements for each sample were made.

The values reported in chapter 5 are the average of the values obtained from the reduced viscosity and the inherent viscosity. Different authors report the formulas to determine the different viscosities.<sup>11</sup>

### 2.3.8 Dynamic Mechanical Thermal Analysis (DMTA)

A Dynamic Mechanical Thermal Analyzer, Triton 2000 DMA from Triton Technology, was used in a single cantilever bending deformation mode to carry out Mechanical Dynamic Thermal Analysis (DMTA). DMA tests using material pockets to analyze powdered materials, as well as the procedure to perform such tests has been reported in the literature.<sup>12</sup> In this work, material pockets were used. A material pocket is a stainless-steel envelope that holds the sample. As stainless steel does not have any relaxation or phase transitions over the temperature range of the instrument, this is an ideal sample mounting material. To prepare the samples, the powder material was put inside the metal pocket. Then, the pocket was folded in half, closed to form a sandwich and placed in the DMTA. The samples were heated from -20 °C to 130 °C at a constant heating rate of 3 °C/min and frequency of 1 Hz. These tests allowed detecting the glass transition temperature ( $T_g$ ), given by the maximum peak in loss tangent,  $\tan \delta$ . This method was used to analyze the copolymers of the Chapter 4 (PET-*ran*-PLA) and the parent homopolymers that formed them.

The same procedure described above was used for measurements of the PET-*b*-Polyether copolymers and their respective parent homopolymers (Chapter 5).

Changing only the temperature range of the analysis, in this case was from -100 °C to 200 °C.

### 2.3.9 Differential Scanning Calorimetry (DSC)

The thermal behavior of the polymers was analyzed by differential scanning calorimetry (DSC), employing a DSC 8500 (PerkinElmer). The instrument was calibrated with indium and tin standards. The DSC scans were collected employing 4.5–5.5 mg samples at heating and cooling rates of 20 °C/min under a nitrogen flow of 20 mL/min.

PET, PLA, PET-*ran*-PLA, Polyethers and PET-*b*-Polyether samples were analyzed using a temperature range from -20 to 270 °C. On the other hand, cycles and linear polymers derived from HT and HF; as well as the triblock copolymers (PLLA-*b*-PHF-*b*-PLLA and PLLA-*b*-PHT-*b*-PLLA), were analyzed in a temperature range of -30–200 °C.

The peaks of temperatures of melting and of cold crystallization,  $T_m$  and  $T_{cc}$  respectively, as well as the latent heats ( $\Delta H_m$  and  $\Delta H_{cc}$ ) reported in the results section were taken from the second heating scans. Only in the case of Cyclic Oligoesters (Chapter 6), the values of  $T_m$  and  $\Delta H_m$ , were obtained from the first heating. The reported values of the crystallization temperature ( $T_c$ ) and its corresponding latent heat ( $\Delta H_c$ ), were taken from the cooling scans. The glass transition temperatures were determined with a heating rate of 40 °C/min after rapidly quenching the sample (ballistic cooling).

#### 2.3.9.1 Non Isothermal studies

The non-isothermal measurements for samples of PET, PLA, PET-*ran*-PLA, Polyethers and PET-*b*-Polyether were performed with the procedure described below:

- 1) Heat from 25 °C to 270 °C at 20 °C/min. (*First Heating*).
- 2) Hold for 3 min. at 270 °C (to erase the thermal history).
- 3) Cool from 270 °C to -20 °C at 20 °C/min. (*Cooling*).
- 4) Hold for 1 min. at -20 °C
- 5) Heat from 25 °C to 270 °C at 20 °C/min. (*Second Heating*).

To analyze the cyclic oligoesters and polyesters derived from hexamethylene terephthalate and hexamethylene furanoate, as well as the triblock copolymers (PLLA-*b*-PHF-*b*-PLLA and PLLA-*b*-PHT-*b*-PLLA), the procedure described was the same, changing only the maximum temperatures to be cooled and heated, at -30 °C and 200 °C, respectively.

#### 2.3.9.2 Isothermal studies

For PET and semi-crystalline PET-*ran*-PLA copolymers, isothermal measurements were performed using the procedure reported by Lorenzo et al.<sup>13</sup>

- 1) Hold for 3 min. at 270 °C (to erase the thermal history).
- 2) Quench from 270 °C to a chosen isothermal crystallization temperature ( $T_c$ ) at 60 °C/min (to avoid crystallization during cooling to  $T_c$ )
- 3) Isothermal crystallization until saturation.
- 4) Heat from  $T_c$  to 270 °C at 20 °C/min.

Because all the samples were able to crystallize on cooling, before starting with the isothermal measurements, the minimum crystallization temperature for each sample was determined. For this purpose, the sample was quenched from the melt until a chosen  $T_c$ , and it was immediately heated again until the melt. These steps were repeated until it was observed that the heating from the chosen  $T_c$  did not show any enthalpy of fusion, where the  $T_c$  that showed this characteristic in the subsequent heating was the minimum crystallization temperature.

To make the isothermal measurements of samples with two crystallization peaks, as is the case of copolymers of PET with polyether, the procedure described below was carried out:

First for the PET in the copolymer:

- 1) Hold for 3 min. at 270 °C (to erase the thermal history).
- 2) Quench from 270 °C to a chosen isothermal crystallization temperature ( $T_c$ ) at 60 °C/min.

- 3) Isothermal crystallization until saturation.
- 4) Heat from  $T_c$  to 270 °C at 20 °C/min.

Where the values of  $T_c$  correspond to values of crystallization temperatures of the PET present in the copolymer, this means that these measurements were made in a temperature range of 150 to 270 °C. Therefore, the polyether present in the copolymer during these measurements was in the melt state. This protocol is represented in Figure 2.2.

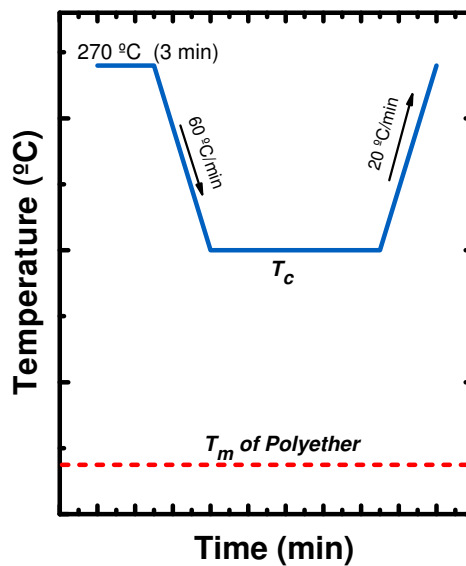


**Figure 2.2.** Schematic representation of the thermal protocol employed for isothermal crystallization experiments of PET in the copolymer.

On the other hand, for the isothermal studies of the polyether in the copolymer, the following was done:

- 1) Hold for 3 min. at 270 °C (to erase the thermal history).
- 2) Cool from 270 °C to a  $T_1$  [ $T_1 = (T_c \text{ of PET in the copolymer}) - 40 \text{ °C}$ ] at 10 °C/min.
- 3) Hold for 10 min. at  $T_1$  (to ensure that all the PET component in the copolymer is crystallized)
- 5) Quench from  $T_1$  to a  $T_{c1}$  at 60 °C/min.
- 6) Isothermal crystallization until saturation.
- 7) Heat from  $T_{c1}$  to  $T_2$  [ $T_2 = (T_m \text{ of Polyether in the copolymer}) + 30 \text{ °C}$ ] at 20 °C/min.
- 8) Hold for 3 min. at  $T_2$ .

- 9) Quench from  $T_2$  to a  $T_{c2}$  at 60 °C/min.
- 10) Isothermal crystallization until saturation.
- 11) Heat from  $T_{c2}$  to  $T_2$  at 20 °C/min.

For each copolymer the values of  $T_1$  and  $T_2$  are those corresponding to the PET and polyether present in the copolymer. The  $T_c$  is the crystallization temperature selected for the polyether. The procedure described above for the isothermal crystallization of Polyether is shown in Figure 2.3.

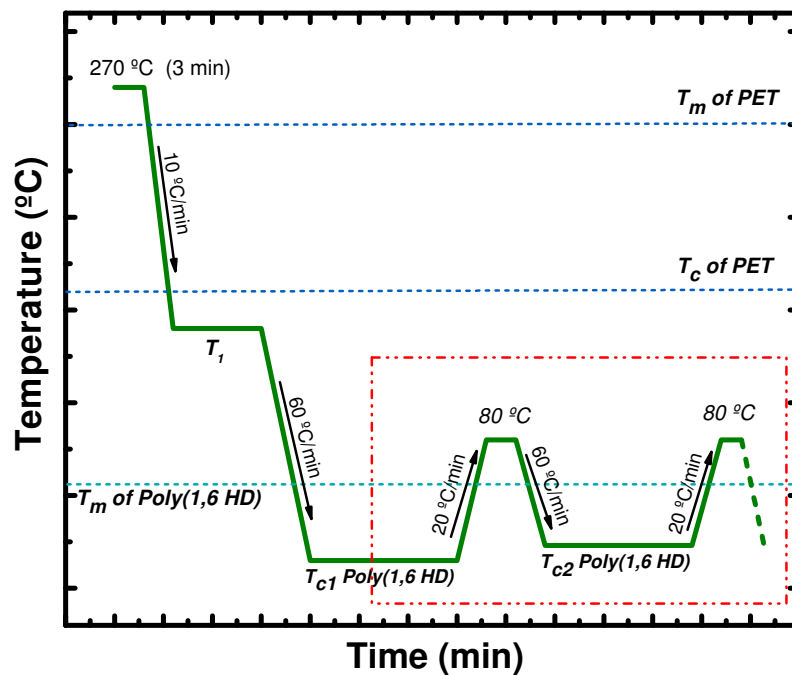


**Figure 2.3.** Schematic representation of the thermal protocol employed for isothermal crystallization experiments of Polyether in the copolymer.

From step 1 to 5 the sample is conditioned to a temperature where the PET is completely crystallized and then in step 6 the first isothermal crystallization of the polyether is measured. Therefore, the measurement of isothermal crystallization of the polyether starts in step 6 and continues in the successive steps. The latter is indicated in the red box in Figure 2.3.

To find the minimum crystallization temperature, for PET and polyether the same procedure described in previous paragraphs was followed, these measurements were again made in the temperature range, in the case of PET where the polyether is completely melted, and in the case of the polyether in the temperature range where the PET is completely crystallized.

### 2.3.10 Flash DSC

A Flash DSC 2+ (Mettler Toledo) is a measuring instrument for rapid differential scanning calorimetry. This equipment was used to measure the glass transition temperatures of some copolymers made from PET and Polyether. The flash DSC 2+ was equipped with Huber TC-100 intracooler. The cooling rate was -4000 K/s and the heating rate was 20 000 K/s.

Before each experiment, the sensor was conditioned and calibrated, after a flow of nitrogen gas was applied to provide an inert atmosphere, maintaining a flow rate of 80 mL/min. For a good contact between the sample and the sensor, the sample was subjected to several heating and cooling runs from 25 to 270 °C (rate of 1000 K/s). The samples were analyzed in a range of -90 to 270 °C.

The general procedure for measurements in every sample was:

- 1) Hold for 0.10 s at 270 °C (to erase the thermal history).
- 2) Cool from 270 °C to -90 °C at -4000 K/s (*Cooling*).
- 3) Hold for 0.10 s at -90 °C
- 4) Heat from -90 °C to 270 °C at 20 000 K/s (*Heating*).

The reported values of  $T_g$  were taken from the heating runs. The results were independent of sample mass. The STARe software was used to analyze the data.

### 2.3.11 Thermogravimetric Analysis (TGA)

Weight loss as a function of temperature was examined by a TGA Q500 (TA instrument) under nitrogen atmosphere. Samples of 5–10 mg were heated from 40 to 600 °C at a rate of 10 °C/min.

### 2.3.12 Simultaneous Wide-Angle and Small-Angle X-ray Scattering (SAXS/WAXS)

The samples in capillaries were examined under non-isothermal conditions by simultaneous WAXS/SAXS performed at beamline BL11-NCD at the ALBA Synchrotron

radiation facility (Barcelona, Spain). In a Linkam THMS600 hot stage coupled to a liquid nitrogen cooling system.

For PET-*ran*-PLA copolymers, the patterns were collected by cooling from 270 °C to 25 °C and subsequently heating from 25 °C to 270 °C. In the case of PET-*b*-Polyether samples the patterns were collected by cooling from 270 °C to -20 °C and subsequently heating from -20 °C to 270 °C. The polyether patterns were collected by cooling from 130 °C to -20 °C and subsequently heating from -20 °C to 130 °C. In the case of triblock copolymers of PLLA-*b*-PHF-*b*-PLLA and PLLA-*b*-PHT-*b*-PLLA, patterns were collected by cooling from 180 °C to -30 °C and subsequently heating from -30 °C to 180 °C. All the measurements were carried out at a rate of 20 °C/min.

The energy of X-ray source was 12.4 keV ( $\lambda=1.0$  Å). WAXS patterns were recorded using a Rayonix LX255-HS detector with an active area of 85 x 255 mm<sup>2</sup> (pixel size 40x40  $\mu\text{m}^2$ ), for PET-*ran*-PLA and PET-*b*-Polyether copolymers, the sample-to-detector distance employed was 154.69 mm with tilt angle of 29.23°, to analyze Polyethers, PHF, PHT, PLLA-*b*-PHF-*b*-PLLA and PLLA-*b*-PHT-*b*-PLLA the sample-to-detector distance employed was 196.14 mm with tilt angle of 30.33°. On the other hand the SAXS patterns were collected using Pilatus 1M detector (from Dectris), with an active area of 168.7 x 179.4 mm<sup>2</sup> (pixel size 172x172  $\mu\text{m}^2$ ), the sample-to-detector distance employed was 6730 mm with a tilt angle of 0°, for measurements of PET-*ran*-PLA and PET-*b*-Polyether samples. When Polyethers, PHF, PHT, PLLA-*b*-PHF-*b*-PLLA and PLLA-*b*-PHT-*b*-PLLA were analyzed the sample-to-detector distance employed was 6790 mm with tilt angle of 0°. The intensity profile was output as the plot of the scattering intensity vs the scattering vector. The scattering vector was calibrated using silver behenate (SAXS) and chromium (III) oxide (WAXS).

### **2.3.13 Polarized Light Optical Microscopy (PLOM) and Atomic Force Microscopy (AFM)**

This technique was employed to study the morphology of PET-*ran*-PLA copolyesters. PLOM was conducted with a Nikon Eclipse E600 POL microscope and a Nikon digital camera DXM200. AFM was performed with a  $\mu\text{TA}^{\text{TM}}$  2990 Micro-Thermal

Analyzer. In the case of PET and its copolymer derivatives of PET-*b*-polyether, the same equipment was used with METLER hot stage with temperature control. Topography images were obtained in contact mode with a current set point of  $-5$  nA. A feedback loop keeps the cantilever deflection constant at the selected set point value while scanning. This is done by applying a voltage to the Z-piezo that was kept constant at 50 V. V-shaped silicon nitride probes (Applied NanoStructures, Inc., Mountain View, CA, USA) with a cantilever length of  $200\ \mu\text{m}$  and a spring constant of  $0.046\ \text{N}\cdot\text{m}^{-1}$  were used. Depending on the size of the images (between  $3$  and  $50\ \mu\text{m}^2$ ), the scanning rates varied from  $3$  to  $50\ \mu\text{m}\cdot\text{s}^{-1}$ . The images were processed using the  $\mu\text{TALab}$  1.01 software package. The tilting effect in height values was corrected by applying a software leveling function, fitting a surface to the observed topography and then subtracting the height values of the fitted surface pixel by pixel from those of the initial image. In this study, a first order plane was used.

Copolymer film samples were prepared by solvent casting at room temperature from solutions prepared by dissolving a known weight of each copolymer in a fixed volume of HFIP ( $c = 25\ \text{mg/mL}$ ). All films were cast from  $20\ \mu\text{L}$  aliquots of the solutions onto glass substrates. After solvent evaporation, the films were melted at temperatures  $10\ ^\circ\text{C}$  above the corresponding melting point during 2 minutes, in order to erase any previous history. Subsequently, the samples were isothermally crystallized at the intermediate temperature between the glass transition ( $T_g$ ) and the melting point ( $T_m$ ) during 20 minutes. For PET and its copolymer derivatives of PET-*b*-polyether, different isothermal crystallization protocols were applied to the samples; at  $T_c$  (as measured by DSC) and at two different levels of undercooling ( $\Delta T=16\ ^\circ\text{C}$  and  $\Delta T=7\ ^\circ\text{C}$ , during 2 hours). After crystallization all samples were quenched to room temperature.

## 2.4 Theoretical Concepts of Thermal Characterization of Polymers

To interpret appropriately the behavior of polymers, it is important to measure their properties and know their structure, morphology and crystallization. But in addition, you must also know the concepts and theories can be applied to the experimental data in order to facilitate the understanding of the information provided by the different characterization techniques.

### 2.4.1 Crystallization in Polymers

The crystallization of polymers can be divided in: <sup>14,15</sup>

- (1) Primary Crystallization: this crystallization has two steps: nucleation (i.e. primary nucleation) and growth (i.e. secondary nucleation). Primary nucleation can occur by spontaneous aggregation of polymeric chain segments (homogenous nucleation) or by the attachment of chains into existing heterogeneities (heterogeneous nucleation). After primary nuclei are formed, these grow by secondary nucleation processes of chains that progressively attach to the existing nuclei. The process of secondary nucleation is also referred to as polymer crystal growth. When a polymer crystallizes from the melt, primary crystallization ends when spherulites impinged on one another. This typically occurs around the half-crystallization time of the entire overall crystallization process.
- (2) Secondary crystallization: In this stage, the crystallization process slows down and other processes can occur such as: the crystallization of interspherulitic material after spherulites impinged on one another, the crystallization of intraspherulitic material, in-filling of spherulites through the secondary nucleation of daughter lamellae (intra-spherulitic crystallization) and thickening of previously formed lamellae. Moreover, the refinement of existing crystals, through the removal of lattice distortions and a combination of thickening and re-crystallization are also possible.

Crystallization can occur only in a range of temperatures limited by the glass transition temperature ( $T_g$ ) and the melting temperature ( $T_m$ ). It is known that the nucleation rate ( $\dot{N}$ ) and the growth rate ( $G$ ) do not depend in the same way on the degree of supercooling. Normally, the maximum of  $\dot{N}$  appears at higher supercooling (see Figure 2.4), at these low temperatures the mobility of the polymer chains is reduced and this favors the nucleation rate generating a greater number of crystals of small size. On the other hand, at higher temperatures the growth rate is favored and fewer nuclei are formed resulting in larger spherulites. <sup>14,15</sup>

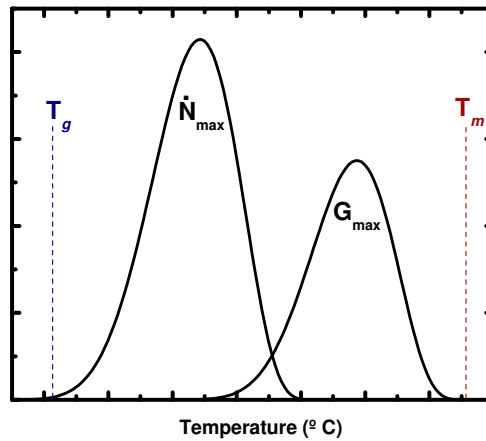


**Figure 2.4** Representation of the nucleation rate ( $\dot{N}$ ) and the crystalline growth rate ( $G$ ) as a function of temperature. (Figure modified) <sup>14</sup>

### 2.4.2 Crystal Growth

The spherulitic growth rate is governed mainly by supercooling, a general representation of the rate of crystal growth as a function of the crystallization temperature is shown in Figure 2.5, in the figure it is observed that the growth rate exhibits a bell shape curve with a maximum. The left hand side of the bell is dominated by diffusion (high supercooling), here the diffusion of the chains tends to be more difficult due to the closeness of the crystallization temperature with the glass transition temperature (increase of the viscosity of the melt). On the other hand, the right side of the bell is controlled by secondary nucleation, where the decrease of the crystallization temperature (increase in supercooling) thermodynamically favors spherulitic growth until diffusion becomes important and the maximum in the curve is reached. <sup>14,15</sup>

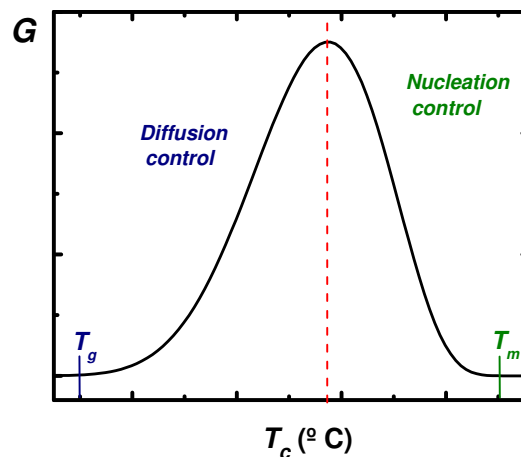


**Figure 2.5** Crystal growth rate ( $G$ ) as a function of the isothermal crystallization temperature.

When a polymer crystallizes from the melt, its transformation to the semi-crystalline state follows nucleation and growth processes that can be monitored by Differential Scanning Calorimetry (DSC) for instance. In this case, DSC can be used to determine overall crystallization rates (that include both nucleation and growth).

### 2.4.3 Structure and Morphology of Polymers

Semicrystalline polymers formed from the melt generally consist of lamellar crystals separated by amorphous regions (Figure 2.6). Axes of the chains are transverse to the faces of the lamellae, which normally are 100-500 Å in thickness; their lateral dimensions are much larger. The regions between the crystal lamellae, measuring 50-200 Å in thickness, exhibit properties approximating to those of the amorphous, non-crystalline polymer, although vestiges of order in the transitional regions are indicated by various measurements.<sup>16</sup>

Typically, the lengths of the polymer chains are many times greater than the lamellar thickness. Hence, each molecule must pass through the same or different lamellae many times. Chains normally fold and reenter the crystal. The manner in which this requirement is met is obviously of the foremost importance in regard to the molecular morphology of the crystal-amorphous interphase. It is well established, that besides folding, chains protrude from the crystalline lamellae and proceed into the interphase for a distance that is significantly beyond what may be regarded as the surface of the crystal.<sup>16</sup>

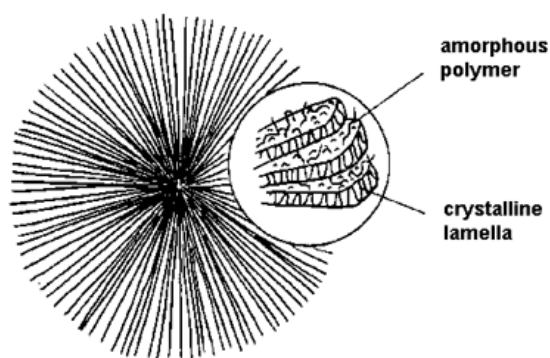


**Figure 2.6** Schematic representation of a spherulite composed from lamellae and amorphous regions.<sup>17</sup>

The semicrystalline polymers have a structure and morphology that can be analyzed by techniques such as: WAXS / SAXS (Wide-Angle X-ray Scattering and Small-Angle X-ray Scattering), PLOM (Polarized Light Optical Microscopy) and AFM (Atomic Force Microscopy) among others.

Crystalline solids consist of regular three-dimensional arrays of atoms. In polymers, the atoms are joined together by covalent bonds along the macromolecular chains. These chains pack together side-by side and lie along one particular direction in the crystals. It is possible to specify the structure of any crystalline solid by defining a regular pattern of atoms that is repeated in the structure. This repeat unit is known as the unit cell and the crystals are made up of stacks of these cells. In polymer crystals, the unit cells are made up of the repeating segments of the polymer chains packed together, often with several segments in each unit cell. The spatial arrangement of the atoms is controlled by the covalent bonding within a particular molecular segment, with the polymer segments held together in the crystals by secondary van der Waals forces or hydrogen bonding. Since the polymer chains lie along one particular direction in the cell and there is only relatively weak secondary bonding between molecules, the crystals have very anisotropic physical properties.<sup>18</sup>

When a crystal structure of a molecular compound is analyzed, both, the relative positions of the atoms on the molecular repeat units and the arrangement of these segments in the unit cell must be determined. This three-dimensional structure is normally determined using X-ray diffraction, involving measurement of the positions and intensities of all the diffraction maxima from a single crystal sample.

If a melt-crystallized polymer is prepared in the form of a thin film, either by sectioning a bulk sample or casting the film directly, and then viewed in an optical microscope using polarized light, a characteristic structure is normally obtained. It consists of entities known spherulites that show a characteristic maltese cross pattern in polarized light. A typical spherulite is shown in Figure 2.7. They are formed by nucleation at different points in the sample and then grow as spherical entities; the growth of the spherulites stops when impingement of adjacent spherulites occurs.<sup>18</sup> Figure 2.7 shows a spherulite viewed through crossed polars to reveal the typical

Maltese Cross extinction pattern. This pattern is caused by the ability of polymeric crystals to reorient the polarization direction of light as they are birefringent.

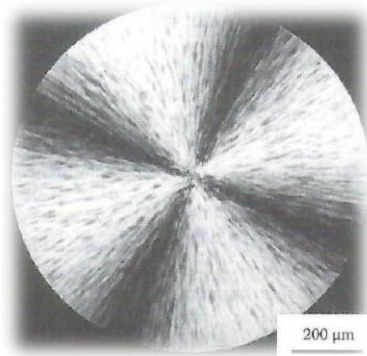


**Figure 2.7** Single spherulite growing in isotactic polystyrene.<sup>18</sup>

Spherulite size, number and morphology of each polymer depends on the chemical structure, molecular weight, crystallization conditions and the density of active nuclei present in the material.

#### 2.4.4 Polymer Crystallization Theories

In this work two theories of crystallization were used, the Avrami theory and the Lauritzen and Hoffman theory. The application of both theories to experimental data obtained is shown in chapters four and five of this thesis. A brief description of these theories is presented below:

##### 2.4.4.1 The Avrami Equation

From the theory of Avrami several useful equations for the study of the crystallization of polymers can be derived to understand crystallization kinetics and its relationship with morphology. Equation 2.1 is the general Avrami relationship, taking into consideration a constant nucleation rate and constant linear growth,<sup>19</sup> can be expressed as:<sup>14,20</sup>

$$1 - V_c(t - t_o) = \exp(-K(t - t_o)^n) \quad (2.1)$$

where  $t$  is the experimental time,  $t_o$  is the induction time before any crystallinity develops,  $V_c$  is the relative volumetric transformed fraction,  $n$  is the Avrami index and  $K$  is the overall crystallization rate constant (i.e., it includes contributions from both nucleation and growth). The Avrami theory usually provides a good fit of the experimental data at least in the conversion range up to the end of the primary crystallization, that is, up to the impingement of spherulites at approximately 50% conversion to the solid semicrystalline state.

The parameter  $n$  (Avrami index) in the equation 2.1, is composed of two terms:<sup>14</sup>

$$n = n_d + n_n \quad (2.2)$$

where  $n_d$  represents the dimensionality of the growing crystals, which should correspond to 1, 2 or 3 for one, two or three-dimensional entities. In the case of polymers, only 2 and 3 are commonly obtained as they represent axialites (two-dimensional lamellar aggregates) and spherulites (superstructural three-dimensional aggregates), respectively. The time dependence of the nucleation is represented by  $n_n$ . Its values should be 0 or 1, where 0 corresponds to purely instantaneous nucleation and 1 to purely sporadic nucleation. However, the nucleation may not be completely sporadic or completely instantaneous, a fact that may lead to non-integer contributions to the Avrami index. Table 2.1 summarizes the different values of  $n$  derived from the combinations of  $n_d$  and  $n_n$ .

**Table 2.1** Description of the different values of Avrami index ( $n$ ).

Avrami index ( $n$ )	$n_d$	$n_n$	Description ( $n_d/ n_n$ )
1	1	0	Rod/Instantaneous
2	1	1	Rod/Sporadic
2	2	0	Axialite/Instantaneous
3	2	1	Axialite/Sporadic
3	3	0	Spherulite/Instantaneous
4	3	1	Spherulite/Sporadic

The Avrami equation can be adjusted to adapt better to experimental polymer crystallization data, where the relative volume fraction ( $V_c$ ) is calculated as:<sup>14</sup>

$$V_c = \frac{W_c}{W_c + \frac{\rho_c}{\rho_a}(1 - W_c)} \quad (2.3)$$

where  $\rho_c$  and  $\rho_a$  are fully crystalline and fully amorphous polymer densities, respectively.  $W_c$  is the crystalline mass fraction in the sample and is calculated from the following equation:<sup>14</sup>

$$W_c = \frac{\Delta H(t)}{\Delta H_{total}} \quad (2.4)$$

where  $\Delta H(t)$  is the enthalpy variation as function of the time spent at a given crystallization temperature and  $\Delta H_{total}$  is the maximum enthalpy value reached at the end of the isothermal crystallization process.

The half-crystallization time ( $\tau_{50\%}$ ), i.e., the time needed to achieve 50% of the relative crystallinity of polymer; it is a parameter that can be used to express the crystallization rate and is calculated as follows:<sup>20</sup>

$$\tau_{50\%} = \left[ \frac{-\ln(1 - V_c)}{k} \right]^{1/n} = \left[ \frac{-\ln(0.5)}{k} \right]^{1/n} \quad (2.5)$$

In order to obtain all the previous parameters, equation 2.1 is linearized and represented as:<sup>14,20</sup>

$$\log[-\ln[1 - V_c(t - t_o)]] = \log k + n \log(t - t_o) \quad (2.6)$$

From this equation some plots can be obtained, where the experimental data were fitted to the Avrami equation using the Origin plug-in developed by Lorenzo *et al.*<sup>20</sup>. One of these graphs is the Figure 2.8(a), where  $\log[-\ln(1 - V_c)]$  is plotted versus  $\log(t - t_o)$ . If the crystallization kinetics follows the Avrami equation, then straight

line is obtained. The Figure 2.8(b) shows the curve of isothermal crystallization from experimental data vs. the curve obtained fitting the data to Avrami equation, and the values of  $\tau_{50\%}$  (theoretical) vs  $\tau_{50\%}$  (experimental). The figure 2.8 demonstrates the good fit provided by the Avrami equation to experimental data.

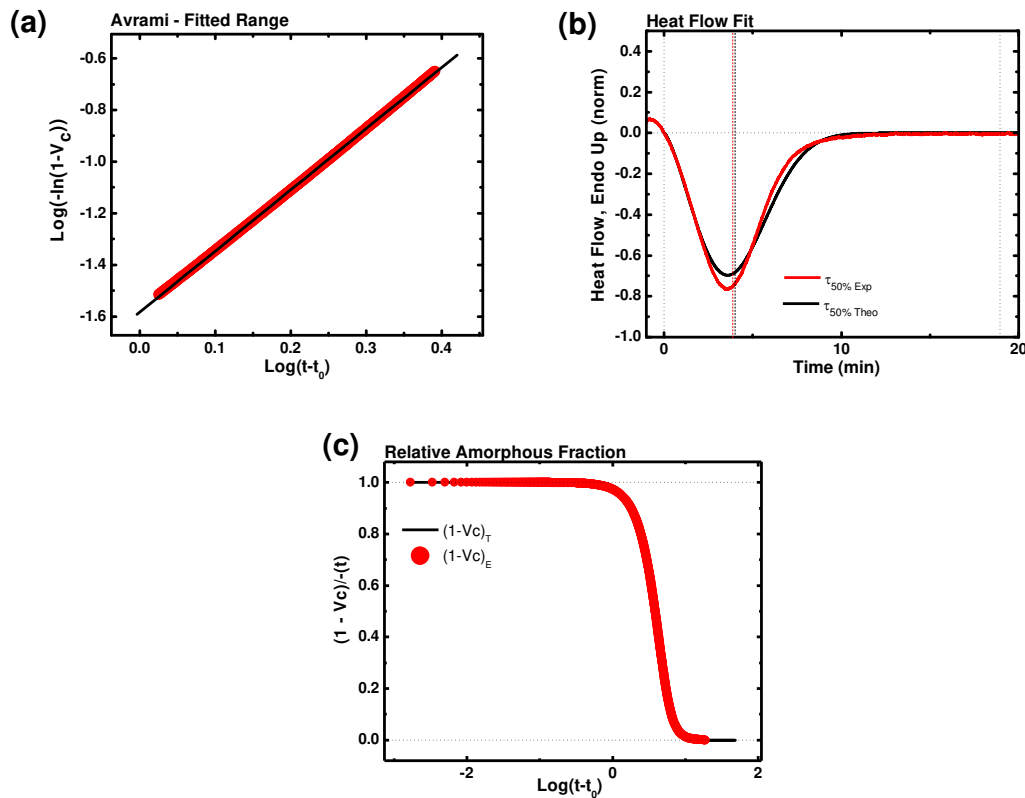


**Figure 2.8.** Plots obtained by Origin: (a) Representation of Avrami equation, (b) Isothermal curve and (c) Untransformed relative amorphous fraction  $(1-V_c)$ , as a function of time.

#### 2.4.4.2 Lauritzen and Hoffman Theory

According to classical crystallization theories, the temperature dependence of the linear spherulitic growth rate ( $G$ ) can be expressed by two exponential factors: the molecular transport term and the nucleation term. On the other hand, the isothermal crystallizations kinetics data can be analyzed with a variety of models in order to quantify the energy barriers associated with the nucleation and crystal growth, one of these models is the Lauritzen and Hoffman (LH) model, which has the advantage of providing analytical expressions for the growth rate as a function of supercooling.<sup>14</sup>

LH model is one of the few models that provides easy-to-use mathematical expressions that are capable of describing well the experimental data (even though the

physical meaning of some of the fitting parameters could be questionable) and therefore it is widely employed.

The LH model equation is expressed as: <sup>14,21</sup>

$$G(T) = G_0 \exp\left(\frac{-U^*}{R(T_C - T_\infty)}\right) \exp\left(\frac{-K_g}{T_C \Delta T f}\right) \quad (2.7)$$

where  $G_0$  is a growth rate constant,  $U^*$  the activation energy for the transport of the chains to the growing nuclei (1,500 cal/mol is generally used),  $R$  is the gas constant,  $T_C$  the isothermal crystallization temperature,  $T_\infty$  is the temperature at which chain mobility ceases and it is usually taken as  $(T_g - 30)$  (K).  $\Delta T$  is the supercooling defined as  $(T_m^0 - T_C)$  where  $T_m^0$  is the equilibrium melting point. The factor  $f$  is a temperature correction term equal to:  $2T_C/(T_C + T_m^0)$ ; and  $K_g$  is a secondary nucleation constant, which is proportional to the energy barrier for secondary nucleation. The parameter  $K_g$  is equal to  $K_g^t$ , which is proportional to the total energy barrier for the overall crystallization (i.e., for both nucleation and growth).

When the isothermal crystallization is determined by spherulitic growth experiments, the energy barrier determined by applying the LH model refers exclusively to secondary nucleation or crystal growth. Instead, when the inverse of half-crystallization time  $1/\tau_{50\%}$  values obtained from DSC isothermal overall crystallization kinetic data is considered, both primary nucleation and crystal growth are considered ( $G(T)$  in equation (2.7) is replaced by  $1/\tau_{50\%}$ ). Therefore, the energetic parameter obtained after applying any classical kinetic crystallization theory to DSC data will include contributions from both processes.

#### 2.4.5 Thermal Properties of Copolymers

Copolymer synthesis offers the ability to alter the properties of homopolymers in the desired direction by the introduction of an appropriately chosen second repeating unit. Properties, such as crystallinity, flexibility,  $T_m$ ,  $T_g$  among other, can be altered by forming copolymers. The values and sometimes even the directions of the

property alteration differ depending on whether random, alternating, or block copolymer are prepared.

In this sense, the crystallinity of a random copolymer is lower than that of either of the respective homopolymers (i.e., the homopolymers corresponding to the two different units) because of the decrease in structural regularity. The melting temperature of any crystalline material formed is usually lower than that of either homopolymer. The  $T_g$  value will be in between those for the two homopolymers.

On the other hand, alternating copolymers have a regular structure, and their crystallinity may not be significantly affected unless one of the repeating units contains rigid, bulky, or excessively flexible chain segments. The  $T_m$  and  $T_g$  values of an alternating copolymer are in between the corresponding values for the homopolymers.

In the case of block copolymers, they show the properties (e.g., crystallinity,  $T_m$ ,  $T_g$ ) present in the corresponding homopolymers as long as the block lengths are not too short. This behavior is typical since A blocks from different polymer molecules aggregate with each other and separately, B blocks from different polymer molecules aggregate with each other. This offers the ability to combine the properties of two very different polymers into the one block copolymer. The properties of block copolymers will be highly dependent on the possible micro-phase segregation of each block. The segregation strength controls the structure and morphology of block copolymers. It is defined by the product of the Flory-Huggins interaction parameter and the polymerization degree. Therefore, phase segregation is more probable when the two comonomers are chemically dissimilar and when the molecular weight is high.

## 2.4 References

- (1) Coady, D. J.; Fukushima, K.; Horn, H. W.; Rice, J. E.; Hedrick, J. L. Catalytic Insights into Acid/Base Conjugates: Highly Selective Bifunctional Catalysts for the Ring-Opening Polymerization of Lactide. *Chemical Communications* **2011**, 47 (11), 3105–3107. <https://doi.org/10.1039/c0cc03987j>.
- (2) Jehanno, C.; flores, I.; Dove, A. P.; Muller, A.; Ruipérez, F.; Sardon, H. Organocatalysed Depolymerisation of PET in a Fully Sustainable Cycle Using Thermally Stable Protic Ionic Salt. *Green Chemistry* **2018**. <https://doi.org/10.1039/C7GC03396F>.
- (3) Gubbels, E.; Jasinska-Walc, L.; Koning, C. E. Synthesis and Characterization of Novel Renewable Polyesters Based on 2,5-Furandicarboxylic Acid and 2,3-Butanediol. *Journal of Polymer Science Part A: Polymer Chemistry* **2013**, 51 (4), 890–898. <https://doi.org/10.1002/pola.26446>.
- (4) Basterretxea, A.; Gabirondo, E.; Jehanno, C.; Zhu, H.; Flores, I.; Müller, A. J.; Etxeberria, A.; Mecerreyes, D.; Coulembier, O.; Sardon, H. Polyether Synthesis by Bulk Self-Condensation of Diols Catalyzed by Non-Eutectic Acid–Base Organocatalysts. *ACS Sustainable Chemistry & Engineering* **2019**, 7 (4), 4103–4111. <https://doi.org/10.1021/acssuschemeng.8b05609>.
- (5) Bossion, A.; Heifferon, K. V.; Meabe, L.; Zivic, N.; Taton, D.; Hedrick, J. L.; Long, T. E.; Sardon, H. Opportunities for Organocatalysis in Polymer Synthesis via Step-Growth Methods. *Progress in Polymer Science* **2019**, 90, 164–210. <https://doi.org/10.1016/j.progpolymsci.2018.11.003>.
- (6) Ben-Haida, A.; Conzatti, L.; Hodge, P.; Manzini, B.; Stagnaro, P. An Introduction to Entropically-Driven Ring-Opening Polymerizations. *Macromolecular Symposia* **2010**, 297 (1), 6–17. <https://doi.org/10.1002/masy.200900109>.
- (7) Hodge, P. Entropically Driven Ring-Opening Polymerization of Strainless Organic Macrocycles. *Chemical Reviews* **2014**, 114 (4), 2278–2312. <https://doi.org/10.1021/cr400222p>.
- (8) Hodge, P. Recycling of Condensation Polymers via Ring-Chain Equilibria: RECYCLING VIA RING-CHAIN EQUILIBRIA. *Polymers for Advanced Technologies* **2015**, 26 (7), 797–803. <https://doi.org/10.1002/pat.3469>.

- 
- (9) Sugihara, S.; Toshima, K.; Matsumura, S. New Strategy for Enzymatic Synthesis of High-Molecular-Weight Poly(Butylene Succinate) via Cyclic Oligomers. *Macromolecular Rapid Communications* **2006**, *27* (3), 203–207. <https://doi.org/10.1002/marc.200500723>.
- (10) Donovan, A. R.; Moad, G. A Novel Method for Determination of Polyester End-Groups by NMR Spectroscopy. *Polymer* **2005**, *46* (14), 5005–5011. <https://doi.org/10.1016/j.polymer.2005.04.032>.
- (11) Krevelen, D. W. van; Nijenhuis, K. te. *Properties of Polymers: Their Correlation with Chemical Structure: Their Numerical Estimation and Prediction from Additive Group Contributions*, 4th, completely rev. ed ed.; Elsevier: Amsterdam, 2009.
- (12) Royall, P. G.; Huang, C.; Tang, S. J.; Duncan, J.; Van-de-Velde, G.; Brown, M. B. The Development of DMA for the Detection of Amorphous Content in Pharmaceutical Powdered Materials. *International Journal of Pharmaceutics* **2005**, *301* (1–2), 181–191. <https://doi.org/10.1016/j.ijpharm.2005.05.015>.
- (13) Lorenzo, A. T.; Arnal, M. L.; Albuerne, J.; Müller, A. J. DSC Isothermal Polymer Crystallization Kinetics Measurements and the Use of the Avrami Equation to Fit the Data: Guidelines to Avoid Common Problems. *Polymer Testing* **2007**, *26* (2), 222–231. <https://doi.org/10.1016/j.polymertesting.2006.10.005>.
- (14) Müller, A. J.; Michell, R. M.; Lorenzo, A. T. Isothermal Crystallization Kinetics of Polymers. In *Polymer Morphology*; Guo, Q., Ed.; John Wiley & Sons, Inc: Hoboken, NJ, USA, 2016; pp 181–203. <https://doi.org/10.1002/9781118892756.ch11>.
- (15) Lorenzo, A. T.; Müller, A. J. Estimation of the Nucleation and Crystal Growth Contributions to the Overall Crystallization Energy Barrier. *Journal of Polymer Science Part B: Polymer Physics* **2008**, *46* (14), 1478–1487. <https://doi.org/10.1002/polb.21483>.
- (16) Flory, P. J.; Yoon, D. Y.; Dill, K. A. The Interphase in Lamellar Semicrystalline Polymers. *Macromolecules* **1984**, *17* (4), 862–868. <https://doi.org/10.1021/ma00134a055>.
- (17) Spherulites and optical properties <https://www.doitpoms.ac.uk/tlplib/polymers/spherulites.php> (accessed Feb 22, 2019).

- (18) Yong, R. J.; Lovell, P. A. Chapter 17 The Crystalline State. In *Introduction to Polymers*; CRC press, 2011; p 688.
- (19) Avrami, M. Granulation, Phase Change, and Microstructure Kinetics of Phase Change. III. *The Journal of Chemical Physics* **1941**, *9* (2), 177–184. <https://doi.org/10.1063/1.1750872>.
- (20) Lorenzo, A. T.; Arnal, M. L.; Albuerne, J.; Müller, A. J. DSC Isothermal Polymer Crystallization Kinetics Measurements and the Use of the Avrami Equation to Fit the Data: Guidelines to Avoid Common Problems. *Polymer Testing* **2007**, *26* (2), 222–231. <https://doi.org/10.1016/j.polymertesting.2006.10.005>.
- (21) Lauritzen, J. I.; Hoffman, J. D. Theory of Formation of Polymer Crystals with Folded Chains in Dilute Solution. *Journal of Research of the National Bureau of Standards Section A: Physics and Chemistry* **1960**, *64A* (1), 73. <https://doi.org/10.6028/jres.064A.007>.

---

# Chapter 3

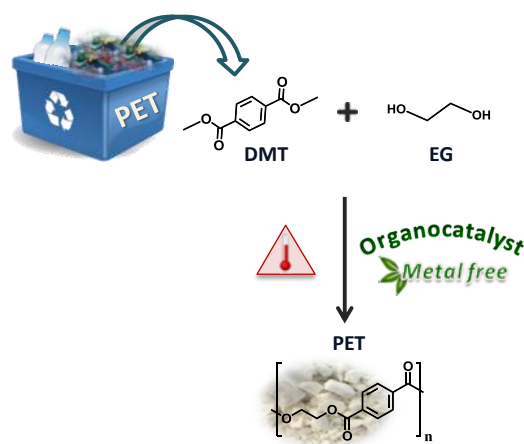
---

## *Screening of Different Organocatalysts for the Sustainable Synthesis of PET*

3.1 Abstract.....	51
3.2 Introduction.....	52
3.3 Results and Discussion.....	54
3.3.1 Screening of Different Catalysts for PET Synthesis.....	54
3.3.2 Optimized Polymerization of PET.....	60
3.4 Conclusions.....	64
3.5 References.....	65

### 3.1 Abstract

Industrially, poly(ethylene terephthalate) (PET) is produced using organometallic catalysts which have shown excellent ability to promote the polymerization at elevated temperatures. However, the catalysts remain permanently in the fabricated item because their removal is very difficult both from a technical and economical point of view. In this work, several organocatalysts have been evaluated as alternative to the industrially applied organometallic catalysts for the bulk polymerization of PET from dimethyl terephthalate (DMT) and ethylene glycol (EG) at high temperatures. The effectiveness of the organic catalysts in PET synthesis is evaluated by SEC, DSC, TGA,  $^1\text{H}$  NMR and FTIR spectroscopy. After screening various organocatalyst families, the results demonstrate that the catalytic activity of 1,8-Diazabicyclo[5.4.0]undec-7-ene: benzoic acid salt (DBU:BA) is competitive in comparison with the conventional organometallic-based catalyst employed in PET synthesis. This ionic salt combines the excellent catalytic ability of organic compounds with the thermal stability of metal-based catalysts, resisting degradation up to  $>250\text{ }^\circ\text{C}$  which is close to the industrial polymerization temperature of PET. Moreover, the dimerization degree of ethylene glycol in the presence of DBU:BA is significantly reduced in comparison to organometallic catalysts which enhances the thermal properties of the synthesized PET using DBU:BA. Thus, organic salts have shown to be promising catalyst for the bulk polymerization of PET and in addition may be a viable option to obtain metal-free PET.



Flores, I.; Demarteau, J.; Müller, A. J.; Etxeberria, A.; Irusta, L.; Bergman, F.; Koning, C.; Sardon, H. Screening of Different Organocatalysts for the Sustainable Synthesis of PET. *Eur. Polym. J.* **2018**, *104*, 170–17.

## 3.2 Introduction

The large development of polymers in various fields has resulted in decades of their application for several uses in our daily life. Poly(ethylene terephthalate) (PET) is one of the most relevant polymers in the world, because of its high durability, excellent mechanical properties, transparency, recyclability and good processability. Moreover, this versatile material keeps a good balance of useful functional properties and low cost. As a consequence of the above, PET has a wide demand in the manufacture of products like textiles, packaging films, packaging products and beverage bottles. This has led to an increase in the production of this polyester, e.g., the Global PET production reached a capacity of 27.8 million tons in 2015.<sup>1</sup>

PET can be prepared by a) the polyesterification of terephthalic acid with ethylene glycol or b) by transesterification of dimethyl terephthalate with ethylene glycol, or c) direct polycondensation of bis (hydroxyethyl) terephthalate or by d) entropically driven ROP of oligoesters.<sup>2-5</sup> The use of catalysts and harsh polymerization conditions, such as high vacuum in combination with high temperatures, are a key factor in producing polymers with high molecular weights and good mechanical properties.

The majority of catalysts used in the polymerization of PET are organometallic such as antimony, germanium, titanium and other compounds, where antimony trioxide is currently the most employed in the production of PET.<sup>2,3,6-11</sup> In spite of having high catalytic activities to synthesize high molecular weight PET, they also have some disadvantages such as their non-biodegradability, in some cases their high toxicity to the human health and environment and, most importantly, the difficulty to be removed from the resulting polymer.<sup>12</sup> Consequently, as the catalyst remains in the fabricated item, during the secondary melt fabrication process or mechanical recycling, side reactions may happen leading to significant property deterioration. Therefore, frequently mechanically-recycled PET generally ends up in secondary products.<sup>13,14</sup>

In the last decade, extensive attempts have been carried out to reduce the toxicity of organometallic catalysts using more benign catalyst systems. In this regard, the utilization of fully organic compounds to promote step growth polymerizations is gaining a lot of attention. While organocatalysis has demonstrated its utility in ring-

opening, anionic, zwitterionic, step growth and group-transfer polymerizations, the use of organocatalysis in polymerization reactions such as stepgrowth polymerizations remain less explored in comparison to more traditional metal-based polymerizations. A key reason for shifting to organocatalysts in polymerization reactions is their ability to be effectively removed from resultant polymers.<sup>15–20</sup>

Several organocatalysts have shown to be effective to catalyze transesterification reactions such as 1,8-Diazabicyclo[5.4.0]undec-7-ene (DBU) or 1,5,7-triazabicyclo[4.4.0]dec-5-ene (TBD). Although these catalysts have been reported in the literature for the depolymerization of PET,<sup>21–26</sup> the use of TBD and DBU in the polymerization of PET has not been described.

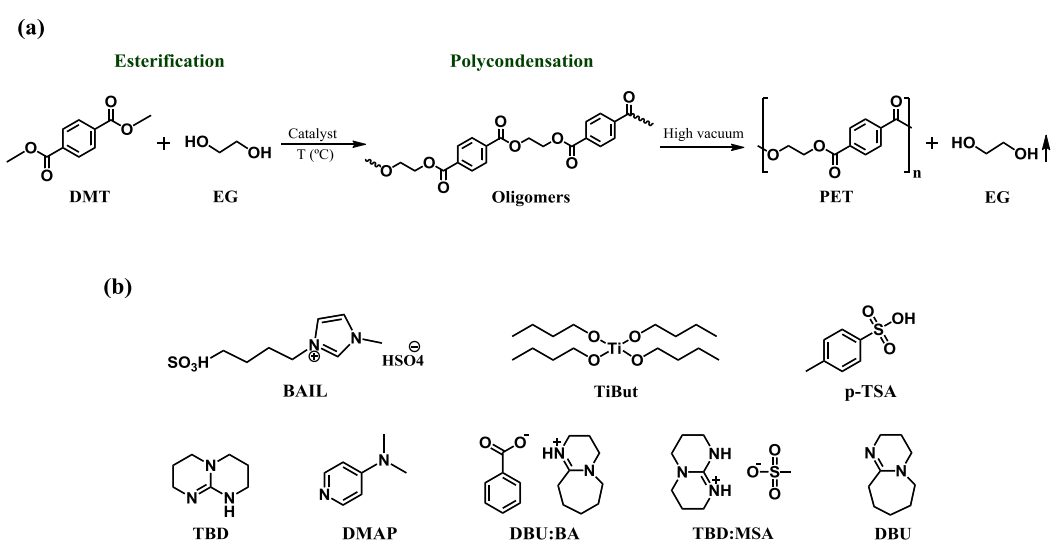
One of the main limitations for the utilization of organocatalysts is their poor thermal stability at temperatures that would be practical for PET polymerization and therefore full or partial thermal degradation of the catalyst may occur during the polymerization.<sup>27</sup> Recently, ionic compounds have emerged as an alternative for carrying out polymerizations at high temperatures. For instance, Peruch et al. prepared some DMAP-based protic ionic compounds to mediate the ROP of L-LA at elevated temperatures.<sup>28</sup> Fradet et al. and Sardon et al. utilized some Brønsted acid ionic liquid to promote polyesterification and ring opening polymerizations, respectively.<sup>29,30</sup> The ability of 1,5,7-triazabicyclo [4.4.0]dec-5-ene (TBD): methane sulfonic acid (MSA) protic ionic compound to catalyze PET depolymerization.<sup>31</sup> was recently demonstrated.

In this chapter, several organocatalysts have been evaluated as alternatives to organometal-based catalyst for the bulk polymerization of poly (ethylene terephthalate) from dimethyl terephthalate (DMT) and ethylene glycol (EG) at high temperatures. Not only conventional organocatalyst such as DMAP, DBU, TBD or p-TSA have been screened but also some ionic compounds, such as 1-(4-sulfobutyl)-3-methylimidazolium hydrogen sulfate (Brønsted acid ionic liquid) or DBU:BA and TBD:MSA protic ionic compounds, have been investigated and compared to titanium tetrabutoxide catalyst. This organometallic catalyst is widely used in the polymerization of Poly (butylene terephthalate) (PBT), but also has been studied as an alternative to reduce environmental impact in the synthesis of PET replacing the highly toxic antimony based catalysts.<sup>6</sup> The effectiveness of the organic catalysts in PET synthesis is evaluated by SEC, DSC, TGA, <sup>1</sup>H NMR and FTIR spectroscopy.

### 3.3 Results and Discussion

#### 3.3.1 Screening of Different Catalysts for PET Synthesis

Organocatalyzed Polymerization of PET was carried out after mixing dimethyl terephthalate (DMT) (1 equiv., 0.015 mol, 3.0 g) and ethylene glycol (EG) (1.4 equiv., 0.021, 1.3 g) in a tubular Schlenk flask in the presence of 5 mol% of catalyst (Scheme 3.1a). The polymerization was performed in two steps. In the first step, the transesterification between dimethyl terephthalate and ethylene glycol was performed at 200 °C for 24 h obtaining oligomers. During the second step, the temperature was maintained and solid state polymerization was continued applying high vacuum and removing the excess of ethylene glycol and methanol, in order to obtain high molecular weights. Different organic catalysts, such as organic acids, p-toluenesulfonic acid (p-TSA) and 1-(4-sulfobutyl)-3-methylimidazolium hydrogen sulfate (BAIL) and commercial organic bases such as diazabicyclo-[5.4.0]undec-7-ene (DBU) or 1,5,7-triazabicyclo[4.4.0]dec-5-ene (TBD) and nucleophilic activator such as 4-Dimethylaminopyridine (DMAP) and some ionic salts such as DBU:BA and TBD:MSA, have been screened in the polymerization (Scheme 3.1b). All these catalysts have been successfully used in transesterification reactions of cyclic esters,<sup>32–34</sup> and therefore have been selected for the synthesis of PET. For comparative purposes TiBut was also included as polymerization control along with an uncatalyzed reaction.



**Scheme 3.1** (a) Organocatalyzed synthesis of PET from DMT and EG (the main condensate is CH<sub>3</sub>OH in step 1 and excess EG in the step 2) and (b) Catalysts employed in the Screening Process.

The polymerization was monitored by FTIR as shown in Figure 3.1 where the infrared spectra of the samples obtained at different reaction times using TBD:MSA (1:1) as catalyst are shown. As can be seen the absorbance of the band centered at  $1430\text{ cm}^{-1}$ ,<sup>35</sup> assigned to the asymmetric bending ( $\delta_{as}$ ) of the methyl groups attached to terephthalate units decreases its intensity with the reaction and a new band assigned to the symmetric bending ( $\delta_{si}$ ) of the methylene groups attached to terephthalate units appears at  $1340\text{ cm}^{-1}$  confirming the advance in the polymerization.

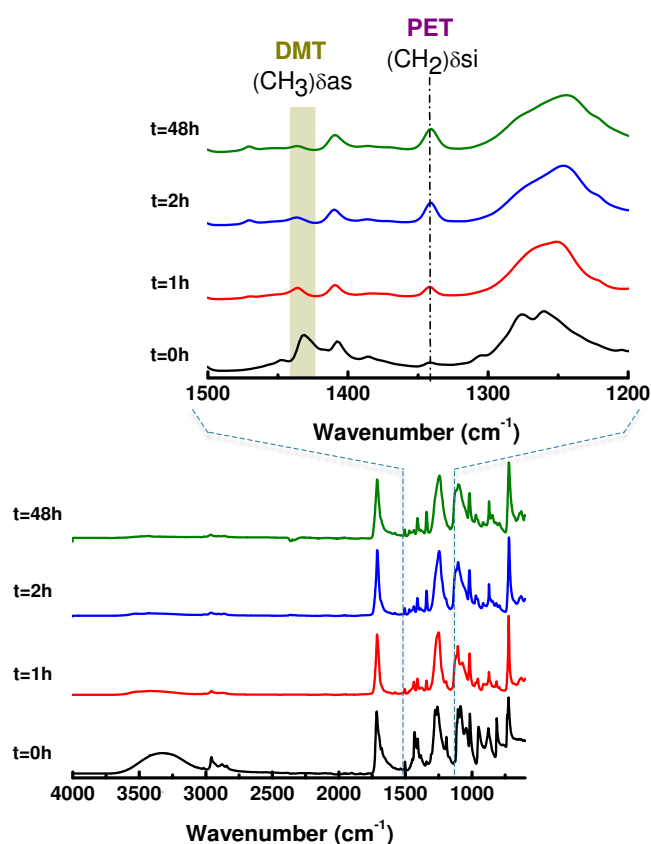


**Figure 3.1.** Infrared Spectra showing the evolution of PET formation at  $200\text{ }^{\circ}\text{C}$  employing TBD:MSA as catalyst.

The monomer conversion was determined using the relative area of this band centered at  $1430\text{ cm}^{-1}$  vs. time for each polymerization using various catalysts. The reaction with TiBut and the uncatalyzed reaction were included as reference to evaluate the effectiveness of organic catalysts (Figure 3.2). It was observed that the rate of polymerization was found to be highly catalyst dependent. Without a catalyst, monomer conversion was less than 50% after 48 h and full conversion was not achieved. Conversely, DBU, DMAP and the salt of DBU:BA exhibited conversions

exceeding 90% after 5 h of reaction time, obtaining a conversion of >98% after 48 h. This was a very favorable result compared to the conversions obtained from TiBut (83% after 5 h and >98% after 48 h). TBD also catalyzed the PET polymerization (84% after 5 h), with final conversion >97% after 48 h. The TBD:MSA (1:1) catalyst yields a conversion of 53% after 5 h and the final conversion was slightly lower (93% after 48 h). Organic acids (p-TSA and BAIL) were found ineffective and gave rather low final conversions of 52 and 38%, respectively, after 48 h. These results demonstrate that the catalyst plays an important role in the polymerization and that the polymerization rate seems to be higher when using DBU, DMAP and DBU:BA (1:1) rather than TiBut to prepare PET.

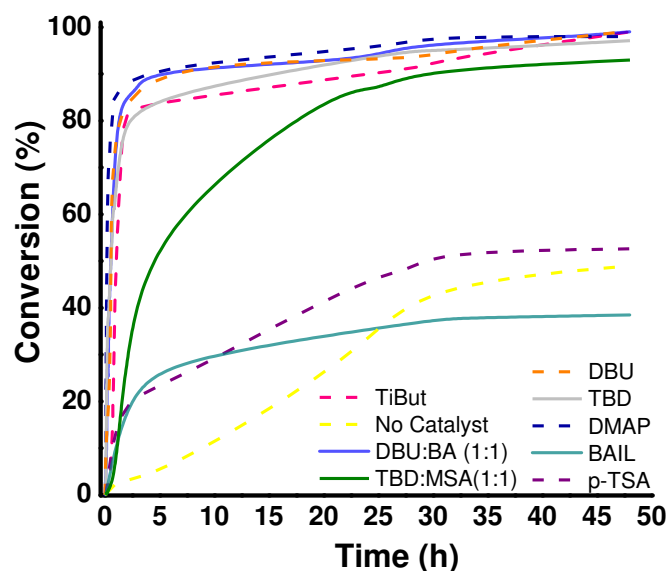


**Figure 3.2.** Conversion to PET at 200 °C monitored by FTIR.

To further confirm the PET synthesis,  $^1\text{H}$  NMR was performed. Figure 3.3 shows  $^1\text{H}$  NMR of both monomers, *viz.* ethylene glycol (EG) and dimethyl terephthalate (DMT), and the  $^1\text{H}$  NMR of PET after 48 h of synthesis using DBU:BA catalyst.<sup>36</sup> As expected, when the polymerization was completed, the characteristic peaks of the ethylene glycol and DMT had disappeared while new peaks assigned to PET at 8.12 ppm (Ar-CH, peak 1) and 4.78 (COO-CH<sub>2</sub>-CH<sub>2</sub>-OCO, peak 2) appeared, confirming the PET synthesis. Together with the signals associated with PET some low intensity signals attributed to dimerization of EG during the polymerization at 4.63 ppm and 4.10 ppm (COO-CH<sub>2</sub>-CH<sub>2</sub>-O-CH<sub>2</sub>-CH<sub>2</sub>-OCO dimer) and some others attributed to PET chain ends at

4.63 ppm and 4.18 ppm (COO-CH<sub>2</sub>-CH<sub>2</sub>-OH) and 4.02 ppm for the CH<sub>3</sub> (COO-CH<sub>3</sub>) were observed.<sup>36,37</sup>

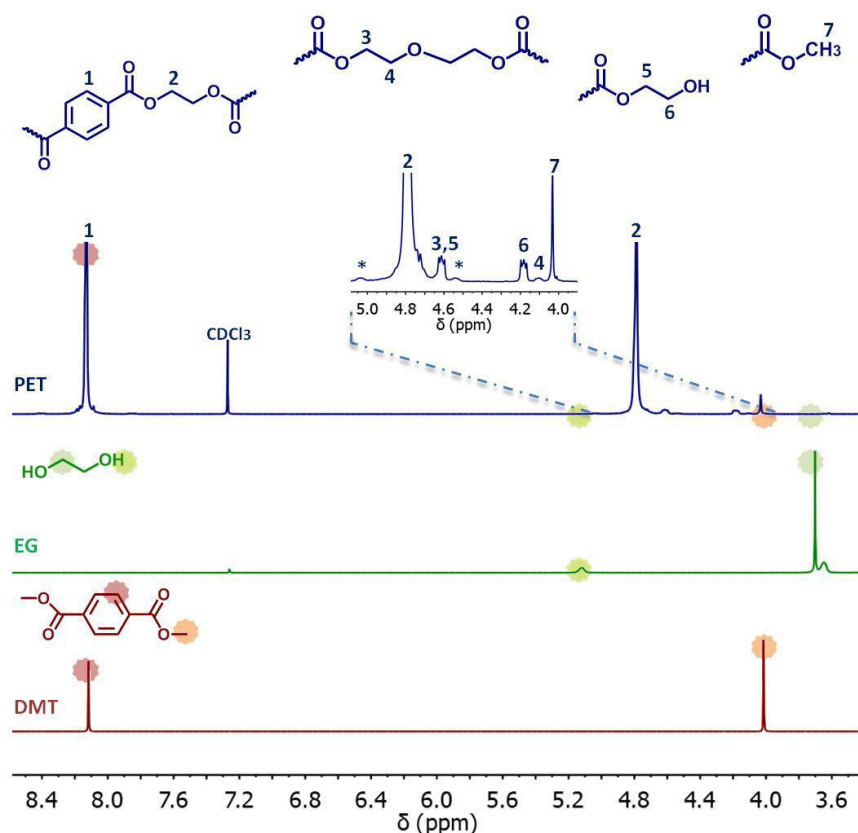


**Figure 3.3.** <sup>1</sup>H NMR spectrum of a synthesized PET at 200 °C using DBU:BA as catalyst, recorded in CDCl<sub>3</sub>/TFA; <sup>13</sup>C satellites (\*).

To more precisely compare catalytic activities, kinetic studies were performed for each catalyst. The reaction proceeded with overall second order kinetics with respect to the monomers  $-d[M]/dt=k[DMT][EG]$ , as confirmed by the linear relationship between time,  $t$  and  $1/(1-p)$ , where  $p$  is the fraction of monomer converted to polymer. Rate constants were obtained for each catalyst (Figure 3.4). The organocatalysts DMAP, TBD and DBU:BA (1:1) showed higher rate constants than the reference metal catalyst.

The high catalytic activity of organocatalysts for PET polymerization is clearly demonstrated (Figure 3.4). Nevertheless, the molecular weights calculated by NMR (Annex A) and measured by SEC (Table 3.1) show that the final molecular weights obtained with organic catalysts are lower than those obtained with the reference metal catalyst after 48 h, at least at 200 °C, while the conversions were similar (Table 3.1). A factor that may influence the molecular weight is the reaction temperature. For

PET synthesis, it has been reported that temperatures above the melting temperature of PET (>250 °C) are required to obtain decent molecular weights.<sup>38,39</sup> With this in mind, it was investigated if using higher temperatures the polymers could reach higher molecular weights.

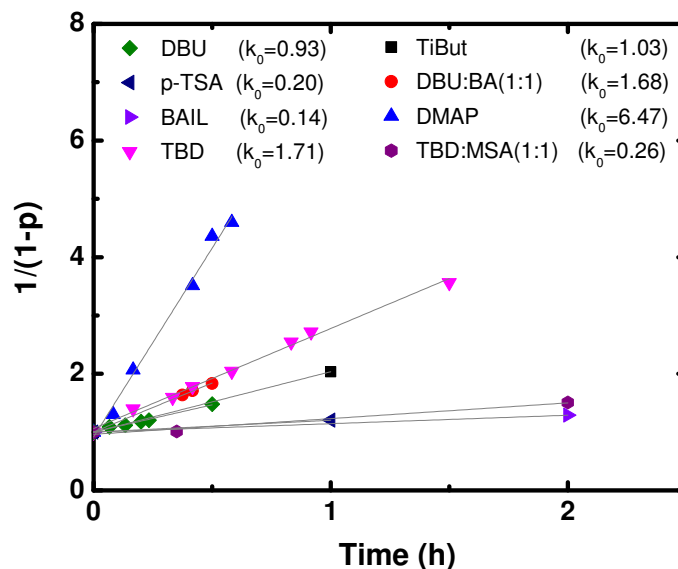


**Figure 3.4.** Linear plot of  $1/(1-p)$  as a function of time for the catalyzed polymerization (at 200 °C).  $K_0$  was determined from the slope.

**Table 3.1** Molecular weights, dispersities and degrees of conversion of synthesized PETs.

Catalyst	$M_{n,NMR}^a$ (kDa)	$M_{n,SEC}^b$ (kDa)	$M_{w,SEC}^b$ (kDa)	$\mathcal{D}^b$	Conversion <sup>c</sup> (%)
None	1.8	1.3	2.3	1.8	49
TiBut	7.2	2.0	4.5	2.2	> 98
DBU:BA (1:1)	5.2	1.5	3.1	2.0	> 98
DMAP	3.8	1.4	2.9	2.1	97
TBD	4.2	1.1	3.1	2.8	97
DBU	4	1.2	3.2	2.5	> 98
p-TSA	0.5	0.7	4.3	5.7	52
BAIL	0.6	0.3	2.7	8.3	38
TBD:MSA (1:1)	1.6	1.1	2.3	2.1	93

PET obtained at 200 °C.

<sup>a</sup>Calculated by NMR.

<sup>b</sup>Measured by SEC in HFIP against PMMA standards.

<sup>c</sup>Final conversion determined by FTIR.

It is well known that one of the limitations of organocatalysts is their stability at high temperatures.<sup>27</sup> As seen in Figure 3.5, when running the polymerization in the presence of TBD, DMAP and DBU, the polymers were colored. Ionic compounds could

offer an interesting alternative due to their strong internal ionic interactions, which increases their thermal stability.<sup>33,40</sup> In this sense, a higher thermal stability for the two ionic compounds DBU:BA and TBD:MSA was assumed rather than DBU, TBD or DMAP, which is confirmed by the absence of color after polymerization in the presence of these two catalysts (Figure 3.5).



**Figure 3.5.** Pictures of PET synthesized with different catalysts.

To further confirm the thermal stability and the absence of volatiles of these two ionic compounds during polymerization, TGA analysis was performed for all catalysts. In Figure 3.6, it can be observed that DBU:BA and TBD:MSA are stable above 200 °C, and therefore they were selected to continue with the screening and to perform the PET polymerization at higher temperatures in order to try to increase the molecular weights.

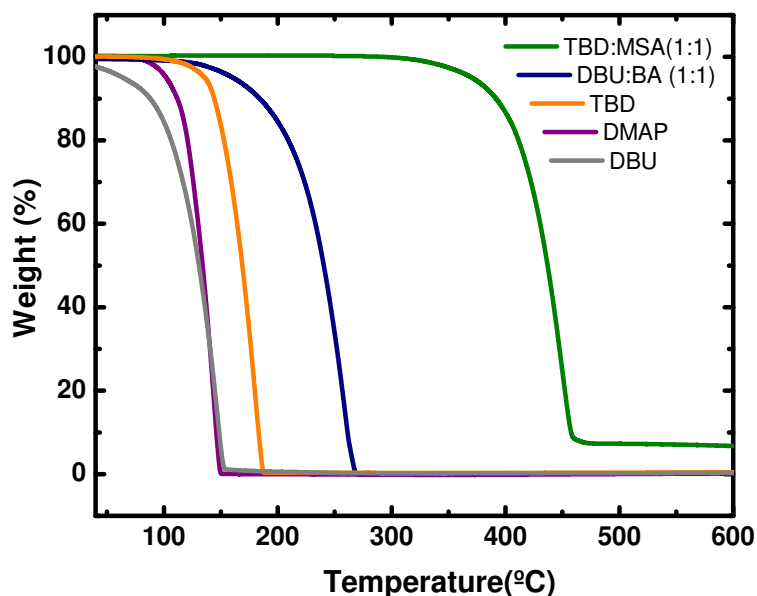


**Figure 3.6.** TGA of organocatalysts employed.

### 3.3.2 Optimized Polymerization of PET

After screening some polymerization conditions, the best results in terms of molecular weight and conversion were obtained running the polymerization in two steps, mimicking the strategy used in the commercial synthesis of PET. In the first step dimethyl terephthalate (DMT) (1 equiv., 0.015 mol, 3.0 g) and ethylene glycol (EG) (1.4 equiv., 0.021 mol, 1.3 g) were mixed in a tubular Schlenk flask in the presence of 5 mol% of catalyst (Scheme 3.1a) and the polymerization was run for 1 h at 250 °C. In this first step PET oligomers were obtained by transesterification. In the second step, high vacuum was applied for 4 h to push the conversion to higher values and to increase the molecular weight by polycondensation. Using these polymerization conditions the two most stable catalysts DBU:BA and TBD:MSA were tested for PET polymerization and compared with TiBut. Although the catalyst TBD:MSA (1:1) gives lower conversion and catalytic activity than DBU:BA (1:1), it is thermally more stable at high temperatures and therefore this compound was also investigated in the polymerization.

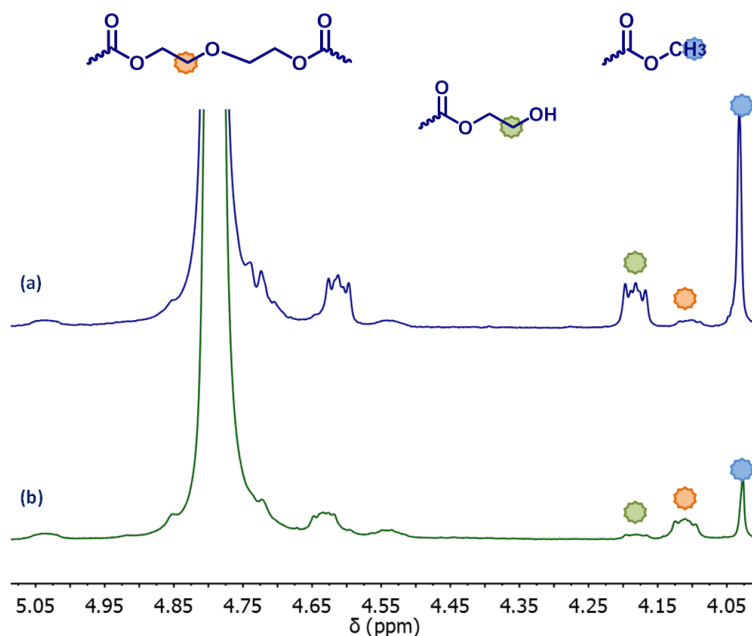


**Figure 3.7.** <sup>1</sup>H NMR spectra of (a) PET synthesized at 200°C and (b) PET synthesized at 250 °C.

As in the previous case NMR measurements were performed to confirm the polymerization and to calculate the molecular weight of PET. Figure 3.7 shows a <sup>1</sup>H

NMR spectrum of the PET sample synthesized with DBU:BA (1:1) as catalyst at 200 °C (a) versus the PET spectrum synthesized at 250 °C using the same catalyst (b). It can be seen that the intensity of the signal corresponding to the protons of the end groups (4.18 ppm for the COO-CH<sub>2</sub>-CH<sub>2</sub>-OH and 4.02 ppm for COO-CH<sub>3</sub>), decreases when PET is synthesized at 250 °C (b), which indicates that the chains formed are longer and therefore the number of end groups decreases. Also, the molecular weight of PET synthesized at 250 °C is higher than that of PET synthesized at 200 °C.

**Table 3.2** Molecular weight and thermal properties of synthesized PETs.

Catalyst	$M_n$ NMR <sup>a</sup> (kDa)	Dimerization <sup>a</sup> (%)	$M_n$ SEC <sup>b</sup> (kDa)	$\mathcal{D}_{SEC}$ <sup>b</sup>	<i>I.V.</i> <sup>b</sup> (dl/g)	$T_m$ <sup>c</sup> (°C)	$T_g$ <sup>c</sup> (°C)	$\Delta H_m$ <sup>c</sup> (J/g)
At 200 °C								
DBU:BA(1:1)	5.2	0.4	1.5	2	---	250.6	67	49
At 250 °C								
TiBut	12	7.6	16.8	4.9	0.35	236.1	70	35
TBD:MSA (1:1)	6.7	0.5	7.3	2.3	0.26	257.7	80	60
DBU:BA(1:1)	18.6	1.4	10.7	2.9	0.26	252	77	52

<sup>a</sup>Calculated by NMR. The dimerization is the degree of ethylene glycol that dimerized before polymerization.

<sup>b</sup>Measured by SEC in HFIP.

<sup>c</sup>Determined by DSC.

From the NMR spectrum the molecular weight was calculated. The results are shown in Table 3.2. In all cases, the molecular weight was greater when increasing the temperature. With the TBD:MSA catalyst, the obtained NMR-based molecular weight ( $M_n=6.7$  kDa) is lower than that obtained with TiBut ( $M_n=12$  kDa). Conversely, the DBU:BA catalyst exhibits a molecular weight calculated by NMR ( $M_n=18.6$  kDa) greater than that obtained with TiBut. To further analyze molecular weights, SEC analysis was performed using hexafluoroisopropanol as eluent. The SEC-based number average molecular weight obtained with the TiBut catalyst (16.8 KDa) is higher than that obtained with DBU:BA (10.7 KDa). Nevertheless, the  $\mathcal{D}$  value obtained with the TiBut catalyst is quite high (4.9) for a polycondensation reaction (Theoretical value without branching being  $\mathcal{D}\approx 2$ ). This rather high  $\mathcal{D}$  could be attributed to some side reactions during PET polymerization in the presence of TiBut. It was reported that TiBut catalyst possess strong affinity to coordinate with PET. Pilatti et al. assumed that this interaction leads to branching, called “quasi networks”, and consequently to an apparent increase of the molecular weight in the melt state which confirms also why

the internal viscosity is higher in the case of TiBut.<sup>41</sup> This phenomenon could explain not only the high  $\bar{M}_w$  obtained using TiBut but also the lower molecular weight calculated by NMR for TiBut. In addition, it was found that in the presence of TiBut the dimerization rate was much higher (7%) than using both organocatalysts. As a consequence, the high content of diethylene glycol units in the polymers can act as a defect in the crystallization of the material and decrease the values in  $T_m$  and  $\Delta H_m$ .<sup>42–44</sup> Basically, any chemical group (different than the PET repeating unit) that is inserted within the PET chains will interrupt the regularity of the PET macromolecules, constituting defects along the chains. Such defects will limit the extent of crystallinity and also the lamellar thickness that the crystals can achieve. As the lamellar thickness is directly proportional to the melting point, the thinner the crystals the lower the  $T_m$  values.

In order to minimize the catalyst loading and to be competitive with industrial PET preparation polymerizations were performed using 100 times less catalyst. As expected the molecular weights (Annex A, Table A.1) were lower as the catalyst loading was reduced. In spite of the decrease in the molecular weight, it should be noted that the results for DBU:BA and TiBut were comparable even at low catalyst loading.

Another important feature strongly determined by the quality of the produced PET is its thermal behavior. Hence, the thermal properties of the different produced PET samples were compared by DSC (Figure 3.8) and TGA (Annex A). Table 3.2 shows the  $T_m$ ,  $T_g$  and  $\Delta H_m$  values of the PET synthesized using the three different catalysts (TiBut, TBD:MSA and DBU:BA) and the two different applied polymerization temperatures.

It was found that the higher the polymerization temperature the higher the molecular weight of PET and consequently the higher the  $T_m$  and  $\Delta H_m$  in all cases. Nevertheless, in the case of PET obtained using TiBut catalyst, for which the molecular weight is the highest, it was found that both the  $T_m$  and the  $\Delta H_m$  were relatively low. This effect was also observed by Pilati et al.<sup>41</sup> when using TiBut catalyst. They concluded that the observed branching could interrupt the linear crystallizable sequences of PET and accordingly the  $T_m$  and the heat of fusion (and concomitantly the

degree of crystallinity). The melting point of the PET obtained with the TBD:MSA (1:1) catalyst of 257.7 °C is close to the melting point of commercial PET grades.

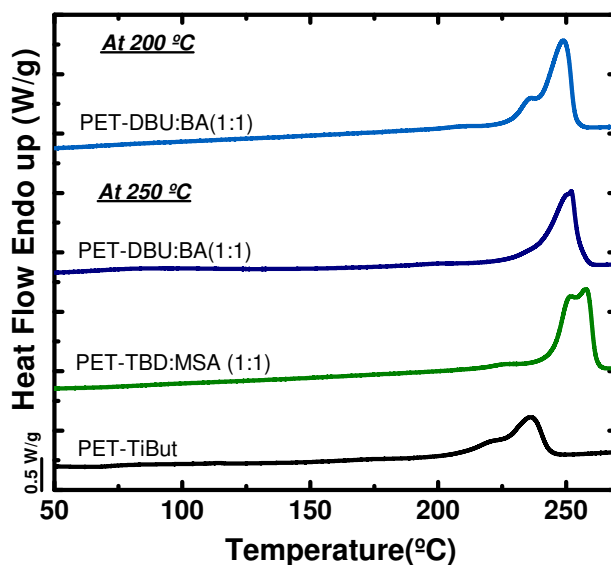


**Figure 3.8.** DSC second heating scans for PET samples obtained with optimized reaction conditions using different catalyst systems (250 °C).

To further confirm the similar thermal characteristics of PET synthesized with organocatalysis, the thermal stability of the polymers was analyzed by TGA (Annex A). These TGA results show that the thermal stability of the PET materials synthesized with organic catalysts is similar to that of the PET synthesized with a metal-based catalyst.<sup>10</sup>

### 3.4 Conclusions

In conclusion, the ability to synthesize PET using organocatalysis has been demonstrated. The protic ionic salt diazabicyclo-[5.4.0]undec-7-ene (DBU): benzoic acid (BA) was found to efficiently activate the polymerization of dimethyl terephthalate and ethylene glycol, while also producing high molecular weights, comparable to organometallic catalyst. Moreover, it was found that although the molecular weight in the presence of DBU:BA ( $M_n=11$  kDa) was slightly lower than using TiBut ( $M_n=16$  kDa), the  $\bar{D}$  obtained was greater in the case of TiBut than DBU:BA (4.9 and 2.9 respectively). It was demonstrated that this high  $\bar{D}$  could be attributed to the higher ability of TiBut to coordinate with PET. This interaction leads to branching and consequently to an apparent increase of the molecular weight. Besides affecting the  $\bar{D}$ , the branching considerably affected the crystallization of PET reducing the  $T_m$  and  $\Delta H_m$  of PET. On the other hand, the degree of dimerization can also influence the value of  $T_m$ . In this sense, it was found that in the presence of DBU:BA catalyst PET with higher crystallinity was produced.

The data obtained in this study reveal that organic ionic compounds have potential for synthesizing metal free PET due to their thermal stability and catalytic activity, and may be a step towards the recyclability of PET due to the absence of metal contaminations.

### 3.5 References

- (1) Plastics insight. Global PET Resin Production Capacity.
- (2) Yin, M.; Li, C.; Guan, G.; Zhang, D.; Xiao, Y. Novel Catalysts Based on Titanium Dioxide/Silicon Dioxide for Poly(Ethylene Terephthalate). *Journal of Applied Polymer Science* **2010**, *115* (4), 2470–2478. <https://doi.org/10.1002/app.30949>.
- (3) Xiao, B.; Wang, L.; Mei, R.; Wang, G. PET Synthesis in the Presence of New Aluminum Catalysts. *Journal of Polymer Research* **2011**, *18* (6), 2221–2227. <https://doi.org/10.1007/s10965-011-9634-2>.
- (4) Švec, P.; Hubená, P.; Růžičková, Z.; Holubová, J.; Pouzar, M.; Merna, J.; Růžička, A. Poly(Ethylene Terephthalate) Synthesis Catalysed by Chelated Sn, Zn and Mg Complexes: Sn-, Zn- and Mg-Based Catalysts for PET Synthesis. *Applied Organometallic Chemistry* **2016**, *30* (1), 20–25. <https://doi.org/10.1002/aoc.3393>.
- (5) Habaue, S.; Takahashi, Y.; Hosogoe, Y.; Yamashita, H.; Kajiwara, M. Poly (Ethylene Terephthalate) Synthesis with Catalysts Derived from Chrysotile Asbestos. *Natural Science* **2010**, *02* (06), 557–562. <https://doi.org/10.4236/ns.2010.26070>.
- (6) Finelli, L.; Lorenzetti, C.; Messori, M.; Sisti, L.; Vannini, M. Comparison between Titanium Tetrabutoxide and a New Commercial Titanium Dioxide Based Catalyst Used for the Synthesis of Poly (Ethylene Terephthalate). *Journal of applied polymer science* **2004**, *92* (3), 1887–1892. <https://doi.org/10.1002/app.20171>.
- (7) Xiao, B.; Wang, L. P.; Mei, R. H.; Wang, G. Y. Ethylene Glycol Aluminum as a Novel Catalyst for the Synthesis of Poly(Ethylene Terephthalate). *Chinese Chemical Letters* **2011**, *22* (6), 741–744. <https://doi.org/10.1016/j.cclet.2010.12.036>.
- (8) Ahmadnian, F.; Reichert, K.-H. Kinetic Studies of Polyethylene Terephthalate Synthesis with Titanium-Based Catalyst. *Macromolecular Symposia* **2007**, *259* (1), 188–196. <https://doi.org/10.1002/masy.200751322>.
- (9) Son, T. W.; Son, H. S.; Kim, W. K.; Lee, D. W.; Kim, K. I.; Jeong, J. H. Preparation of PET Using Homogeneous Catalysts. II. Effect of BHPP, NPG and PD in Sb<sub>2</sub>O<sub>3</sub> Glycol Solution Catalysts. *Fibers and Polymers* **2000**, *1* (1), 6–11. <https://doi.org/10.1007/BF02874870>.
- (10) Ahmadnian, F.; Velasquez, F.; Reichert, K.-H. Screening of Different Titanium (IV) Catalysts in the Synthesis of Poly(Ethylene Terephthalate). *Macromolecular*

- Reaction Engineering* **2008**, *2* (6), 513–521.  
<https://doi.org/10.1002/mren.200800021>.
- (11) Rosu, R. F.; Shanks, R. A.; Bhattacharya, S. N. Synthesis and Characterisation of Branched Poly(Ethylene Terephthalate). *Polym. Int.* **1997**, *42* (3), 267–275.  
[https://doi.org/10.1002/\(SICI\)1097-0126\(199703\)42:3<267::AID-PI712>3.0.CO;2-Z](https://doi.org/10.1002/(SICI)1097-0126(199703)42:3<267::AID-PI712>3.0.CO;2-Z).
- (12) Shaikh, I. R. Organocatalysis: Key Trends in Green Synthetic Chemistry, Challenges, Scope towards Heterogenization, and Importance from Research and Industrial Point of View. *Journal of Catalysts* **2014**, *2014*, 1–35.  
<https://doi.org/10.1155/2014/402860>.
- (13) National Association for PET Container Resources. *Report on Postconsumer PET Container Recycling Activity in 2016*; 2017.
- (14) Avadanei, M.; Drobotă, M.; Stoica, I.; Rusu, E.; Barboiu, V. Surface Morphology and Amide Concentration Depth Profile of Aminolyzed Poly(Ethylene Terephthalate) Films. *Journal of Polymer Science Part A: Polymer Chemistry* **2010**, *48* (23), 5456–5467. <https://doi.org/10.1002/pola.24354>.
- (15) Ottou, W. N.; Sardon, H.; Mecerreyes, D.; Vignolle, J.; Taton, D. Update and Challenges in Organo-Mediated Polymerization Reactions. *Progress in Polymer Science* **2016**, *56*, 64–115. <https://doi.org/10.1016/j.progpolymsci.2015.12.001>.
- (16) Zhang, X.; Fevre, M.; Jones, G. O.; Waymouth, R. M. Catalysis as an Enabling Science for Sustainable Polymers. *Chemical Reviews* **2018**, *118* (2), 839–885.  
<https://doi.org/10.1021/acs.chemrev.7b00329>.
- (17) Sardon, H.; Pascual, A.; Mecerreyes, D.; Taton, D.; Cramail, H.; Hedrick, J. L. Synthesis of Polyurethanes Using Organocatalysis: A Perspective. *Macromolecules* **2015**, *48* (10), 3153–3165. <https://doi.org/10.1021/acs.macromol.5b00384>.
- (18) MacMillan, D. W. C. The Advent and Development of Organocatalysis. *Nature* **2008**, *455* (7211), 304–308. <https://doi.org/10.1038/nature07367>.
- (19) Bertelsen, S.; Jørgensen, K. A. Organocatalysis—after the Gold Rush. *Chemical Society Reviews* **2009**, *38* (8), 2178. <https://doi.org/10.1039/b903816g>.
- (20) Dalko, P. I.; Moisan, L. In the Golden Age of Organocatalysis. *Angewandte Chemie International Edition* **2004**, *43* (39), 5138–5175.  
<https://doi.org/10.1002/anie.200400650>.

- (21) Jin, L.; Wu, Y.; Kim, C.; Xue, Y. Theoretical Study on the Aminolysis of Ester Catalyzed by TBD: Hydrogen Bonding or Covalent Bonding of the Catalyst? *Journal of Molecular Structure: THEOCHEM* **2010**, *942*, 137–144. <https://doi.org/10.1016/j.theochem.2009.12.012>.
- (22) Fukushima, K.; Coulembier, O.; Lecuyer, J. M.; Almegren, H. A.; Alabdulrahman, A. M.; Alsewailem, F. D.; Mcneil, M. A.; Dubois, P.; Waymouth, R. M.; Horn, H. W.; et al. Organocatalytic Depolymerization of Poly(Ethylene Terephthalate). *Journal of Polymer Science Part A: Polymer Chemistry* **2011**, *49* (5), 1273–1281. <https://doi.org/10.1002/pola.24551>.
- (23) Fukushima, K.; Coady, D. J.; Jones, G. O.; Almegren, H. A.; Alabdulrahman, A. M.; Alsewailem, F. D.; Horn, H. W.; Rice, J. E.; Hedrick, J. L. Unexpected Efficiency of Cyclic Amidine Catalysts in Depolymerizing Poly(Ethylene Terephthalate). *Journal of Polymer Science Part A: Polymer Chemistry* **2013**, *51* (7), 1606–1611. <https://doi.org/10.1002/pola.26530>.
- (24) Fukushima, K.; Lecuyer, J. M.; Wei, D. S.; Horn, H. W.; Jones, G. O.; Al-Megren, H. A.; Alabdulrahman, A. M.; Alsewailem, F. D.; McNeil, M. A.; Rice, J. E.; et al. Advanced Chemical Recycling of Poly(Ethylene Terephthalate) through Organocatalytic Aminolysis. *Polym. Chem.* **2013**, *4* (5), 1610–1616. <https://doi.org/10.1039/C2PY20793A>.
- (25) Horn, H. W.; Jones, G. O.; Wei, D. S.; Fukushima, K.; Lecuyer, J. M.; Coady, D. J.; Hedrick, J. L.; Rice, J. E. Mechanisms of Organocatalytic Amidation and Trans-Esterification of Aromatic Esters As a Model for the Depolymerization of Poly(Ethylene) Terephthalate. *The Journal of Physical Chemistry A* **2012**, *116* (51), 12389–12398. <https://doi.org/10.1021/jp304212y>.
- (26) Simona Nica; Anamaria Hanganu; Anca Tanase; Monica Duldner; STELA IANCU; Constantin Draghici; Petru Ivan Filip; Emeric Bartha. Glycolytic Depolymerization of Polyethylene Terephthalate (PET) Wastes Organic vs. Metal-Catalysis. *REV. CHIM. BUCHAREST* **2015**, *66* (8), 1105–1111.
- (27) Mezzasalma, L.; Dove, A. P.; Coulembier, O. Organocatalytic Ring-Opening Polymerization of L-Lactide in Bulk: A Long Standing Challenge. *European Polymer Journal* **2017**, *95*, 628–634. <https://doi.org/10.1016/j.eurpolymj.2017.05.013>.

- (28) Kadota, J.; Pavlović, D.; Hirano, H.; Okada, A.; Agari, Y.; Bibal, B.; Deffieux, A.; Peruch, F. Controlled Bulk Polymerization of L-Lactide and Lactones by Dual Activation with Organo-Catalytic Systems. *RSC Advances* **2014**, *4* (28), 14725. <https://doi.org/10.1039/c4ra01239a>.
- (29) Zhang, S.; Lemaire, V.; Féret, A.; Lefebvre, H.; Tessier, M.; Fradet, A. Synthesis of Linear and Hyperbranched Polyesters in Brønsted Acid Ionic Liquids. *Polym. Chem.* **2013**, *4* (5), 1538–1545. <https://doi.org/10.1039/C2PY20888A>.
- (30) Basterretxea, A.; Gabirondo, E.; Sanchez-Sanchez, A.; Etxeberria, A.; Coulembier, O.; Mecerreyes, D.; Sardon, H. Synthesis and Characterization of Poly ( $\epsilon$ -Caprolactam-Co-Lactide) Polyesteramides Using Brønsted Acid or Brønsted Base Organocatalyst. *European Polymer Journal* **2017**, *95*, 650–659. <https://doi.org/10.1016/j.eurpolymj.2017.05.023>.
- (31) Jehanno, C.; Flores, I.; Dove, A. P.; Müller, A. J.; Ruipérez, F.; Sardon, H. Organocatalysed Depolymerisation of PET in a Fully Sustainable Cycle Using Thermally Stable Protic Ionic Salt. *Green Chemistry* **2018**, *20* (6), 1205–1212. <https://doi.org/10.1039/C7GC03396F>.
- (32) Simón, L.; Goodman, J. M. The Mechanism of TBD-Catalyzed Ring-Opening Polymerization of Cyclic Esters. *The Journal of Organic Chemistry* **2007**, *72* (25), 9656–9662. <https://doi.org/10.1021/jo702088c>.
- (33) García-Argüelles, S.; García, C.; Serrano, M. C.; Gutiérrez, M. C.; Ferrer, M. L.; del Monte, F. Near-to-Eutectic Mixtures as Bifunctional Catalysts in the Low-Temperature-Ring-Opening-Polymerization of  $\epsilon$ -Caprolactone. *Green Chem.* **2015**, *17* (6), 3632–3643. <https://doi.org/10.1039/C5GC00348B>.
- (34) Llevot, A.; Grau, E.; Carlotti, S.; Grelier, S.; Cramail, H. Renewable (Semi)Aromatic Polyesters from Symmetrical Vanillin-Based Dimers. *Polym. Chem.* **2015**, *6* (33), 6058–6066. <https://doi.org/10.1039/C5PY00824G>.
- (35) Pretsch, E.; Clerc, T.; Seibl, J.; Simon, W. *Tablas Para La Determinación Estructural Por Métodos Espectroscópicos*, Segunda edición española.; Springer-Verlag Ibérica: España, 1998.
- (36) Pospiech, D.; Korwitz, A.; Komber, H.; Voigt, D.; Jehnichen, D.; Muller, J.; Janke, A.; Hoffmann, T.; Kretzschmar, B. In Situ Synthesis of Poly(Ethylene Terephthalate)/Layered Silicate Nanocomposites by Polycondensation. *High*

- Performance Polymers* **2007**, *19* (5–6), 565–580.  
<https://doi.org/10.1177/0954008307081199>.
- (37) de Ilarduya, A. M.; Muñoz-Guerra, S. Chemical Structure and Microstructure of Poly(Alkylene Terephthalate)s, Their Copolyesters, and Their Blends as Studied by NMR. *Macromolecular Chemistry and Physics* **2014**, *215* (22), 2138–2160.  
<https://doi.org/10.1002/macp.201400239>.
- (38) Shin, J.; Lee, Y.; Park, S. Optimization of the Pre-Polymerization Step of Polyethylene Terephthalate (PET) Production in a Semi-Batch Reactor. *Chemical Engineering Journal* **1999**, *75* (1), 47–55. [https://doi.org/10.1016/S1385-8947\(98\)00097-7](https://doi.org/10.1016/S1385-8947(98)00097-7).
- (39) Di Serio, M.; Tesser, R.; Ferrara, A.; Santacesaria, E. Heterogeneous Basic Catalysts for the Transesterification and the Polycondensation Reactions in PET Production from DMT. *Journal of Molecular Catalysis A: Chemical* **2004**, *212* (1–2), 251–257.  
<https://doi.org/10.1016/j.molcata.2003.10.032>.
- (40) Miran, M. S.; Kinoshita, H.; Yasuda, T.; Susan, Md. A. B. H.; Watanabe, M. Physicochemical Properties Determined by  $\Delta pK_a$  for Protic Ionic Liquids Based on an Organic Super-Strong Base with Various Brønsted Acids. *Physical Chemistry Chemical Physics* **2012**, *14* (15), 5178. <https://doi.org/10.1039/c2cp00007e>.
- (41) Pilati, F.; Toselli, M.; Messori, M.; Manzoni, C.; Turturro, A.; Gattiglia, E. G. On Specific Factors Affecting the Crystallization of PET: The Role of Carboxyl Terminal Groups and Residual Catalysts on the Crystallization Rate. *Polymer* **1997**, *38* (17), 4469–4476.
- (42) Chen, J.-W.; Chen, L.-W. The Kinetics of Diethylene Glycol Formation in the Preparation of Polyethylene Terephthalate. *Journal of Polymer Science Part A: Polymer Chemistry* **1998**, *36*, 3073–3080.
- (43) Chen, J.-W.; Chen, L.-W. The Kinetics of Diethylene Glycol Formation from Bis-Hydroxyethyl Terephthalate with Antimony Catalyst in the Preparation of PET. *Journal of Polymer Science Part A: Polymer Chemistry* **1999**, *37*, 1797–1803.
- (44) Chen, L.-W.; Chen, J.-W. Kinetics of Diethylene Glycol Formation from Bis-Hydroxyethyl Terephthalate with Proton Catalyst in the Preparation of Poly(Ethylene Terephthalate). *Journal of Applied Polymer Science* **2000**, *75* (10), 1221–1228.

---

# Chapter 4

---

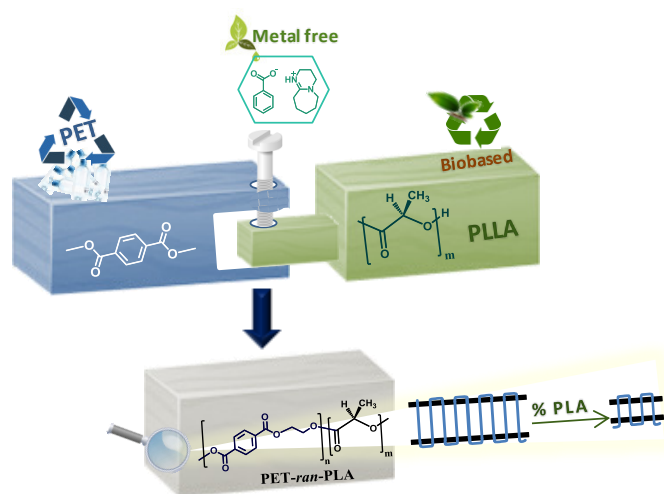
*PET-ran-PLA partially degradable random copolymers prepared by organocatalysis:  
Effect of PLA incorporation on  
crystallization and morphology.*

4.1 Abstract.....	71
4.2 Introduction.....	72
4.3 Results and Discussion.....	74
4.3.1 Synthesis and Characterization of the Copolyesters.....	74
4.3.2 Effect of PLA Content in the Thermal Properties of PET	78
4.3.3 Isothermal Crystallization Kinetics.....	84
4.3.4 Determination of Parameters derived by SAXS.....	93
4.3.5 Hydrolytic Degradation of Copolymers.....	97
4.4 Conclusions.....	98
4.5 References.....	99

## 4.1 Abstract

PET is a non-biodegradable polymer whose hydrolytic degradation can take decades. Intensive research is being performed to accelerate its hydrolytic degradation without significantly affecting its properties. In this work, PET was combined with PLA, a well-known biodegradable polymer, and the effect of PLA content in the crystallization of the PET component has been investigated in detail. In order to make the process sustainable, PET was polymerized using monomers that can be derived from PET chemical recycling (dimethyl terephthalate) and using organocatalysis (metal-free catalysts). First, low molecular weight telechelic PLA was prepared from the organocatalyzed ROP of L-lactide followed by step-growth copolymerization with PET oligomers. The random copolymerization was confirmed by FTIR and  $^1\text{H}$  NMR.

WAXS and SAXS demonstrated that PLA units interrupt the average crystallizable PET sequences, decreasing its lamellar thickness, melting point and crystallinity. The copolymers exhibited a micro-spherulitic PET morphology that changed to axialitic at relatively high contents of PLA. Preliminary hydrolytic degradation experiments demonstrate the potential degradation character of the prepared copolymers. Considering the degradability of the copolymers obtained together with the green synthetic route employed, the copolymers produced represent a step towards revalorization of PET recycled monomers for the production of sustainable materials.



Flores, I.; Etxeberria, A.; Irusta, L.; Calafel, I.; Vega, J.F.; Martínez-Salazar, J.; Sardon, H.; Müller, A. J. PET-ran-PLA partially degradable random copolymers prepared by organocatalysis: Effect of PLA incorporation on crystallization and morphology. *ACS Sustainable Chemistry & Engineering* **2019**, (Accepted).

## 4.2 Introduction

Polyethylene terephthalate (PET) is one of the most widely used polymers due to its combination of good mechanical, thermal and permeability properties. PET is used for the manufacture of containers (beverages, oils, dairy products, cosmetics, etc.), in practically any packaging format (jugs, bottles, tray).<sup>1-3</sup> In spite of the available infrastructure for collecting and sorting PET products implemented worldwide, only 20-30 % of PET is recycled, mostly by physical recycling methods, leading to poor properties of recycled products that eventually end up in landfills or incineration. As PET is not biodegradable and its hydrolytic degradation can take decades, it generates a large amount of waste, which has caused pollution and accumulation problems in different ecosystems.<sup>3-5</sup>

In line with the above, one possibility to create new materials with higher ability to degrade in the environment is by co-polymerizing PET with poly (lactic acid) or PLA. PLA is a biobased and biodegradable polymer that can be obtained from renewable sources (corn, starch, sugar). PLA has properties that can be compared with other thermoplastic materials such as poly styrene (PS) and poly propylene (PP).<sup>6</sup> On the other hand, it has been shown that the incorporation of aliphatic chains within the aromatic polyester tends to improve the degradability of PET.<sup>7</sup>

The idea of combining the degradability of PLA with a polymer with superior mechanical properties but not degradable like PET has been previously explored.<sup>2,7-13</sup> However, in all these previous works, metal catalysts are used for the formation of copolymers, and their residues are not environmentally friendly.<sup>14</sup> In recent years various metal-free catalysts (organocatalysts) have been shown to be effective for the preparation of various polymers and copolymers<sup>15-23</sup> that include PLA and PET components. Within these organocatalysts, the protic ionic salt diazabicyclo-[5.4.0]undec-7-ene (DBU): benzoic acid (BA) is very interesting. This organocatalytic system is effective in promoting the polymerization of PLLA. It has been recently shown that it can also be effective in polymerizing PET, as it has the required thermal stability at high temperatures.<sup>22,23</sup>

In this work, the results of the synthesis and characterization of PET-*ran*-PLA random copolyesters, made from low molecular weight telechelic PLLA and oligomers

of PET (derived from dimethyl terephthalate, DMT, which can be obtained from PET waste) are reported.

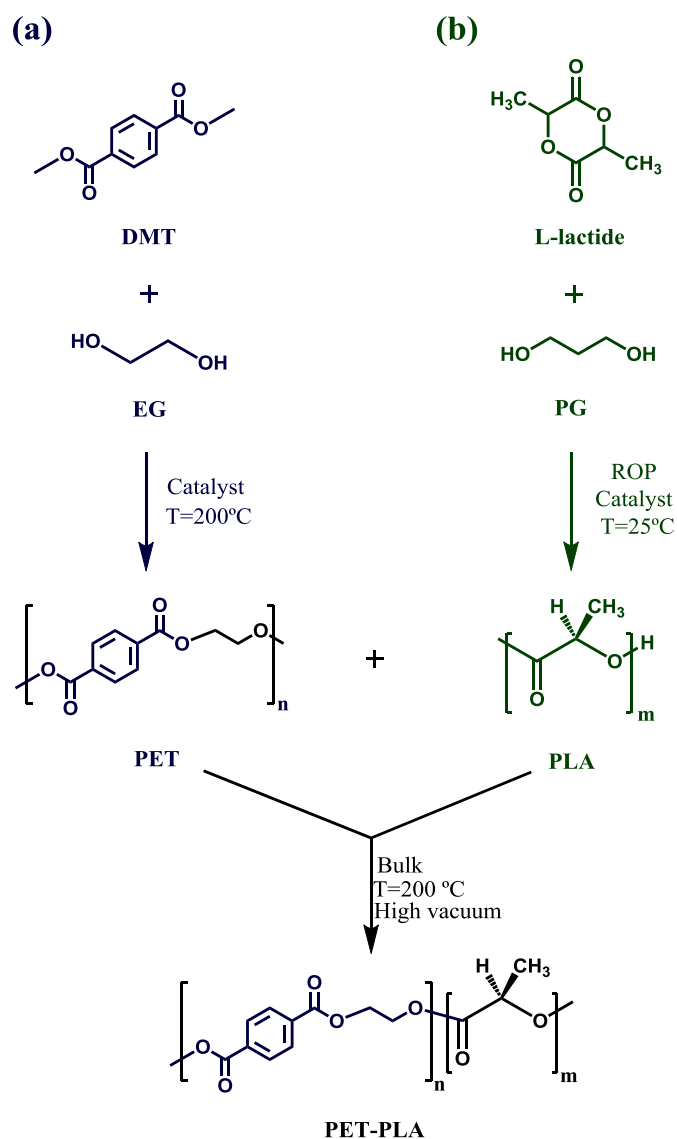
DMT was selected because it is one of the most successful monomers obtained from the chemical recycling of PET by methanolysis. A promising trend in polymer chemistry is to produce new polymers using plastic waste as the chemical source. This waste should be perceived as a new resource that must be reincorporated into the life cycle of plastics, thus completing a cycle in their circular economy. According to estimates, the potential annual energy savings that could be achieved from recycling all global plastic waste is equivalent to 3.5 billion barrels of oil per year. Industries for sorting and recycling PET already exists, hence, PET is an ideal candidate for applying chemical recycling concepts.<sup>1,3,4,15,24-27</sup> Finally in order to make the process more sustainable, the copolymers are formed using a metal-free catalyst (DBU: BA), i.e., an organocatalyst. Apart from using a new green and sustainable novel approach towards the synthesis of PET-*ran*-PLA copolymers by employing organocatalysis, their structure, morphology and crystallization kinetics has been studied in detail by DSC, SAXS, WAXS, AFM, DMTA and PLOM.

## 4.3 Results and Discussion

### 4.3.1 Synthesis and Characterization of the Copolyesters

The synthesis of PET-*ran*-PLA copolymers was carried out in two steps. The organocatalyst DBU:BA was selected because it has been reported to be effective for the homopolymerization of both PLLA and PET.<sup>20,22,23</sup> Therefore, it is expected that it displays catalytic activity favoring the formation of PET-*ran*-PLA copolymers.

First telechelic PLA (Poly (L-lactic acid)) was synthesized by ROP using DBU:BA as catalyst, using 1,3-propanediol as initiator (1/50 ratio). The polymerization was confirmed by <sup>1</sup>H NMR following the diagnostic peaks related to the PLA formation (Figure 4.1).



**Scheme 4.1.** Organocatalyzed Synthesis of PET-*ran*-PLA.

To further characterize the PLA homopolymer, SEC analysis was performed to find that the experimental molecular weight ( $M_n = 8.1$  kDa) was similar to the targeted one. Then, the synthesis of PET oligomers was carried out. Dimethyl terephthalate (DMT) was reacted with excess ethylene glycol (EG) for 2 h, in the presence of the same DBU:BA organocatalyst, to form PET oligomers. Afterwards, the preformed PLA was added to the PET oligomers (Scheme 4.1) to complete the copolymerization.

To demonstrate that the copolymerization took place, detailed NMR studies were performed. In Figure 4.1 the characteristic peaks associated with PET-*co*-PLA copolymerization can be observed at 5.43 ppm, a signal attributed to the *Terephthalate-Lactide* links, (Ar-COO-CHCH<sub>3</sub>CO, peak 1), 4.66 ppm for the *Terephthalate-Ethylene glycol-Lactide* links (Ar-COO-CH<sub>2</sub>-CH<sub>2</sub>-OCOCHCH<sub>3</sub>-O, peak 2) and 1.69 ppm assigned to *Terephthalate-Lactide* links (Ar-COO-CHCH<sub>3</sub>CO, peak 3).<sup>7,8,11,12</sup> Furthermore, the characteristic peaks from PET units (8.12 ppm, Ar-CH and 4.78 ppm, COO-CH<sub>2</sub>-CH<sub>2</sub>-OCO) and lactide units (5.28 ppm, COO-CHCH<sub>3</sub>O and 1.56 ppm, COO-CHCH<sub>3</sub>O) are presented in the NMR analysis.<sup>12</sup>

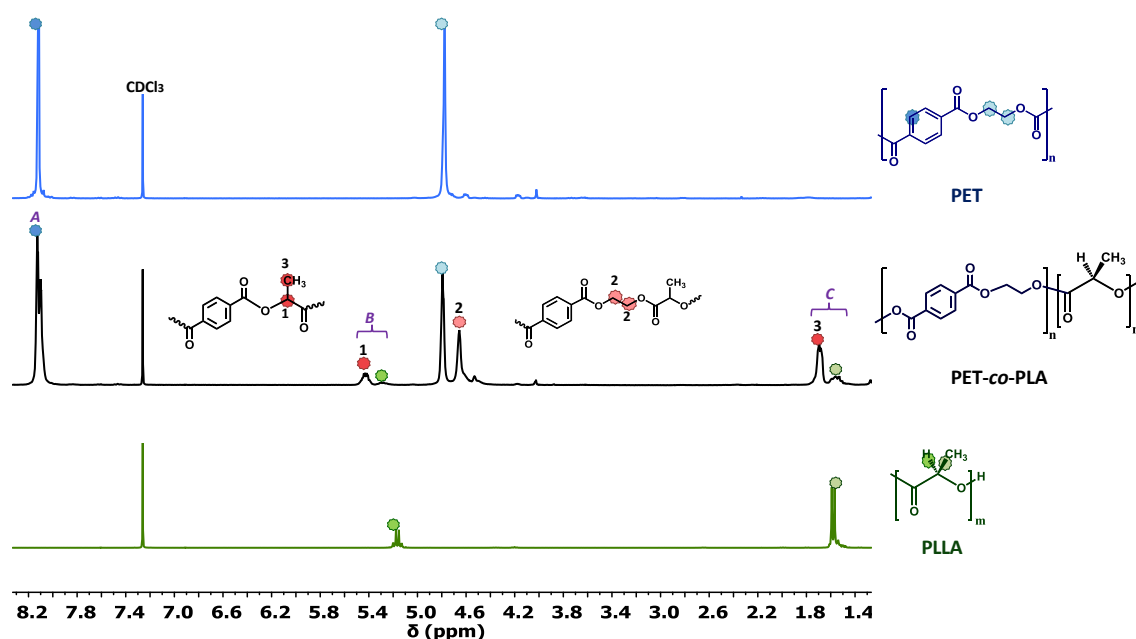


**Figure 4.1.** <sup>1</sup>H NMR spectrum of PET<sub>63</sub>PLA<sub>37</sub> in CDCl<sub>3</sub>/TFA.

To further ensure the formation of PLA-*co*-PET copolymers, it was performed an extraction of the copolymers in a solvent that was selective for PLA (CHCl<sub>3</sub>) and the PET/PLA composition was subsequently measured (Table B.1, Annex B). It was

observed that the resulting composition was very similar to that observed when the copolymers are diluted in  $\text{CHCl}_3/\text{TFA}$  (a solvent mixture that dilutes both PET and PLA). This result suggests that the materials prepared are indeed copolymers.

To further confirm the presence of PET and PLA, a qualitative analysis by FTIR was carried out. In Figure 4.2, the scale expanded infrared spectra of different copolymers are shown. As can be seen, the bands assigned to the C = O group stretching appear at 1755 and 1718  $\text{cm}^{-1}$  for PLLA and PET respectively. Moreover, the band belonging to the C-O-C asymmetric stretching of PLA appears at 1188  $\text{cm}^{-1}$  and in the case of PET it is observed at 1252  $\text{cm}^{-1}$ . All these bands indicate the presence of both types of units (PET and PLA) in the copolymer.<sup>7,28</sup>

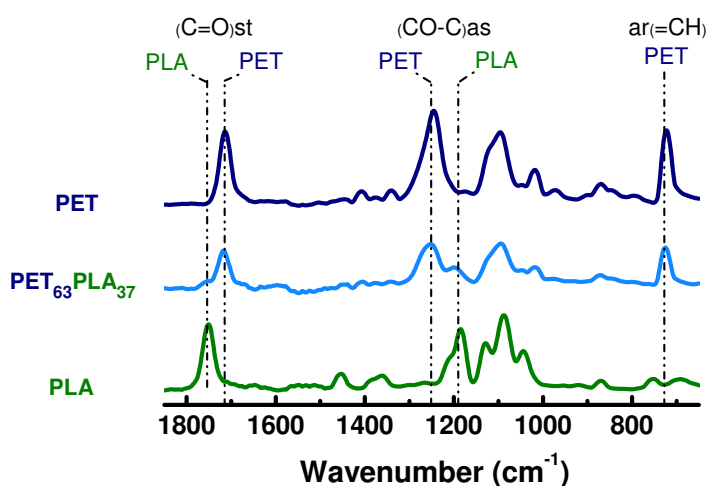


**Figure 4.2.** Infrared Spectra of Copolymers PET-ran-PLA.

After confirming the successful copolymerization between PET and PLA, copolymers with different compositions have been prepared in order to investigate the effect of different PLA ratios on the thermal properties and crystallization of PET. The final composition was calculated using  $^1\text{H}$  NMR spectroscopy.

Assuming that the formation of the copolymer is partially based on the transesterification reactions between PET and PLA, and taking into account that such reactions could produce isolated lactyl units, the PET/PLA ratio has been calculated considering the lactyl group as the repeating unit following the expression below:

$$(T) = \frac{A/4}{A/4 + (B + C)/4} \quad (4.1)$$

where ( $T$ ) is the mole fraction of the terephthalate in the copolymer, A, B and C the integrals of the signals at 8.12, 5.5-5.2 and 1.8-1.4, respectively. The final compositions were similar to the targeted ones and compositions from 100 mol % of PET to 13 mol % of PET were obtained. On the other hand, using  $^1\text{H}$  NMR, the degree of randomness ( $\eta$ ) was calculated (Equation B-2, Annex B). The value in all copolymers tends to 1 indicating that they are mostly random copolymers ( $\eta = 1$ ).

As will be shown later, PLLA loses the crystallization ability after being subject to the copolymerization conditions employed here. Epimerization could lead to the reduction of stereopurity. In case of racemization, the number of mmm sequences would decrease, the  $^{13}\text{C}$  NMR spectra are presented in Annex B. A simple analysis of the carbonyl signals showed that, assuming Bernoullian statistics,  $P_{mm}$  decreased from 0.963 to 0.910 values for the PLA after copolymerization, meaning that epimerization was occurring during the co-polymerization step.<sup>29</sup>

**Table 4.1** Composition, Degree of randomness and Molecular Weight of Polymers.

Sample	PET / PLA		$\eta^a$	$M_n^b$ kDa	$M_w^b$ kDa	$\mathcal{D}^b$
	% mass ratio <sup>a</sup>	% mol ratio <sup>a</sup>				
PET	100/0	100/0	---	1.35	2.95	2.2
PET <sub>95</sub> PLA <sub>05</sub>	98/02	95/05	0.95	1.3	3.05	2.3
PET <sub>88</sub> PLA <sub>12</sub>	95/05	88/12	0.98	1.5	3.45	2.3
PET <sub>84</sub> PLA <sub>16</sub>	93/07	84/16	1.14	1.2	4.3	3.6
PET <sub>81</sub> PLA <sub>19</sub>	92/08	81/19	1.13	1.35	3.05	2.3
PET <sub>79</sub> PLA <sub>21</sub>	91/09	79/21	1.12	-	-	-
PET <sub>76</sub> PLA <sub>24</sub>	90/10	76/24	1.14	1.86	4.9	2.6
PET <sub>63</sub> PLA <sub>37</sub>	82/18	63/37	1.26	2.85	6.75	2.4
PET <sub>26</sub> PLA <sub>74</sub>	48/52	26/74	1.35	4.35	9.75	2.2
PET <sub>13</sub> PLA <sub>87</sub>	28/72	13/87	0.93	4.85	9.25	1.9
PLLA	0/100	0/100	---	8.1 <sup>c</sup>	9.7 <sup>c</sup>	1.1 <sup>c</sup>

<sup>a</sup>Calculated by NMR. <sup>b</sup>Measured by GPC in HFIP against PMMA standards.

<sup>c</sup>Measured by GPC in THF according to PS standards (Curves in SI).

In order to complete the characterization, the molecular weights and polydispersity index ( $\mathcal{D}$ ) of each polymer synthesized was analyzed by SEC-GPC (Table

4.1). In all cases, low or moderate molecular weights were obtained and it was found an increase in molecular weight as the amount of PLA was increased in the copolymer.

The limited molecular weights obtained (both in PET and in the copolymers) are probably due to the temperature at which the reactions are carried out (200 °C), since it has been reported that for PET synthesis an increase from 200 to 250 °C in reaction temperature, generates an increase in the molecular weight of the PET obtained.<sup>22</sup> However, in this work PET was copolymerized with PLA at lower temperatures than desired (200 °C), as PLA tends to degrade at higher temperatures. It was found that higher temperatures were completely inefficient for copolymerization, as PLA degradation was highly pronounced. Therefore, the polymerization temperature restrictions limited the growth of PET chains in the copolymerization process, as reflected in the low molecular weights obtained.

#### 4.3.2 Effect of PLA Content in the Thermal Properties of PET

Although PET has excellent thermal properties, its use may be limited in certain applications because of the high crystallinity it can develop in the low molecular weight range. As a result of the above, several investigations have reported PET copolymers with poly (butylene succinate), poly (ethylene succinate), poly (lactic acid), etc., with the aim of modifying the properties of PET especially in terms of its crystallinity. These investigations show that the crystallization of PET is highly affected by the presence of comonomeric chains randomly distributed along the chains. For instance, Muñoz-Guerra et al. found that only copolymers containing 90 mol % or more of ethylene terephthalate units were able to crystallize in PET copolymers.<sup>2,9,30-</sup>  
32

The second DSC heating scans (the first heating scans, as well as the cooling scans from the melt are shown in Annex B) of selected samples are shown in Figure 4.3, where the calorimetric properties exhibit large differences depending on copolymer composition.

The PLA sample shown in Figure 4.3 is a neat PLA sample that was thermally treated to simulate the conditions applied during copolymer synthesis. The DSC

heating scan shows that the sample is incapable of crystallization (Figure 4.3), which indicates that the reaction conditions (time and temperature) affect the crystallization ability of PLA. As it is well known, a racemization larger than 4 mol% (content of D greater than 4 mol%) is enough to significantly reduce the crystallization of PLA.<sup>33</sup> In this case, the racemization of PLA after the thermal conditions is slightly superior to this value, thus, crystallization did not occur.

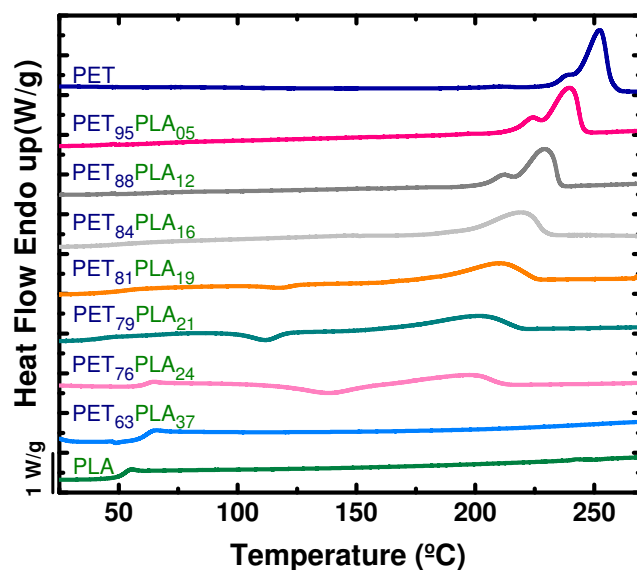


**Figure 4.3.** DSC second heating scans for the PET-*ran*-PLA copolymers and the parent homopolymers.

As explained above, the synthetic conditions employed also lead to a randomized structure in the copolymers and they can be considered random copolymers of PET and PLA. In fact, the DSC results are consistent with a random structure in the copolymers, as the PET component was only able to crystallize for copolymer compositions with 76 mol% PET or more. The decrease in  $T_m$  values, as PLA content in the comonomer increases, is another evidence of the frequent interruptions of the linear crystallizable sequences of PET repeating units by PLA repeating units. As PLA cannot crystallize and has different chain repeating units, it is excluded to the amorphous regions during PET crystallization, limiting the lamellar thickness obtained and therefore the melting point of the PET crystals. Evidences for such decreases in lamellar thickness were obtained by SAXS and will be presented below.

The neat PET has a fairly low number average molecular weight that allows it to crystallize until saturation during cooling from the melt (see Figure B.5, Annex B), hence it does not display cold-crystallization during the second heating run. A similar behavior is observed in the random copolymers until 16 mol% incorporation of PLA. Beyond that, cold crystallization is observed in the second heating scans, indicating that the sample was not able to crystallize fully during cooling from the melt at 20 °C/min.

Table 4.2 displays  $T_c$ ,  $T_m$ , and  $T_g$  values. The latent heats of crystallization, fusion and cold crystallization ( $\Delta H_c$ ,  $\Delta H_m$ ,  $\Delta H_{cc}$ ) shown in Table 4.2 are normalized values for each sample that were calculated by dividing the enthalpy by the respective mass fraction. In this same table, the value of  $\Delta H_{mF}$  is shown and this is obtained by subtracting the value of the  $\Delta H_{cc}$  from  $\Delta H_m$  (taken from the same table).  $\Delta H_{mF}$  was employed to calculate the degree of crystallinity of the samples at room temperature.

Figure 4.4 shows a summary of the non-isothermal calorimetric results where  $T_c$ ,  $T_m$  and the degree of crystallinity ( $X_c$ ) have been plotted as a function of PLA content in the copolymers. The monotonic decrease in these three variables as a function of PLA content and the fact that beyond 37 mol% of PLA the samples are incapable of crystallization are all consistent with full exclusion of PLA units from the crystallites developed by the PET component.

**Table 4.2** Thermal Properties of Synthesized PET, PLA and PET-co-PLA copolymers.

Sample	Mass fraction	Cooling			2 <sup>nd</sup> . Heating				
		$T_c$ (°C) <sup>a</sup>	$\Delta H_c$ (J/g) <sup>a</sup>	$T_m$ (°C) <sup>a</sup>	$\Delta H_m$ (J/g) <sup>a</sup>	$T_{cc}$ (°C) <sup>a</sup>	$\Delta H_{cc}$ (J/g) <sup>a</sup>	$\Delta H_{mF}$ (J/g) <sup>a</sup>	$T_g$ (°C) <sup>b</sup>
PET	1	213.5	56	252.6	51	---	---	51	99
PET <sub>95</sub> PLA <sub>05</sub>	0.98	197.1	54	239.4	53	---	---	53	100
PET <sub>88</sub> PLA <sub>12</sub>	0.95	182.1	48	229.2	48	---	---	48	91
PET <sub>84</sub> PLA <sub>16</sub>	0.93	149.6	44	219.1	45	---	---	45	93
PET <sub>81</sub> PLA <sub>19</sub>	0.92	135.1	36	210	42	118.1	3	39	82
PET <sub>79</sub> PLA <sub>21</sub>	0.91	123.7	25	201.7	41	111.9	9	32	---
PET <sub>76</sub> PLA <sub>24</sub>	0.90	125	6	196.9	28	138.2	16	12	81
PET <sub>63</sub> PLA <sub>37</sub>	0.82	---	---	---	---	---	---	---	70
PET <sub>26</sub> PLA <sub>74</sub>	0.48	---	---	---	---	---	---	---	60
PET <sub>13</sub> PLA <sub>87</sub>	0.28	---	---	---	---	---	---	---	63
PLA	---	---	---	139	16	112.2	15	---	62
PLA**	---	---	---	---	---	---	---	---	56

<sup>a</sup>Determined by DSC. <sup>b</sup>Obtained by DMTA. PLA\*\* is PLA that was subjected to the same conditions of time and temperature as the copolymer, but without the presence of PET.

To corroborate that the crystallization observed in DSC corresponds to PET, measurements were carried out by WAXS, to analyze the crystalline structure obtained in the synthesized materials at different temperatures. Daubeny et al. determined the crystal structure of PET from drawn fibers. The reported unit cell is triclinic, with  $a = 4.56 \text{ \AA}$ ,  $b = 5.94 \text{ \AA}$ ,  $c = 10.75 \text{ \AA}$ ,  $\alpha = 98 \frac{1}{2}^\circ$ ,  $\beta = 118^\circ$ ,  $\gamma = 112^\circ$ .<sup>34</sup>

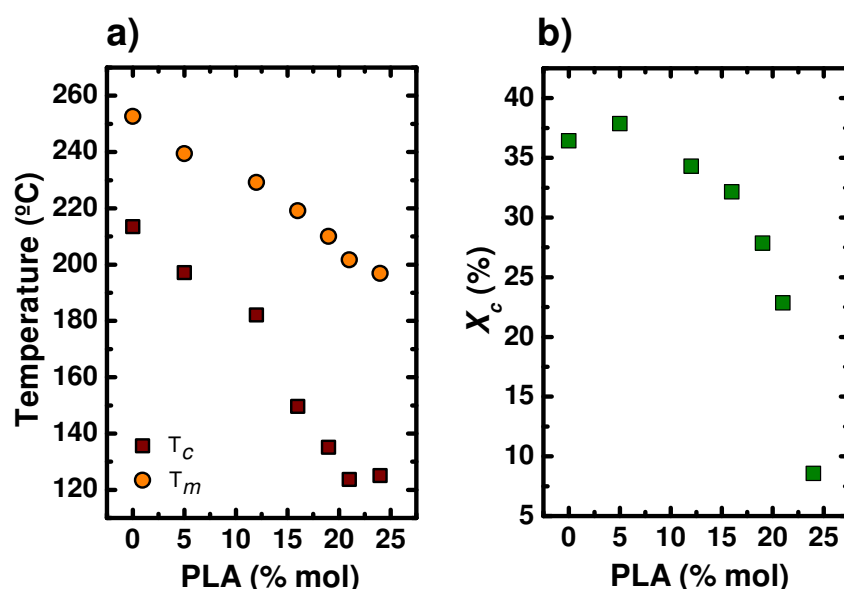


**Figure 4.4.** (a) Values of  $T_m$  and  $T_c$  as a function of composition for PET-*ran*-PLA random copolymers and (b)  $X_c$  versus composition for PET-*ran*-PLA.

Figure 4.5(a) shows WAXS diffractograms taken at the synchrotron during cooling a PET sample at  $20 \text{ }^\circ\text{C}/\text{min}$  and are therefore comparable to the conditions employed by DSC. The reflections observed in Figure 4.5(a) at  $2\theta$  values of 10.69, 11.63, 14.15, 14.93, 17.11, 18.33, 21.40 and 27.80 correspond to diffraction from the following crystalline planes within the PET triclinic unit cell: (011), (010), (111), (110), (100), (111), (111), (105), thus proving (together with NMR and FTIR) that the PET was obtained with the green synthetic route proposed here.<sup>34-41</sup>

Figure 4.5(b) corresponding to the  $\text{PET}_{95}\text{PLA}_{05}$  copolymer shows intense reflections that are also characteristic of PET, but also the total absence of peaks corresponding to crystalline PLA. This behavior is also observed in the rest of the semicrystalline copolymers that were synthesized (WAXS patterns for all copolymers can be found in Annex B).

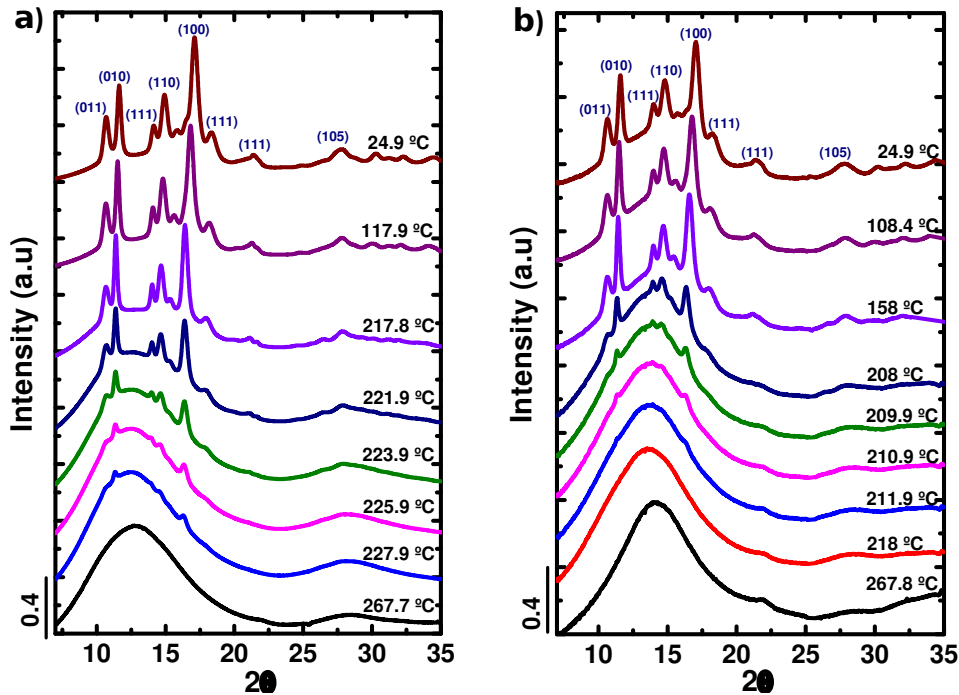


**Figure 4.5.** Real time synchrotron WAXS diffraction patterns for samples (a) PET and (b) PET<sub>95</sub>PLA<sub>05</sub>, cooled from the 270 °C to 25 °C at 20 °C/min.

The WAXS results are consistent with the DSC measurements, as it is observed that when the amount of PLA in the copolymers increases, the intensity and area under the PET crystalline peaks decreased (indicating a reduction in crystallinity degree) while the temperature at which the materials started to crystallize from the melt also decreased. This trend is already evident for the PET<sub>95</sub>PLA<sub>05</sub> copolymer (see Figure 4.5(b)).

The exclusion of PLA comonomeric units from the PET crystal lattice was also corroborated by the WAXS results. The lattice parameters obtained at constant temperatures are insensitive to copolymer composition, a classic behavior of comonomer exclusion (see Figure B.11, Annex B).

In some cases, DSC was not sensitive enough to measure the  $T_g$  of some of the semi-crystalline samples, as the change in  $C_p$  associated with  $T_g$  was very small. Therefore, DMTA tests were employed to measure the  $T_g$  values of all the samples obtained, which are listed in the table 4.2 and represented in Figure B.13 (Annex B). Only one  $\alpha$  relaxation with high intensity (see the prominent maxima at temperatures between 60 and 100 °C in Figure B.13) for all compositions was found. This  $\alpha$  relaxation is the mechanical manifestation of the  $T_g$ . The observation of a single  $T_g$  for all

copolymers corroborates the random character of the copolymers. Due to this, it is expected that they do not exhibit any phase segregation in the melt, a fact that was corroborated by SAXS and shown later.

The  $T_g$  values of the copolyesters are in between the  $T_g$  values of the two parent homopolymers and are composition dependent. The trend in  $T_g$  values versus composition can be fitted to semi-empirical equations. Figure 4.6 shows the fit of the experimental  $T_g$  data to the Gordon Taylor equation (Eq. (4.2)), which can be written as:

$$T_{g, \text{copolymer}} = \frac{w_1 T_{g,1} + k_{GT}(1 - w_1) T_{g,2}}{w_1 + k_{GT}(1 - w_1)} \quad (4.2)$$

where  $T_{g,1}$  and  $T_{g,2}$  are the glass transition temperatures of homopolymers 1 and 2, respectively;  $w_1$  is the mass fraction of homopolymer 1 and  $k_{GT}$  is the Gordon-Taylor parameter.<sup>42</sup> A satisfactory fit was obtained with a  $k_{GT}=10$  indicating a behavior which is also typical of random copolymers.

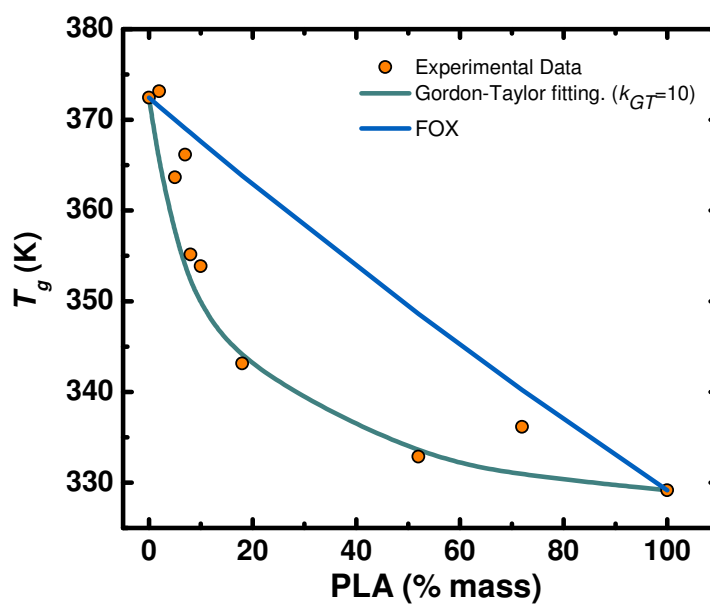


**Figure 4.6.**  $T_g$  values for the synthesized copolymers ( $\text{PET}_x\text{PLA}_y$ ) as a function of the content of PLA and their fitting with the Gordon-Taylor equation and the Fox equation.

In Figure 4.6 the Fox equation is also represented. It is clearly appreciated that this equation does not provide a good fit for the trend observed in the experimentally determined  $T_g$  values versus composition. The Fox equation predicts a trend much

closer to a simple rule of mixtures that is characteristic of random copolymers where the two chemical repeat units are very similar. In the case of PET-*ran*-PLA, that is not the case (one repeat unit is aromatic while the other is aliphatic) and stronger deviations from a simple rule of mixtures are expected and described semi-empirically by the Gordon-Taylor equation.

### 4.3.3 Isothermal Crystallization Kinetics

Spherulites constitute the most common morphological texture of polymers crystallized from the melt. The nucleation and crystallization kinetics controls the spherulitic texture, which in turn can greatly affect the mechanical properties of the polymer. The observations performed by Polarized Light Optical Microscopy (PLOM) indicated that the nucleation density was very high even for neat PET and very small spherulites were observed. The nucleation density increased even further in the copolymers. The morphological texture was therefore micrometric at sizes around 1 micron or less and growth rate measurements of superstructural structures like spherulites was therefore impossible to carry out. The microspherulitic textures were observed by AFM and are presented in a subsequent section.

As PLOM could not be used to study growth kinetics, DSC was used in order to determine overall isothermal crystallization rates (which include both nucleation and growth) of PET and the PET components within the copolyesters.

Figure 4.7(a) shows the inverse of the half crystallization time ( $1/\tau_{50\%}$ ), which is proportional to the experimentally determined overall crystallization rate (that includes both nucleation and growth), as a function of isothermal crystallization temperatures ( $T_c$ ) for neat PET and all copolyesters where the PET component was able to crystallize.

The overall crystallization rate of polymeric materials is a complex function of primary nucleation and growth. When it can be measured in a very wide temperature range, the inverse of the half-crystallization time as a function of  $T_c$  displays a bell shape curve.<sup>43,44</sup> At low supercoolings (right hand side of the bell shape curve), both primary and secondary nucleation processes dominate the kinetics. As the driving

force for crystallization increases, i.e., as supercooling increases, the crystallization rate increases until a critical  $T_c$  value is reached. At this critical  $T_c$ , the crystallization rate goes through a maximum as diffusion starts to dominate the crystallization kinetics. The transport of chains to the growth front is increasingly retarded as melt viscosity increases when temperature decreases. So, in this diffusion dominated part of the bell shape curve (left hand side of the curve), at very large supercoolings, the crystallization rate decreases with  $T_c$  until it becomes zero at  $T_g$ .

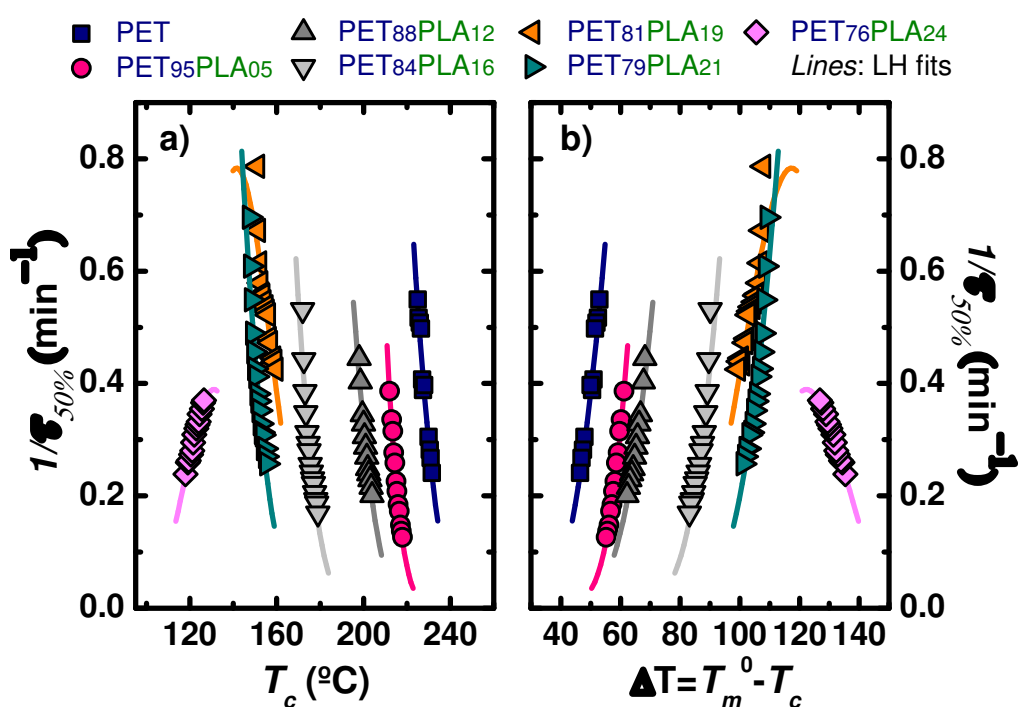


**Figure 4.7.** (a) Overall crystallization rate ( $1/\tau_{50\%}$ ) as a function of isothermal crystallization temperature ( $T_c$ ) and (b) Overall crystallization rate ( $1/\tau_{50\%}$ ) as a function of the supercooling ( $T_m^0 - T_c$ ), for neat PET and for the PET-*ran*-PLA copolymers.

The PET homopolymer sample prepared in this work has a very low molecular weight ( $M_w=2.950$  g/mol) and that explains its very fast crystallization kinetics. Figure 4.7 shows that only data at low supercooling was collected, as any attempt to lower the  $T_c$  value resulted in crystallization during cooling to  $T_c$  (which was performed at 60 °C/min). Therefore, only data belonging to the right-hand-side crystallization bell shape curve was measured for this PET homopolymer sample. Its crystallization rate, expressed as the inverse of the half-crystallization time, varied between approximately 0.24 and 0.55 min<sup>-1</sup> in a  $T_c$  range of 225 and 231.5 °C. Lu and Hay reported values

between 0.1 and 0.2 min<sup>-1</sup> for a  $T_c$  range of 213 and 222 °C.<sup>35</sup> These slower overall crystallization rates are consistent with their higher molecular weight commercial PET sample ( $M_w=16.000$  g/mol).

Figure 4.7(a) shows that as the amount of PLA increases in the copolymers, the  $T_c$  range needed for crystallization decreases. This is consistent with the trend already observed in the non-isothermal crystallization results (see Figure B.5, Annex B). As explained above, when PET is randomly copolymerized with PLA, interruptions of the linear crystallizable sequences by the PLA comonomeric units occur at random places in the chains. As the amount of PLA increases, the concentration of “defects” (i.e., PLA comonomeric units) also increases and the average crystallizable length of PET sequences decreases.

It is anticipated that the equilibrium melting temperature of PET also decreases as PLA comonomer is incorporated in the copolymer chains. The values of  $T_m^0$  have been calculated by the Flory-Huggins theory (see Annex B) and the data in Figure 4.7(a) has been represented in Figure 4.7(b) as a function of supercooling. Only part of the horizontal shift of the  $1/\tau_{50\%}$  versus  $T_c$  curves in Figure 4.7(a) is related to the change in  $T_m^0$  values (as calculated by the Flory-Huggins theory), as readily observed in Figure 4.7(b).

A remarkable and novel result is also shown in Figure 4.7(a). Notice how the trend in crystallization kinetics with temperature, changes from nucleation control (where the crystallization rate increases as  $T_c$  decreases) to diffusion control (where the crystallization rate decreases as  $T_c$  decreases), when the amount of PLA increases from 21 mol % to 24 mol %. This result is due to the high amount of PLA comonomer, which almost reaches the maximum tolerable level for the crystallization of the PET molecules in the copolymer, thereby hindering the diffusion of PET chains to the crystallization front.

Figure 4.8 shows the dramatic decrease in PET final crystallinity (developed during isothermal crystallization) as the amount of PLA in the copolymer increases, evidencing topological restrictions of the average PET chain segments to crystallize. The values reported in Figure 4.8 are normalized with respect to the weight PET content in the copolymer. For the PET<sub>76</sub>PLA<sub>24</sub> sample (whose weight composition is 90% PET and 10% PLA, see Table 4.1), approximately 14% of the PET sequences were

able to crystallize (at 120 °C), according to Figure 4.8. Therefore, in this copolymer sample, the final total crystalline content (i.e., PET crystals) after isothermal crystallization at 120 °C was only 12.6% (i.e., the 14% of 90 wt%) and there were 87.4% mixed molten PLA-*ran*-PET chains in the material. As crystallization proceeds from a single melt phase, the diffusion of the shorter crystallizable PET chain sequences is the slow step (or dominating step) in the overall crystallization kinetics of this particular copolymer (as shown in Figure 4.7(a)).

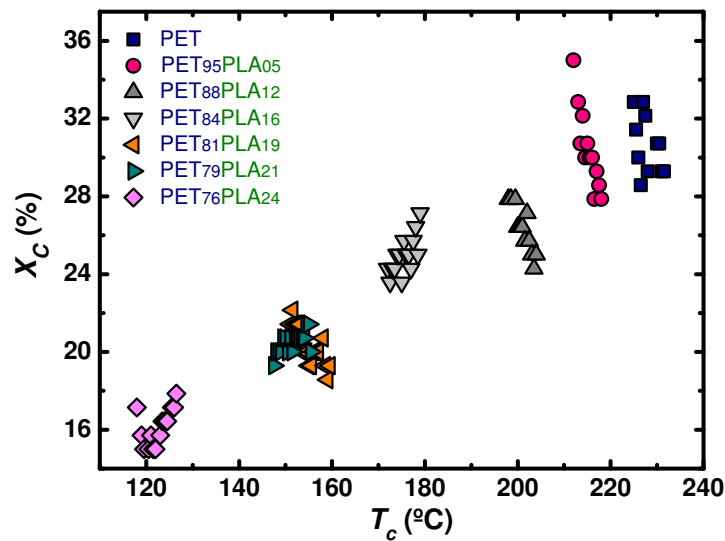


**Figure 4.8.** Percentage crystallinity ( $X_c$ ) of the PET component as a function of the isothermal crystallization temperature ( $T_c$ ).

The Avrami and the Lauritzen and Hoffman theories provide useful analytical equations that when properly handled represent valuable tools to understand crystallization kinetics and its relationship with morphology. The Avrami equation,<sup>45</sup> can be expressed as:<sup>43,46</sup>

$$1 - V_c(t - t_o) = \exp(-K(t - t_o)^n) \quad (4.3)$$

where  $t$  is the experimental time,  $t_o$  is the induction time before any crystallinity develops,  $V_c$  is the relative volumetric transformed fraction,  $n$  is the Avrami index and  $K$  is the overall crystallization rate constant. The experimental data were fitted to the Avrami equation using the Origin plug-in developed by Lorenzo *et al.*<sup>46</sup>

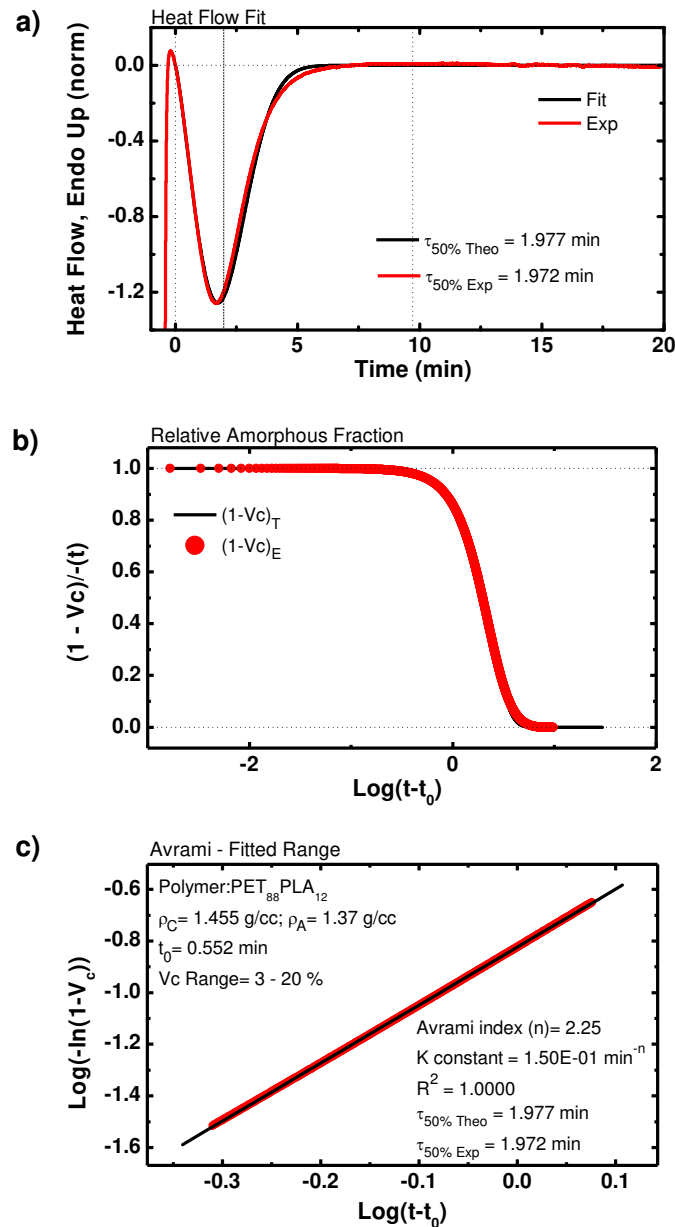


**Figure 4.9.** (a, b, c) Experimental Data compared with fits to the Avrami equation for PET<sub>88</sub>PLA<sub>12</sub>.

The Avrami equation generally fits well the primary crystallization range. This is why, the fits are usually performed at low conversion values (3-20%).<sup>46</sup> An example of the excellent agreement between the Avrami model and the experimental data is shown in Figure 4.9. The experimental DSC isotherms were compared with the Avrami predictions and an example is provided in Figure 4.9(a). The agreement is excellent in the primary crystallization range (i.e., until approximately the peak value, where the growing spherulites or axialites impinge on one another), as indicated by the correlation coefficient of 1 in the limited conversion range of 3-20% in Figure 4.9(c).

Surprisingly, the agreement is also very good in the secondary crystallization range, a fact that maybe connected with the low molecular weight of the PET synthesized here.

The values obtained for  $K^{1/n}$  (isothermal crystallization rate constant) are shown in Figure 4.10(a). The value of  $K$  has units of  $\text{min}^{-1}$ , i.e., they depend on the  $n$  value or Avrami index value. Therefore, in order to be able to compare  $K$  values with comparable units,  $K$  was elevated to the power  $1/n$ . As  $K$  is proportional to the overall crystallization rate, it has a tendency that is practically the same as the one shown in Figure 4.7, also attesting for the good fit to the Avrami equation.

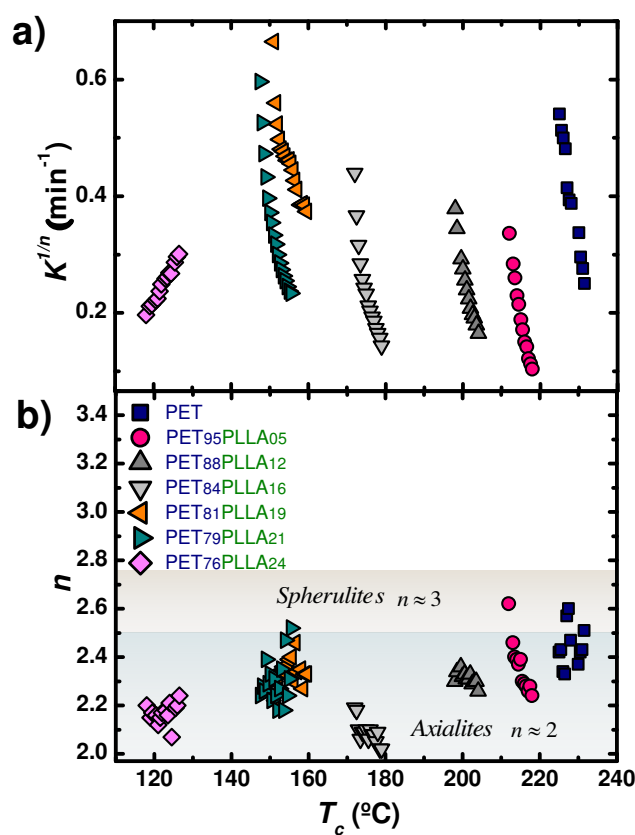


**Figure 4.10.** (a) Isothermal crystallization rate constant ( $K^{1/n}$ ) as a function of crystallization temperature ( $T_c$ ) and (b) Avrami index ( $n$ ) as a function of isothermal crystallization temperature ( $T_c$ ).

Applying the Avrami equation, values of  $n$  (i.e., Avrami index) for neat PET and PET phase in the copolymers were calculated and plotted in Figure 4.10(b), where it is appreciated that a range of values from 2 to 2.8 were obtained. In principle,  $n=3$  (or  $n=2.5-3.4$  which can be approximated to 3) indicates the presence of instantaneously

nucleated spherulites or sporadically nucleated axialites, while  $n=2$  is typically associated in polymers with instantaneously nucleated axialites. Observations performed by Polarized Optical Microscopy did show that even in neat PET, the nucleation density was very high and therefore the superstructures observed were very small, even at very high  $T_c$  values, were small spherulites were indeed observed. In such cases, the development of 3D spherulites is usually limited by the impingement with neighboring superstructures and in many cases, axialitic structures can be developed.

To complement the previous results and to check if the formation of spherulites and axialites could be observed, the materials were studied by atomic force microscopy (AFM). For each material, solvent cast films (see Chapter 2) were crystallized isothermally from the melt. The crystallization temperature ( $T_c$ ) selected for each sample is intermediate between  $T_g$  and  $T_m$ . Figure 4.11 shows the topography of pure PET versus PET<sub>88</sub>PLA<sub>12</sub>, where apparent spherulites are observed whose size is around 1  $\mu\text{m}$ . As only the surface of the film is being observed by AFM, it is not easy to distinguish between 3D or 2D lamellar packing, however the tight radial lamellar packing is characteristic of spherulites. These images are very similar to those obtained for PET<sub>95</sub>PLA<sub>05</sub> and PET<sub>84</sub>PLA<sub>16</sub> both at an optical and topographical level.

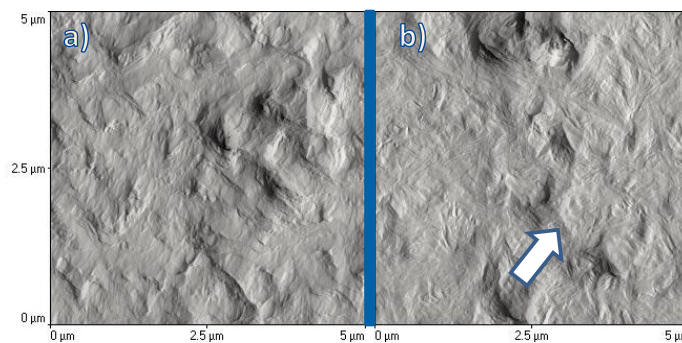


**Figure 4.11.** Micrographs observed by AFM for a film of (a) neat PET at  $T_c=190$  °C and (b) PET<sub>88</sub>PLA<sub>12</sub> at  $T_c=160$  °C.

An apparent transition from spherulites to axialites was observed in the compositions of 81 to 79 mol % PET (Figure 4.12). It is expected that as the amount of PLA in the copolymers increases, the development of 3D order becomes more difficult and only axialites could be observed. The difficulty in developing 3D superstructures or

spherulites arises when the linear crystallizable sequences get too short. These PET sequences must find each other both intra and intermolecularly in order to develop superstructures.

The information obtained by AFM and PLOM confirms that the PLA has a significant effect on the crystallinity of the PET in the copolymers, therefore the morphology and crystallization behavior of each sample is a function of the amount of PLA present.

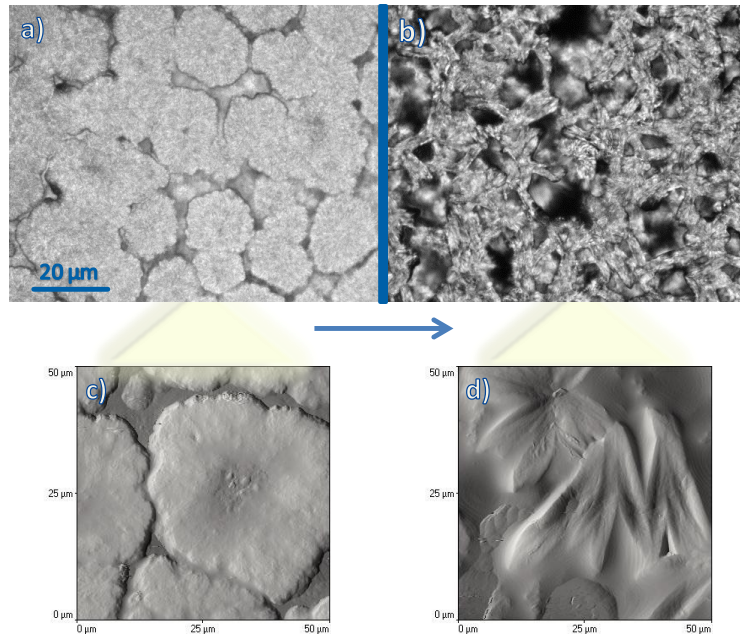


**Figure 4.12.** Micrographs observed by PLOM and AFM for a film of PET<sub>81</sub>PLA<sub>19</sub> at  $T_c=148$  °C (a, c), where a spherulitic morphology is apparent, and PET<sub>79</sub>PLA<sub>21</sub> at  $T_c=145$  °C (b, d), where clear axialites are observed.

The growth rate  $G(T)$  of the crystals can be predicted by the Lauritzen and Hoffman theory which is expressed as: <sup>47</sup>

$$G(T) = G_0 \exp\left(\frac{-U^*}{R(T_c - T_\infty)}\right) \exp\left(\frac{-K_g}{T_c \Delta T f}\right) \quad (4.4)$$

where  $G_0$  is a growth rate constant,  $U^*$  the activation energy for the transport of the chains to the growing nuclei (1,500 cal/mol is generally used),  $R$  is the gas constant,  $T_c$  the isothermal crystallization temperature,  $T_\infty$  is the temperature at which chain mobility ceases and it is usually taken as  $T_g-30$  (K).  $\Delta T$  is the supercooling defined as  $(T_m^0 - T_c)$  where  $T_m^0$  is the equilibrium melting point. The factor  $f$  is a

temperature correction term equal to:  $2T_c/(T_c + T_m^0)$ ; and  $K_g$  is a secondary nucleation constant, which is proportional to the energy barrier for secondary nucleation.

When the Lauritzen and Hoffman theory is applied to DSC data,  $G(T)$  in equation (4.4) is replaced by the inverse of the experimental half-crystallization time and the equation can then predict overall crystallization rates (which include both nucleation and growth).<sup>48</sup> Figure 4.7 shows the good fit of the experimental data to the LH theory (solid lines) for the overall crystallization rate. In this case, the parameter  $K_g$  is equal to  $K_g^T$ , which is proportional to the total energy barrier for the overall crystallization (i.e., for both nucleation and growth). In this work,  $T_m^0$  was calculated by the Flory-Huggins theory for random copolymers assuming complete exclusion of PLA comonomeric units (see Annex B).

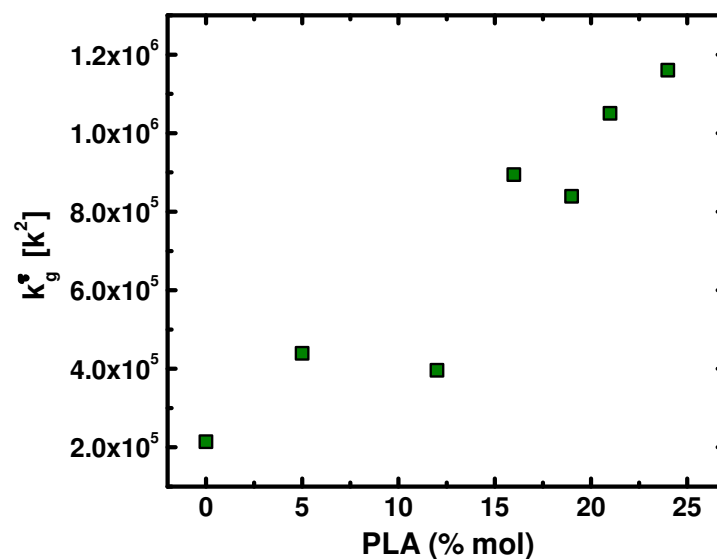


**Figure 4.13.** Values of  $k_g^T$  derived from LH fitting plotted as a function of PLA content.

Figure 4.13 clearly shows that when the amount of PLA increases in the copolymer the value of  $K_g^T$  is larger, indicating that the energy barrier to overcome for nucleation and growth increases as PET average crystallizable sequences get shorter.

#### 4.3.4 Determination of Parameters derived by SAXS

In order to study the effect that introducing PLA sequences in PET chains has on the lamellar periodicity (long period), as well as on the lamellar thickness of the copolymers, SAXS experiments were carried out for all the copolymer synthesized.

Experiments similar to those carried out by WAXS were conducted using SAXS (in fact, they were measured simultaneously at the synchrotron source). Figure 4.14 shows the SAXS results at different temperatures for (a) PET and (b) PET<sub>95</sub>PLA<sub>05</sub> samples, where the Lorentz corrected intensity is plotted as a function of the scattering vector  $q$ .

The SAXS curves exhibit a clear intense maximum due to the scattering caused by the periodic lamellar stacks (i.e., long period). The intensity of this maximum decreases as the amount of PLA increases in the copolymers. Such behavior indicates that lamellar stacking is increasingly difficult as PLA content increases and crystallinity degree decreases, as expected.

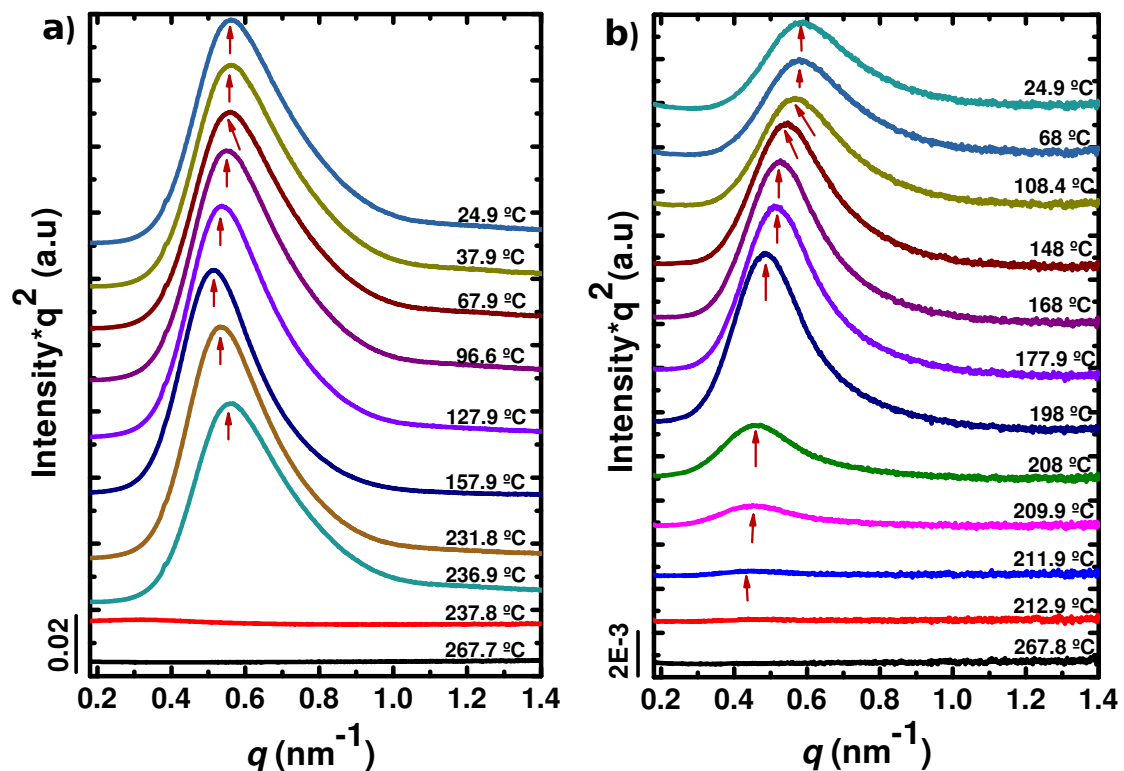


**Figure 4.14.** Lorentz-corrected SAXS profiles for (a) PET and (b) PET<sub>95</sub>PLA<sub>05</sub>, with intensity as a function of scattering vector. Data taken of samples cooled from the 270 °C to 25 °C at 20 °C/min.

When the PET crystals in the copolymer melt, the SAXS curves do not display any signal in Figure 4.14, indicating that a melt mixed phase is obtained, as expected for random copolymers.

In all samples, the long periods ( $d^*$ ) at different temperatures were estimated by Eq. (4.5) from  $q_{max}$  values taken from the Lorentz corrected plots ( $I^*q^2$  versus  $q$ ).

$$d^* = \frac{2\pi}{q_{max}} \quad (4.5)$$

Figure 4.15(a) shows that the value of  $d^*$  at low temperatures is a function of composition, as it tends to decrease with increases in PLA. This is expected for random copolymers where comonomer exclusion dominates, as upon increasing PLA co-units, the average linear crystallizable PET segments decrease in length causing a decrease in both crystallinity and lamellar thickness, as represented in Figure 4.15(b) and explained below. The long period also increased with temperature, as the amorphous content increases, especially above 150 °C (data not shown), where melting can start in some of the samples.

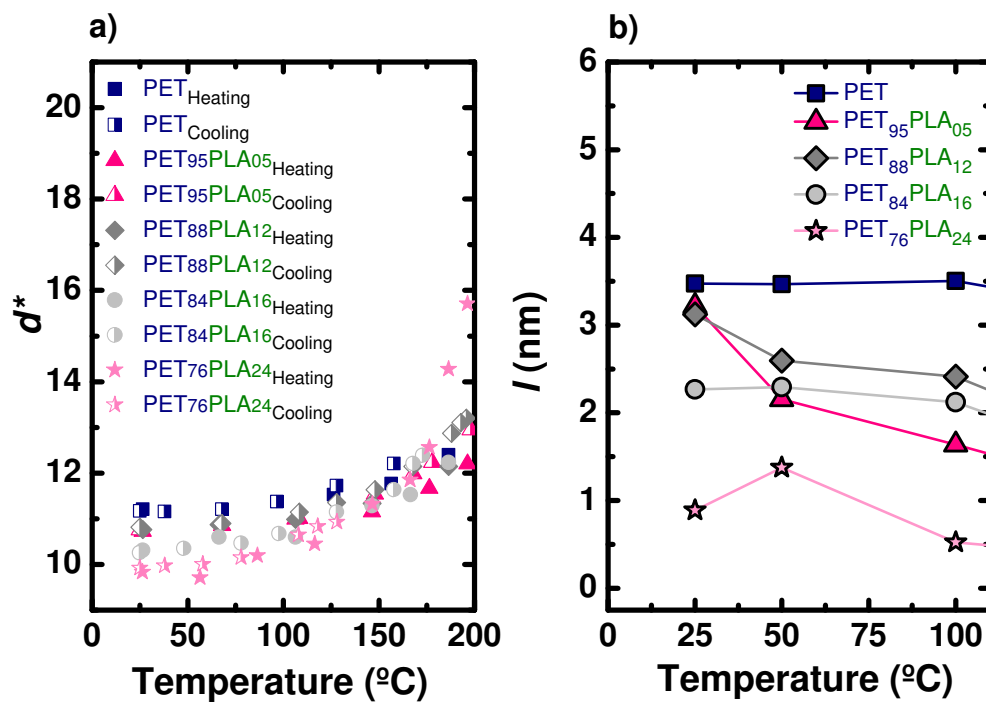


**Figure 4.15.** (a) Long periods ( $d^*$ ) calculated from SAXS data as a function of temperature and (b) lamellar thickness ( $l$ ) calculated from WAXS/SAXS data as a function of temperature.

Parameters such as the degree of crystallinity of each phase and the lamellar thickness ( $l$ ), can be calculated from the analysis of data obtained from WAXS, SAXS and DSC. For the calculation of an average lamellar thickness ( $l$ ) the following approximation was used:

$$l = d^* \cdot X_c \quad (4.6)$$

where  $X_c$  is the crystalline mass fraction and can be calculated from the enthalpy of fusion of the phase under consideration ( $\Delta H_m$ ), the enthalpy of fusion of a 100% crystalline sample and the weight fraction of the phase under consideration ( $W$ ) using Eq. (4.7).

$$X_c = \frac{\Delta H_m}{\Delta H_{m(100\%)} W} \quad (4.7)$$

Table 4.3 show the values of  $X_c$  determined by DSC by Eq.(4.7). From table 4.2,  $\Delta H_{mF}$  was taken for each sample, which is the normalized value of the latent heat of fusion  $\left(\frac{\Delta H_m - \Delta H_{cc}}{W}\right)$ , then  $X_c$  was calculated by dividing  $\Delta H_{mF}$  by  $\Delta H_{m(100\%)}$  (140 J/g).<sup>49</sup> Using these values the lamellar thickness ( $l$ ) was calculated and plotted in Figure 4.15(b) as a function of copolymer composition.

The lamellar thickness values generally decrease when the amount of PLA increases in these random copolymers as expected, since the average crystallizable PET sequences are decreasing in length. As the lamellar thickness values depend on the crystallinity degree employed to calculate them according to equation 4.6, the degree of crystallinity by WAXS was also calculated (an example is provided in Annex B, see Figure B.12). Table 4.3 lists the lamellar thickness calculated with crystallinity values derived from both DSC and WAXS and the values and trends are fully consistent with one another.

In order to complete the study, the average extended chain segments ( $L$ ) of the PET component within the copolymers was calculated. In order to determine these values, the number of terephthalate units joined together belonging to the PET ( $L_T$ ) was required, which can be determined from <sup>1</sup>H NMR using the equation below:

$$L_T = \frac{2(T)}{(LT)} \quad (4.8)$$

where  $(T)$  is the mole fraction of terephthalate units in the copolymer and  $(LT)$  is the molar fraction of the exchange dyad in the copolymer (the unit where lactyl or LA is attached to the terephthalate unit), these parameters were obtained by NMR.

$L_T$  values could explain the ability of copolymers to crystallize, as it will be seen and the values are presented in Table 4.3. It is observed that the number average chain length ( $L$ ) of PET segments decreases when the amount of PLA increases in the copolymer, as PLA breaks the regularity of the PET chains. It is also observed that PET segments within the synthesized copolymers do not crystallize with extended chains ( $L \neq l$ ) and therefore, form folds when crystallizing. The number of folds ( $NF$ ) tends to decrease with the increase of PLA in the copolyesters, with the exception of the last composition, where the lamellar thickness ( $l$ ) is so small due to the low crystallinity of the material that the average shorter chain can fold several times and does not follow the trend of the rest of materials. Figure 4.16 schematically shows the behavior described above.

**Table 4.3** Long Period ( $d^*$ ), Crystalline Fraction ( $X_c$ ), Lamellar Thickness ( $l$ ), Number average sequential length ( $L_T$ ), Chain Length ( $L$ ) and Number of Folds ( $NF$ ).

Sample	$d^*$	$X_c$		$l$ (nm)		$L_T$	$L$ (nm)	$NF$	
		WAXS	DSC	WAXS	DSC			WAXS	DSC
PET	11.210	0.31	0.36	3.5	4.1	---	29	8.4	7.1
PET <sub>95</sub> PLLA <sub>05</sub>	10.728	0.30	0.38	3.2	4.1	19.1	21	6.4	5.1
PET <sub>88</sub> PLLA <sub>12</sub>	10.764	0.29	0.34	3.1	3.7	8.7	9	3	2.8
PET <sub>84</sub> PLLA <sub>16</sub>	10.309	0.22	0.32	2.3	3.3	5.4	6	2.6	1.8
PET <sub>76</sub> PLLA <sub>24</sub>	9.834	0.09	0.08	0.90	0.8	3.6	4	4.4	5.0

- Values of  $X_c$  and  $d^*$  calculated with data from WAXS and SAXS respectively at 25 °C.

- Values of  $L_T$  calculated by NMR.

- For Copolymers  $L = L_T * 10.75 \text{ \AA}$  (from unit cell of PET).<sup>34</sup>

- In case of PET  $L = (Mn \text{ by NMR} / 192) * 10.75 \text{ \AA}$ .

-  $NF = L/l$  from this table.

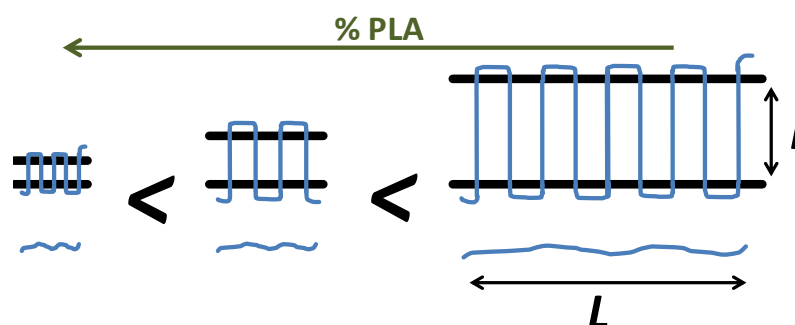


**Figure 4.16.** Changes in ( $l$ ) and ( $L$ ) as a function of the amount of PLA in the copolymer. The scheme depicts how chain segments crystallize within the random PET-*ran*-PLA copolymers.

### 4.3.5 Hydrolytic Degradation of Copolymers

Selected samples were subjected to hydrolytic degradation, as indicated in the experimental part. The samples were periodically examined by NMR during 10 weeks exposure to a phosphate buffer solution. Figure 4.17 shows how the PLA content in mol% changes in the copolymers with incubation time. Except for the copolymer sample with only 5% PLA, all others exhibit a decrease in PLA content as incubation time increases. This indicates that the PLA repeating units covalently linked to PET repeating units in the copolymers can be degraded by hydrolysis, thus showing the partially degradable character of these copolymers.

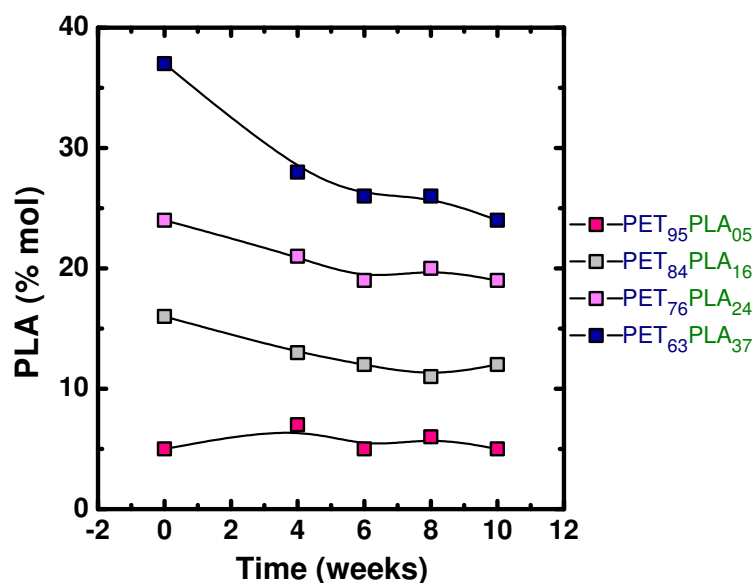


**Figure 4.17.** PLA content in the indicated copolymer samples determined by NMR as a function of incubation time in a phosphate buffer (pH=7.4) solution at 37 °C.

## 4.4 Conclusions

In this work, new PET materials potentially susceptible to hydrolytic degradation were synthesized using organocatalysis, following a sustainable synthetic route, where PET was copolymerized with bio-based PLA. The random copolymerization was confirmed by  $^1\text{H}$  NMR and FTIR. Different PET-*ran*-PLA copolymers were prepared and the structure, morphology and crystallization of the PET component were studied. By DSC and WAXS it was found that the PET component within the PET-*ran*-PLA copolymers was able to crystallize up to 24 mol % of PLA. Nevertheless, the quality and quantity of these crystals were significantly affected by the PLA content which considerably reduced the crystallization kinetics, as well as the lamellar thickness measured by isothermal crystallization from the melt and SAXS respectively. A novel result found, was the radical change from nucleation to diffusion control, in the temperature dependence of the overall isothermal crystallization rate, when the PLA content approached the maximum tolerable limit for PET crystallization. It was found that the morphology of PET crystals could change from micron size spherulites to axialites when increasing the PLA content, as the nucleation rate also increased considerably by PLA incorporation.

Finally, preliminary hydrolytic degradation experiments were able to demonstrate the partial degradation character of the prepared copolymers, as the PLA component undergoes hydrolysis in a buffer phosphate at 37 °C after a few weeks incubation time.

In addition, this work shows a way to take advantage of monomers derived from chemical recycling of PET (such as DMT) to synthesize copolymers, giving an added value to the waste generated from PET. On the other hand, the use of a bio-based polymer, such as PLA that is obtained from renewable sources and is biodegradable, leaves a lower ecological footprint than non-bio-based polymers. And all the above in conjunction with the use of organic catalysts (metal-free) contributes to finding synthetic paths that respect as much as possible the environment.

## 4.5 References

- (1) Rahimi, A.; García, J. M. Chemical Recycling of Waste Plastics for New Materials Production. *Nature Reviews Chemistry* **2017**, *1* (6), 0046. <https://doi.org/10.1038/s41570-017-0046>.
- (2) Sousa, A. F.; Vilela, C.; Matos, M.; Freire, C. S. R.; Silvestre, A. J. D.; Coelho, J. F. J. Polyethylene Terephthalate: Copolyesters, Composites, and Renewable Alternatives. In *Poly(Ethylene Terephthalate) Based Blends, Composites and Nanocomposites*; Elsevier, 2015; pp 113–141. <https://doi.org/10.1016/B978-0-323-31306-3.00007-5>.
- (3) Sinha, V.; Patel, M. R.; Patel, J. V. Pet Waste Management by Chemical Recycling: A Review. *Journal of Polymers and the Environment* **2010**, *18* (1), 8–25. <https://doi.org/10.1007/s10924-008-0106-7>.
- (4) Plastics Europe; EPRO. *Plásticos: Situación 2017*; 2018; p 47.
- (5) Zhang, X.; Fevre, M.; Jones, G. O.; Waymouth, R. M. Catalysis as an Enabling Science for Sustainable Polymers. *Chemical Reviews* **2018**, *118* (2), 839–885. <https://doi.org/10.1021/acs.chemrev.7b00329>.
- (6) Castro-Aguirre, E.; Iñiguez-Franco, F.; Samsudin, H.; Fang, X.; Auras, R. Poly(Lactic Acid)—Mass Production, Processing, Industrial Applications, and End of Life. *Advanced Drug Delivery Reviews* **2016**, *107*, 333–366. <https://doi.org/10.1016/j.addr.2016.03.010>.
- (7) Namkajorn, M.; Petchsuk, A.; Opaprakasit, M.; Opaprakasit, P. Synthesis and Characterizations of Degradable Aliphatic-Aromatic Copolyesters from Lactic Acid, Dimethyl Terephthalate and Diol: Effects of Diol Type and Monomer Feed Ratio. *Express Polymer Letters* **2010**, *4* (7), 415–422. <https://doi.org/10.3144/expresspolymlett.2010.52>.
- (8) Ben Gara, M.; Kammoun, W.; Delaite, C. Synthesis and Characterization of Aliphatic-Aromatic Copolyesters PET-PLA from PET Waste and Lactide. *Journal of New Technology and Materials* **2016**, *6* (1), 42–48. <https://doi.org/10.12816/0043923>.
- (9) Acar, I.; Kaşgöz, A.; Özgümüş, S.; Orbay, M. Modification of Waste Poly(Ethylene Terephthalate) (PET) by Using Poly(L-Lactic Acid) (PLA) and Hydrolytic Stability.

- Polymer-Plastics Technology and Engineering* **2006**, 45 (3), 351–359.  
<https://doi.org/10.1080/03602550600553267>.
- (10) Buasri, A.; Juengrungchaiwattana, S. Preparation and Characterization of PET-PLA Copolyester from Waste PET and Lactic Acid (LA). *Chiang Mai J. Sci.* **2011**, 38, 619–624.
- (11) Opaprakasit, M.; Petchsuk, A.; Opaprakasit, P.; Chongprakobkit, S. Effects of Synthesis Conditions on Chemical Structures and Physical Properties of Copolyesters from Lactic Acid, Ethylene Glycol and Dimethyl Terephthalate. *Express Polymer Letters* **2009**, 3 (7), 458–468.  
<https://doi.org/10.3144/expresspolymlett.2009.56>.
- (12) Olewnik, E.; Czerwiński, W.; Nowaczyk, J.; Sepulchre, M.-O.; Tessier, M.; Salhi, S.; Fradet, A. Synthesis and Structural Study of Copolymers of L-Lactic Acid and Bis(2-Hydroxyethyl Terephthalate). *European Polymer Journal* **2007**, 43 (3), 1009–1019.  
<https://doi.org/10.1016/j.eurpolymj.2006.11.025>.
- (13) Kumar, K. S.; Selvaraj, V.; Alagar, M. Synthesis of PET-PLA/Drug Nanoparticles and Their Effect with Gold Nanoparticles for Controlled Drug Release in Cancer Chemotherapy. *Research Letters in Nanotechnology* **2008**, 2008, 1–4.  
<https://doi.org/10.1155/2008/389512>.
- (14) Shaikh, I. R. Organocatalysis: Key Trends in Green Synthetic Chemistry, Challenges, Scope towards Heterogenization, and Importance from Research and Industrial Point of View. *Journal of Catalysts* **2014**, 2014, 1–35.  
<https://doi.org/10.1155/2014/402860>.
- (15) Jehanno, C.; Flores, I.; Dove, A. P.; Müller, A. J.; Ruipérez, F.; Sardon, H. Organocatalysed Depolymerisation of PET in a Fully Sustainable Cycle Using Thermally Stable Protic Ionic Salt. *Green Chemistry* **2018**, 20 (6), 1205–1212.  
<https://doi.org/10.1039/C7GC03396F>.
- (16) Hu, S.; Zhao, J.; Zhang, G.; Schlaad, H. Macromolecular Architectures through Organocatalysis. *Progress in Polymer Science* **2017**, 74, 34–77.  
<https://doi.org/10.1016/j.progpolymsci.2017.07.002>.
- (17) Ottou, W. N.; Sardon, H.; Mecerreyes, D.; Vignolle, J.; Taton, D. Update and Challenges in Organo-Mediated Polymerization Reactions. *Progress in Polymer Science* **2016**, 56, 64–115. <https://doi.org/10.1016/j.progpolymsci.2015.12.001>.

- (18) Kadota, J.; Pavlović, D.; Hirano, H.; Okada, A.; Agari, Y.; Bibal, B.; Deffieux, A.; Peruch, F. Controlled Bulk Polymerization of L-Lactide and Lactones by Dual Activation with Organo-Catalytic Systems. *RSC Advances* **2014**, *4* (28), 14725. <https://doi.org/10.1039/c4ra01239a>.
- (19) Mezzasalma, L.; Dove, A. P.; Coulembier, O. Organocatalytic Ring-Opening Polymerization of L-Lactide in Bulk: A Long Standing Challenge. *European Polymer Journal* **2017**, *95*, 628–634. <https://doi.org/10.1016/j.eurpolymj.2017.05.013>.
- (20) Radzinski, S. C.; Foster, J. C.; Matson, J. B. Preparation of Bottlebrush Polymers via a One-Pot Ring-Opening Polymerization (ROP) and Ring-Opening Metathesis Polymerization (ROMP) Grafting-Through Strategy. *Macromolecular Rapid Communications* **2016**, *37* (7), 616–621. <https://doi.org/10.1002/marc.201500672>.
- (21) Qin, Y.; Zhu, L.; Luo, S. Organocatalysis in Inert C–H Bond Functionalization. *Chemical Reviews* **2017**, *117* (13), 9433–9520. <https://doi.org/10.1021/acs.chemrev.6b00657>.
- (22) Flores, I.; Demarteau, J.; Müller, A. J.; Etxeberria, A.; Irusta, L.; Bergman, F.; Koning, C.; Sardon, H. Screening of Different Organocatalysts for the Sustainable Synthesis of PET. *European Polymer Journal* **2018**, *104*, 170–176. <https://doi.org/10.1016/j.eurpolymj.2018.04.040>.
- (23) Coady, D. J.; Fukushima, K.; Horn, H. W.; Rice, J. E.; Hedrick, J. L. Catalytic Insights into Acid/Base Conjugates: Highly Selective Bifunctional Catalysts for the Ring-Opening Polymerization of Lactide. *Chemical Communications* **2011**, *47* (11), 3105. <https://doi.org/10.1039/c0cc03987j>.
- (24) Bartolome, L.; Imran, M.; Gyoo, B.; A., W.; Hyun, D. Recent Developments in the Chemical Recycling of PET. In *Material Recycling - Trends and Perspectives*; Achilias, D., Ed.; InTech, 2012. <https://doi.org/10.5772/33800>.
- (25) Du, S.; Valla, J. A.; Parnas, R. S.; Bollas, G. M. Conversion of Polyethylene Terephthalate Based Waste Carpet to Benzene-Rich Oils through Thermal, Catalytic, and Catalytic Steam Pyrolysis. *ACS Sustainable Chemistry & Engineering* **2016**, *4* (5), 2852–2860. <https://doi.org/10.1021/acssuschemeng.6b00450>.

- (26) Al-Sabagh, A. M.; Yehia, F. Z.; Eshaq, Gh.; Rabie, A. M.; ElMetwally, A. E. Greener Routes for Recycling of Polyethylene Terephthalate. *Egyptian Journal of Petroleum* **2016**, *25* (1), 53–64. <https://doi.org/10.1016/j.ejpe.2015.03.001>.
- (27) Sharma, V.; Parashar, P.; Srivastava, P.; kumar, S.; Agarwal, D. D.; Richharia, N. Recycling of Waste PET-Bottles Using Dimethyl Sulfoxide and Hydrotalcite Catalyst. *Journal of Applied Polymer Science* **2013**, *129* (3), 1513–1519. <https://doi.org/10.1002/app.38829>.
- (28) Sriromreun, P.; Opaprakasit, P. Miscibility and Hydrolytic Degradability of Polylactic Acid/Poly (Ethylene Terephthalate-Co-Lactic Acid) Blends. *Chiang Mai J. Sci.* **2014**, *41*, 691–703.
- (29) Coudane, J.; Ustariz-Peyret, C.; Schwach, G.; Vert, M. More about the Stereodependence OfDD AndLL Pair Linkages during the Ring-Opening Polymerization of Racemic Lactide. *Journal of Polymer Science Part A: Polymer Chemistry* **1997**, *35* (9), 1651–1658. [https://doi.org/10.1002/\(SICI\)1099-0518\(19970715\)35:9<1651::AID-POLA6>3.0.CO;2-U](https://doi.org/10.1002/(SICI)1099-0518(19970715)35:9<1651::AID-POLA6>3.0.CO;2-U).
- (30) Deng, L.-M.; Wang, Y.-Z.; Yang, K.-K.; Wang, X.-L.; Zhou, Q.; Ding, S.-D. A New Biodegradable Copolyester Poly(Butylene Succinate-Co-Ethylene Succinate-Co-Ethylene Terephthalate). *Acta Materialia* **2004**, *52* (20), 5871–5878. <https://doi.org/10.1016/j.actamat.2004.09.002>.
- (31) Li, X.; Liu, R.; Zhong, L.; Gu, L. Antielectrostatic Poly(Ether Ester) Block Copolymer of Poly(Ethylene Terephthalate-Co-Isophthalate)-Poly(Ethylene Glycol). *Journal of Applied Polymer Science* **2003**, *89* (6), 1696–1701. <https://doi.org/10.1002/app.12311>.
- (32) Coleman, D. Block Copolymers: Copolymerization of Ethylene Terephthalate and Polyoxyethylene Glycols. *Journal of Polymer Science* **1954**, *14* (73), 15–28. <https://doi.org/10.1002/pol.1954.120147303>.
- (33) Müller, A. J.; Ávila, M.; Saenz, G.; Salazar, J. Crystallization of PLA-Based Materials. In *Poly(lactic acid) Science and Technology*; Cambridge, UK, 2015; pp 66–98.
- (34) de P. Daubeny, R.; Bunn, C. W. The Crystal Structure of Polyethylene Terephthalate. *Proceedings of the Royal Society A: Mathematical, Physical and Engineering Sciences* **1954**, *226* (1167), 531–542. <https://doi.org/10.1098/rspa.1954.0273>.

- (35) Lu, X. F.; Hay, J. N. Isothermal Crystallization Kinetics and Melting Behaviour of Poly(Ethylene Terephthalate). *Polymer* **2001**, *42* (23), 9423–9431. [https://doi.org/10.1016/S0032-3861\(01\)00502-X](https://doi.org/10.1016/S0032-3861(01)00502-X).
- (36) Rwei, S. P.; Lin, W. P.; Wang, J. F. Synthesis and Characterization of Biodegradable and Weather-Durable PET/PEG/NDC Copolymers. *Colloid and Polymer Science* **2012**, *290* (14), 1381–1392. <https://doi.org/10.1007/s00396-012-2662-6>.
- (37) Tan, L. C.; Zhou, W. H.; Huang, Y. L.; Chen, Y. W. Sequential Structure, Crystallization, and Properties of Biodegradable Poly(Ethylene Terephthalate-Co-Ethylene Oxide-Co-Lactide) Copolyester. *Journal of Macromolecular Science, Part B* **2014**, *53* (7), 1231–1243. <https://doi.org/10.1080/00222348.2014.901870>.
- (38) Canetti, M.; Bertini, F. Crystalline and Supramolecular Structure Evolution of Poly(Ethylene Terephthalate) during Isothermal Crystallization and Annealing Treatment by Means of Wide and Small Angle X-Ray Investigations. *European Polymer Journal* **2010**, *46* (2), 270–276. <https://doi.org/10.1016/j.eurpolymj.2009.10.019>.
- (39) Zhao, M. L.; Li, F. X.; Yu, J. Y.; Wang, X. L. Preparation and Characterization of Poly(Ethylene Terephthalate) Copolyesters Modified with Sodium-5-Sulfo-Bis-(Hydroxyethyl)-Isophthalate and Poly(Ethylene Glycol). *Journal of Applied Polymer Science* **2014**, *131* (3), 1–9. <https://doi.org/10.1002/app.39823>.
- (40) Chen, B.; Gu, L. Isothermal Crystallization and Melting Behavior of 2-Methyl-1,3-Propanediol Substituted Sulfonated Poly(Ethylene Terephthalate) Copolyesters. *Journal of Applied Polymer Science* **2010**, *117* (4), 2454–2463. <https://doi.org/10.1002/app.32119>.
- (41) Wang, Z. G.; Hsiao, B. S.; Fu, B. X.; Liu, L.; Yeh, F.; Sauer, B. B.; Chang, H.; Schultz, J. M. Correct Determination of Crystal Lamellar Thickness in Semicrystalline Poly(Ethylene Terephthalate) by Small-Angle X-Ray Scattering. *Polymer* **2000**, *41* (5), 1791–1797. [https://doi.org/10.1016/S0032-3861\(99\)00327-4](https://doi.org/10.1016/S0032-3861(99)00327-4).
- (42) Van Krevelen D. W.; Te Nijenhuis K. *Properties of Polymers: Their Correlation with Chemical Structure; Their Numerical Estimation and Prediction from Additive Group Contributions*, fourth.; Elsevier: Oxford, 2009.

- 
- (43) Müller, A. J.; Michell, R. M.; Lorenzo, A. T. Isothermal Crystallization Kinetics of Polymers. In *Polymer Morphology*; Guo, Q., Ed.; John Wiley & Sons, Inc: Hoboken, NJ, USA, 2016; pp 181–203. <https://doi.org/10.1002/9781118892756.ch11>.
- (44) Schultz, J. M. *Polymer Crystallization: The Development of Crystalline Order in Thermoplastic Polymers*; Oxford University Press: Oxford, 2001.
- (45) Avrami, M. Granulation, Phase Change, and Microstructure Kinetics of Phase Change. III. *The Journal of Chemical Physics* **1941**, *9* (2), 177–184. <https://doi.org/10.1063/1.1750872>.
- (46) Lorenzo, A. T.; Arnal, M. L.; Albuerne, J.; Müller, A. J. DSC Isothermal Polymer Crystallization Kinetics Measurements and the Use of the Avrami Equation to Fit the Data: Guidelines to Avoid Common Problems. *Polymer Testing* **2007**, *26* (2), 222–231. <https://doi.org/10.1016/j.polymertesting.2006.10.005>.
- (47) Lauritzen, J. I.; Hoffman, J. D. Theory of Formation of Polymer Crystals with Folded Chains in Dilute Solution. *Journal of Research of the National Bureau of Standards Section A: Physics and Chemistry* **1960**, *64A* (1), 73. <https://doi.org/10.6028/jres.064A.007>.
- (48) Lorenzo, A. T.; Müller, A. J. Estimation of the Nucleation and Crystal Growth Contributions to the Overall Crystallization Energy Barrier. *Journal of Polymer Science Part B: Polymer Physics* **2008**, *46* (14), 1478–1487. <https://doi.org/10.1002/polb.21483>.
- (49) Van Krevelen D. W. *Properties of Polymers. Chapter 5: Calorimetric Properties.*, Third.; Elsevier: Amsterdam, 1997.

---

# Chapter 5

---

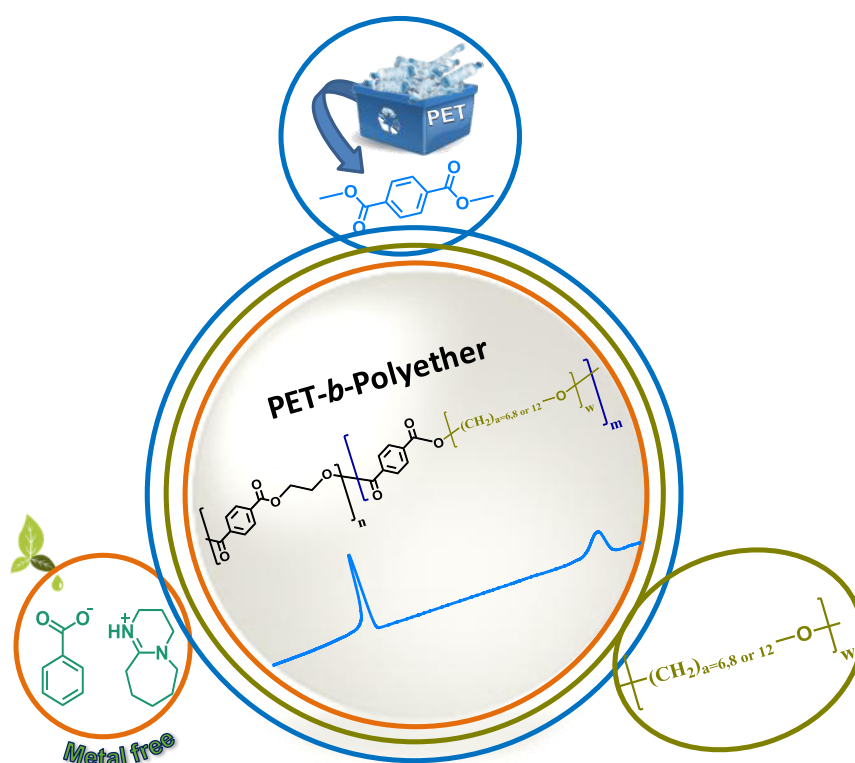
## *Organocatalyzed Polymerization of PET-*b*-Polyether Copolymers*

5.1 Abstract.....	106
5.2 Introduction.....	107
5.3 Results and Discussion.....	109
5.3.1 Synthesis and Characterization of Copolymers .....	109
5.3.2 Non-isothermal Properties.....	113
5.3.2.1 Phase Separation in Block Copolymers.....	118
5.3.3 Isothermal Crystallization Kinetics.....	120
5.3.4 Determination of Parameters derived by WAXS.....	128
5.3.5 Determination of Parameters derived by SAXS.....	130
5.3.6 Morphology.....	138
5.4 Conclusions.....	141
5.5 References.....	142

## 5.1 Abstract

Several works have studied the copolymerization of PET with other polymers with the intention of modifying the properties of PET and making functional materials for applications in which neat PET could not be used. In this work, PET was copolymerized with polyether, following a green synthetic route. PET was polymerized using dimethyl terephthalate (a monomer that can be derived from chemically recycling PET waste) and using an organic catalyst (metal-free catalyst).

New materials (multiblock copolymers) were synthesized, where each copolymer combines the properties of the two homopolymers (PET and polyether) and exhibits properties different from those shown individually by the homopolymers. Characterization techniques such as NMR, TGA, DSC, flash DSC, DMTA, WAXS and SAXS were used to analyze the synthesized copolymers. The thermal properties and the crystallization of these materials are strongly affected by the PET/Polyether composition. For some compositions double crystalline materials were successfully obtained. The copolymers showed a single phase in the melt state and one phase segregation in the amorphous state. All copolymers present a micro-spherulitic morphology.



## 5.2 Introduction

The trend to combine two or more homopolymers with the expectation of obtaining new materials (copolymers) with different properties from those of the parent homopolymers has increased. In this sense, as polyethylene terephthalate (PET) is one of the most popular polymers in the manufacture of multiple products, it has been the subject of a large amount of research where it has been copolymerized with various polymers to modify its properties, for example crystallinity, degradability and degree of hydrophilicity, among others.<sup>1</sup>

One possibility is to copolymerize PET with other low molecular weight polyols in order to impart different properties to the PET. Among the different copolymers studied, poly(ether ester) copolymers are a kind of interesting synthetic target because they have a "hard" segment corresponding to PET (high  $T_g$  and  $T_m$ ) and another "soft" segment corresponding to the polyether with (low  $T_g$  and  $T_m$ ).<sup>2</sup> This union results in a new material whose properties are not a simple function of the individual components.<sup>2,3</sup> Moreover, the soft segment of polyethers and the hard segments of PET can coexist providing in some cases improvement in the mechanical properties, toughness or chemical resistance of PET.<sup>4</sup> Due to the above, these materials have aroused scientific and industrial interest, since they exhibit a rich variety of thermal behaviors that are related to the composition and chemical structure characteristic of the segmented copolymer.<sup>2,3,5,6</sup> However, to employ these materials in potential applications, a basic understanding of their properties is necessary.

For instance, in the middle of the 20th century, Coleman copolymerized PET with a polyether (polyethylene glycol, PEG) with the intention that PET in fiber form would be more hydrophilic and therefore easier to colour.<sup>7</sup> These copolymers (PET-co-PEG) have been studied by researchers whose work has focused on several aspects (biodegradability, phase-change characteristics and shape-memory effects, in addition to hydrophilicity).<sup>3,5,6,8-11</sup>

Understanding the behavior of these copolymers is complex, because several probable reactions can occur in the process of formation of the copolymer and this generates a large number of heterogeneities (several unions between the initial monomers).<sup>6</sup> On the other hand, the crystallization of copolymers with two

crystallizable blocks (PET and PEG), has been studied in some works.<sup>3,6,10</sup> In these systems where both segments (hard and soft) in the copolymer are able to crystallize, the crystallization process is complex because each component (segment) affects the properties of the other and vice versa, depending on composition.<sup>2,3,10</sup> This means that the copolymer structure can be manipulated and the properties of the material to be obtained can be optimized, adapting them to specific applications.<sup>8,9,11</sup>

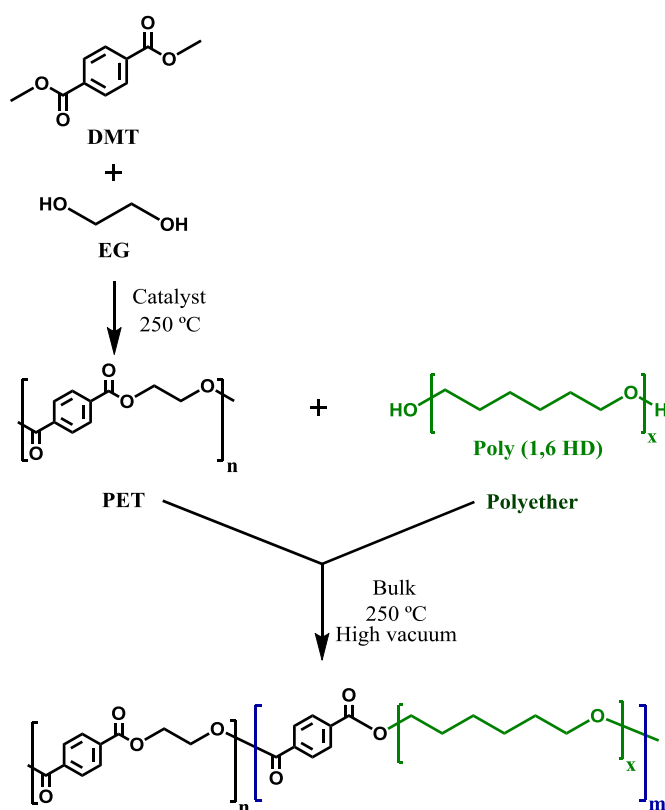
Normally, poly(ether ester) copolymers are synthesized by condensation polymerization of relatively low molecular weight telechelic polyether diols with polyester monomers at high temperatures.<sup>2,4,8,9</sup> This process produces multiblock copolymers with polyester which have shown the ability to co-crystallize. The multiblock copolymers show double crystallinity and properties from the polyether and PET segments, as revealed by DSC experiments. To date, all the multiblock poly(ether ester) copolymers are based on polyethers with 2,3 or 4 methylene units.<sup>2,4-6,9,12</sup> The main reason behind this limitation is that telechelic polyethers have been solely prepared by the ring-opening polymerization of the corresponding cyclic ethers, such as oxiranes, oxetanes, or tetrahydrofuran and using the aforementioned method, larger size polyethers cannot be obtained because of the extreme stability of the cyclic ethers.<sup>13-15</sup> Recently attention has been paid for the preparation of medium-to-long aliphatic polyethers by the bulk self-condensation of alcohols. This method allows the preparation of telechelic polyethers with a number of methylene units ranging from 6 to 12 units and melting temperatures between 54 and 85 °C.<sup>16</sup>

In this work PET and Polyether multiblock copolymers have been prepared using telechelic polyether based on 6 methylene units. The copolymers were prepared using an organic catalyst (DBU:BA). It is expected that using telechelic polyethers with different methylene units the melting temperature of the soft polyether segment could be varied on demand obtaining double crystalline poly(ether ester) copolymers with tunable melting temperature. To understand the behavior of these materials, the effect of the PET/polyether composition on the thermal properties of each of the segmented copolymers obtained is analyzed.

## 5.3 Results and Discussion

### 5.3.1 Synthesis and Characterization of Copolymers

With the intention of using organocatalysis to promote the copolymerization of PET with polyether, an organic catalyst (DBU:BA) was selected based on its demonstrated effectiveness in the homopolymerization of PET and the copolymerization of PET with other polyesters.<sup>17</sup> The synthesis of PET-*mb*-Polyether copolymers by several stages was carried out. First, the dimethyl terephthalate (DMT) was reacted with excess ethylene glycol (EG) in the presence of an organocatalyst (DBU:BA) forming oligomers of PET for 1.5 h. Then, the polyether was added to PET oligomers (Scheme 5.1) to complete the copolymerization. The Polyether has been synthesized by the step-growth polymerization of 1,6 diols in the presence of MSA:TBD catalyst as previously described.<sup>16</sup> In order to obtain Poly (ether ester) copolymers able to co-crystallize polyether with molecular weight of 3468 (g/mol) was employed in the copolymerization.



**Scheme 5.1.** Organocatalyzed Synthesis of PET-*mb*-Polyether.

To confirm the copolymerization between PET and the polyether  $^1\text{H}$  and  $^{13}\text{C}$  NMR were used. Figure 5.1 shows an  $^1\text{H}$  NMR spectrum of a copolymer of PET with Poly (1,6 HD). After performing the polymerization, the characteristic peaks from PET units (4.78 ppm,  $\text{COO-CH}_2\text{-CH}_2\text{-OCO}$ ) and Poly (1,6 HD) units (3.63 ppm,  $-\text{O}[\text{CH}_2\text{-(CH}_2)_4\text{-CH}_2\text{-O-}]$ , 1.63 ppm,  $-\text{O}[\text{CH}_2\text{-CH}_2\text{-(CH}_2)_2\text{-CH}_2\text{-CH}_2\text{-O-}]$  and 1.34 ppm,  $-\text{O}[(\text{CH}_2)_2\text{-CH}_2\text{-CH}_2\text{-(CH}_2)_2\text{-O-}]$  could be appreciated in Figure 5.1.<sup>16,17</sup> In addition, a new peak could be observed in the  $^1\text{H}$  NMR spectra related to the PET-*mb*-Polyether links at 4.40 ppm (peak 1) assigned to *Terephthalate-Polyether* ( $\text{Ar-CH-COO-CH}_2\text{-CH}_2\text{-CH}_2\text{-CH}_2\text{-CH}_2\text{-CH}_2\text{-O-}$ ).<sup>9</sup> On the other hand, the peak around 8.12 ppm suggest the presence of PET-*mb*-Polyether links corresponding to *Terephthalate-Polyether* ( $\text{Ar-CH-COO}[\text{CH}_2]_6\text{-O-}$ ) and *Terephthalate-Ethylene glycol-Polyether* ( $\text{Ar-CH-COO-CH}_2\text{-CH}_2\text{-O}[\text{CH}_2]_6\text{-O-}$ ). However, in this position the signal of PET-*mb*-Polyether link seems to be overlapped with the Ar-CH signal corresponding to neat PET. Therefore, it is not convincingly possible to assign a single signal to this position.

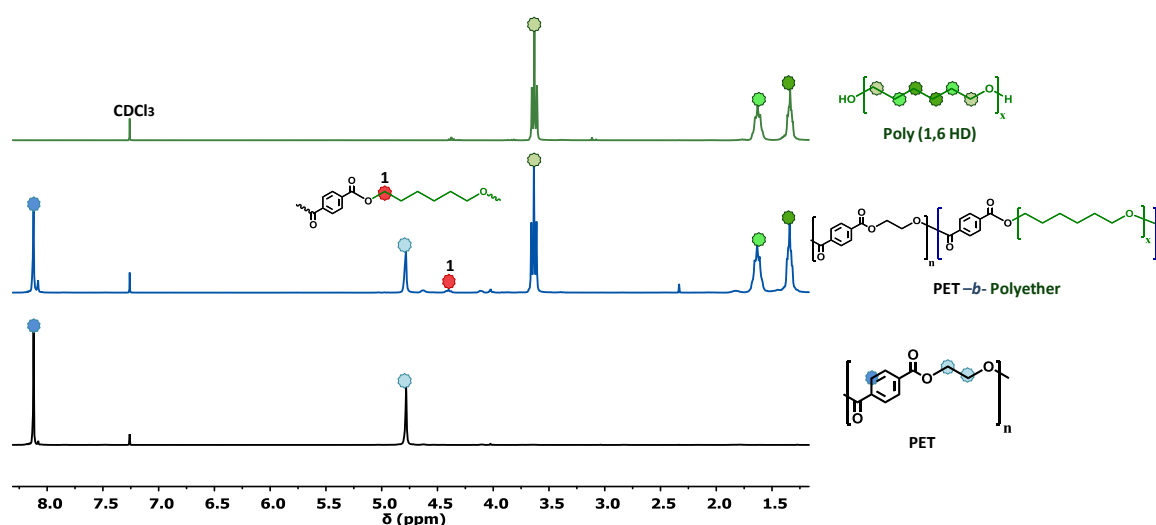


**Figure 5.1.**  $^1\text{H}$  NMR spectrum of  $\text{PET}_{34}\text{Poly}(1,6 \text{ HD})_{66}$  in  $\text{CDCl}_3/\text{TFA}$ .

With the purpose of showing more clearly the PET bonds with polyether,  $^{13}\text{C}$  NMR tests were carried out. Some of these spectra are shown in Figure 5.2. Starting at the signal corresponding to quaternary C of the aromatic ring, a different chemical environment of the copolymer dyads is reflected. The signals at 134.55 and 134.19 ppm correspond to Polyether-*Terephthalate*-Polyether (PE-PE) and Ethylene glycol-*Terephthalate*-Ethylene glycol dyads (EG-EG), respectively, while the signals at 134.77

and 133.97 ppm correspond to interchange dyads: Polyether-*Terephthalate*-Ethylene glycol (PE-EG or EG-PE). However, due to the fact that only copolymers rich in polyether (%mol superior to 10) showed clearly these signals, two additional copolymers were synthesized in order to characterize adequately the copolymer microstructure: PET<sub>03</sub>Poly(1,6 HD)<sub>97</sub> and PET<sub>01</sub>Poly(1,6 HD)<sub>99</sub>. The spectra of these latter compositions are shown in Figure 5.2, in addition, in this figure it is appreciated that when the amount of polyether increases in the sample, the signal at 134.19 ppm decreases, while the signal at 134.55 ppm increases.

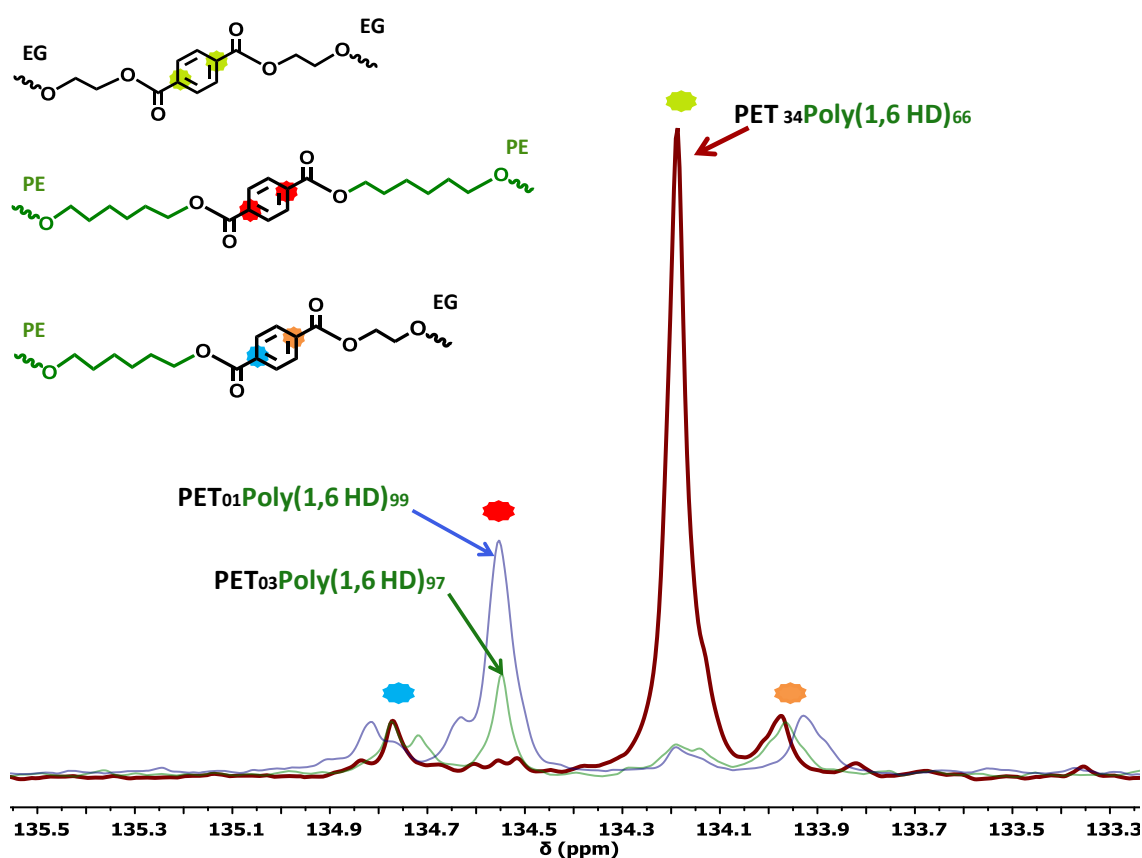


**Figure 5.2.**  $^{13}\text{C}$  NMR spectrum of PET-*mb*-Poly(1,6 HD) in  $\text{CDCl}_3/\text{TFA}$ .

Once the successful copolymerization of PET with Polyether was demonstrated, copolymers with different compositions PET-*mb*-Poly (1,6 HD) were prepared, with the intention of comparing the properties of the copolymers and verifying if the composition affects significantly the properties of the materials obtained.

The experimental values of number average sequential length ( $L_i$ ) and the degree of the randomness ( $\eta$ ) were obtained using data from  $^{13}\text{C}$  NMR (equations in

Annex C). However, these experimental values were determined only for the three copolymers shown in the Figure 5.2 (see Table C.1, Annex C) due to the factor, that the intensities of the signals corresponding to the interchange PE-EG dyad were very small in the copolymers with less than 9 % mole of polyether. Thus, the error involved in the calculation of the  $L_i$  and  $\eta$  parameters was large leading to erroneous values.

In Table C.1 (Annex C), it is appreciated that for the copolymers shown in Figure 5.2 the value of  $\eta$  tends to 1 indicating that ethylene glycol and polyether are reacting randomly with terephthalic units. Taking into account the polymeric nature of polyether, the random reaction leads to the formation of a multi-block copolymer, where each of the different blocks forming the copolymer are randomly distributed. Considering that all the obtained experimental values of  $\eta$  were close to 1, for compositions of 9 to 80 mol% of polyether present in the copolymer, it seems feasible to suppose that copolymers with a molar percentage of polyether between 0 and 9 % will also have a random character. This assumption allows calculating the theoretical number of average sequence length for copolymers with molar percentages lower than 9 % of polyether. The results are shown in Table 5.1. In the case of PET-*mb*-Poly(1,6 HD) copolymers, the parameter  $L_{EG}$ , which represents units of PET, decreases from 38 to 10, in a range of Poly(1,6 HD) content from 0 to 10 mol%, while  $L_{PE}$  varies from 1 to 1.1, which means that practically all the polyether units are isolated.

**Table 5.1** Composition, Number average sequential length and Intrinsic Viscosity of Polymers.

Sample	PET / Polyether		Number average sequential length <sup>a</sup>		$\eta^a$	I.V. <sup>b</sup> (dL/g)	Mn <sup>c</sup> KDa
	% mass ratio <sup>a</sup>	% mol ratio <sup>a</sup>	$L_{EG}$ (PET)	$L_{PE}$ (Polyether)			
PET	100/0	100/0	---	---	---	0.23 ( $\pm$ 0.02)	3.5
PET <sub>68</sub> Poly(1,6 HD) <sub>32</sub>	68/32	97.4/2.6	38.6	1.03	---	0.31 ( $\pm$ 0.01)	4.9
PET <sub>64</sub> Poly(1,6 HD) <sub>36</sub>	64/36	97/03	33.4	1.03	---	0.40 ( $\pm$ 0)	5.0
PET <sub>61</sub> Poly(1,6 HD) <sub>39</sub>	61/39	96.5/3.5	28.9	1.04	---	0.42 ( $\pm$ 0.02)	4.9
PET <sub>34</sub> Poly(1,6 HD) <sub>66</sub>	34/66	90/10	10.4	1.11	0.99	0.45 ( $\pm$ 0.01)	4.4
Poly(1,6 HD)	0/100	0/100	---	---	---	0.10 ( $\pm$ 0.02)	---

<sup>a</sup>Calculated by NMR only for PET<sub>34</sub>Poly(1,6 HD)<sub>66</sub> sample. For the rest of copolymers, assuming their random character, theoretical values are given. In the case of  $L_{PE}$  the second decimal is given in order to show the produced small changes. <sup>b</sup>Measured by viscosimetry. <sup>c</sup>Determined by GPC in HFIP against PMMA standards for PET and copolymers.

To measure the molecular weights of the copolymers by GPC, first a solvent (HFIP) that diluted both components of the copolymer (PET and polyether) was used,

however this solvent degraded the polyether and therefore the measurements obtained were erroneous. On the other hand, when a solvent ( $\text{CHCl}_3$ ) that only dissolves the polyether was used, only very low molecular weight chains were obtained and the rest of the chains remained unparsed. For this reason, the intrinsic viscosity of the materials was measured.

Table 5.1 shows the values of intrinsic viscosity (*I.V.*) for homopolymers and copolymers, it can be seen that for the series of copolymers of PET with Poly 1,6 HD the viscosity seems to increase, which could be related to an increase in molecular weight of the copolymers when the polyether is bound to PET.

The intrinsic viscosity of the copolymers obtained is generally larger than those of the homopolymers. This result can also be taken as a proof that PET and the polyether are copolymerized and as a consequence generate materials with viscosities higher than those of the parent homopolymers.

### 5.3.2 Non-isothermal Properties

The thermal stability of the obtained polymers was studied and the TGA results are reported in Figure 5.3(a). Figure 5.3(b) shows that the thermal stability of the copolymers depends on their composition. Furthermore, it is appreciated that increasing the amount of polyether in the copolymer generates a decrease in the thermal stability of the materials.

To analyze the thermal properties of the synthesized materials, tests were carried out using differential scanning calorimetry (DSC). In Figure 5.4, two types of polyethers are shown, neat Poly (1,6 HD) (without heat treatment) and Poly (1,6 HD) that was thermally treated to simulate the conditions applied during copolymer synthesis. The curves show that the  $T_m$  of the treated polyether is lower as compared to that of the untreated polyether. This is confirmed by the information reported in Table 5.2 and what is shown in Figure 5.5 (a), where it can be seen that the value of  $T_m$  and  $T_c$  are lower for the thermally treated polyether vs the untreated polyether. In addition, in Figure 5.5(b), it is also observed that the degree of crystallinity ( $X_c$ ) of the polyether decreases when it is subjected to the heat treatment. All the above indicates

that the reaction conditions (time and temperature) affect the thermal properties of the polyether.

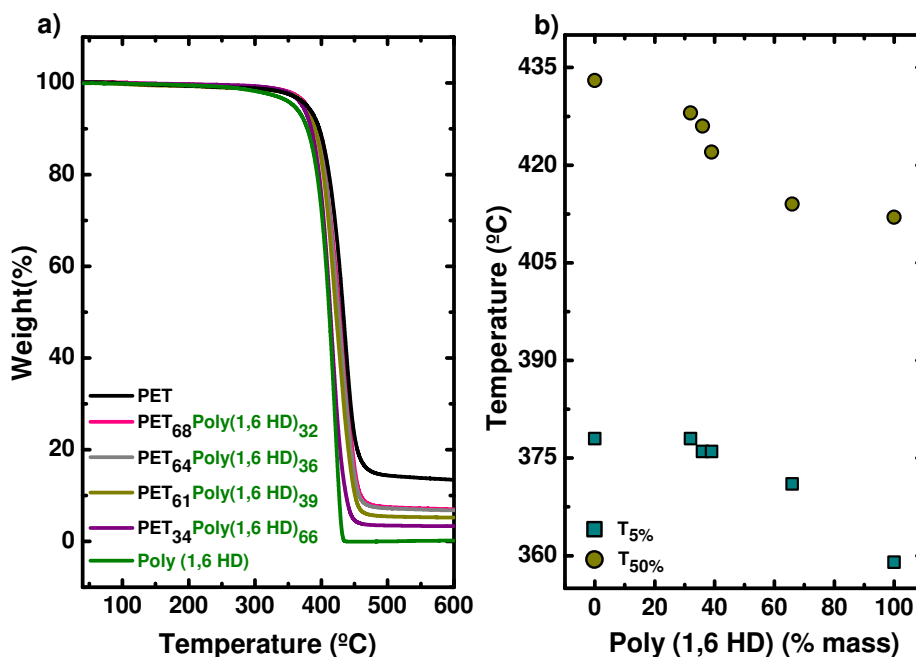


**Figure 5.3.** (a) TGA of Copolymers PET-*mb*-Poly (1,6 HD) and (b) Temperature at which the copolymers lose 5 and 50% of their weight.

PET-*mb*-PEG multi-block copolymers have been reported in the literature, where PET segments act as the crystalline region and PEG segments as the amorphous region.<sup>8,9</sup> In addition to the above, there are also some works that apart from the non-isothermal crystallization, analyze more details of the thermal behavior of these materials.<sup>2,3,5,6,8-10</sup>

So far, no PET-*mb*-polyether copolymers have been reported in the literature with a polyether of a repeating unit with more than 4 methylene groups. In this sense, this work shows copolymers of PET linked to a polyether with a chain size never used before (6 carbons), where multi-block copolymers were obtained.

In Figure 5.4, the DSC heating curves (second heating scans) obtained from the homopolymers and copolymers of PET-*mb*-Poly (1,6 HD) are reported. All compositions show curves with two melting peaks, except for the PET<sub>68</sub>Poly(1,6 HD)<sub>32</sub>. For this composition, the melting peak of the polyether phase is almost undetectable as shown in Figure 5.4 and Table 5.2. In the rest of the copolymers where two melting peaks are appreciated, one corresponds to the PET phase and the other belongs to the Polyether

(first heating and cooling are shown in Annex C). It is observed that when the amount of polyether increases in the copolymer, the peak intensity corresponding to the polyether component increases and the peak intensity corresponding to the PET component decreases.

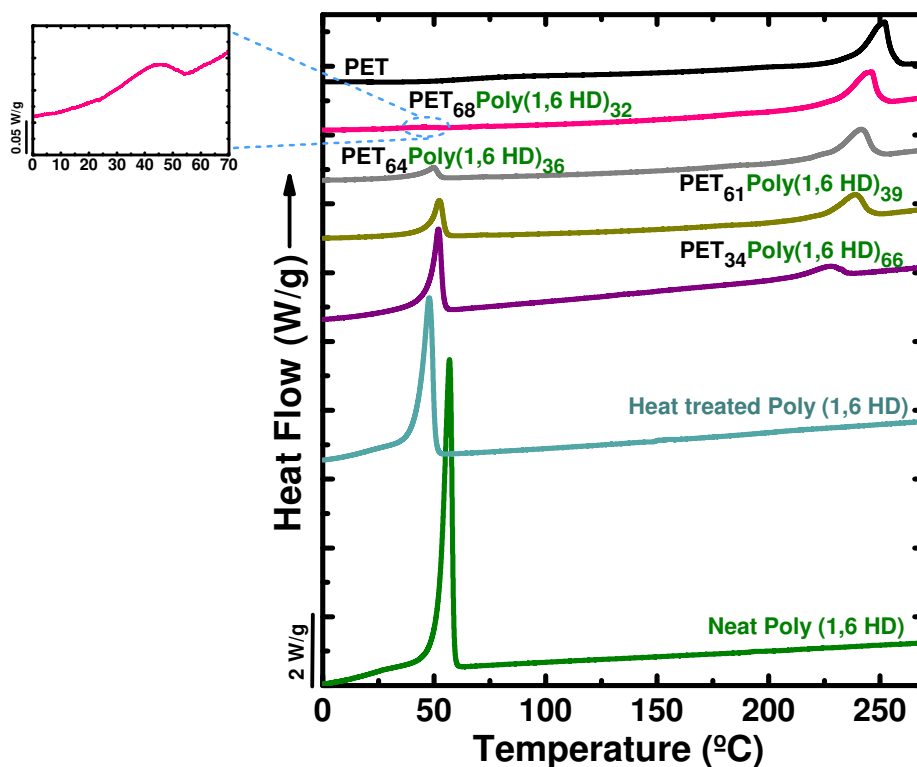


**Figure 5.4.** DSC second heating scans for the PET-*mb*-Poly (1,6 HD) copolymers and the parent homopolymers.

In addition, it is observed that when the amount of PET increases in the copolymer, the  $T_m$  of the polyether crystals decreases. This could be due to the fact that the PET phase crystallizes first upon cooling from the melt, and if its content is large, it can induce confinement effects on the polyether chains that limit its crystallization and lamellar thickness (which is proportional to  $T_m$ ). On the other hand, when the amount of polyether increases, the  $T_m$  of the PET crystals decreases as the average length of the linear crystallizable PET sequences decrease, as determined by NMR and reported in Table 5.1.<sup>3,5,10</sup>

**Table 5.2** Thermal Properties of Synthesized Polymers.

Sample	Cooling				2nd. Heating			
	PET		Polyether		PET		Polyether	
	$T_c$ (°C) <sup>a</sup>	$\Delta H_c$ (J/g) <sup>a</sup>	$T_c$ (°C) <sup>a</sup>	$\Delta H_c$ (J/g) <sup>a</sup>	$T_m$ (°C) <sup>a</sup>	$\Delta H_m$ (J/g) <sup>a</sup>	$T_m$ (°C) <sup>a</sup>	$\Delta H_m$ (J/g) <sup>a</sup>
PET	197.9	-54	-	-	252	53	-	-
PET <sub>68</sub> Poly(1,6 HD) <sub>32</sub>	185.5	-66	1.3	-6	246.1	62	42.7	6
PET <sub>64</sub> Poly(1,6 HD) <sub>36</sub>	183.9	-62	24.4	-25	241.3	56	49.7	28
PET <sub>61</sub> Poly(1,6 HD) <sub>39</sub>	177.5	-51	28.3	-56	238.6	49	52.3	56
PET <sub>34</sub> Poly(1,6 HD) <sub>66</sub>	160.6	-44	30.7	-71	227.1	38	51.9	74
Poly(1,6 HD)	-	-	39.4	-130	-	-	56.8	141
Poly(1,6 HD)*	-	-	30.9	-100	-	-	47.7	110

<sup>a</sup>Determined by DSC. \*It is Polyether that was put to the same conditions of time and temperature as the copolymer, but without the presence of PET.

\* $\Delta H_c$  and  $\Delta H_m$  are normalized values, were calculated by dividing the enthalpy by the respective mass fraction of the component that crystallizes (PET or Polyether)

Table 5.2 displays  $T_c$  and  $T_m$  values.  $\Delta H_m$  was employed to calculate the degree of crystallinity ( $X_c$ ) of the phases (PET or Polyether) at room temperature.  $X_c$  can be calculated from the enthalpy of fusion of the phase under consideration ( $\Delta H_m$ ), the enthalpy of fusion of a 100% crystalline sample and the weight fraction of the phase under consideration ( $W$ ) using Eq. (5.1).

$$X_c = \frac{\Delta H_m}{\Delta H_{m(100\%)}W} \quad (5.1)$$

The value of  $\Delta H_{m(100\%)}$  for polyether was calculated following the procedure reported in the literature [250 J/g for Poly (1,6 HD)].<sup>18</sup> In the case of PET the value was taken from Physical Properties of Polymers Handbook (140 J/g).<sup>19</sup>

The results of the non-isothermal analysis of the polymers obtained can be summarized in Figure 5.5, where  $T_c$ ,  $T_m$  and the degree of crystallinity ( $X_c$ ) have been plotted as a function of the polyether or PET content in the copolymers. Figure 5.5(a) shows that by increasing the content of polyether in the copolymer the  $T_m$  and  $T_c$  of the PET component decrease. The effect of the polyether component on the crystallization of the PET component in the copolymer is that at the temperature that the PET phase crystallizes, the polyether phase is in the melt. Therefore, in principle, if the polyether component is immiscible with the PET component, one would not expect

any influence on the PET phase, unless its quantity would be lower than 20%. Two reasons may explain a melting point depression of the PET component: a) the average sequence length of PET segments in the copolymer decrease with the increase in polyether or b) the copolymers are miscible in the melt. In this way, the polyether chains could act as a plasticizer for the PET crystals when they melt. The fact that the crystallinity of the PET component decrease with increases in polyether content is also an evidence of a decrease in crystallization ability, that could be compatible with smaller average PET sequences in the chain.

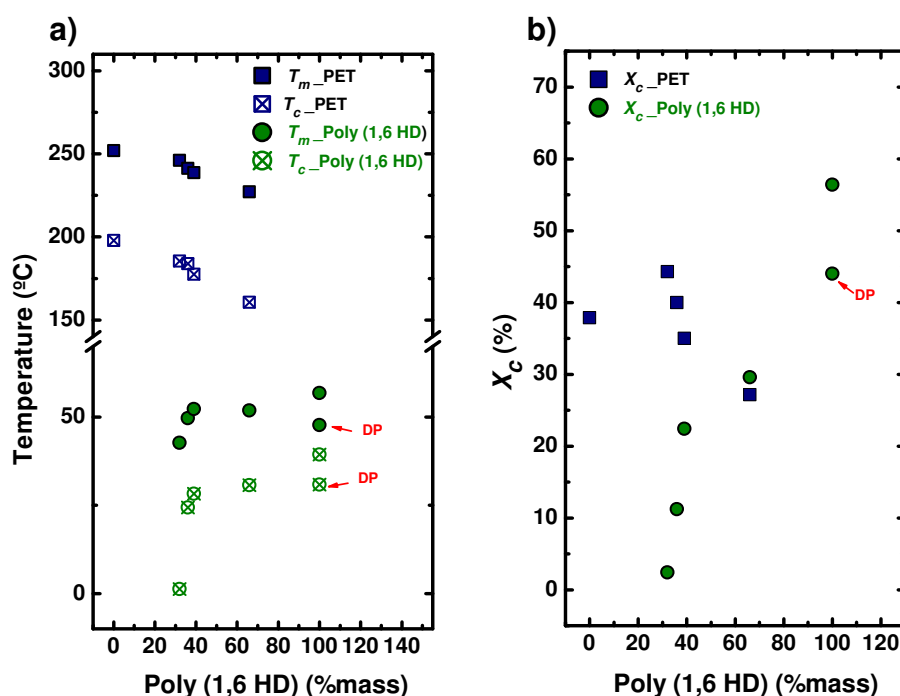


**Figure 5.5.** (a) Values of  $T_m$  and  $T_c$  as a function of composition for PET-*mb*-Poly (1,6 HD) and (b)  $X_c$  versus composition for PET-*mb*-Poly (1,6 HD). (The points indicated with DP, are values of the thermally treated polyether).

On the other hand when the amount of PET increases in the copolymer, the  $T_m$  and  $T_c$  of the polyether decrease and the crystallinity dramatically decreases. The PET phase crystallizes first and forms crystals that restrict the mobility of the polyether covalently bonded chains. A topological confinement effect is produced that increase with the amount of PET in the copolymer.<sup>2,3,5,10</sup> In the literature it is reported that for block copolymers formed by PET and PEO, the crystallization of the PET blocks exerts a strong influence on the crystallization process, crystallinity and on the final soft segment morphology (PEO).<sup>3</sup>

The behavior of the obtained PET-*mb*-Poly (1,6 HD) copolymers can be described as follows: above the melting point of the PET, the copolymer forms a single phase melt. As the temperature is decreased, the PET blocks crystallize while the polyether chains remain in the melt state. When the temperature is further reduced to  $T < T_m$  (Poly (1,6 HD)), the segments of Poly (1,6 HD) also crystallize, and a double crystalline copolymer is generated. A similar behavior has been reported for copolymers of PET with PEO.<sup>3</sup>

### 5.3.2.1 Phase Separation in Block Copolymers

Some authors have reported that when there are block copolymers where different macromolecules (PET or PBT and PEG) are covalently bound, macrophase separation cannot take place, however a microphase separation can occur. This separation is favored by the increase in molecular weight of Polyester or Polyether that form the copolymer. But if the molecular weight remains constant, an increase in the amount of PET in the copolymer causes an increase in crystallinity which can favor a microphase separation.<sup>9,12</sup>

The  $T_g$  of the segments (PET and Polyether) that form the copolymer is usually a characteristic parameter for evaluating the microphase separation in many segmented copolymer systems and gives important information about the microphase structure. It has been reported that in PET copolymer systems with PEG, the  $T_g$  value of the PEG present in the copolymer is usually higher than that of pure PEG, which indicates the existence of a mixture in the amorphous phase containing both segments (PEG and non-crystallized segments of PET), where the PET segments reinforce the soft phase and this increases the  $T_g$  of the PEG.<sup>2</sup>

Analyzing the effect of the polyether component on the  $T_g$  of the PET component in the copolymer (PET and PEG), it has been reported that the motion of molecules and chains of PEG in the rubbery state can influence significantly the glass transition of PET, decreasing the  $T_g$  of PET in the copolymer in comparison with the  $T_g$  of the PET.<sup>11,20</sup>

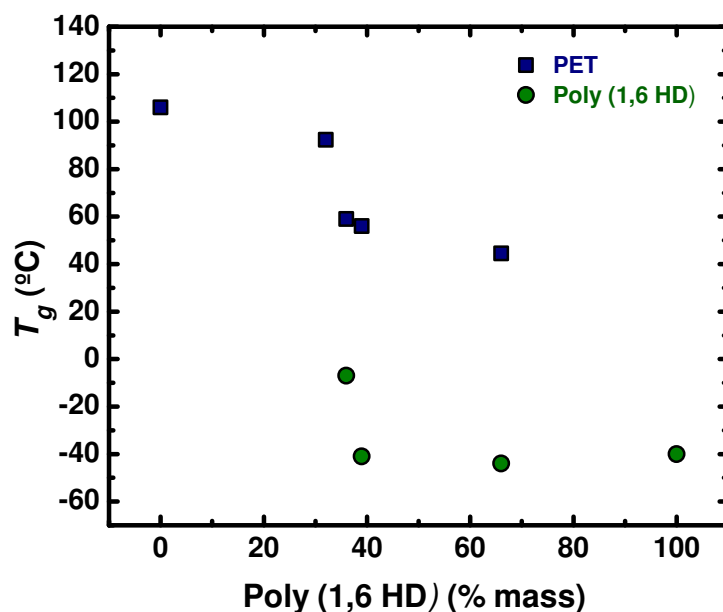


**Figure 5.6.**  $T_g$  values of copolymers  $\text{PET}_x\text{Poly}(1,6\text{ HD})_y$  as a function of Polyether content in the copolymer (by DMTA).

DMTA tests were employed to measure the  $T_g$  values of all the samples obtained, which are listed in Table 5.3. Two  $T_g$  are appreciated in Figure 5.6 for the copolymers obtained. Figure 5.6 shows that some PET-*mb*-poly(1,6 HD) copolymers exhibit two  $T_g$  values corresponding to a PET rich phase and a Poly(1,6 HD) rich phase. The  $T_g$  values corresponding to the PET rich phase tend to decrease as the polyether content increases and are all lower than those of neat PET. This indicates that a PET rich phase is formed, where a small amount of polyether chains are dissolved in PET and therefore plasticize and depress the  $T_g$  value. On the polyether composition side, the  $T_g$  of the polyether in the copolymer tends to increase when the amount of PET increases, at least for some of the values, also indicating the formation of a polyether rich phase that contains a small amount of PET chains.

**Table 5.3** Glass Transition Temperature of the PET-*mb*-Poly (1,6 HD).

	DMTA		flashDSC	
	PET $T_g$ (°C)	Polyether $T_g$ (°C)	PET $T_g$ (°C)	Polyether $T_g$ (°C)
PET	106	---	104	---
PET <sub>68</sub> Poly(1,6 HD) <sub>32</sub>	92.4	---	91.9	-31.5
PET <sub>64</sub> Poly(1,6 HD) <sub>36</sub>	59	-7	---	---
PET <sub>61</sub> Poly(1,6 HD) <sub>39</sub>	56	-41	---	---
PET <sub>34</sub> Poly(1,6 HD) <sub>66</sub>	44.5	-44	37.9	-52.8
Poly (1,6 HD)	---	-40	---	-59.6

The DSC measurements were useful to detect both crystallization and melting transition, but because of the high crystallinity content in the copolymer samples, the  $T_g$  was not detected. Therefore, ultra fast DSC was performed in a FlashDSC 2 equipment by Mettler Toledo. The rates employed were -4000 K/s and 20 000 K/s for cooling and heating, respectively. The samples were analyzed in a range of -90 to 270 °C. The flashDSC was used to rapidly quenched the materials and taking advantage of the much lower crystallinity determining  $T_g$  values (the curves of these tests are shown in Figure C.3, Annex C). In Figure 5.7 it can be seen that the two copolymers [PET<sub>68</sub>Poly(1,6 HD)<sub>32</sub> and PET<sub>34</sub>Poly(1,6 HD)<sub>66</sub>] show two  $T_g$ , suggesting that there is a microphase separation in the copolymer amorphous phase.

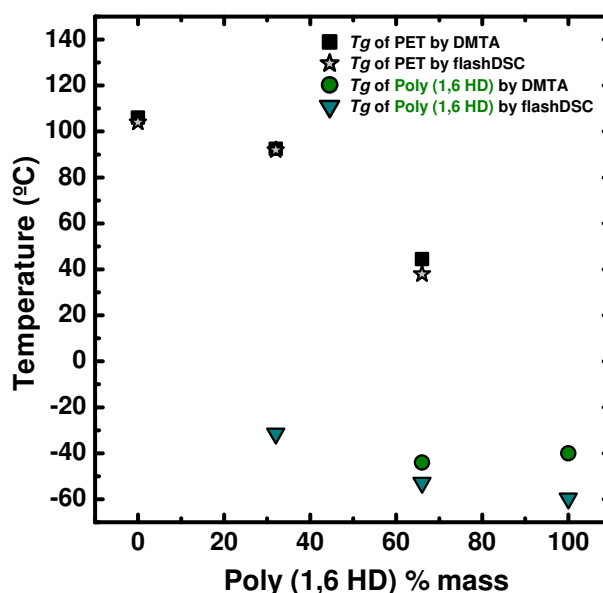


**Figure 5.7.**  $T_g$  values of some copolymers PET<sub>x</sub>Poly (1,6 HD)<sub>y</sub> as a function of Polyether content in the copolymer.

On the other hand, the values of  $T_g$  obtained by flash DSC (Table 5.3) are very similar to those obtained by DMTA, therefore both techniques can be useful for  $T_g$  measurements in this type of segmented copolymers.

### 5.3.3 Isothermal Crystallization Kinetics

The crystallization kinetics of the double crystallizable block copolymers is very interesting and may be different from that of crystallizable block copolymers or semi-

crystalline homopolymers. However, such crystallization behavior is commonly complicated due to the concurrent effects of several factors, such as confinement, geometry, glass transition temperature, morphology among others.

In the present work, the isothermal crystallization of neat PET and PET-*mb*-Poly (1,6 HD) of different compositions has been measured by DSC. Figure 5.8(a) shows the inverse of the half crystallization time ( $1/\tau_{50\%}$ ), which is proportional to the experimentally determined overall crystallization rate (that includes both nucleation and growth), as a function of isothermal crystallization temperatures ( $T_c$ ) for neat PET and all copolymers where the PET component was able to crystallize. At the crystallization temperatures employed to crystallize the PET component, the polyether chains are in the melt state (Figure 2.2, experimental section).

Figure 5.8(a) shows that neat PET crystallizes faster than the PET blocks present in the copolymers. In addition, the crystallization rate decreases as the amount of polyether in the copolymer increases.

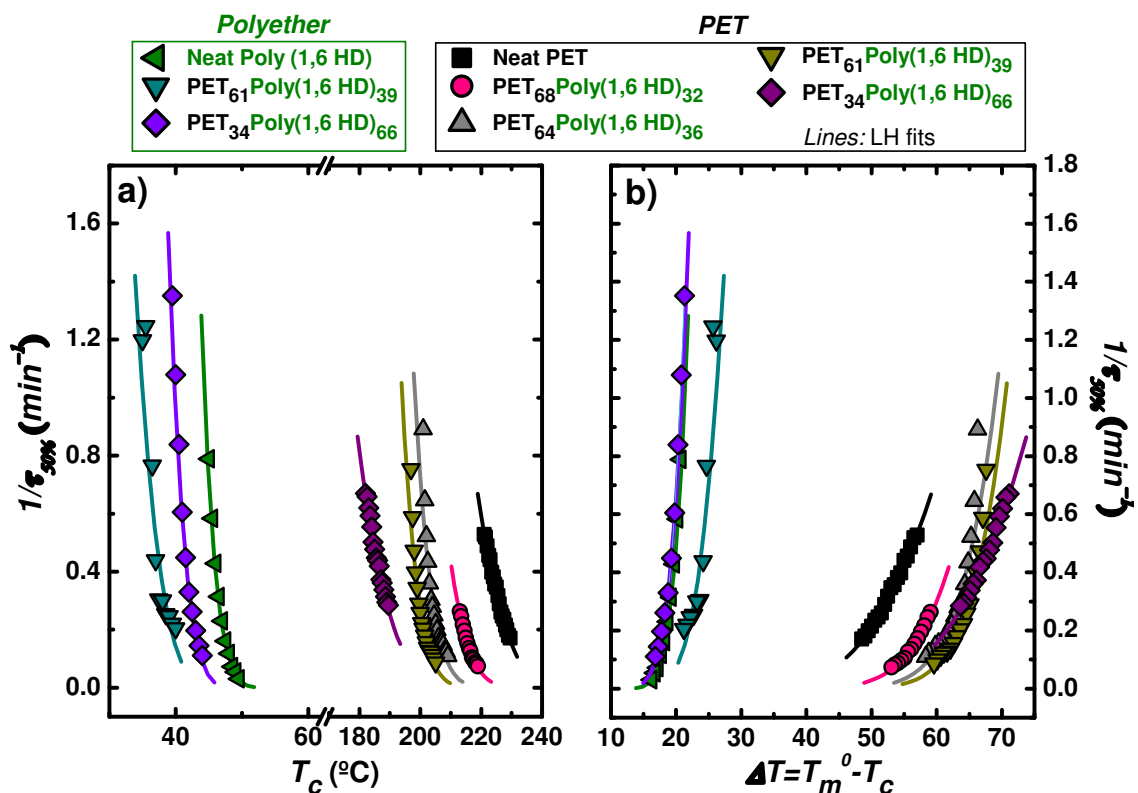


**Figure 5.8.** (a) Overall crystallization rate ( $1/\tau_{50\%}$ ) as a function of isothermal crystallization temperature ( $T_c$ ) and (b) Overall crystallization rate ( $1/\tau_{50\%}$ ) as a function of the supercooling ( $T_m^0 - T_c$ ), for neat PET, neat Poly (1,6 HD) and for the PET-*mb*-Poly (1,6 HD) copolymers

It is anticipated that the equilibrium melting temperature of PET should also decrease as the polyether is incorporated in the copolymer chains. The values  $T_m^0$  were determined and the data in Figure 5.8(a) has been represented in Figure 5.8(b) as a function of supercooling. It can be appreciated that the curves as a function of supercooling are closer together (the range in terms of temperature interval is narrower as compared to the range in  $T_c$  values), as the supercooling will consider the thermodynamic differences between the copolymers.

In this work, the crystallization rate of the polyether components in the copolymers was determined after a previous crystallization of the PET component, as explained in the experimental section (Figure 2.3).

Figure 5.8(a) shows the crystallization behavior of the poly (1,6 HD) component present in the copolymers vs the pure polyether. The crystallization rate of the polyether blocks in the copolymers is slower than that of the homopolymer and also when the amount of PET in the copolymer increases, the crystallization rate of the Poly (1,6 HD) chains decreases. The previously formed PET crystals are probably restricting the crystallization of the polyether phase. It is expected that the equilibrium melting temperature of Polyether also decreases as PET is incorporated in the copolymer chains. With experimental values of  $T_m^0$  the data in Figure 5.8(a) has been represented in Figure 5.8(b) as a function of supercooling.

If the two components are miscible, both in the melt and in the amorphous state, then it is possible that PET chains crystallize from homogeneous chains, forming spherulites that grow until impingement. The internal region of such spherulites contain PET lamellae plus interlamellar amorphous regions formed by melt polyether chains covalently bonded with the PET chains. Not all PET chains crystallize. In fact only a minority since the crystallinity of the PET component decreases with polyether content in the copolymer, from around 45% down to 10% as shown in Figure 5.9. Inside the previously formed PET spherulitic templates is where the polyether blocks have to crystallize. In these interlamellar PET regions, the polyether chains will be confined and their confinement will increase as PET increases in the copolymers, thereby restricting their crystallization ability. A similar behavior has been observed in melt miscible block and random copolymers.<sup>10,21,22</sup>

Figure 5.9 shows the crystallinity of each of the segments (PET and Polyether) in the copolymer during the isothermal crystallization. Despite some fluctuations in the values, in general terms, the crystallinity is greatly reduced when the content of the component under consideration decreases within the copolymer.

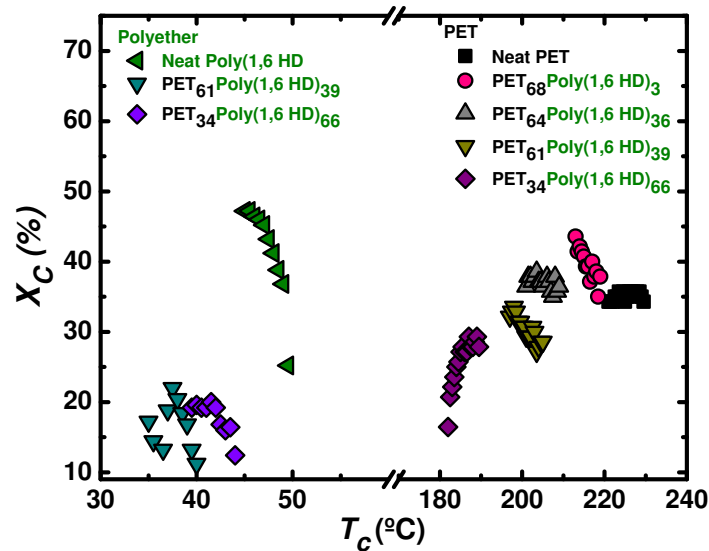


**Figure 5.9.** Percentage of crystallinity ( $X_c$ ) as a function of the isothermal crystallization temperature ( $T_c$ ) for PET-*mb*-Poly (1,6 HD).

The Avrami and the Lauritzen and Hoffman theories are usually employed to fit crystallization kinetics data. The Avrami equation,<sup>23</sup> can be expressed as:<sup>24,25</sup>

$$1 - V_c(t - t_0) = \exp(-K(t - t_0)^n) \quad (5.2)$$

where  $t$  is the experimental time,  $t_0$  is the induction time before any crystallinity develops,  $V_c$  is the relative volumetric transformed fraction,  $n$  is the Avrami index and  $K$  is the overall crystallization rate constant. The experimental data were fitted to the Avrami equation using the Origin plug-in developed by Lorenzo *et al.*<sup>24</sup>

The Avrami equation generally fits well the primary crystallization range. This is why, the fits are usually performed at low conversion values (3-20%).<sup>24</sup> An example of the good agreement between the Avrami model and the experimental data of PET (neat PET and PET component in the copolymer) is shown in Figure 5.10(a,b). The experimental DSC isotherms were compared with the Avrami predicted ones. The agreement is excellent in the primary crystallization range (i.e., until approximately the

peak value, where the growing spherulites or axialites impinge on one another), as indicated by the correlation coefficient of 1 in the limited conversion range of 3-20%, but also beyond 20% as experimental and fitted curves are overlapped on each other in Figure 5.10(a,b) until at least 50% conversion.

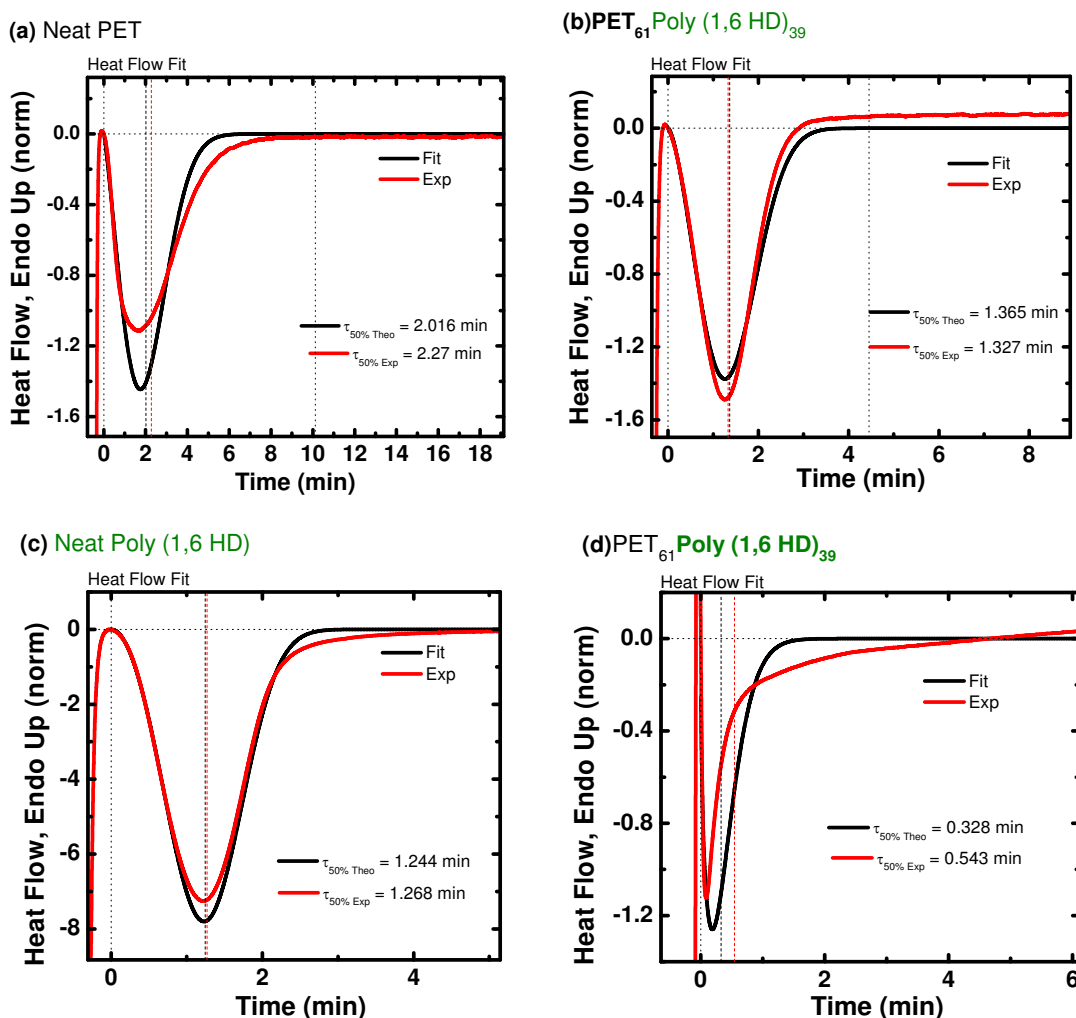


**Figure 5.10.** Experimental Data compared with fits to the Avrami equation for (a, b) neat PET and PET segment in PET<sub>61</sub>Poly(1,6 HD)<sub>39</sub>, respectively. (c, d) neat Poly(1,6 HD) and Poly(1,6 HD) segment in PET<sub>61</sub>Poly(1,6 HD)<sub>39</sub>, respectively.

In the case of neat polyether a good fit between the Avrami model and the experimental DSC data was also observed until at least 50% conversion (Figure 5.10(c)). On the other hand, Avrami seems to fit well only for the primary crystallization (3-20% conversion) of the polyether segment in the copolymer. Above 20% the fit between the Avrami model and the experimental data has certain deviations which are shown in Figure 5.10(d). These deviations may be due to the fact

that the polyether crystallizes in the presence of semi-crystalline PET, which seems to affect the crystallization process of the polyether.

For both PET and Poly (1,6 HD) present in the copolymers, parameters derived from isothermal crystallization were obtained. The values obtained for  $K^{1/n}$  (isothermal crystallization rate constant) are shown in Figure 5.11(a). The value of  $K$  has units of  $n^{-1}$ , i.e., they depend on the  $n$  value or Avrami index value. Therefore, in order to be able to compare  $K$  values with comparable units,  $K$  is elevated to the power  $1/n$ . As  $K^{1/n}$  is proportional to the overall crystallization rate, it has a tendency that is practically the same as the one shown in Figure 5.8(a).

Applying the Avrami equation, values of  $n$  (i.e., Avrami index) for neat polymers (PET and Polyether) and PET and polyether components in the copolymers were calculated and plotted in Figure 5.11(b). It is appreciated that for PET, a range of values from 2 to 3.2 were obtained. In principle,  $n=3$  (or  $n=2.5-3.2$  which can be approximated to 3) indicates the presence of instantaneously nucleated spherulites or sporadically nucleated axialites, while  $n=2$  is typically associated in polymers with instantaneously nucleated axialites.

Figure 5.11(b) also reports Avrami index values for neat polyether and for the polyether blocks within the copolymers. Values between 3 and 4 were obtained for the neat Poly(1,6 HD), which correspond to instantaneous and sporadic nucleated spherulites respectively. On the other hand, a very interesting behavior has been found for the polyether phase of two copolymers examined. The Avrami index first decreases to 2 in the case of the copolymer with 34% PET, indicating that only 2D crystals can be formed instantaneously within the previously crystallized PET superstructural aggregates (which correspond for this copolymer to axialites). Then a dramatic reduction of the Avrami index is observed as  $n$  values of 0.91 to 1.5 are obtained for the copolymer with 61% PET. In this case, Avrami indexes of 1 or lower have been extensively reported for confined crystallization in the minority phases of diblock copolymers and also in the case of nanocomposites with very large amounts of nano-fillers.<sup>26-29</sup> The reason for this behavior is related to the difficulties experienced by confined materials to be nucleated. When this happened, the nucleation becomes the slow step or dominating step in the overall crystallization kinetics, as growth tends

to be much faster than nucleation. Therefore, the crystallization kinetics transforms into a first order kinetics dominated by nucleation.

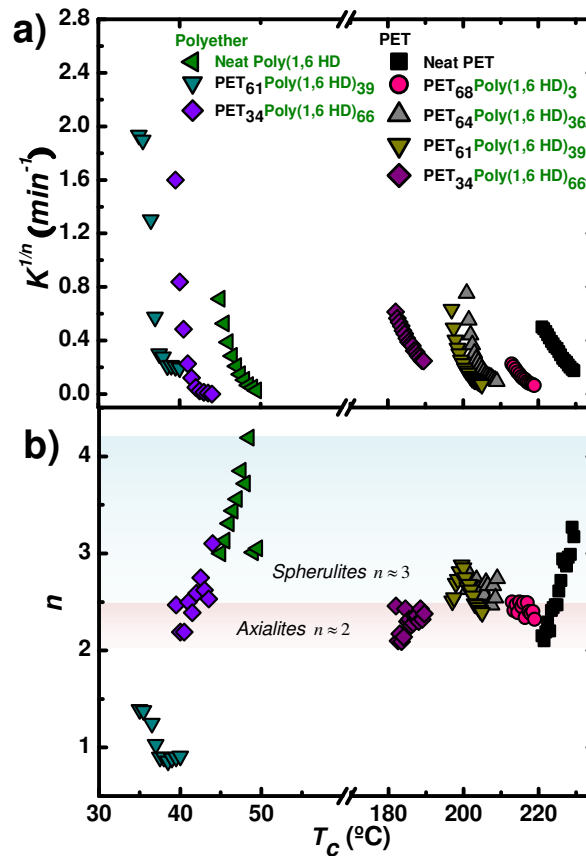


**Figure 5.11.** (a) Isothermal crystallization rate constant ( $K^{1/n}$ ) as a function of crystallization temperature ( $T_c$ ) and (b) Avrami index ( $n$ ) as a function of isothermal crystallization temperature ( $T_c$ ), for PET-*mb*-Poly (1,6 HD).

The growth rate  $G(T)$  of the crystals can be predicted by the Lauritzen and Hoffman theory which is expressed as:<sup>30</sup>

$$G(T) = G_0 \exp\left(\frac{-U^*}{R(T_c - T_\infty)}\right) \exp\left(\frac{-K_g}{T_c \Delta T f}\right) \quad (5.3)$$

where  $G_0$  is a growth rate constant,  $U^*$  the activation energy for the transport of the chains to the growing nuclei (1,500 cal/mol is generally used),  $R$  is the gas constant,  $T_c$  the isothermal crystallization temperature,  $T_\infty$  is the temperature at which chain mobility ceases and it is usually taken as  $T_g - 30$  (K).  $\Delta T$  is the supercooling defined as  $(T_m^0 - T_c)$  where  $T_m^0$  is the equilibrium melting point. The factor  $f$  is a

temperature correction term equal to:  $2T_c/(T_c + T_m^0)$ ; and  $K_g$  is a secondary nucleation constant, which is proportional to the energy barrier for secondary nucleation.

When the Lauritzen and Hoffman theory is applied to DSC data,  $G(T)$  in equation (5.3) is replaced by the inverse of the experimental half-crystallization time and the equation can then predict overall crystallization rates (which include both nucleation and growth).<sup>31</sup> Figure 5.8(a) shows the good fit of the experimental data to the LH theory (solid lines) for the overall crystallization rate. In this case, the parameter  $K_g$  is equal to  $K_g^T$ , which is proportional to the total energy barrier for the overall crystallization (i.e., for both nucleation and growth). In this work,  $T_m^0$  was obtained from experimental data.

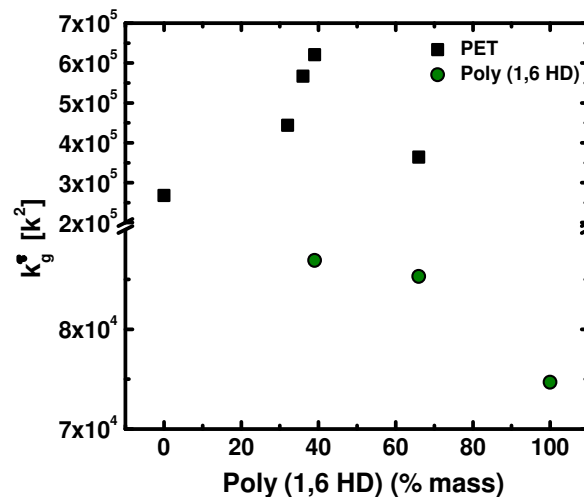


**Figure 5.12.** Values of  $k_g^T$  derived from LH fitting plotted as a function of Poly (1,6 HD) content.

Figure 5.12 shows the value of  $K_g^T$  depending on the amount of Poly (1,6 HD) in the copolymer. For Poly (1,6 HD) when the amount of polyether increases in the copolymer the value of  $K_g^T$  is lower, indicating that the energy barrier to overcome for nucleation and growth decreases as the average crystallizable sequences of Poly (1,6 HD) are longer. For PET, the energy barrier seems to be greater in all copolymers versus neat PET, which indicates that the polyether complicates the PET component crystallization process. The results are consistent with both the isothermal crystallization kinetics and the non-isothermal behavior of the copolymers, as

crystallization of each component within the copolymer is always slower and more difficult than for the neat components.

### 5.3.4 Determination of parameters derived by WAXS

To analyze the crystalline structure of the materials, these were characterized by WAXS. In the case of homopolymers [PET and poly (1,6 HD)] their diffractograms are shown in Annex C, where each homopolymer exhibits a unit cell type, in the case of PET a triclinic unit cell is appreciated and in the case of the polyether a monoclinic cell is observed. In both cases the crystalline planes characteristic of each one are appreciated (Table 5.4).<sup>16,32-37</sup> In this same table the diffraction spacings ( $d$ ) were calculated according to Bragg's Law. These results are consistent with the crystalline structures reported for PET and poly (1,6 HD) in the literature.<sup>16,34,36,37</sup>

**Table 5.4** Values of  $q$ ,  $2\theta$ , Crystalline Planes and  $d_{hkl}$  of Homopolymers.

<i>Crystalline Reflections</i>	$q$ (nm <sup>-1</sup> )	$2\theta$	Planes	$d_{hkl}$ (nm)
<b>PET</b>				
<b>1</b>	11.63	10.94	011	0.540
<b>2</b>	12.59	11.84	010	0.499
<b>3</b>	15.36	14.47	111	0.409
<b>4</b>	16.18	15.24	110	0.388
<b>5</b>	18.51	17.46	100	0.339
<b>6</b>	19.84	18.71	111	0.317
<b>7</b>	23.02	21.75	111	0.273
<b>8</b>	29.68	28.16	105	0.212
<b>Poly (1,6 HD)</b>				
<b>9</b>	14.01	13.19	020	0.449
<b>10</b>	17.04	16.06	110	0.369

Figure 5.13 shows WAXS results for PET<sub>64</sub>Poly(1.6 HD)<sub>36</sub> and PET<sub>34</sub>Poly(1.6 HD)<sub>66</sub>, where the appearance of reflections corresponding to both homopolymers can be seen (Table 5.4). With respect to the PET component, it can be seen that the intensity of its reflections is larger in Figure 5.13(a) vs Figure 5.13(b), suggesting that when the composition of the polyether increases, the amount of PET crystals in the copolymer decreases as expected. On the polyether side the opposite effect occurs.

From the above, it can be said that depending on the PET/polyether composition the intensity of the reflections of both components in the copolymer will

be more or less appreciated, considering that both components affect the crystallinity values. This behavior is appreciated in the diffractograms of the series of copolymers formed by PET and Poly (1,6 HD) and shown in the Annex C.

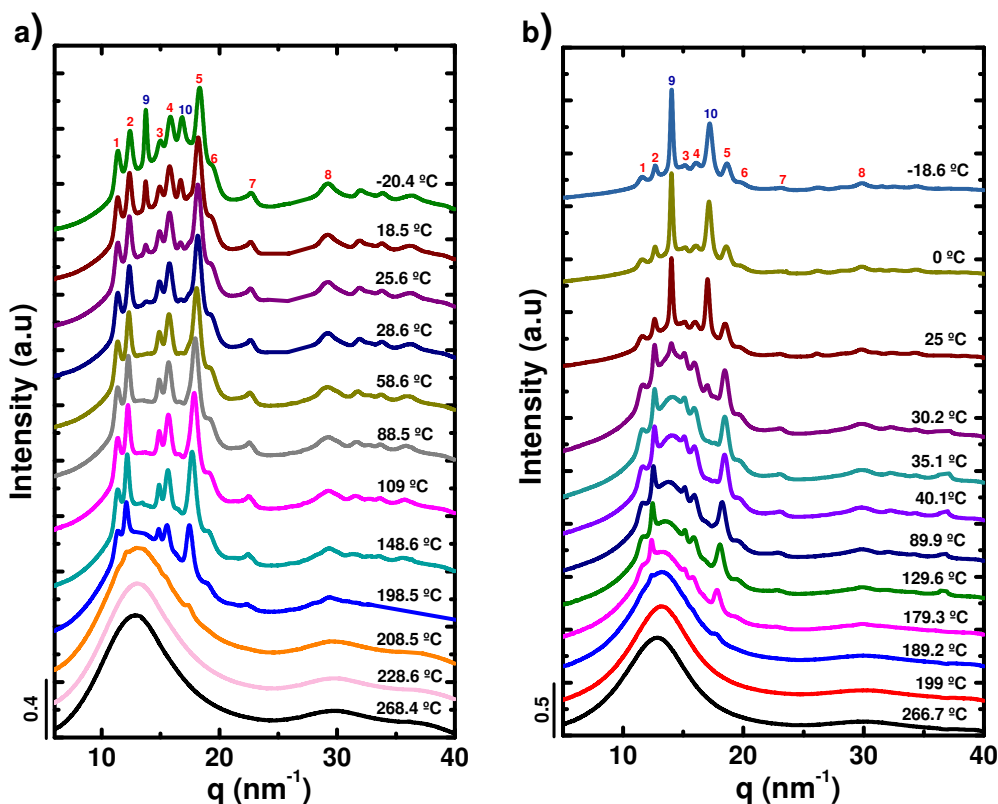


**Figure 5.13.** Real time synchrotron WAXS diffraction patterns for samples (a) PET<sub>64</sub>Poly (1,6 HD)<sub>36</sub> and (b) PET<sub>34</sub>Poly (1,6 HD)<sub>66</sub>, cooled from the 270 °C to -20 °C at 20 °C/min.

In summary, X-ray diffraction has shown that the crystalline structure of copolymers exhibits two types of unit cells: the triclinic unit cell corresponding to PET and the monoclinic unit cell corresponding to Poly (1,6 HD), corroborating the presence of both homopolymers in the copolymer, which had already been shown by NMR and DSC.

When the temperature is above the melting point of both components, a bimodal amorphous halo can be observed for both copolymers (notice the absence of crystalline reflections, i.e., sharp peaks) in Figure 5.13. This Figure also shows the gradual appearance of both PET and polyether reflections as the samples are cooled from the melt, depending on the crystallization temperature of each of the materials.

Because the difference in  $T_c$  between the components is large, the sequential appearance of PET and polyether reflections is clearly visible.

The average interplanar distance ( $d_{hkl}$ ) for all reflections in every copolymer was calculated using Bragg's law. The values of  $d_{hkl}$  taken at constant temperature are generally independent of composition as the variations observed are not significant (Figure 5.14).

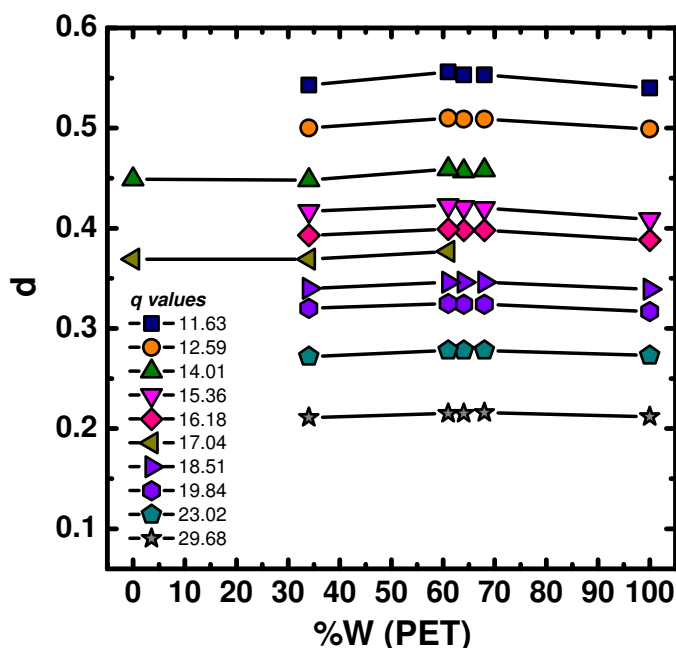


Figure 5.14. Interplanar distance ( $d_{hkl}$ ) for all reflections at 25 °C.

The results obtained by WAXS demonstrate the presence of PET and Poly (1,6 HD) crystals in the copolymers.

### 5.3.5 Determination of parameters derived by SAXS

In order to study the behavior of the lamellar periodicity (long period) of a segmented copolymer, such as the PET-*mb*-Poly (1,6 HD), as well as the lamellar thickness of the copolymers, SAXS experiments were carried out at the same measurement conditions as the WAXS (in fact, SAXS/WAXS were measured simultaneously at the synchrotron source).

Figure 5.15 shows the SAXS results at different temperatures for (a) PET<sub>64</sub>Poly(1,6 HD)<sub>36</sub> and (b) PET<sub>34</sub>Poly(1,6 HD)<sub>66</sub> samples, where the Lorentz corrected

intensity is plotted as a function of the scattering vector  $q$ . PET<sub>64</sub>Poly(1,6 HD)<sub>36</sub> exhibits clear intense maximum due to the scattering caused by the periodic lamellar stacks (i.e., long period). The intensity of this maximum is due to both PET and polyether crystalline lamellar components. At temperatures above 60 °C, only PET component lamellae cause the scattering, as the polyether component is in the melt. At temperatures below 60 °C, the maximum intensity is a mixture of periodic lamellar stacks of PET and polyether components. The temperature of 60 °C is taken in relation to the results of Table 5.2, which indicate that the melting point of the polyether is around 50 °C, this means that above 60 °C the polyether is completely molten. The above can also be corroborated by reviewing the SAXS of the homopolymers and the WAXS results (Annex C).

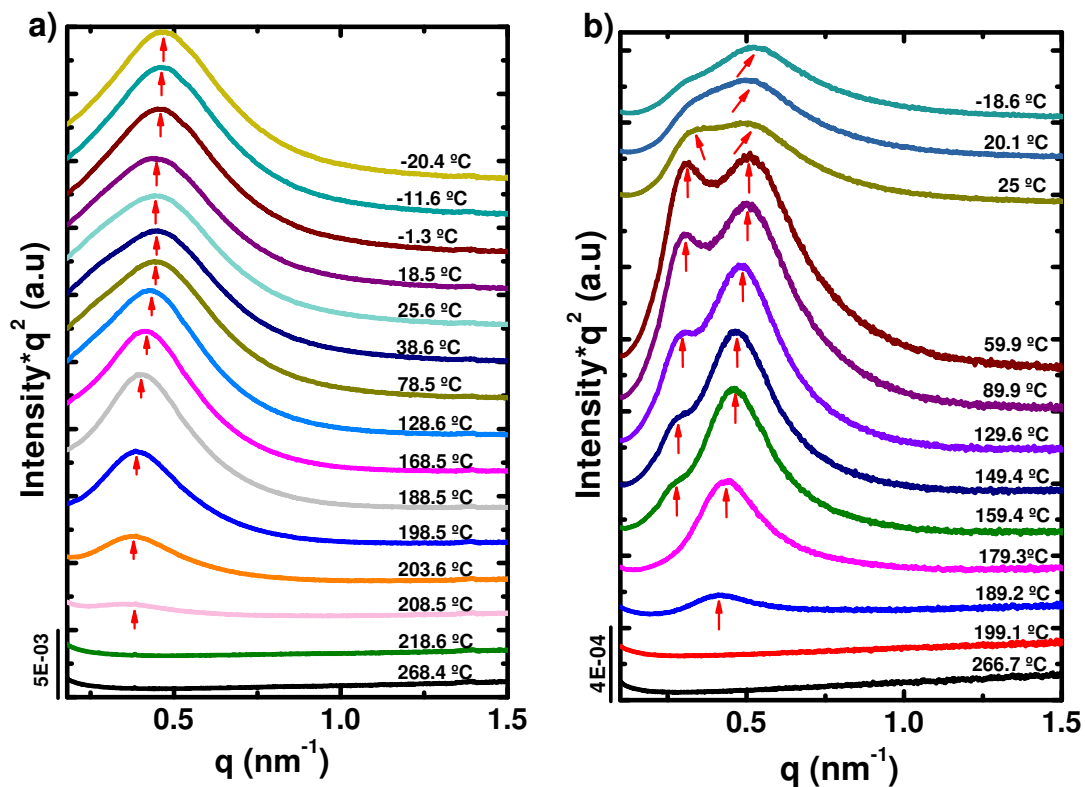


**Figure 5.15.** Lorentz-corrected SAXS profiles for (a) PET<sub>64</sub>Poly(1,6 HD)<sub>36</sub> and (b) PET<sub>34</sub>Poly(1,6 HD)<sub>66</sub>, with intensity as a function of scattering vector. Data taken of samples cooled from the 270 °C to -20 °C at 20 °C/min.

On the other hand in Figure 5.15(b), two peaks can be observed which do not correspond to two diffraction orders (as they are not located at  $q$  values which are twice each other, as for first and second order). In this case, it could be possible that

one peak is due to the scattering from PET lamellae and the other to polyether lamellae. However, there are temperatures where a single signal is appreciated and can correspond to the PET and polyether together or only to the PET depending on the temperature of measurement.

In Figure 5.15 it is also appreciated that when the crystals of the copolymers are melted the SAXS curves show no signal, indicating that there is no phase segregation in the melt state in the copolymers. This behavior was appreciated in the rest of the copolymers synthesized (Annex C). This demonstrates that the copolymers prepared here form a single phase melt, as their segregation strength is too low.

The segregation strength that could exist between PET and Poly (1,6 HD) was calculated ( $\chi N$ ). First, the Flory-Huggins interaction parameter ( $\chi$ ) between PET and poly (1,6 HD) was determined using the following equation: <sup>38</sup>

$$\chi = \frac{V_1}{RT} (\delta_1 - \delta_2)^2 \quad (5.4)$$

where  $V_1$  is the molar volume of the solvent ( $\text{m}^3/\text{mol}$ ),  $R$  is the gas constant ( $8.314 \text{ J/K}\cdot\text{mol}$ ),  $T$  is the temperature ( $298.15 \text{ K}$ ) and  $\delta_1, \delta_2$  are the solubility parameters of solvent and solute respectively ( $\text{J/m}^3$ )<sup>1/2</sup>. To apply this equation to PET-Polyether system, it is necessary to consider the PET as the solute and the Polyether as the solvent. The value of  $\delta_1$  was calculated by the Method of Hoftzyer and Van Krevelen using the data and the procedure reported in the literature ( $19.03 \text{ (MJ/m}^3\text{)}^{1/2}$ ). <sup>39</sup> In the case of PET,  $\delta_2$  was obtained from tables ( $20.5 \text{ (MJ/m}^3\text{)}^{1/2}$ ). <sup>39</sup> On the other hand  $V_1$  for Polyether was calculated from  $V_1 = m/\rho$  ( $9.523\text{E-}05 \text{ m}^3/\text{mol}$ ). Considering all the parameters previously describe, the interaction parameter  $\chi$  was calculated and value of  $\chi=0.08$  was obtained. The book of Hiemenz and Lodge reports that when the value predicted by Equation 5.4 is less than 0.3, Equation 5.5 is much more reliable for estimating the value of  $\chi$ . <sup>38</sup>

$$\chi = \frac{V_1}{RT} (\delta_1 - \delta_2)^2 + 0.34 \quad (5.5)$$

Because the value of  $\chi$  calculated with the Eq. 5.4 was less than 0.3, the value considered for  $\chi$  was determined with the Eq., 5.5, the new value obtained was  $\chi=0.42$ .

The value of  $N$  (total degree of polymerization) was calculated by equation 5.6:

$$N = \frac{(Mn_A * \Phi_A) + (Mn_B * \Phi_B)}{(Mnr_A * \Phi_A) + (Mnr_B * \Phi_B)} \quad (5.6)$$

where  $Mn_A$  is the molecular weight of the PET block,  $Mn_B$  is the molecular weight of the polyether block (3468 g/mol),  $\Phi_A$  and  $\Phi_B$  are the molar fractions of PET and polyether respectively, present in the copolymer.  $Mnr_A$  is the molecular weight of the repetitive unit of PET (192 g/mol) and  $Mnr_B$  is the molecular weight of the repetitive unit of Poly(1,6 HD) (100 g/mol). The values of  $N$  were calculated for every copolymer and the results are shown in Table 5.5.

**Table 5.5** Molecular weights,  $N$  and  $\chi N$  of Copolymers.

Sample	$Mn^a$ (g/mol) PET block	$N$	$\chi N$
PET <sub>68</sub> Poly(1,6 HD) <sub>32</sub>	7411	36	15.1
PET <sub>64</sub> Poly(1,6 HD) <sub>36</sub>	6413	34	14.4
PET <sub>61</sub> Poly(1,6 HD) <sub>39</sub>	5549	33	13.9
PET <sub>34</sub> Poly(1,6 HD) <sub>66</sub>	1997	32	13.5

<sup>a</sup>Calculated by  $Mn=(L_{EG}$  from Table 5.1)\*(192 g/mol)

The segregation strength ( $\chi N$ ) between PET and Poly (1,6 HD) was calculated multiplying  $\chi$  by  $N$ . The results are appreciated in Table 5.5. In a diblock copolymer, ( $\chi N$ ) is the parameter that controls the segregation between blocks A and B. Generally segregation is classified into three regimes: weak, intermediate and strong. There is no well-defined criterion to separate these regimes, however there are works that discuss this issue, the articles reported by Matsen and Bates, indicate that  $\chi N \leq 10$  represents a copolymer without phase segregation, when  $\chi N \approx 12$  indicates the beginning of a weak to intermediate segregation and a value of  $\chi N \approx 50$  indicates the beginning of a segregation from intermediate to strong.<sup>40,41</sup>

For all copolymers, the  $\chi N$  values are below 50 which indicate a weak to intermediate segregation strength in these systems, tending more to weak

segregation, because the values of  $\chi N$  are closer to 12. This means that a miscible or weakly segregated state in the melt would be predicted for a PET-*mb*-Poly(1,6 HD) diblock copolymer. As the polymers prepared here are multiblocks, the presence of multiple covalent bonds between PET and Poly(1,6 HD) will increase the miscibility of the system. So, it is reasonable to assume that in the melt state, these multiblock copolymers should be in a single phase, as will be demonstrated by SAXS experiments.

Considering the data obtained by SAXS, the long periods ( $d^*$ ) at different temperatures were estimated by Eq. (5.7) from  $q_{max}$  values taken from the Lorentz corrected plots ( $I^*q^2$  versus  $q$ ).

$$d^* = \frac{2\pi}{q_{max}} \quad (5.7)$$

Figure 5.16(a) shows the value of  $d^*$  in a range of temperatures as a function of the composition. Long periods tend to increase with temperature, as lamellae melt and are separated by increasingly larger amorphous intervening layers. This expected behavior can be observed for all materials in Figure 5.16(a).

It can be seen that all copolymers exhibit trends with two types of behavior in Figure 5.16(a). It seems that below 60 °C copolymers tend to have a behavior similar to the homopolyether, however the value of long period ( $d^*$ ) corresponds to both PET and polyether components, that is, the long period value of each component cannot be given separately. The behavior of neat polyether in Figure 5.16 (a), suggests that the homopolymer is already melted above 55 °C. Hence, above 55 °C the values of  $d^*$  in the copolymers correspond only to PET.

Parameters such as the degree of crystallinity ( $X_c$ ) and the lamellar thickness ( $l$ ) of each copolymer are shown in Figure 5.16(b) and (c) respectively. These parameters were calculated from the analysis of data obtained from WAXS and SAXS. For the calculation of an average lamellar thickness ( $l$ ) the following approximation was used:

$$l = d^* \cdot X_c \quad (5.8)$$

As the lamellar thickness values depend on the crystallinity degree according to equation 5.8, the degree of crystallinity by WAXS was also calculated (an example is provided in Annex C).

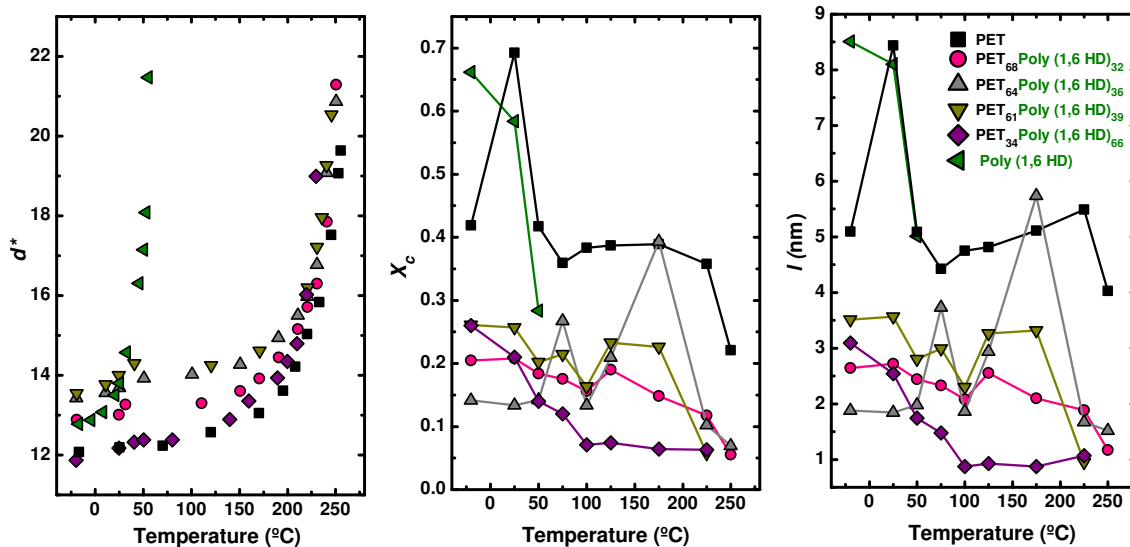


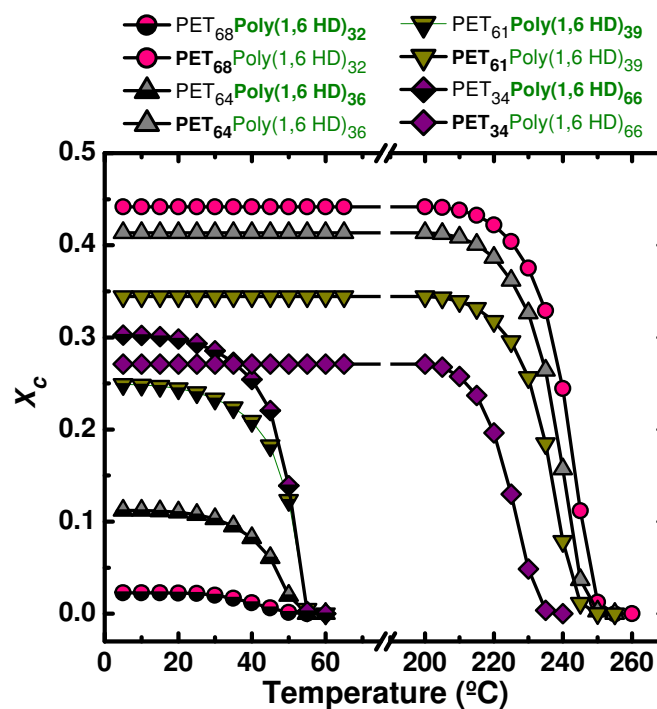
**Figure 5.16.** (a) Long periods ( $d^*$ ) calculated from SAXS data as a function of temperature, (b) degree of crystallinity ( $X_c$ ) calculated from WAXS data as a function of temperature and (c) lamellar thickness ( $l$ ) calculated from WAXS/SAXS data as a function of temperature.

The values of the lamellar thickness in Figure 5.16(c) include the lamellar thickness of the polyether and the PET, i.e., a single value of ( $l$ ) represents the sum of the lamellar thickness of the PET plus the lamellar thickness of the Polyether. The same goes for the value of the degree of crystallinity ( $X_c$ ), where in the Figure 5.16(b), the crystallinity of the copolymer at a given temperature is the sum of the crystallinity of the PET plus the crystallinity of the Polyether.

In Figure 5.16(b, c) it is clearly appreciated that below 60 °C, lamellae of PET and Polyether are present in the copolymer, which leads to a crystallinity formed by lamellae of both components in the copolymer (PET and polyether). Above 55 °C, the values of lamellar thickness and degree of crystallinity in the copolymer correspond only to the PET component, since the only existing lamella at these temperatures would be those of PET.

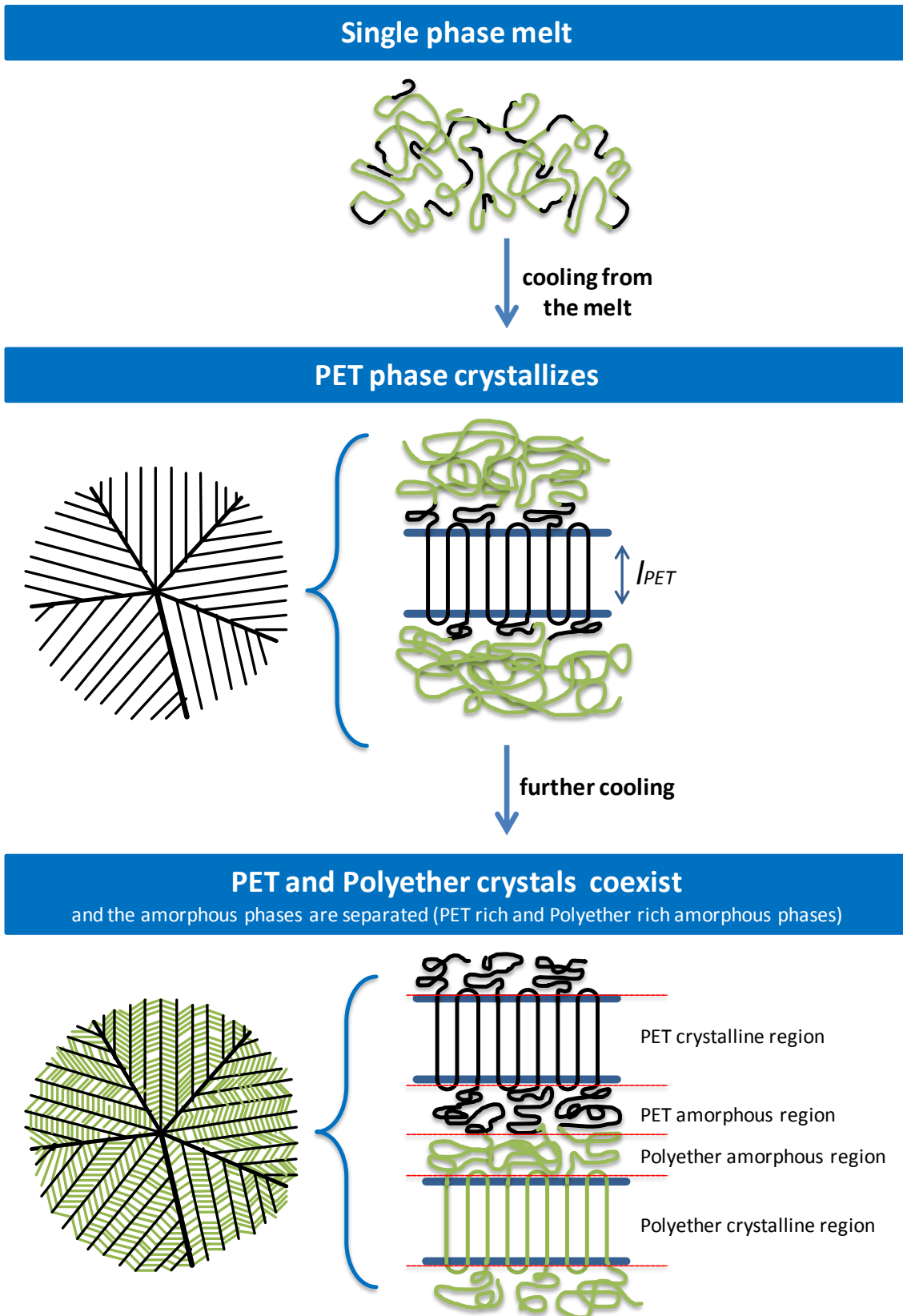
In order to clarify at what temperature ranges there is a mixture of PET and polyether crystals or only PET crystals, the degree of crystallinity at different temperatures was obtained by DSC using Eq. (5.1).

Figure 5.17 shows the degree of crystallinity of the polyether and PET separately at different temperatures (during the heating of the samples), it can be clearly seen that below 60 °C both the PET and the polyether component present a certain degree of crystallinity which means that below this temperature lamella of both components are present in the copolymer. The above corroborates what is shown in Figure 5.13 with data obtained from WAXS. From 60 °C onwards it is observed that the crystallinity of the copolymers is due solely to the PET component, since the polyether present in each of the copolymers is already in the melt state. In addition, this Figure 5.17, was useful to distinguish which components (PET and polyether) give the crystallinity to the copolymers under a given temperature range.



**Figure 5.17.** ( $X_c$ ) Calculated from DSC data at different temperatures for PET-*mb*-Poly (1,6 HD) copolymers.

Even though by DSC it is possible to distinguish the crystallinity of each one of the components, the lamellar thickness ( $l$ ) of each one of the components separately, cannot be calculated because according to the Eq. 5.8 the value of  $l$  depends on both the degree of crystallinity ( $X_c$ ) and the long period ( $d^*$ ), where the value of this last parameter obtained by SAXS contains contributions from both PET and polyether components (below 55 °C).



**Figure 5.18.** A schematic drawing of the formation of the PET-*mb*-Polyether.

Considering all the results shown in the previous pages, in Figure 5.18 shows an approximate scheme of how the semi-crystalline structure develops in these multi-block copolymers. In the melt state, both PET and Polyether chain segments within the multi-block copolymer form a single phase, as demonstrated by SAXS. Subsequently, the copolymer is cooled to a temperature at which only PET segments can crystallize forming lamellae (whose periodicity was determined by SAXS) arranged in spherulites. On the other hand, the polyether chains remain in the melt together with some PET chain segments that did not crystallize in the interlamellar regions within the PET spherulitic templates. Upon further cooling, the polyether chain segments are able to crystallize inside the previously formed PET spherulites. During crystallization, the amorphous regions of both components undergo phase separation, as two  $T_g$ s are detected by DMTA and FlashDSC measurements.

### 5.3.6 Morphology

The materials obtained were analyzed by Polarized Light Optical Microscopy (PLOM) and Atomic Force Microscopy (AFM). As can be seen in Figure 5.19, PET samples show a micro-spherulitic morphology, independent of the degree of undercooling.

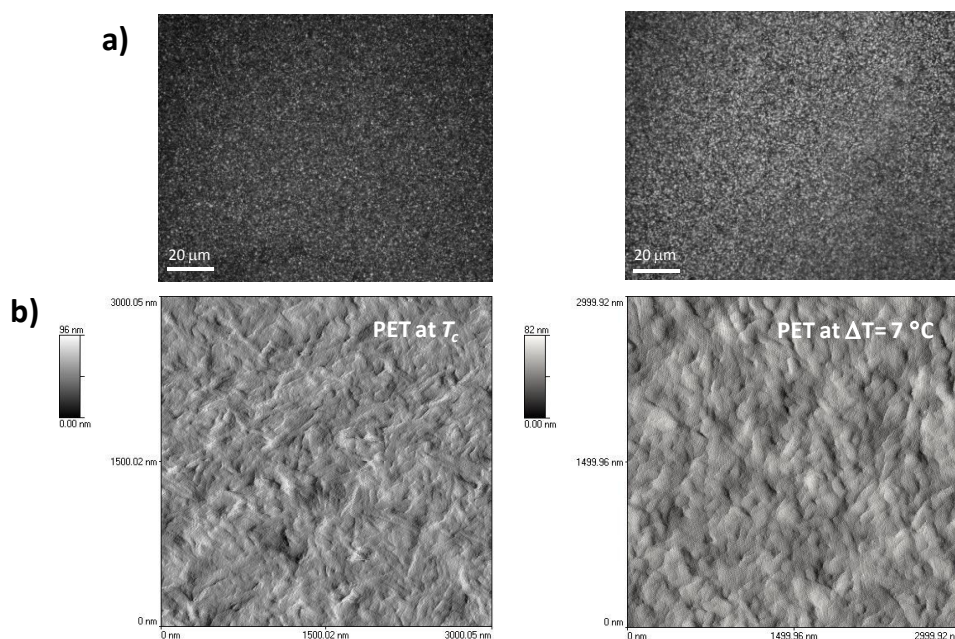


**Figure 5.19.** Morphological details of PET sample crystallized at  $T_c$  (left) and  $\Delta T = 7^\circ\text{C}$  (right) by optical microscopy (a) and AFM (b).

On the contrary, the polyether samples in Figure 5.20 show a clear axialitic morphology. In Figure 5.21, the morphological aspects of the copolymer samples PET-*mb*-poly (1,6 H,D), with variable PET/polyether content ratio can be observed. Neither PLOM nor AFM indicate any differences in copolymer samples morphology with different polyether content.

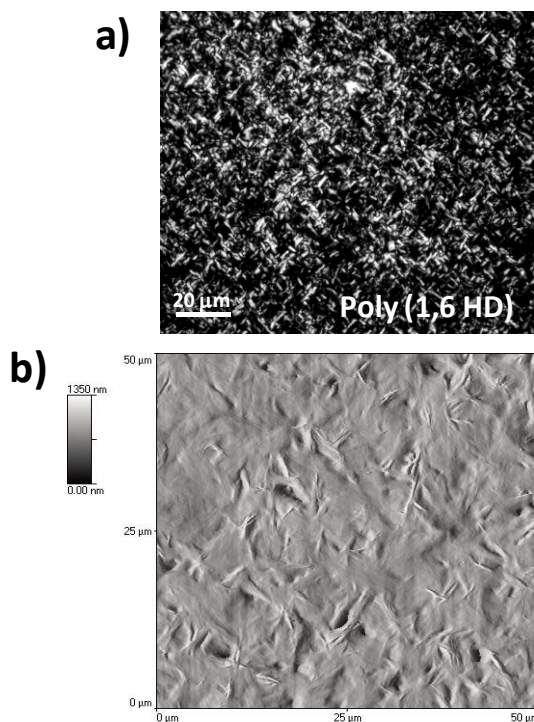


**Figure 5.20.** Morphological details of polyether sample quenched at room temperature by optical microscopy (a) and AFM (b).

In summary, similar morphological features have been found for all copolymer samples prepared at the different thermal conditions regardless of the amount of polyether in the copolymers. All copolymer samples show a micro-spherulitic morphology completely dominated by PET, even for the compositions rich in polyether. These results corroborate the morphological model depicted in Figure 5.18. As the PET component is the first to crystallize from a homogeneous melt, it forms micron size spherulitic templates (filled with molten PET chains and polyether chains) that grow until impingement with one another. Because the size of the spherulitic templates is so small, it is very difficult to observe differences, as the dominant feature is the external “skeleton” or micro-spherulitic templates.

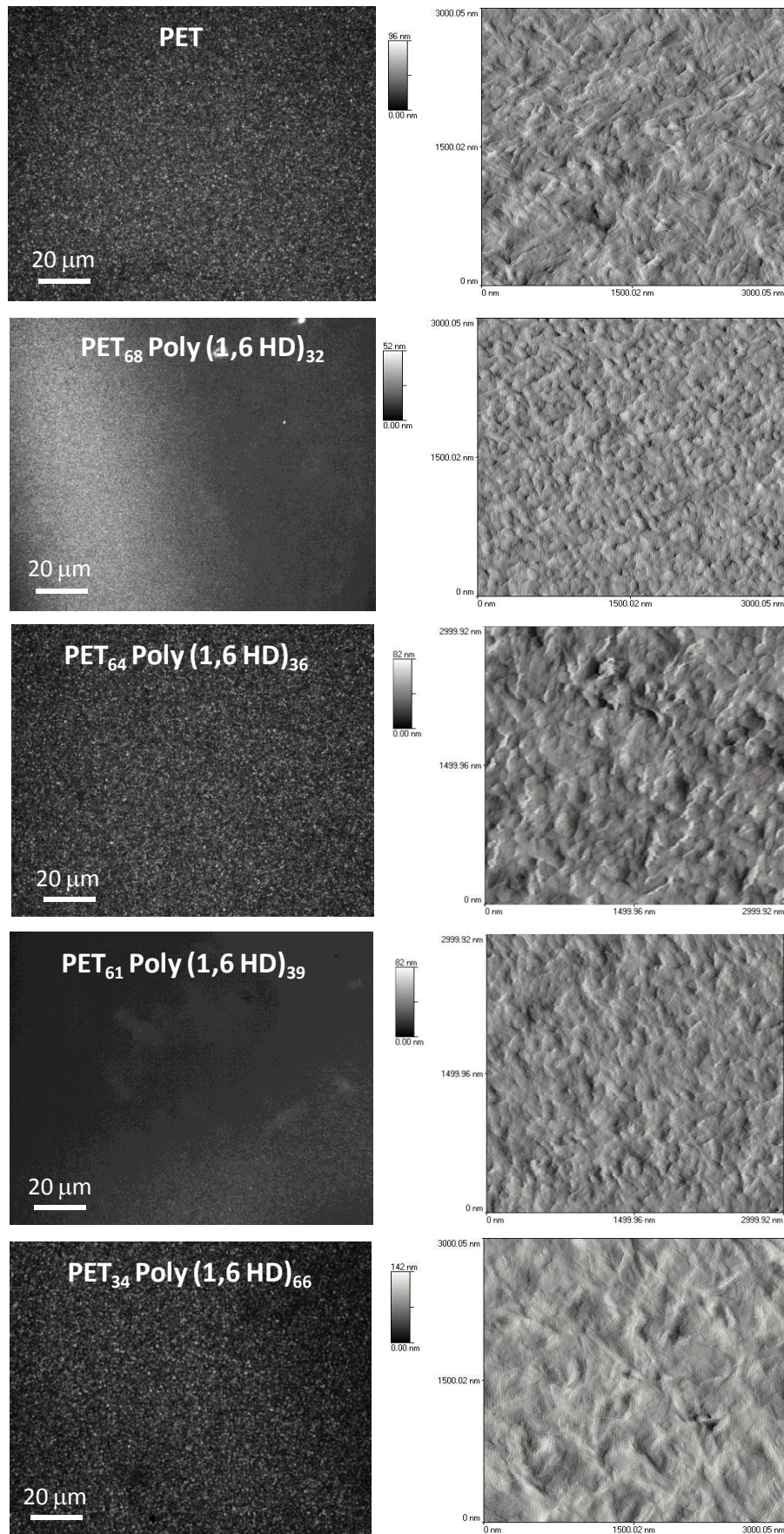


**Figure 5.21.** Morphological details of copolymer PET-*mb*-Poly(1,6 HD) samples crystallized at  $T_c$ : optical microscopy (left) and AFM (right).

## 5.4 Conclusions

PET-*mb*-polyether copolymers were synthesized and characterized. The materials showed that both components in the copolymer (PET and Polyether) are able to crystallize at their respective crystallization temperatures giving rise to a double crystalline polymeric material. The thermal properties of the copolymers were affected by the PET/Polyether composition, resulting in multiblock copolymers with different crystallinities and different ranges of glass transition temperatures. The crystallization rate of each of the components in the copolymer was largely dependent on PET/polyether composition.

These copolymers appear to have a very low segregation between the components that form them, in the melt state, as they are characterized by low molecular weights. Therefore, the copolymers exhibit a single phase in the melt. However, upon cooling from the melt, and after the PET phase is able to crystallize, phase segregation occurs within the amorphous phases in the copolymer, as evidenced by the presence of two  $T_{gs}$ .

In this work, PET-*mb*-Polyether copolymers with different ratios PET/Polyether were obtained. Therefore, a library of new materials adapted to various applications can be obtained by simply modifying the PET/Polyether composition which plays an important role on the thermal properties of the materials.

It should be noted that a micro-spherulitic morphology was found for all copolymer samples regardless polyether content present in the copolymers, as the PET component is the first to crystallize from a mixed melt forming micro-spherulitic templates that totally dominate the resulting morphology.

## 5.5 References

- (1) Sousa, A. F.; Vilela, C.; Matos, M.; Freire, C. S. R.; Silvestre, A. J. D.; Coelho, J. F. J. Polyethylene Terephthalate: Copolyesters, Composites, and Renewable Alternatives. In *Poly(Ethylene Terephthalate) Based Blends, Composites and Nanocomposites*; Elsevier, 2015; pp 113–141. <https://doi.org/10.1016/B978-0-323-31306-3.00007-5>.
- (2) Wang, M.; Zhang, L.; Ma, D. Degree of Microphase Separation in Segmented Copolymers Based on Poly(Ethylene Oxide) and Poly(Ethylene Terephthalate). *European Polymer Journal* **1999**, *35* (7), 1335–1343. [https://doi.org/10.1016/S0014-3057\(99\)00030-0](https://doi.org/10.1016/S0014-3057(99)00030-0).
- (3) Li, W.; Kong, X.; Zhou, E.; Ma, D. Isothermal Crystallization Kinetics of Poly(Ethylene Terephthalate)–Poly(Ethylene Oxide) Segmented Copolymer with Two Crystallizing Blocks. *Polymer* **2005**, *46* (25), 11655–11663. <https://doi.org/10.1016/j.polymer.2005.09.067>.
- (4) Huang, W.; Wan, Y.; Chen, J.; Xu, Q.; Li, X.; Yang, X.; Li, Y.; Tu, Y. One Pot Synthesis and Characterization of Novel Poly(Ether Ester) Mutiblock Copolymers Containing Poly(Tetramethylene Oxide) and Poly(Ethylene Terephthalate). *Polym. Chem.* **2014**, *5* (3), 945–954. <https://doi.org/10.1039/C3PY00932G>.
- (5) Kong, X.; Yang, X.; Zhou, E.; Ma, D. Nonisothermal Crystallization Kinetics of Ethylene Terephthalate–Ethylene Oxide Segmented Copolymers with Two Crystallizing Segments. *European Polymer Journal* **2000**, *36* (6), 1085–1090. [https://doi.org/10.1016/S0014-3057\(99\)00186-X](https://doi.org/10.1016/S0014-3057(99)00186-X).
- (6) Ma, D.; Wang, M.; Wang, M.; Zhang, X.; Luo, X. Compositional Heterogeneity, Thermostable, and Shape Memory Properties of Ethylene Oxide–Ethylene Terephthalate Segmented Copolymer with Long Soft Segment. *Journal of Applied Polymer Science* **1998**, *69* (5), 947–955. [https://doi.org/10.1002/\(SICI\)1097-4628\(19980801\)69:5<947::AID-APP14>3.0.CO;2-L](https://doi.org/10.1002/(SICI)1097-4628(19980801)69:5<947::AID-APP14>3.0.CO;2-L).
- (7) Coleman, D. Block Copolymers: Copolymerization of Ethylene Terephthalate and Polyoxyethylene Glycols. *Journal of Polymer Science* **1954**, *14* (73), 15–28. <https://doi.org/10.1002/pol.1954.120147303>.

- 
- (8) Hu, J.; Yu, H.; Chen, Y.; Zhu, M. Study on Phase-Change Characteristics of PET-PEG Copolymers. *Journal of Macromolecular Science, Part B* **2006**, *45* (4), 615–621. <https://doi.org/10.1080/00222340600770210>.
- (9) Qian, Z.; Li, S.; He, Y.; Liu, X. Synthesis and in Vitro Degradation Study of Poly(Ethylene Terephthalate)/Poly(Ethylene Glycol) (PET/PEG) Multiblock Copolymer. *Polymer Degradation and Stability* **2004**, *83* (1), 93–100. [https://doi.org/10.1016/S0141-3910\(03\)00229-5](https://doi.org/10.1016/S0141-3910(03)00229-5).
- (10) Kong, X.; Yang, X.; Li, G.; Zhao, X.; Zhou, E.; Ma, D. Nonisothermal Crystallization Kinetics: Poly(Ethylene Terephthalate)–Poly(Ethylene Oxide) Segmented Copolymer and Poly(Ethylene Oxide) Homopolymer. *European Polymer Journal* **2001**, *37* (9), 1855–1862. [https://doi.org/10.1016/S0014-3057\(01\)00046-5](https://doi.org/10.1016/S0014-3057(01)00046-5).
- (11) Chun, B. C.; Cha, S. H.; Chung, Y.-C.; Cho, J. W. Enhanced Dynamic Mechanical and Shape-Memory Properties of a Poly(Ethylene Terephthalate)-Poly(Ethylene Glycol) Copolymer Crosslinked by Maleic Anhydride. *Journal of Applied Polymer Science* **2002**, *83* (1), 27–37. <https://doi.org/10.1002/app.2228>.
- (12) Deschamps, A. A.; Grijpma, D. W.; Feijen, J. Poly(Ethylene Oxide)/Poly(Butylene Terephthalate) Segmented Block Copolymers: The Effect of Copolymer Composition on Physical Properties and Degradation Behavior. *Polymer* **2001**, *42* (23), 9335–9345. [https://doi.org/10.1016/S0032-3861\(01\)00453-0](https://doi.org/10.1016/S0032-3861(01)00453-0).
- (13) Dreyfuss, M. P.; Dreyfuss, P. A 'Living' Polymer after Cationic Initiation. *Polymer* **1965**, *6* (2), 93–95.
- (14) Perry, S.; Hibbert, H. Studies on Reactions Relating to Carbohydrates and Polysaccharides. LXI. The Mechanism of Polymerization of Ethylene Oxide. *J. Am. Chem. Soc.* **1940**, *62* (10), 2599–2604.
- (15) Vandenberg, E. J. Organometallic Catalysts for Polymerizing Monosubstituted Epoxides. *Journal of Polymer Science* **1960**, *47* (149), 486–489. <https://doi.org/10.1002/pol.1960.1204714947>.
- (16) Basterretxea, A.; Gabirondo, E.; Jehanno, C.; Zhu, H.; Flores, I.; Müller, A. J.; Etxeberria, A.; Mecerreyes, D.; Coulembier, O.; Sardon, H. Polyether Synthesis by Bulk Self-Condensation of Diols Catalyzed by Non-Eutectic Acid–Base Organocatalysts. *ACS Sustainable Chemistry & Engineering* **2019**, *7* (4), 4103–4111. <https://doi.org/10.1021/acssuschemeng.8b05609>.

- (17) Flores, I.; Demarteau, J.; Müller, A. J.; Etxeberria, A.; Irusta, L.; Bergman, F.; Koning, C.; Sardon, H. Screening of Different Organocatalysts for the Sustainable Synthesis of PET. *European Polymer Journal* **2018**, *104*, 170–176. <https://doi.org/10.1016/j.eurpolymj.2018.04.040>.
- (18) Van Krevelen, D. W.; Te Nijenhuis, K. Calorimetric Properties. In *Properties of Polymers*; Elsevier, 2009; pp 109–128. <https://doi.org/10.1016/B978-0-08-054819-7.00005-4>.
- (19) *Physical Properties of Polymers Handbook*, 2nd ed.; Mark, J. E., Ed.; Springer: New York, 2006.
- (20) Wang, B.; Zhang, M.; Zhang, J. M.; He, C. Q.; Dai, Y. Q.; Wang, S. J.; Ma, D. Z. Compositional and Temperature Dependence of Free Volume in Segmented Copolymer PETrPEO Studied by Positron Annihilation Lifetime Measurement. **1999**, *11*.
- (21) Castillo, R. V.; Müller, A. J. Crystallization and Morphology of Biodegradable or Biostable Single and Double Crystalline Block Copolymers. *Progress in Polymer Science* **2009**, *34* (6), 516–560. <https://doi.org/10.1016/j.progpolymsci.2009.03.002>.
- (22) Pérez-Camargo, R. A.; Arandia, I.; Safari, M.; Cavallo, D.; Lotti, N.; Soccio, M.; Müller, A. J. Crystallization of Isodimorphic Aliphatic Random Copolyesters: Pseudo-Eutectic Behavior and Double-Crystalline Materials. *European Polymer Journal* **2018**, *101*, 233–247. <https://doi.org/10.1016/j.eurpolymj.2018.02.037>.
- (23) Avrami, M. Granulation, Phase Change, and Microstructure Kinetics of Phase Change. III. *The Journal of Chemical Physics* **1941**, *9* (2), 177–184. <https://doi.org/10.1063/1.1750872>.
- (24) Lorenzo, A. T.; Arnal, M. L.; Albuerne, J.; Müller, A. J. DSC Isothermal Polymer Crystallization Kinetics Measurements and the Use of the Avrami Equation to Fit the Data: Guidelines to Avoid Common Problems. *Polymer Testing* **2007**, *26* (2), 222–231. <https://doi.org/10.1016/j.polymertesting.2006.10.005>.
- (25) Müller, A. J.; Michell, R. M.; Lorenzo, A. T. Isothermal Crystallization Kinetics of Polymers. In *Polymer Morphology*; Guo, Q., Ed.; John Wiley & Sons, Inc: Hoboken, NJ, USA, 2016; pp 181–203. <https://doi.org/10.1002/9781118892756.ch11>.

- (26) Michell, R. M.; Lorenzo, A. T.; Müller, A. J.; Lin, M.-C.; Chen, H.-L.; Blaszczyk-Lezak, I.; Martín, J.; Mijangos, C. The Crystallization of Confined Polymers and Block Copolymers Infiltrated Within Alumina Nanotube Templates. *Macromolecules* **2012**, *45* (3), 1517–1528. <https://doi.org/10.1021/ma202327f>.
- (27) Michell, R. M.; Blaszczyk-Lezak, I.; Mijangos, C.; Müller, A. J. Confinement Effects on Polymer Crystallization: From Droplets to Alumina Nanopores. *Polymer* **2013**, *54* (16), 4059–4077. <https://doi.org/10.1016/j.polymer.2013.05.029>.
- (28) Müller, A. J.; Arnal, M. L.; Trujillo, M.; Lorenzo, A. T. Super-Nucleation in Nanocomposites and Confinement Effects on the Crystallizable Components within Block Copolymers, Miktoarm Star Copolymers and Nanocomposites. *European Polymer Journal* **2011**, *47* (4), 614–629. <https://doi.org/10.1016/j.eurpolymj.2010.09.027>.
- (29) Castillo, R. V.; Arnal, M. L.; Müller, A. J.; Hamley, I. W.; Castelletto, V.; Schmalz, H.; Abetz, V. Fractionated Crystallization and Fractionated Melting of Confined PEO Microdomains in PB-*b*-PEO and PE-*b*-PEO Diblock Copolymers. *Macromolecules* **2008**, *41* (3), 879–889. <https://doi.org/10.1021/ma0718907>.
- (30) Lauritzen, J. I.; Hoffman, J. D. Theory of Formation of Polymer Crystals with Folded Chains in Dilute Solution. *Journal of Research of the National Bureau of Standards Section A: Physics and Chemistry* **1960**, *64A* (1), 73. <https://doi.org/10.6028/jres.064A.007>.
- (31) Lorenzo, A. T.; Müller, A. J. Estimation of the Nucleation and Crystal Growth Contributions to the Overall Crystallization Energy Barrier. *Journal of Polymer Science Part B: Polymer Physics* **2008**, *46* (14), 1478–1487. <https://doi.org/10.1002/polb.21483>.
- (32) Kobayashi, S.; Tadokoro, H. Structural Studies on Polyethers,  $[-(\text{CH}_2)_m\text{-O}]_n$ . VI The Higher Members with  $M=6-10,12$ . *Makromol. Chem.* **1968**, *112*, 225–241.
- (33) de P. Daubeny, R.; Bunn, C. W. The Crystal Structure of Polyethylene Terephthalate. *Proceedings of the Royal Society A: Mathematical, Physical and Engineering Sciences* **1954**, *226* (1167), 531–542. <https://doi.org/10.1098/rspa.1954.0273>.

- (34) Lu, X. F.; Hay, J. N. Isothermal Crystallization Kinetics and Melting Behaviour of Poly(Ethylene Terephthalate). *Polymer* **2001**, *42* (23), 9423–9431. [https://doi.org/10.1016/S0032-3861\(01\)00502-X](https://doi.org/10.1016/S0032-3861(01)00502-X).
- (35) Rwei, S. P.; Lin, W. P.; Wang, J. F. Synthesis and Characterization of Biodegradable and Weather-Durable PET/PEG/NDC Copolymers. *Colloid and Polymer Science* **2012**, *290* (14), 1381–1392. <https://doi.org/10.1007/s00396-012-2662-6>.
- (36) Tan, L. C.; Zhou, W. H.; Huang, Y. L.; Chen, Y. W. Sequential Structure, Crystallization, and Properties of Biodegradable Poly(Ethylene Terephthalate-Co-Ethylene Oxide-Co-Lactide) Copolyester. *Journal of Macromolecular Science, Part B* **2014**, *53* (7), 1231–1243. <https://doi.org/10.1080/00222348.2014.901870>.
- (37) Zhao, M. L.; Li, F. X.; Yu, J. Y.; Wang, X. L. Preparation and Characterization of Poly(Ethylene Terephthalate) Copolyesters Modified with Sodium-5-Sulfo-Bis-(Hydroxyethyl)-Isophthalate and Poly(Ethylene Glycol). *Journal of Applied Polymer Science* **2014**, *131* (3), 1–9. <https://doi.org/10.1002/app.39823>.
- (38) Hiemenz, P. C.; Lodge, T. P. *Polymer Chemistry*, second.; CRC press, 2007.
- (39) Krevelen, D. W. van; Nijenhuis, K. te. *Properties of Polymers: Their Correlation with Chemical Structure: Their Numerical Estimation and Prediction from Additive Group Contributions*, 4th, completely rev. ed ed.; Elsevier: Amsterdam, 2009.
- (40) Matsen, M. W.; Bates, F. S. Block Copolymer Microstructures in the Intermediate-Segregation Regime. *The Journal of Chemical Physics* **1997**, *106* (6), 2436–2448. <https://doi.org/10.1063/1.473153>.
- (41) Matsen, M. W.; Bates, F. S. Unifying Weak- and Strong-Segregation Block Copolymer Theories. *Macromolecules* **1996**, *29* (4), 1091–1098. <https://doi.org/10.1021/ma951138i>.

---

# Chapter 6

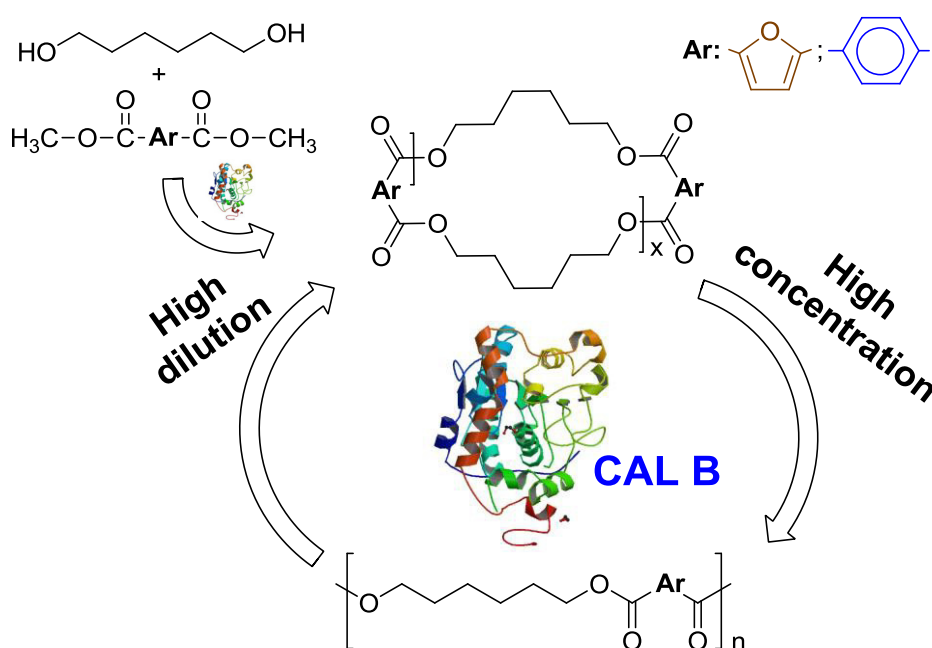
---

*Synthesis of Aromatic–Aliphatic Polyesters by  
Enzymatic Ring Opening Polymerization of  
Cyclic Oligoesters and their  
Cyclodepolymerization for a Circular Economy.*

6.1 Abstract.....	148
6.2 Introduction.....	149
6.3 Results and Discussion.....	151
6.4 Conclusions.....	158
6.5 References.....	159

## 6.1 Abstract

Cyclic oligomers of hexamethylene furanoate and hexamethylene terephthalate were obtained from 1,6-hexanediol and the corresponding methyl esters using *Candida antarctica* Lipase B (CALB) enzyme catalyst. HPLC, MALDI-TOF MS and NMR analyses showed that mixtures composed from cyclic dimer up to heptamer were obtained almost quantitatively. Subsequently, these cycles were polymerized by ring opening polymerization (ROP) mediated by CALB to obtain semi-crystalline polymers. In addition, it has been shown that the polymers obtained from the ROP process could be transformed into cyclic oligomers in high yields using enzymatic cyclodepolymerization, thereby recycling the polymer in a circular biosynthetic path.



Flores, I.; Martínez de Ilarduya, A.; Sardon, H.; Müller, A. J.; Muñoz-Guerra, S. Synthesis of Aromatic–Aliphatic Polyesters by Enzymatic Ring Opening Polymerization of Cyclic Oligoesters and Their Cyclodepolymerization for a Circular Economy. *ACS Appl. Polym. Mater.* **2019**, *1* (3), 321-325.

## 6.2 Introduction

The production of plastics obtained from petrochemical resources is not sustainable.<sup>1</sup> Physical or chemical recycling is among the possible solutions associated with the disposal of plastic waste. In the latter case, after the recycling process, monomers are obtained which can be used again to obtain the polymers, allowing a circular alternative for these residues.<sup>2</sup> In the case of aromatic-aliphatic polyesters such as PET, different chemical recycling methods have been proposed to obtain the monomers such as methanolysis, glycolysis, hydrolysis or aminolysis.<sup>3</sup> For aliphatic polyesters Chen et al.<sup>4</sup> developed a method in which changing the reaction conditions could select the direction of the chemical equilibrium toward the formation of cyclic monomer or polymer, allowing the preparation of polyesters with infinite recyclability. A similar idea was used by Shaver et al.<sup>5</sup> to prepare a new biodegradable aromatic-aliphatic polyester by ROP that could be easily depolymerized to monomer using a very active aluminium salen catalyst.

One of the most interesting approaches where the reaction conditions can be used to select the direction of the monomer-polymer equilibrium is the entropically driven ring opening polymerization of macrocycles (ED-ROP). Macrocycles with 14 or more atoms have very small transannular interactions so that the negative Gibbs free energy required for their opening is mainly due to the positive entropy generated by the increase in conformational flexibility entailed in the polymerization. This situation can be reverted at high dilutions where the translational entropy of the macrocycles prevails and the equilibrium shifts to the formation of the cycles.<sup>6-8</sup> For instance, the ROP of cyclic oligoesters, which is mainly entropically driven, has been explored as a clean route for the synthesis of high molecular weight polyesters. The almost athermal character of these reactions has been corroborated by the work of He et al.,<sup>9</sup> which reported small values of  $\Delta H_p$  between -1 and -2  $\text{kJ}\cdot\text{mol}^{-1}$  and values of  $\Delta S_p$  between 10 and 17  $\text{J}\cdot\text{mol}^{-1}\cdot\text{K}^{-1}$  for some alkylene terephthalate cyclic oligomers, which were calculated from cycles/polymer equilibrium concentrations at different polymerization temperatures. In this reaction, as opposed to polycondensation, no by-products are generated, and high molecular weight polymers can be obtained in short reaction times.<sup>10</sup> The reaction can be catalyzed by metallic,<sup>11</sup> organometallic<sup>12</sup> and organic<sup>13</sup>

catalysts or enzymes.<sup>14–16</sup> The main drawback of this methodology is that, the synthesis of the cyclic oligomeric precursors is laborious, affords low yields and in some cases acid chloride derived reagents are used to obtain the initial macrocycles.<sup>17</sup>

Cyclic oligoesters derived from aliphatic diols such as ethylene glycol, 1,4-butanediol or 1,6-hexanediol and aromatic diacids, such as terephthalic or furandicarboxylic acids, have been usually obtained by high dilution condensation (HDC) of diols and acid dichlorides or by cyclodepolymerization (CDP) in solution at high temperatures.<sup>12,17–20</sup> In these cases the final products are contaminated by linear oligomeric species that have to be removed by column chromatography or by other techniques, such as selective precipitation, if high molecular weight polyesters want to be produced by ROP.<sup>17–20</sup>

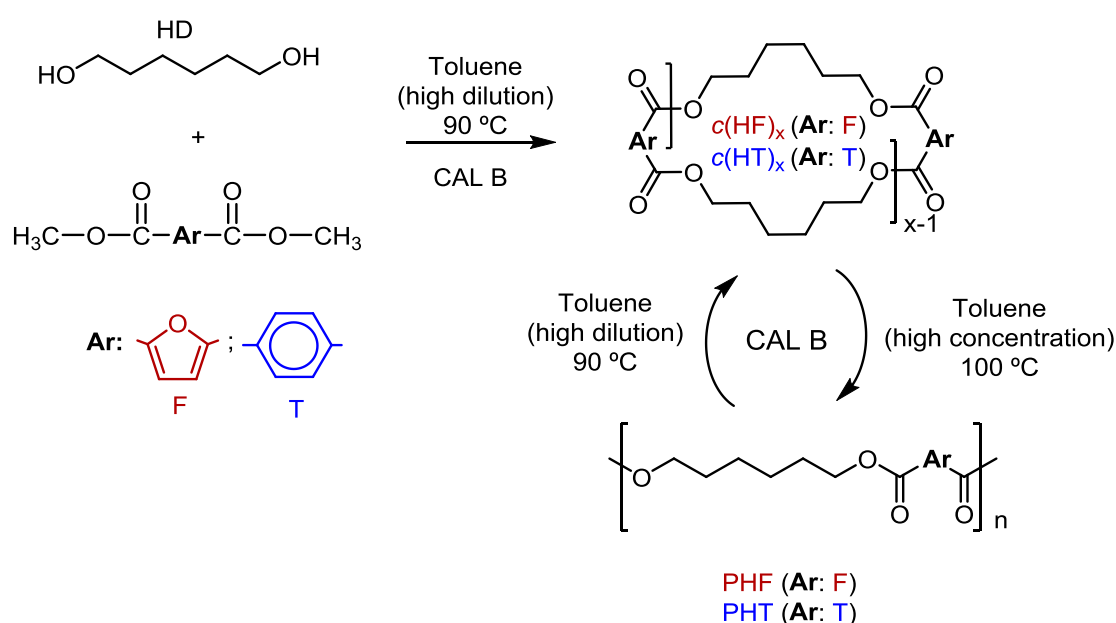
Although the enzymatic synthesis of cyclic aliphatic oligoesters,<sup>16</sup> and the use of enzymes for preparation of aliphatic polyesters from different macrolactones, such as globalide or pentadecalactone has been reported in the literature,<sup>21,22</sup> the use of enzymes for the production of more interesting technological aliphatic-aromatic cyclic oligoesters or polyesters has been scarcely studied.<sup>23</sup> Only a few reports mention the possibility of formation of cyclic oligomeric species as side products in the enzymatic polymerization of dimethyl furanoate and diols of different lengths.<sup>24</sup>

In this contribution, the synthesis of cyclic oligomers of hexamethylene terephthalate and hexamethylene furanoate is reported. An enzymatic reaction using *Candida antarctica* lipase B enzyme was performed by avoiding the use of acid chloride derived reagents. These cycles were obtained in high yields and they were found to be able to polymerize with the concurrence of the same enzyme. Additionally, the ability of CALB to favor the cyclodepolymerization of the polyesters upon selection of the appropriate conditions was shown, thereby corroborating that these cycles could be recovered in high yields, opening a recycling pathway for further polymerization.

### 6.3 Results and Discussion

The chemical route followed for the synthesis of hexamethylene furanoate and hexamethylene terephthalate cyclic oligomers, their cyclopolymerization, and their recovery by cyclodepolymerization is depicted in Scheme 6.1.

The first step was to synthesize cycles from 1,6 Hexanediol (HD) combined with dimethyl terephthalate (DMT) or dimethyl furanoate (DMF), later the cycles were opened by ROP to obtain the linear polymers. The linear polymers were then taken to be cyclodepolymerized and cyclic oligomers obtained again.



**Scheme 6.1.** Enzymatic synthesis of  $c(\text{HF})_x$  and  $c(\text{HT})_x$  cyclic oligomers, their cyclopolymerization and the cyclodepolymerization of their respective polyesters

The cyclization reaction was carried out in toluene solution under mild and high dilution conditions in the presence of enzymes. Its evolution was followed by HPLC and  $^1\text{H}$  NMR analysis of aliquots taken at scheduled times.

The presence of small amounts of cyclic oligomers mixed with other species, such as short linear oligomers, was detected after 7 hours of reaction. However, after 1 day of reaction, the non-cyclic structures fully disappeared (Annex D, Figures D1 to D4).  $^1\text{H}$  NMR spectra showed the almost complete disappearance of signals corresponding to the methyl and hydroxymethylene protons after 1 day of reaction. To further confirm the non-presence of linear structures, HPLC and GPC analysis were

performed, confirming that only cyclic species were present. To evaluate the thermodynamics of the process, the reaction was maintained for 7 days, during this period, ROP reactions or changes in the content of the different cycle species were not observed, indicating that the thermodynamic equilibrium was reached from the first 24 hours of reaction (1 day), see Figures D5 and D6 (Annex D). The presence of CALB was essential because no reaction was observed in the absence of this enzyme after 7 days (Annex D, Figures D7 and D8).

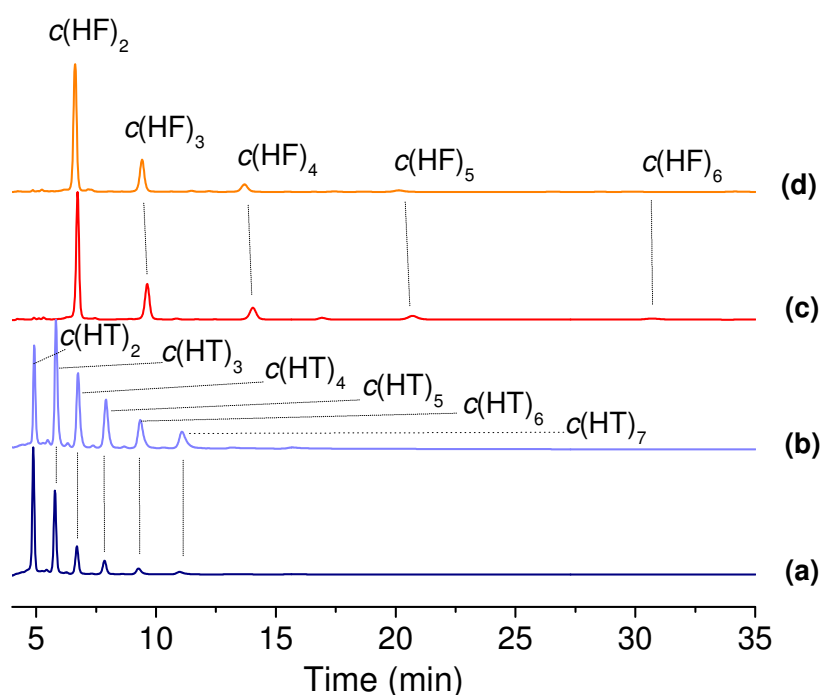


**Figure 6.1.** HPLC chromatograms of the crude product obtained after 7 days of enzymatic HDC: a)  $c(\text{HT})_x$  and c)  $c(\text{HF})_x$ , and after 3 days of enzymatic CDP: b)  $c(\text{HT})_x$  and d)  $c(\text{HF})_x$ .

More detail evaluation of HPLC crude reaction products after 7 days (Figure 6.1) reveals that cyclic oligomeric species from dimer to hexamer<sub>7</sub> for the hexamethylene furanoate and to heptamer for the hexamethylene terephthalate derivatives were the main products. In addition, it is clearly observed that their relative contents rapidly decreased with cycle size in both cases in accordance with a thermodynamically controlled process as described by Jacobson-Stockmayer model, in which the concentration of cyclics obtained is proportional to approximately the  $5/2$  power of cyclic size.<sup>25</sup> It has to be mentioned that the content of cyclic dimer was clearly superior for the  $c(\text{HF})_x$  cycles than for  $c(\text{HT})_x$ . It seems that the furanoate 2,5 substitution, as compared to the terephthalate 1,4 substitution favors the ring closure

of smaller cycles for the former. A similar effect has been observed for PBT cycles obtained by CDP, where the content of cyclic dimer was lower than predicted by both, a modified Jacobson/Stockmayer<sup>26</sup> and RIS theories and attributed to its high ring strain.<sup>27</sup> No linear oligomers were detected at longer retention times. The assignment of different HPCL peaks was carried out by comparison with the MALDI-TOF MS spectra obtained from these samples (Annex D, Figures D9 and D10). On the other hand, the content of the different oligomeric  $c(\text{HT})_x$  cycles was not far from that obtained by cyclodepolymerization of PHT in solution at high temperatures using organometallic catalyst.<sup>18</sup>

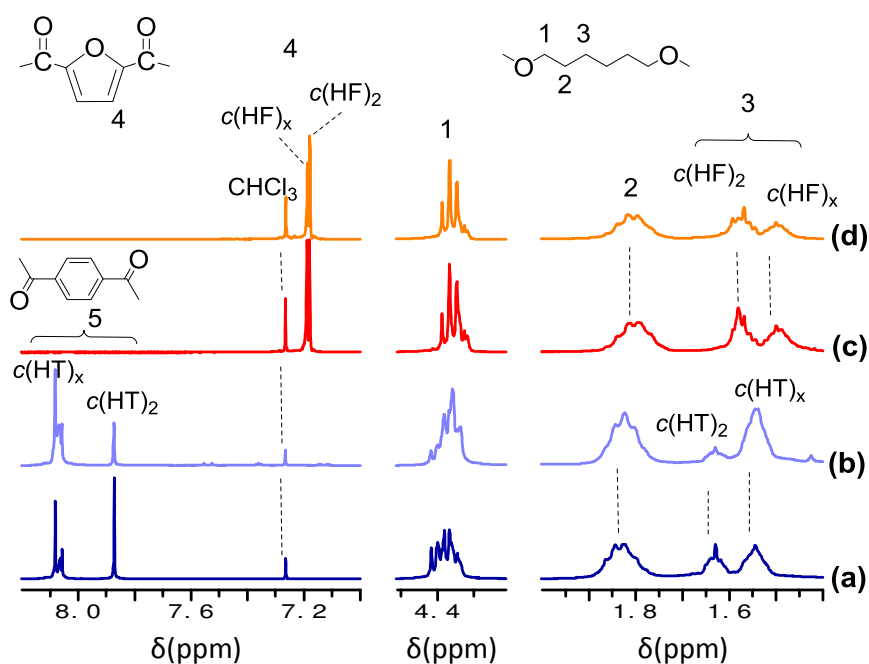


**Figure 6.2.**  $^1\text{H}$  NMR of the crude product obtained after 7 days of enzymatic HDC (down) and 3 days of enzymatic CPD (up). a) and b)  $c(\text{HT})_x$ , c) and d)  $c(\text{HF})_x$ .

The results obtained by HPLC were corroborated by  $^1\text{H}$  NMR (Figure 6.2). In these spectra, signals due to small cyclic species, such as dimers, appeared clearly resolved and downfield and upfield shifted for the interior methylenes (3) and aromatic protons (4,5) respectively. Such displacements were, most probably due to the magnetic anisotropy effects caused by the electrons circulation in the aromatic rings, an effect that has been observed in other related cycles.<sup>17,28</sup>

The thermal stability of the synthesized cycles was evaluated by TGA analysis under inert atmosphere. The TGA thermograms in Figure 6.3 show that both types of

cycles were thermally stable up to around 250-270 °C. They decomposed in a single step with temperatures of maximum decomposition rate at 379 and 389 °C for  $c(\text{HF})_x$  and  $c(\text{HT})_x$  respectively, and with remaining weights at 600 °C about 3 wt% (Table 6.1).

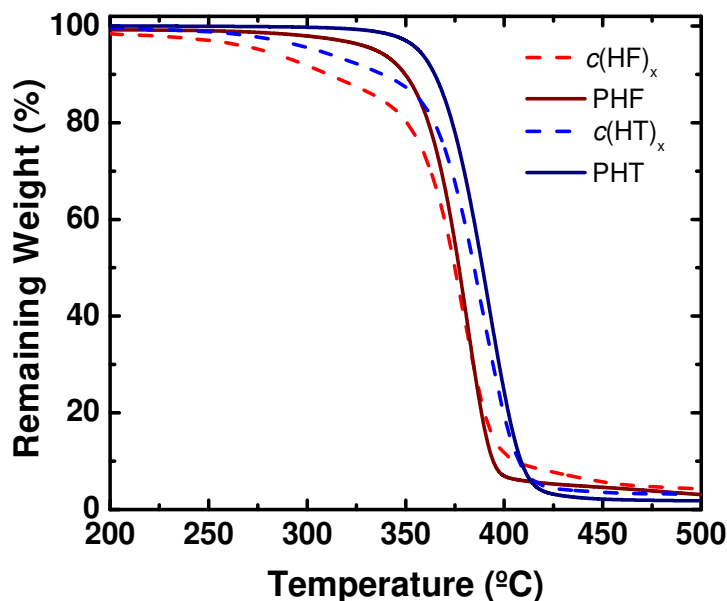


**Figure 6.3.** TGA analysis of  $c(\text{HF})_x$ ,  $c(\text{HT})_x$ , and PHF, PHT derived polymers.

DSC data recorded from as synthesized samples showed that both types of cyclic oligomers display endotherms at around 92-93 °C. These peaks are broad due to the melting of the different size crystallites belonging to different cyclic species and showed melting enthalpies of 24 and 41 J g<sup>-1</sup> for  $c(\text{HF})_x$  and  $c(\text{HT})_x$  respectively (Figure 6.4).

After the first heating treatment both type cycles were not able to crystallize and flat thermograms were observed in the second heating scans (Annex D, Figure D11). The thermal properties observed allow concluding that these cycles could be processed for bulk polymerization by ROP at temperatures between 100-250 °C in the presence of a catalyst.

The suitability of  $c(\text{HT})_x$  and  $c(\text{HF})_x$  to be polymerized by ROP in the presence of CALB to give PHT and PHF polyesters, respectively, was then evidenced. As most of ED-ROP, the polymerization could be carried out at higher monomer concentration. Hence, the reaction was accomplished at 100 °C using higher cycles concentration.<sup>16</sup> After 24 h, polymers with weight average molecular weights of 8.9 and 15 Kg mol<sup>-1</sup> were attained for PHT and PHF respectively (Table 6.1). Control test carried out

without enzymes showed that no reaction took place under same conditions and the cyclic oligomers were recovered at the end of reaction. The polyesters showed dispersities around 1.7-2.5, which are in accordance with the values observed for polymers obtained by entropically driven ring opening polymerization.<sup>6,7</sup>

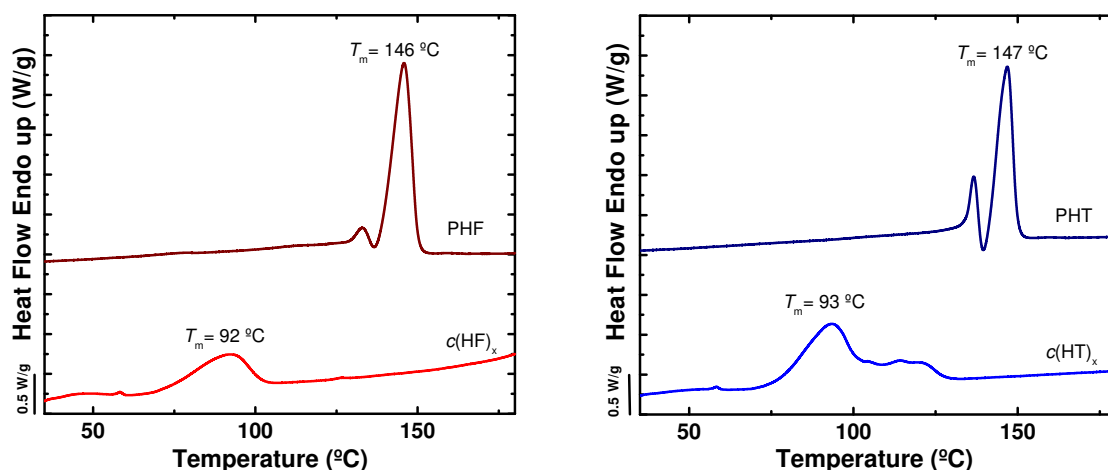


**Figure 6.4.** DSC thermograms of  $c(\text{HF})_x$  and  $c(\text{HT})_x$  cyclic oligomers (1st. heating) and their PHF and PHT derived polymers (2nd. heating).

**Table 6.1.** Molecular weights and thermal properties of  $c(\text{HT})_x$  and  $c(\text{HF})_x$  cyclic oligomers and PHT, PHF derived polymers.

Sample	Molecular Weights				TGA			DSC				
								First heating		Second heating		
	$M_n^a$ kDa	$M_n^b$ kDa	$M_w^b$ kDa	$\mathcal{D}^b$	$^oT_d^c$ (°C)	$\text{max}T_d^d$ (°C)	$R_w^e$ (%)	$T_g$ (°C)	$T_m$ (°C)	$\Delta H_m$ ( $\text{J}\cdot\text{g}^{-1}$ )	$T_m$ (°C)	$\Delta H_m$ ( $\text{J}\cdot\text{g}^{-1}$ )
$c(\text{HT})_x$	-	-	-	-	305	389	2.6	-	93	41	-	-
$c(\text{HF})_x$	-	-	-	-	277	379	3.2	-	92	24	-	-
PHT	10.5	3.6	8.9	2.5	356	393	1.3	11	148	51	136/147	6/35
PHF	6.9	9.1	15.0	1.7	335	382	1.6	15	147	75	146	60

<sup>a</sup>  $M_n$  determined by  $^1\text{H}$  NMR and using trichloroacetyl isocyanate (TAI) derivatizing agent (Annex D, Figures D14 and D15).<sup>29</sup>

<sup>b</sup>  $M_n$ ,  $M_w$  and dispersities determined by GPC.

<sup>c</sup> Temperature at which 5% weight loss was observed in the TGA traces recorded at  $10\text{ °C min}^{-1}$ .

<sup>d</sup> Temperature of maximum degradation rate.

<sup>e</sup> Remaining weight at  $600\text{ °C}$ .

PHT and PHF polyesters were recovered as white powders and characterized by  $^1\text{H}$  NMR (Figure 6.5). Signals due to cyclic oligomers disappeared, whereas new signals characteristic of linear species were detected. Moreover, a small triplet at 3.6 ppm was observed and assigned to the  $-\text{CH}_2\text{OH}$  end group.

The thermal stability of PHT and PHF polyesters here obtained was found to be slightly higher than that of their respective cyclic oligomers (Figure 6.3). The onset temperature increased around  $50\text{ }^\circ\text{C}$  and the maximum decomposition rate temperature around  $3\text{ }^\circ\text{C}$  in both cases (Table 6.1). In accordance with data reported for these polymers in the literature, PHT showed better thermal stability than PHF.<sup>18,23</sup> DSC scans recorded for these polyester samples are depicted in Figure 6.4 and showed that both of them were semicrystalline polymers with melting temperatures of  $147$  and  $146\text{ }^\circ\text{C}$  for PHT and PHF, respectively, not far from those observed for the same polyesters obtained by melt polycondensation.<sup>23,30,31</sup>

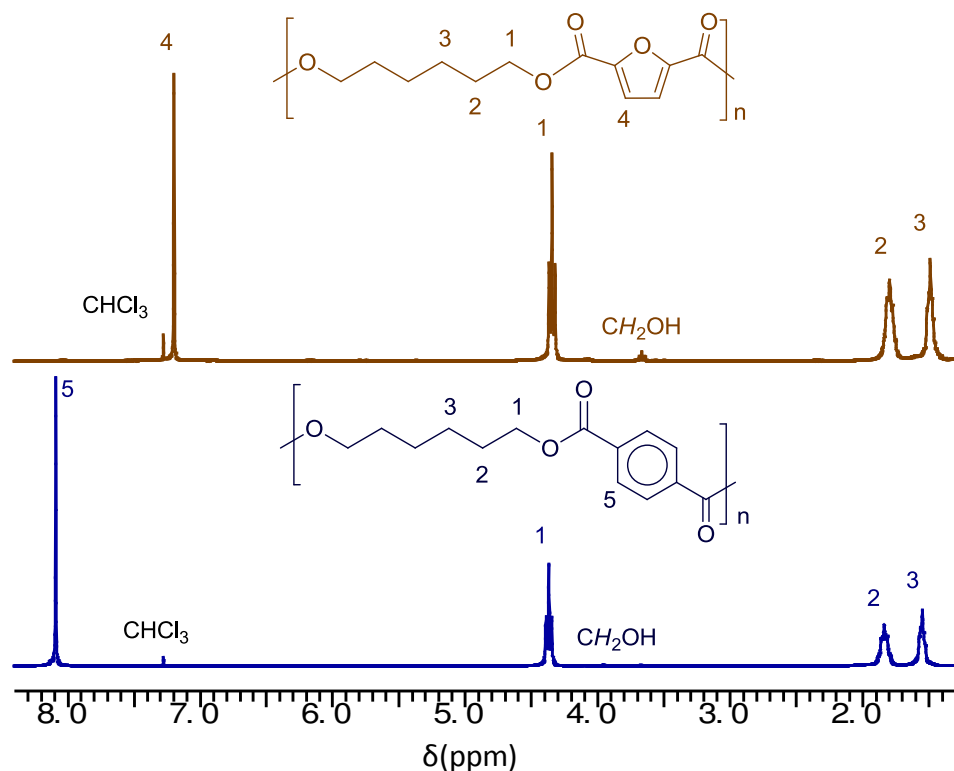


**Figure 6.5.**  $^1\text{H}$  NMR of PHF (top) and PHT (bottom) obtained by enzymatic ROP of  $c(\text{HF})_x$  and  $c(\text{HT})_x$  respectively.

The two melting peaks observed for PHT may be due to the presence of different polymorphs or to a crystalline reorganization process taking place during the heating scan.<sup>31</sup> Samples recorded at different heating rates showed these two peaks with almost no differences in both melting temperatures and enthalpies (Annex D, Figure D11). Further experiments are needed to ascertain their precise origin (e.g., WAXS as a function of temperature). The glass transition temperatures determined from rapidly melt quenched samples were around 11 and 15 °C for PHT and PHF respectively.

To determine if this enzymatic process could be used as a recycling tool, a preliminary essay with samples of previously synthesized polyesters were subjected to cyclodepolymerization in solution in the presence and absence of CALB. This CDP reaction, carried out under conditions similar to those used for enzymatic cyclization, was followed by <sup>1</sup>H NMR (Annex D, Figures D12 and D13). Both <sup>1</sup>H NMR (Figure 6.2b and 6.2d) and HPLC data showed that, in the presence of CALB, oligomeric cycles were obtained almost quantitatively after 72 hours of reaction, being the dimer the predominant species for PHF and the trimer for PHT (Figure 6.1b and 6.1d). The linear polymer was recovered at the end of reaction in the absence of CALB enzyme, showing its biocatalytic effect for the intramolecular transesterification reaction.

## 6.4 Conclusions

In summary, it can be concluded that cyclic oligoesters derived from dimethyl terephthalate and dimethyl furanoate and 1,6-hexanediol can be obtained in high yields by enzymatic cyclization. The successful polymerization of these cycles by enzymes has been proven, and even more interestingly, the cyclodepolymerization that converts the polyester into cyclic oligoesters has been also demonstrated. The approach here described can be extrapolated to the synthesis of other cycles of higher industrial interest, such as those derived from ethylene glycol or 1,4-butanediol and aromatic diesters, which are usually obtained by HDC or CDP. One drawback of these enzymatic reactions is that longer reaction times are required to be accomplished if compared with those assisted by metallic or organometallic catalysts. This limitation is susceptible to being solved by using a more efficient enzyme able to work at higher temperatures.

## 6.5 References

- (1) Sardon, H.; Dove, A. P. Plastics Recycling with a Difference. *Science* **2018**, *360* (6387), 380–381. <https://doi.org/10.1126/science.aat4997>.
- (2) Hong, M.; Chen, E. Y.-X. Chemically Recyclable Polymers: A Circular Economy Approach to Sustainability. *Green Chemistry* **2017**, *19* (16), 3692–3706. <https://doi.org/10.1039/C7GC01496A>.
- (3) Al-Sabagh, A. M.; Yehia, F. Z.; Eshaq, Gh.; Rabie, A. M.; ElMetwally, A. E. Greener Routes for Recycling of Polyethylene Terephthalate. *Egyptian Journal of Petroleum* **2016**, *25* (1), 53–64. <https://doi.org/10.1016/j.ejpe.2015.03.001>.
- (4) Hong, M.; Chen, E. Y.-X. Completely Recyclable Biopolymers with Linear and Cyclic Topologies via Ring-Opening Polymerization of  $\gamma$ -Butyrolactone. *Nature Chemistry* **2016**, *8* (1), 42–49. <https://doi.org/10.1038/nchem.2391>.
- (5) Lizundia, E.; Makwana, V. A.; Larrañaga, A.; Vilas, J. L.; Shaver, M. P. Thermal, Structural and Degradation Properties of an Aromatic–Aliphatic Polyester Built through Ring-Opening Polymerisation. *Polymer Chemistry* **2017**, *8* (22), 3530–3538. <https://doi.org/10.1039/C7PY00695K>.
- (6) Hodge, P. Entropically Driven Ring-Opening Polymerization of Strainless Organic Macrocycles. *Chemical Reviews* **2014**, *114* (4), 2278–2312. <https://doi.org/10.1021/cr400222p>.
- (7) Strandman, S.; Gautrot, J. E.; Zhu, X. X. Recent Advances in Entropy-Driven Ring-Opening Polymerizations. *Polym. Chem.* **2011**, *2* (4), 791–799. <https://doi.org/10.1039/C0PY00328J>.
- (8) Albertsson, A.-C.; Varma, I. K.; Srivastava, R. K. Polyesters from Large Lactones. In *Handbook of Ring-Opening Polymerization*; Dubois, P., Coulembier, O., Raquez, J.-M., Eds.; Wiley-VCH Verlag GmbH & Co. KGaA: Weinheim, Germany, 2009; pp 287–306. <https://doi.org/10.1002/9783527628407.ch11>.
- (9) He, C.; Zhu, X.; Li, X.-H.; Yang, X.-M.; Tu, Y.-F. Thermodynamics of Aromatic Cyclic Ester Polymerization in Bulk. *Chinese Journal of Polymer Science* **2019**, *37* (1), 89–93. <https://doi.org/10.1007/s10118-018-2161-4>.
- (10) Brunelle, D. J. Cyclic Oligomer Chemistry. *Journal of Polymer Science Part A: Polymer Chemistry* **2008**, *46* (4), 1151–1164. <https://doi.org/10.1002/pola.22526>.

- (11) Youk, J. H.; Kambour, R. P.; MacKnight, W. J. Polymerization of Ethylene Terephthalate Cyclic Oligomers with Antimony Trioxide<sup>†</sup>. *Macromolecules* **2000**, *33* (10), 3594–3599. <https://doi.org/10.1021/ma991838d>.
- (12) Brunelle, D. J.; Bradt, J. E.; Serth-Guzzo, J.; Takekoshi, T.; Evans, T. L.; Pearce, E. J.; Wilson, P. R. Semicrystalline Polymers via Ring-Opening Polymerization: Preparation and Polymerization of Alkylene Phthalate Cyclic Oligomers. *Macromolecules* **1998**, *31* (15), 4782–4790. <https://doi.org/10.1021/ma971491j>.
- (13) Pinaud, J.; Tang, R.; Gimello, O.; Robin, J.-J. Organocatalyzed Ring-Opening Polymerization of Cyclic Butylene Terephthalate Oligomers. *Journal of Polymer Science Part A: Polymer Chemistry* **2017**, *55* (9), 1611–1619. <https://doi.org/10.1002/pola.28534>.
- (14) Jiang, Y.; Loos, K. Enzymatic Synthesis of Biobased Polyesters and Polyamides. *Polymers* **2016**, *8* (7), 243. <https://doi.org/10.3390/polym8070243>.
- (15) Albertsson, A.; Srivastava, R. Recent Developments in Enzyme-Catalyzed Ring-Opening Polymerization☆. *Advanced Drug Delivery Reviews* **2008**, *60* (9), 1077–1093. <https://doi.org/10.1016/j.addr.2008.02.007>.
- (16) Sugihara, S.; Toshima, K.; Matsumura, S. New Strategy for Enzymatic Synthesis of High-Molecular-Weight Poly(Butylene Succinate) via Cyclic Oligomers. *Macromolecular Rapid Communications* **2006**, *27* (3), 203–207. <https://doi.org/10.1002/marc.200500723>.
- (17) Fleckenstein, P.; Rosenboom, J.-G.; Storti, G.; Morbidelli, M. Synthesis of Cyclic (Ethylene Furanoate) Oligomers via Cyclodepolymerization. *Macromolecular Reaction Engineering* **2018**, *12* (4), 1800018. <https://doi.org/10.1002/mren.201800018>.
- (18) González-Vidal, N.; Martínez de Ilarduya, A.; Herrera, V.; Muñoz-Guerra, S. Poly(Hexamethylene Terephthalate- Co -Caprolactone) Copolyesters Obtained by Ring-Opening Polymerization. *Macromolecules* **2008**, *41* (12), 4136–4146. <https://doi.org/10.1021/ma702464k>.
- (19) Pfister, D.; Storti, G.; Tancini, F.; Costa, L. I.; Morbidelli, M. Synthesis and Ring-Opening Polymerization of Cyclic Butylene 2,5-Furandicarboxylate. *Macromolecular Chemistry and Physics* **2015**, *216* (21), 2141–2146. <https://doi.org/10.1002/macp.201500297>.

- (20) Carlos Morales-Huerta, J.; Martínez de Ilarduya, A.; Muñoz-Guerra, S. Poly(Alkylene 2,5-Furandicarboxylate)s (PEF and PBF) by Ring Opening Polymerization. *Polymer* **2016**, *87*, 148–158. <https://doi.org/10.1016/j.polymer.2016.02.003>.
- (21) van der Meulen, I.; de Geus, M.; Antheunis, H.; Deumens, R.; Joosten, E. A. J.; Koning, C. E.; Heise, A. Polymers from Functional Macrolactones as Potential Biomaterials: Enzymatic Ring Opening Polymerization, Biodegradation, and Biocompatibility. *Biomacromolecules* **2008**, *9* (12), 3404–3410. <https://doi.org/10.1021/bm800898c>.
- (22) Bisht, K. S.; Henderson, L. A.; Gross, R. A.; Kaplan, D. L.; Swift, G. Enzyme-Catalyzed Ring-Opening Polymerization of  $\omega$ -Pentadecalactone<sup>†</sup>. *Macromolecules* **1997**, *30* (9), 2705–2711. <https://doi.org/10.1021/ma961869y>.
- (23) Jiang, Y.; Woortman, A. J. J.; Alberda van Ekenstein, G. O. R.; Loos, K. A Biocatalytic Approach towards Sustainable Furanic–Aliphatic Polyesters. *Polymer Chemistry* **2015**, *6* (29), 5198–5211. <https://doi.org/10.1039/C5PY00629E>.
- (24) Cruz-Izquierdo, Á.; van den Broek, L. A. M.; Serra, J. L.; Llama, M. J.; Boeriu, C. G. Lipase-Catalyzed Synthesis of Oligoesters of 2,5-Furandicarboxylic Acid with Aliphatic Diols. *Pure and Applied Chemistry* **2015**, *87* (1), 59–69. <https://doi.org/10.1515/pac-2014-1003>.
- (25) Jacobson, H.; Stockmayer, W. H. Intramolecular Reaction in Polycondensations. I. The Theory of Linear Systems. *The Journal of Chemical Physics* **1950**, *18* (12), 1600–1606. <https://doi.org/10.1063/1.1747547>.
- (26) Ercolani, G.; Mandolini, L.; Mencarelli, P. Kinetic Treatment of Irreversible Cyclooligomerization of Bifunctional Chains and Its Relevance to the Synthesis of Many-Membered Rings. *Macromolecules* **1988**, *21* (5), 1241–1246. <https://doi.org/10.1021/ma00183a011>.
- (27) Hubbard, P. A.; Brittain, W. J.; Mattice, W. L.; Brunelle, D. J. Ring-Size Distribution in the Depolymerization of Poly(Butylene Terephthalate). *Macromolecules* **1998**, *31* (5), 1518–1522. <https://doi.org/10.1021/ma971275a>.
- (28) de Ilarduya, A. M.; Muñoz-Guerra, S. Chemical Structure and Microstructure of Poly(Alkylene Terephthalate)s, Their Copolyesters, and Their Blends as Studied by

- 
- NMR. *Macromolecular Chemistry and Physics* **2014**, *215* (22), 2138–2160. <https://doi.org/10.1002/macp.201400239>.
- (29) Donovan, A. R.; Moad, G. A Novel Method for Determination of Polyester End-Groups by NMR Spectroscopy. *Polymer* **2005**, *46* (14), 5005–5011. <https://doi.org/10.1016/j.polymer.2005.04.032>.
- (30) Papageorgiou, G. Z.; Tsanaktsis, V.; Papageorgiou, D. G.; Chrissafis, K.; Exarhopoulos, S.; Bikiaris, D. N. Furan-Based Polyesters from Renewable Resources: Crystallization and Thermal Degradation Behavior of Poly(Hexamethylene 2,5-Furan-Dicarboxylate). *European Polymer Journal* **2015**, *67*, 383–396. <https://doi.org/10.1016/j.eurpolymj.2014.08.031>.
- (31) Ghosh, A. K.; Woo, E. M.; Sun, Y.-S.; Lee, L.-T.; Wu, M.-C. Characterization and Analyses on Complex Melting, Polymorphism, and Crystal Phases in Melt-Crystallized Poly(Hexamethylene Terephthalate). *Macromolecules* **2005**, *38* (11), 4780–4790. <https://doi.org/10.1021/ma0473667>.

# Chapter 7

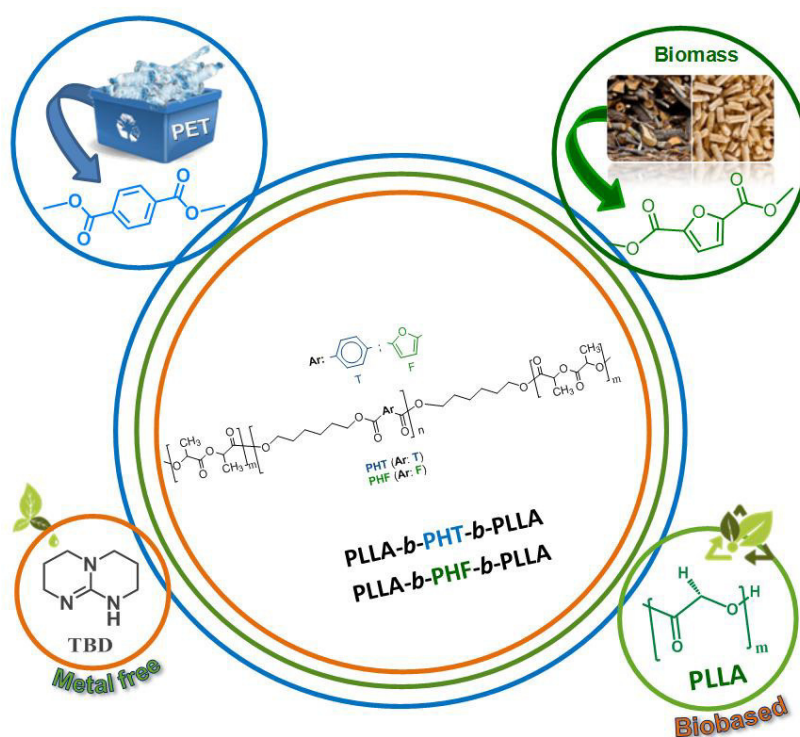
## *Triblock Copolymers using PHF or PHT with L-lactide: Synthesis and Characterization.*

7.1 Abstract.....	164
7.2 Introduction.....	165
7.3 Results and Discussion.....	167
7.3.1 Synthesis of Triblock Copolymers.....	167
7.3.2 Thermal Characterization.....	171
7.3.3 Characterization of the Crystalline Structure.....	176
7.4 Conclusions.....	189
7.5 References.....	190

## 7.1 Abstract

Two series of new triblock copolymers of the ABA type were successfully obtained using an organic catalyst (metal-free catalyst) to promote copolymerization. In both series A is poly (lactic acid) (a biobased polymer). In the first series B is poly (hexamethylene terephthalate) which was polymerized using dimethyl terephthalate and in the second series, B is poly (hexamethylene furanoate) which was synthesized with dimethyl furanoate (monomer derived from biomass).

The materials obtained were characterized from the molecular, thermal and structural point of view by NMR, viscosimetry, TGA, DSC, WAXS and SAXS. The results obtained show that the PLLA bound to PHT or PHF forming the triblock copolymers does not crystallize. PHT and PHF blocks can crystallize and their thermal and structural properties ( $T_m$ ,  $T_c$ ,  $X_c$  and lamellar thickness) do not depend on PLLA content until PLLA concentration is very high and topological restrictions difficult crystallization. PLLA copolymers with PHT or PHF show a single  $T_g$  suggesting that the components are miscible in the amorphous state. On the other hand, a single phase in the molten state was appreciated in almost all copolymers, showing the miscibility of the components in the molten state.



## 7.2 Introduction

The concern for the current environmental conditions and especially for those caused by the contamination of plastics, has generated interest in the production of biodegradable and/or biobased polymers.<sup>1</sup> Biobased polymers reduce the environmental footprint caused by the manufacture of plastics, on the other hand biodegradable polymers at the end of their life cycle tend to disintegrate and this helps to reduce the amount of plastic waste in landfills.<sup>1</sup>

In this sense, poly (lactic acid) (PLA) is one of the polymers that have gained large popularity because it is biobased, biodegradable and has good properties for some applications in the packaging industry and in the biomedical field.<sup>1-4</sup> However, several studies have focused on improving their properties by mixing PLA with other polymers to form copolymers, where copolymerization offers the opportunity to adapt the final properties of the materials.<sup>4</sup> In chapter 4 it is shown that one potential method to improve the properties of PLA is to combine it with aromatic polyesters such as PET to enhance the thermal stability and mechanical properties. Nevertheless, it is found that due to the harsh polymerization conditions for polycondensation (above 200 C), PLA tended to epimerize decreasing substantially the molecular weight of the final copolyesters.

Ring Opening Polymerization is another method to prepare polyesters from cyclic monomers. Although this procedure has been used for the synthesis of a great diversity of polymers, its application to the preparation of aromatic-aliphatic polyesters is less studied. The milder reaction conditions required and the minimization of undesirable sub-products, are appreciated advantages of ROP over conventional polycondensation. Thus, Muñoz et al., employed this method for the preparation of random copolymers based on PCL-co-PHF.

In this sense, it is believed that the ROP could be highly suitable to obtain well defined aliphatic-aromatic copolyesters based on PLLA. These copolymers containing in their chemical structure PLA have shown potential as compatibilizers in polymer mixtures.<sup>5-7</sup>

As shown in the previous chapter, Poly (hexamethylene terephthalate) (PHT) is an aromatic polyester with good mechanical properties and chemical resistance could

be successfully prepared from the polymerization of macrocycles by enzymes.<sup>8</sup> The presence of the flexible hexamethylene segment in the polyester chain, generates that the PHT has a relative low melting temperature (140 °C), which could be an advantage during material processing and for ROP process.<sup>9,10</sup> Similarly, poly (hexamethylene 2,5-furan dicarboxylate) (PHF), has similar properties together with the advantage this monomer is derived from renewable sources. Due to its good properties, this polymer can be used in some applications where polyesters such as terephthalates are usually employed.<sup>11-13</sup> While the polymerization was demonstrated, the ability to obtain well defined telechelic low molecular weight polyesters that can be further employed for the ROP of other esters has not been studied.

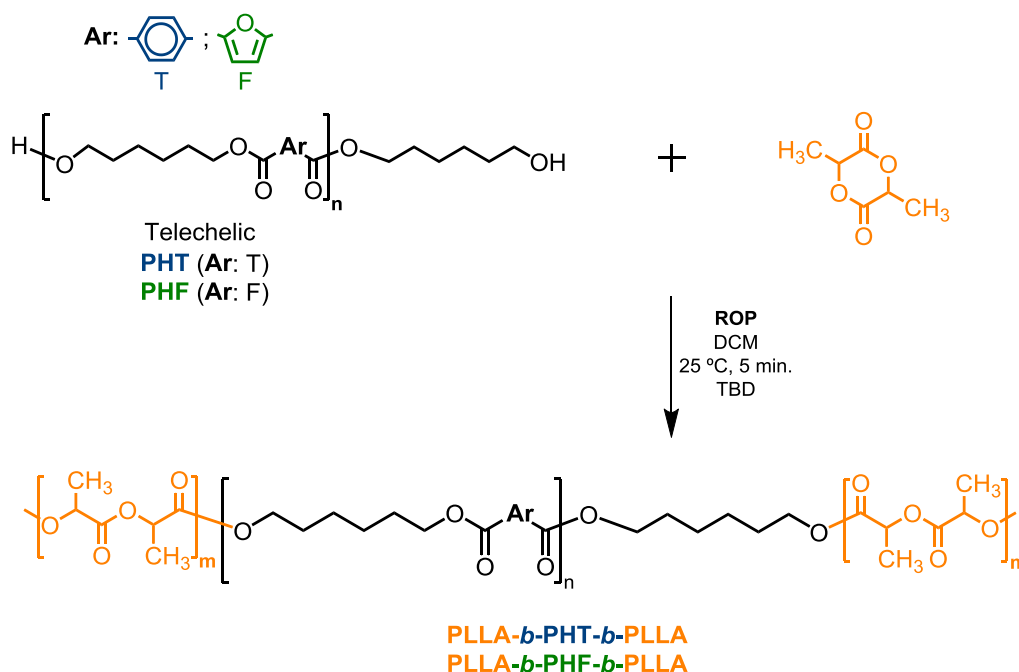
In this work, ABA triblock copolymers were synthesized using metal free approaches. First, the synthesis of cyclic oligomers of hexamethylene terephthalate and hexamethylene furanoate by enzymatic reaction using *Candida antarctica* lipase B(CALB) enzyme was carried out as in the previous chapter followed by the controlled ROP of these macrocycles to obtain low molecular weight telechelic polyester diols. These macrodiols were further employed for the ROP of L-LA in order to obtain triblock copolymers with different PLLA contents. The thermal behavior of the materials was analyzed to understand the effect of the composition of PLLA-*b*-PHT-*b*-PLLA or PLLA-*b*-PHF-*b*-PLLA on the properties of the copolymers.

## 7.3 Results and Discussions

### 7.3.1 Synthesis of Triblock Copolymers

In this chapter, the triblock copolymers were synthesized using TBD as catalyst, due to the effectiveness shown by this catalyst to copolymerize PLA with other polymers and form triblock copolymers.<sup>14,15</sup> Due to the above, it is expected that the TBD has a catalytic activity that promotes the formation of triblock copolymers (PLLA-*b*-PHT-*b*-PLLA and PLLA-*b*-PHF-*b*-PLLA).

First, the oligomers derived from HT or HF, were synthesized according to procedure described in detail in chapter 6. Where it is mentioned that telechelics from HT and HF were obtained by ROP using CALB as a catalyst, a diol (1,6 Hexanediol) was employed as initiator (1/12 ratio). The polymerization of both telechelics was confirmed by <sup>1</sup>H NMR and their characteristic peaks are observed in the Figures 7.1 and 7.2.



**Scheme 7.1.** Synthesis of Triblock Copolymers.

The obtained telechelics had a theoretical molecular weight of 3,000. When making the calculation of the experimental molecular weight by NMR the value of  $M_n$  was similar to the theoretical. After this characterization that corroborated the

formation of low molecular weight telechelic polyester diols, the corresponding oligomers (PHT or PHF) were used as initiator for the ring opening polymerization of L-lactide in the presence of the TBD catalyst. Due to the fact that the telechelic oligomer has two hydroxyl end groups, the final copolymer is expected to have an ABA triblock structure (Scheme 7.1) if no transesterification takes place during the ROP process.

The copolymerization reaction was followed by both GPC and NMR.  $^1\text{H}$  NMR spectra of PLLA-*b*-PHT-*b*-PLLA triblock copolymers (Figures 7.1 and 7.2) revealed that the hydroxyl end groups of the telechelic oligomers acted as initiators in the ROP of L-lactide. Signals corresponding to the methylene end groups of PHT and PHF downfield shifted as a consequence of the esterification reaction taking place with the lactide monomer. No signals were observed at 3.66 for both series indicating that all end groups initiated the ROP of lactide monomer.

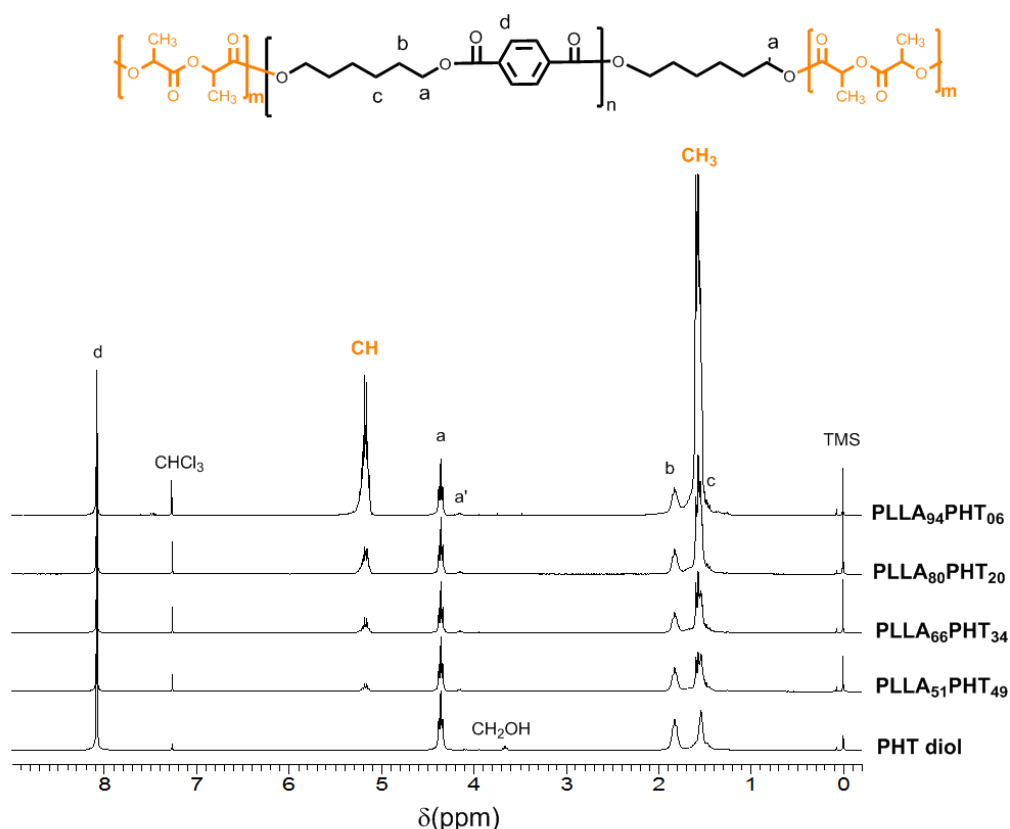


**Figure 7.1.**  $^1\text{H}$  NMR spectra of PHT diol and PLLA-*b*-PHT-*b*-PLLA copolyesters with peak assignments.

The copolymer composition (Table 7.1) was determined by integration of signals appearing at 5.15 ppm corresponding to the methine protons of lactate units

and signals appearing at around 4.30 and 4.15 ppm corresponding to a and a' methylenes respectively of the hexamethylene furanoate and hexamethylene terephthalate units.

In order to confirm the triblock structure of the copolymers obtained,  $^{13}\text{C}$  NMR spectra were carried out for both series. Figures E1 and E2 (Annex E), show full  $^{13}\text{C}$  NMR spectra for PLLA-*b*-PHAr-*b*-PLLA copolymers with peak assignments. As it is well documented, carbonyl as well as non-protonated aromatic carbons are very sensitive to sequence distributions.<sup>16</sup> In the spectra of both series, signals due to carbonyls of PHT and PHF blocks appear as single peaks (Figure 7.3), which indicates that no transesterification took place during ROP of L-lactide initiated by the telechelic PHT and PHF oligomers. On the other hand, the carbonyl signal of PLLA blocks appears split as a consequence of monomer racemization during polymerization. This splitting was more evident as the molecular weight increased or triblock copolymer was enriched in lactate units.

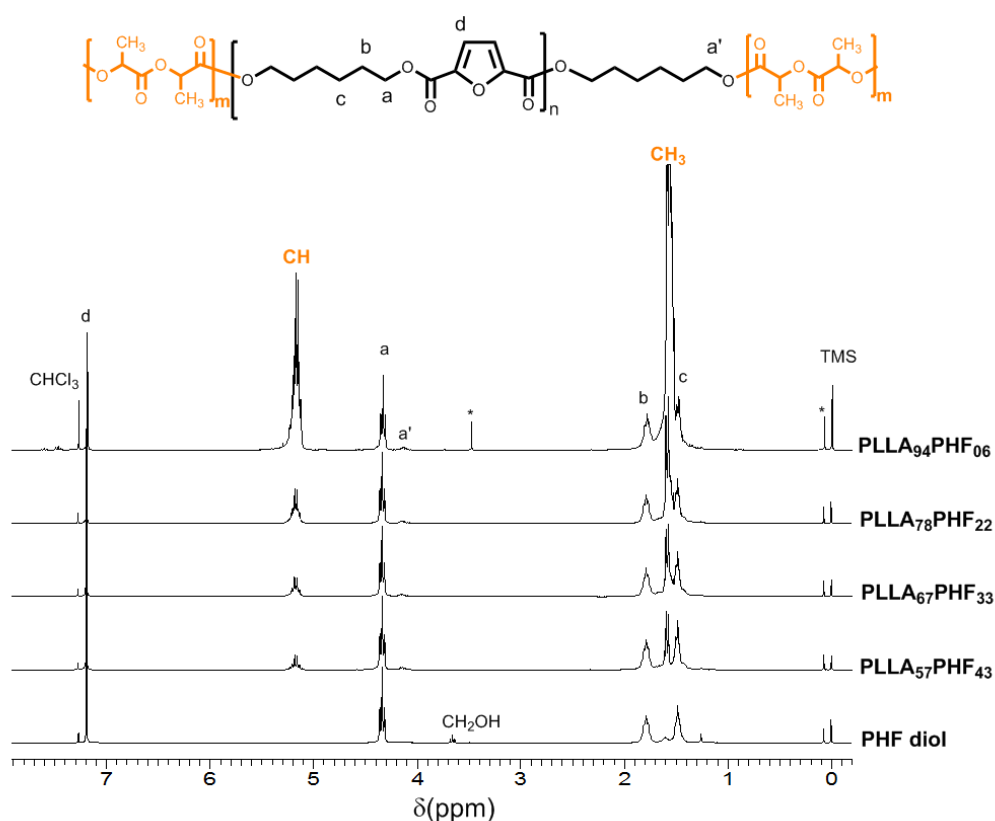


**Figure 7.2.**  $^1\text{H}$  NMR spectra of PHF diol and PLLA-*b*-PHF-*b*-PLLA copolyesters with peak assignments. (\*) Signals of methanol and silicon oil impurities.

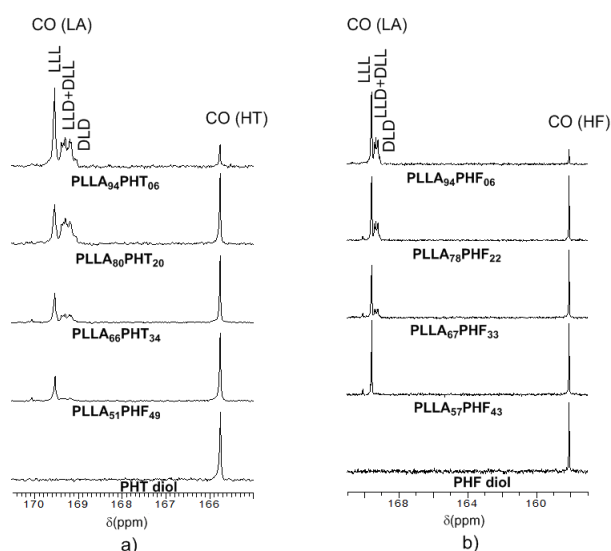


**Figure 7.3.**  $^{13}\text{C}$  NMR spectra of a) PHT diol and PLLA-*b*-PHT-*b*-PLLA copolyesters and b) PHF diol and PLLA-*b*-PHF-*b*-PLLA copolyesters in the region of carbonyl peaks.

GPC chromatograms for both series are compared in Figure 7.4. For both PHT and PHF telechelic oligomers, broad bands with dispersity index ( $\mathfrak{D}$ ) of 2.2 are observed at high volume elution. On the other hand, it is clearly observed that these bands are clearly displaced at lower retention times by copolymerization and this displacement is more evident as the copolymers increase the content in lactate units. Monomodal bands with lower values of  $\mathfrak{D}$  were observed for both series, indicating that L-lactide monomer is exclusively initiated by both PHT and PHF telechelic oligomers. Number and weight average molar masses and dispersity index  $\mathfrak{D}$  obtained from these chromatograms are collected in Table 7.1.

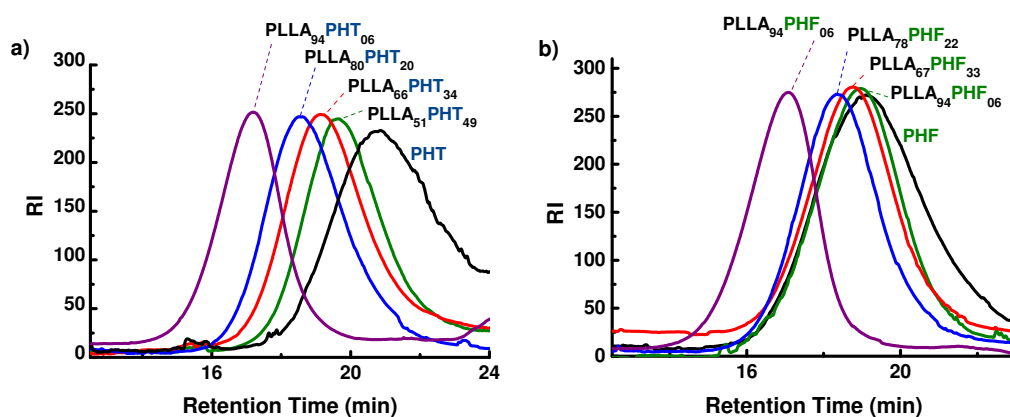


**Figure 7.4.** GPC chromatograms of a) PHT and PLLA-*b*-PHT-*b*-PLLA copolyesters and b) PHF and PLLA-*b*-PHF-*b*-PLLA copolyesters.

**Table 7.1** Composition, Molecular Weight and Block Lengths of Synthesized Polymers.

Sample	NMR					GPC			
	% mass ratio		% mol ratio		L-PHT-L <sup>a</sup>	$M_n$	$M_n$	$M_w$	$\bar{D}$
	HT	Lactic	HT	Lactic					
PHT	100	-	100	-	-	3300	1650	3600	2.2
PLLA <sub>51</sub> PHT <sub>49</sub>	77	23	49	51	07:14:07	4400	3650	6750	1.8
PLLA <sub>66</sub> PHT <sub>34</sub>	64	36	34	66	14:14:14	5350	4750	9150	1.9
PLLA <sub>80</sub> PHT <sub>20</sub>	46	54	20	80	28:14:28	7550	7400	12650	1.8
PLLA <sub>94</sub> PHT <sub>06</sub>	18	82	6	94	110:14:110	19300	18800	29000	1.5
	HF	Lactic	HF	Lactic	L-PHF-L				
PHF	100	-	100	-	-	3900	4750	10500	2.2
PLLA <sub>57</sub> PHF <sub>43</sub>	71	29	43	57	11:16:11	5440	7050	12250	1.7
PLLA <sub>67</sub> PHF <sub>33</sub>	62	38	33	67	16:16:16	6350	8300	13000	1.6
PLLA <sub>78</sub> PHF <sub>22</sub>	48	52	22	78	30:17:30	8400	9650	15600	1.6
PLLA <sub>94</sub> PHF <sub>06</sub>	17	83	6	94	116:14:116	20200	22600	31800	1.4

<sup>a</sup> Number of L units [poly (lactic acid)] and number of repetitive units of PHT or PHF present in the blocks.

### 7.3.2 Thermal Characterization

The obtained triblock copolymers were thermally characterized. The thermal stability of materials made with PLLA and PHT as well as the materials made with PLLA and PHF showed similar trend. In both cases, it is observed that when the amount of PLLA in the copolymers is increased, the thermal stability decreases (Figure 7.5). However, when the amount of PLLA present in the copolymer is 94%, the thermal stability seems to increase and closely resembles that of pure PLLA.<sup>17</sup>

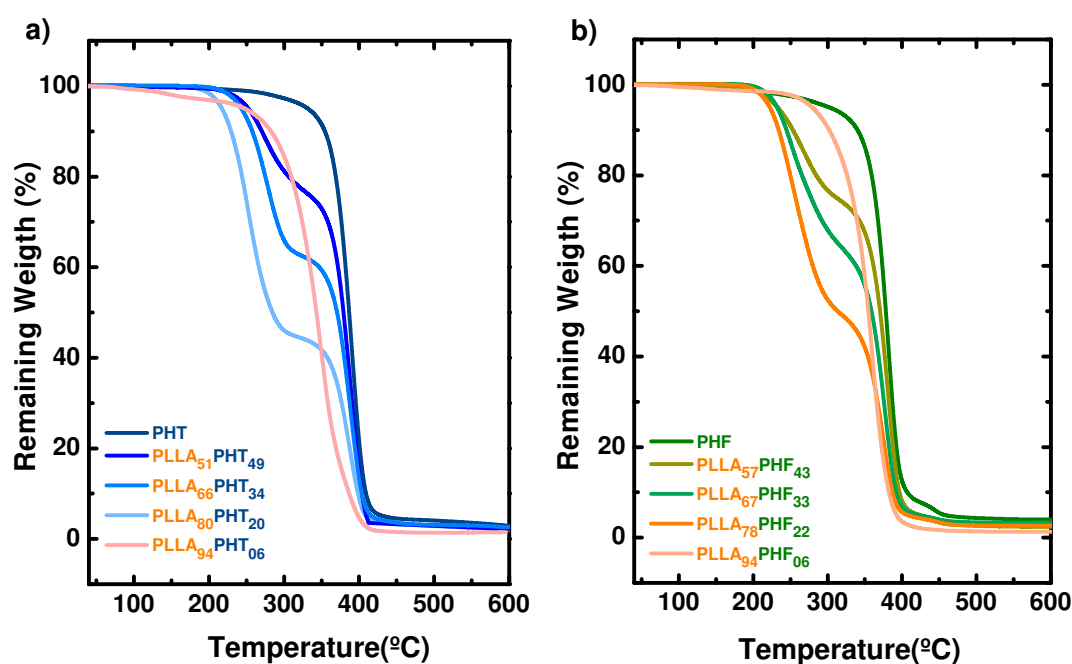


**Figure 7.5.** TGA of (a) triblock copolymers PLLA-*b*-PHT-*b*-PLLA and (b) triblock copolymers PLLA-*b*-PHF-*b*-PLLA.

Both copolymer families showed two stages of degradation, the first stage could be attributed to the PLLA and the second to the PHT or PHF present in the copolymer. To corroborate the above, a comparison between the percentage by weight of PHT and PHT present in each copolymer (Table 7.1) versus the amount in weight that remains at the end of the first stage (Figure 7.5), can be performed. For example, the copolymer with 51 mol % of PLLA has 77 % by weight of PHT according to Table 7.1, this same copolymer in the Figure 7.5(a) at the end of the first stage (the PLLA has degraded) appears to have a remaining weight of approximately 76%, which corresponds to the PHT present in the copolymer. This comparison can be applied to the rest of the copolymers, where the weight percentage values obtained in Table 7.1 are similar to those shown in Figure 7.5.

On the other hand in Figure E.3 in Annex E, the temperatures at which the materials loose 5 and 10% of their weight ( $T_{5\%}$  and  $T_{50\%}$ ), respectively are observed. It is appreciated that by increasing the amount of PLLA in the copolymer the values of  $T_{5\%}$  and  $T_{50\%}$  tend to decrease. But, when the amount of PLLA present in the copolymer is 94%, the values seem to increase.

The data shown above suggest that in both series of copolymers the PLLA affects the thermal stability of the PHT or PHT to a point where the amount of PLLA is so large that from this point the copolymer tends to have a thermal stability very similar to neat PLLA.

**Table 7.2** Thermal Properties of Triblock Copolymers.

Sample	DSC							
	Cooling				Second heating			
	$T_g$ (°C)	$T_c$ (°C)	$\Delta H_c$ (J/g)	$T_{cc}$ (°C)	$\Delta H_{cc}$ (J/g)	$T_m$ (°C)	$\Delta H_m$ (J/g)	$\Delta H_{mf}$ (J/g)
Telechelic PHT	-8	105.3	-46	-	-	139.2	46	46
PLLA <sub>51</sub> PHT <sub>49</sub>	16	104.4	-48	-	-	138.9	49	49
PLLA <sub>66</sub> PHT <sub>34</sub>	35	102.4	-47	-	-	139.8	44	44
PLLA <sub>80</sub> PHT <sub>20</sub>	32	93	-50	-	-	139.7	48	48
PLLA <sub>94</sub> PHT <sub>06</sub>	43	53.4	-11	64.5	-13	134.6	33	20
Telechelic PHF	-5	91.8	-57	122.5	-1	141.3	59	58
PLLA <sub>57</sub> PHF <sub>43</sub>	13	83.8	-62	-	-	138.9	62	62
PLLA <sub>67</sub> PHF <sub>33</sub>	18	76	-13	79.3	-40	135.8	60	20
PLLA <sub>78</sub> PHF <sub>22</sub>	18	73.6	-10	86.3	-46	136.7	52	6
PLLA <sub>94</sub> PHF <sub>06</sub>	45	-	-	114.5	-8	138.1	12	4

The thermal properties of the copolymers from PLLA with PHT or PHF ( $T_g$ ,  $T_m$ ,  $T_c$ ,  $T_{cc}$  and  $\Delta H$ ) were measured using differential scanning calorimetry (DSC). The values of these parameters are shown in the Table 7.2. In this table  $\Delta H_c$ ,  $\Delta H_m$  and  $\Delta H_{cc}$  are normalized values (i.e.  $\Delta H = \frac{\Delta H}{W}$ , where  $W$  is the mass fraction of the phase that crystallizes). From this same table  $\Delta H_{mF}$  represents the value the subtraction of ( $\Delta H_m - \Delta H_{cc}$ ).

DSC second heating scans are shown in Figure 7.6 for the PLLA-*b*-PHT-*b*-PLLA triblock copolymers. In these triblock copolymers, it was found that the PLLA blocks are not able to crystallize (this was corroborated by WAXS and will be shown below). The glass transition temperature is observed around 30 °C followed by melting at much higher temperatures (around 140 °C). The melting transition occurs when PHT crystals melt. On the other hand, the presence of a single  $T_g$  could suggest that the PLLA and PHT components are miscible in the amorphous state.

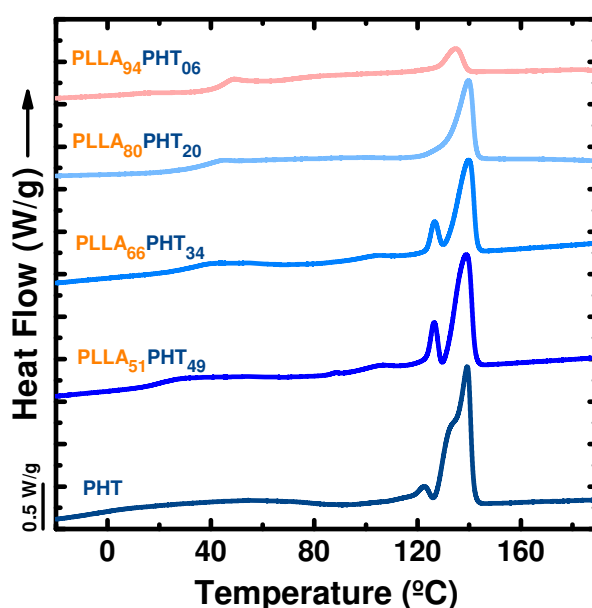


**Figure 7.6.** DSC second heating scans for the PHT and PLLA-*b*-PHT-*b*-PLLA.

Two melting peaks, or a bimodal melting peak, are observed in neat PHT and in two of the copolymers. These double melting peaks can be assigned to the melting of two different PHT polymorphs. According to literature, it has been reported that PHT exhibits more than one melting peak. This is because this polymer crystallizes in three crystalline forms:  $\alpha$ ,  $\beta$  and  $\gamma$ , where depending on the thermal conditions to which the

crystal has been exposed before a measurement the formation of different polymorphs can be expected.<sup>9,18–22</sup>

It has been reported that when the PHT is annealed at temperatures close to 140 °C or higher, the beta form tends to be more stable. On the other hand, when the PHT is annealed at low or moderate temperatures (<140 °C), there is a mixture of crystals of the alpha and beta forms. There is a third crystalline form ( $\gamma$ ), which is usually found in solvent-induced crystallization at room temperature.<sup>9,19,22</sup>

In this work prior to the measurements in DSC, the materials were annealed at 200 °C for 3 minutes, in order to erase their thermal history, from the above and according to the literature it is expected that the DSC scan will show two melting peaks corresponding to a beta crystalline ( $\beta$ ) form.<sup>9</sup> Wu *et al.*, report a peak around 145 °C and another of 138 °C, where the higher value is usually considered as the melting point of PHT, these values can vary depending on the molecular weight and the cooling and heating conditions of the samples.<sup>9</sup>

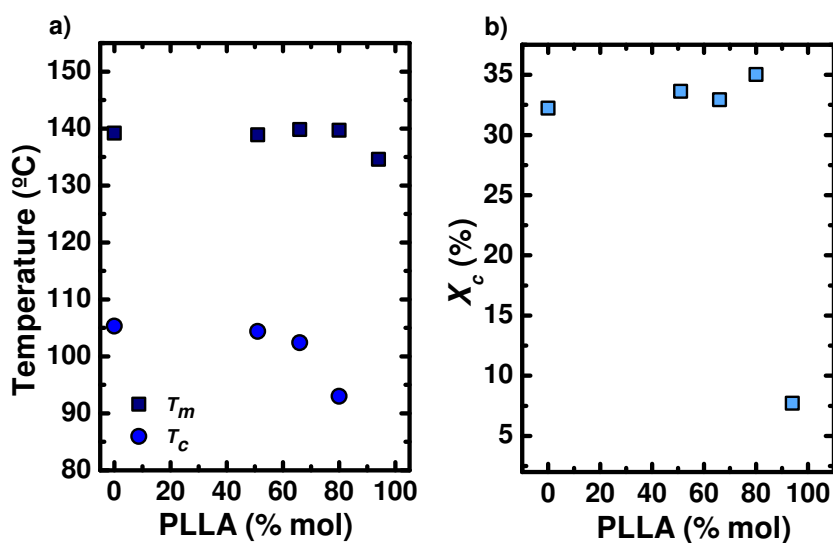


**Figure 7.7.** For PLLA-*b*-PHT-*b*-PLLA copolymers: (a) Values of  $T_m$  and  $T_c$  as a function of composition and (b)  $X_c$  versus composition composition.

Figure 7.6 shows a PHT with two peaks, one corresponding to the melting point of the polymer (140 °C) and another next value below the  $T_m$  (123 °C), this corroborates what is described in the previous paragraph, indicating that the form  $\beta$  for PHT is observed in Figure 7.6. In this same figure, for the copolymers with two peaks, it can also be suggested that they are due to the PHT polymorphism and that  $\beta$ -

form is the one that predominates in these materials. However, to corroborate the above WAXS studies were carried out and are described below.

In the case of copolymers with 80 and 94 mol % of PLLA, only one melting peak is observed, this could be related to the high amount of PLLA in the copolymer (Figure 7.6). The thermal properties ( $T_m$  and  $T_c$ ) of the PHT versus the copolymers formed are similar to each other, indicating that the PLLA does not affect crystallization behavior to a high degree (Figure 7.7.). On the other hand, the crystallinity of the PHT block does not vary with composition except when 94% PLLA is present in the copolymer (Figure 7.7(b)). The percentage crystallinity ( $X_c$ ) was calculated by dividing  $\Delta H_c$  (obtained from the cooling run) by  $\Delta H_m^0$  (142.7 J/g for PHT) and then multiplying by 100%.<sup>23</sup> During cooling all polymers exhibited a single crystallization peak (Figure E.4, Annex E).

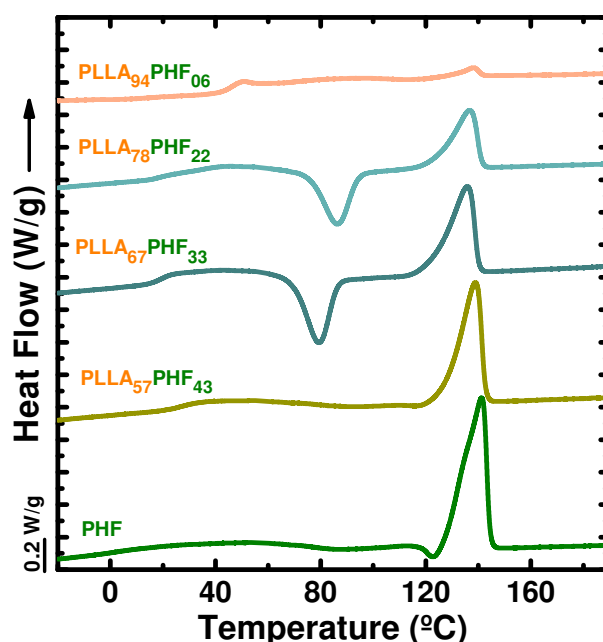


**Figure 7.8.** DSC second heating scans for the PHF and PLLA-*b*-PHF-*b*-PLLA.

The series of copolymers made from PLLA and PHF was also thermally characterized. Figure 7.8 shows the thermal behavior of neat PHF and the PHF block within the PLLA-*b*-PHF-*b*-PLLA triblock copolymers. All materials exhibit melting endotherms. Above 57 mol% of PLLA, a pronounced cold crystallization exotherm is observed in the copolymers, indicating that the sample is not able to fully crystallize during the previous cooling run. Cold-crystallization processes (with rather low

associated enthalpies) are also observed in the DSC heating scan of neat PHF at approximately 80 °C and just before melting at 120 °C.

In this series of copolymers the thermal properties ( $T_m$  and  $T_c$ ) as well as the crystallinity ( $X_c$ ) are affected by the presence of PLLA (Figure 7.9), where the trend suggests a decrease of these parameters when the amount of PLLA in the copolymer increases, except for  $T_m$  values. This can be explained by the cold-crystallization and reorganization processes that occur during the heating scans. To calculate ( $X_c$ ) a value of  $\Delta H_m^o$  (143 J/g) was taken from the literature.<sup>12</sup> During cooling from the melt, neat PHF and the PHF block within the copolymers exhibited a single crystallization peak (Figure E.5, Annex E).

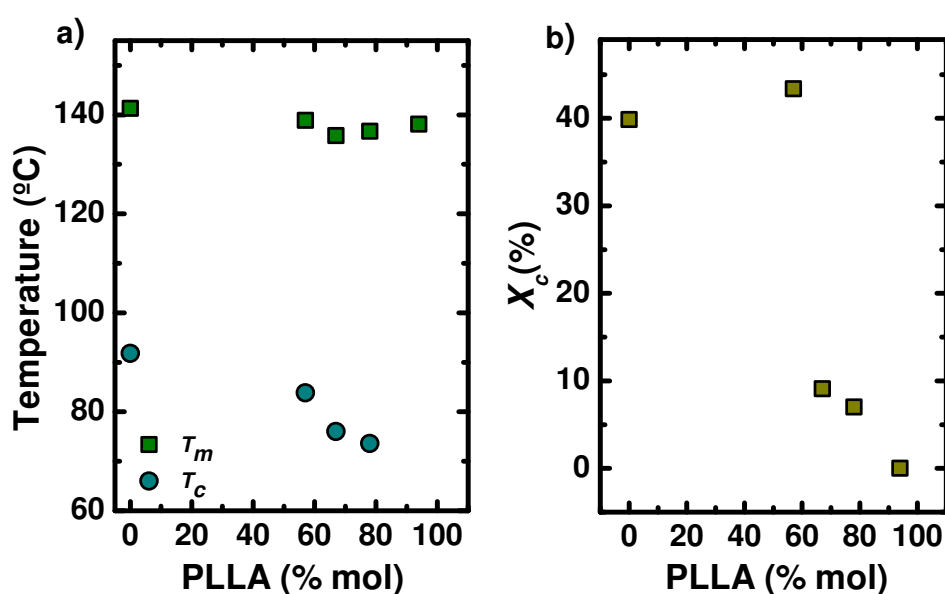


**Figure 7.9.** Thermal transitions for PLLA-*b*-PHF-*b*-PLLA copolymers: (a) Values of  $T_m$  and  $T_c$  as a function of composition and (b)  $X_c$  versus composition.

### 7.3.3 Characterization of the Crystalline Structure

#### 7.3.3.1 PLLA-*b*-PHT-*b*-PLLA Copolymers

The structural characterization was performed by WAXS for both polymer series. For the copolymers derived from PHT with PLLA, it was first shown that only PHT crystals were formed, as their different crystalline forms are appreciated in the diffractogram (Figure 7.10).<sup>9,18,19</sup> In addition, the crystalline parameters characteristic

of this homopolymer are shown in Table 7.3, and they all match with those reported in the literature.<sup>19,20</sup>

**Table 7.3** Crystal cell parameters and crystal forms of PHT.

Crystal form designations	$\alpha$	$\beta$	$\gamma$
Crystal geometry	monoclinic	triclinic	triclinic
a(nm)	0.91	0.48	0.53
b(nm)	1.72	0.57	1.39
c(nm)	1.55	1.57	1.55

Figure 7.10 shows that depending on the temperature a specific PHT polymorph (alpha, beta or gamma) predominate in the structure, which is coherent with that described in several works<sup>9,19,20</sup>.

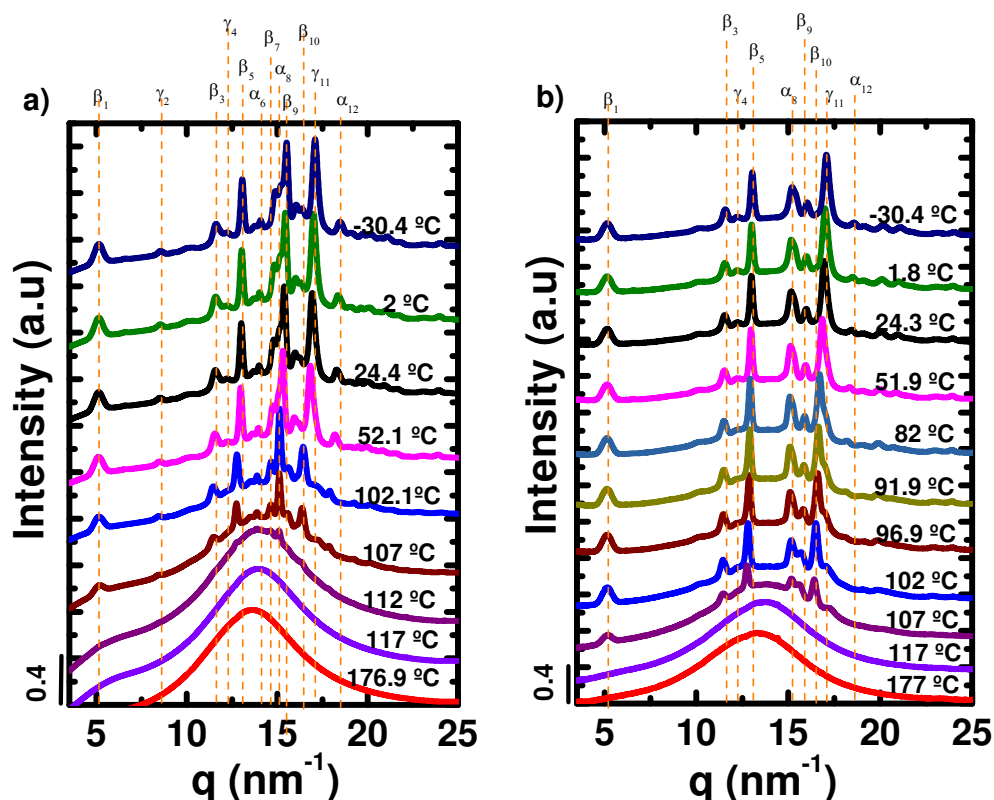
A comparison can be made in Figure 7.10 (a) and (b) between the temperature dependence of the crystalline structure of neat PHF and the PHF block within PLLA<sub>51</sub>PHT<sub>49</sub> copolymer respectively. The presence of PLLA blocks affects the crystallization of PHT block. For example, at 24 °C, the crystalline forms exhibited by neat PHT are different from that shown by the copolymer (Figure 7.10 (b)), but it is also observed that the variety of crystalline forms appreciated in the PHT decrease in the copolymer.

Table 7.4 shows the values obtained from  $2\theta$ , crystalline planes and the diffraction spaces ( $d_{hkl}$ , calculated according to Bragg's Law) for the PHT. These values are in accordance with those reported by different authors.<sup>9,18–20,24,25</sup>

**Table 7.4** Values of  $q$ ,  $2\theta$ , Crystalline Planes and  $d_{hkl}$  of PHT.

Crystal form designations	$q(\text{nm}^{-1})$	$2\theta$	Planes	$d_{hkl}(\text{nm})$
$\beta_1$	5.11	4.80	---	1.23
$\gamma_2$	8.56	8.05	---	0.734
$\beta_3$	11.66	10.97	---	0.539
$\gamma_4$	12.25	11.53	100	0.513
$\beta_5$	13.08	12.31	100	0.480
$\alpha_6$	14.08	13.25	200	0.446
$\beta_7$	14.65	13.79	101	0.429
$\alpha_8$	15.11	14.23	130	0.416
$\beta_9$	15.60	14.69	---	0.403
$\beta_{10}$	16.40	15.45	110	0.383
$\gamma_{11}$	17.10	16.11	120	0.367
$\alpha_{12}$	18.46	17.41	131	0.340

The WAXS results of the whole series of copolymers indicate that when the amount of PLLA in the copolymers increased, the intensity of the crystalline peaks decreased while the temperature at which the materials started to crystallize from the melt also decrease. In the case of the copolymer with 94 mol% of PLLA, no crystallization peak was exhibited in the diffractogram. The diffractograms of the rest of copolymers are shown in the Annex E.



**Figure 7.10.** Real time synchrotron WAXS diffraction patterns for samples (a) PHT and (b) PLLA<sub>51</sub>PHT<sub>49</sub>, cooled from 180 °C to -30 °C at 20 °C/min.

In order to study the effect that the PLLA has on the lamellar periodicity (long period), as well as on the lamellar thickness of the copolymers, SAXS experiments were carried out for copolymers derived from PHT and PLLA. Figure 7.11 shows the SAXS results at different temperatures for (a) PHT and (b) PLLA<sub>51</sub>PHT<sub>49</sub> samples, where the Lorentz corrected intensity is plotted as a function of the scattering vector  $q$ .

The materials exhibited a clear intense maximum due to the scattering caused by the periodic lamellar stacks (i.e., long period). The intensity of this maximum decreased as the amount of PLLA increased in the copolymers. In the melt state,

except for the copolymer with 94% PLLA, all copolymers do not exhibit any signal, indicating that there is no phase segregation and there is a mixed phase in the melt (Annex E). In the case of the copolymer with 94% of PLLA, a signal in the melt state is appreciated, which suggests the existence of phase segregation in the copolymer (Figure E.11, Annex E).

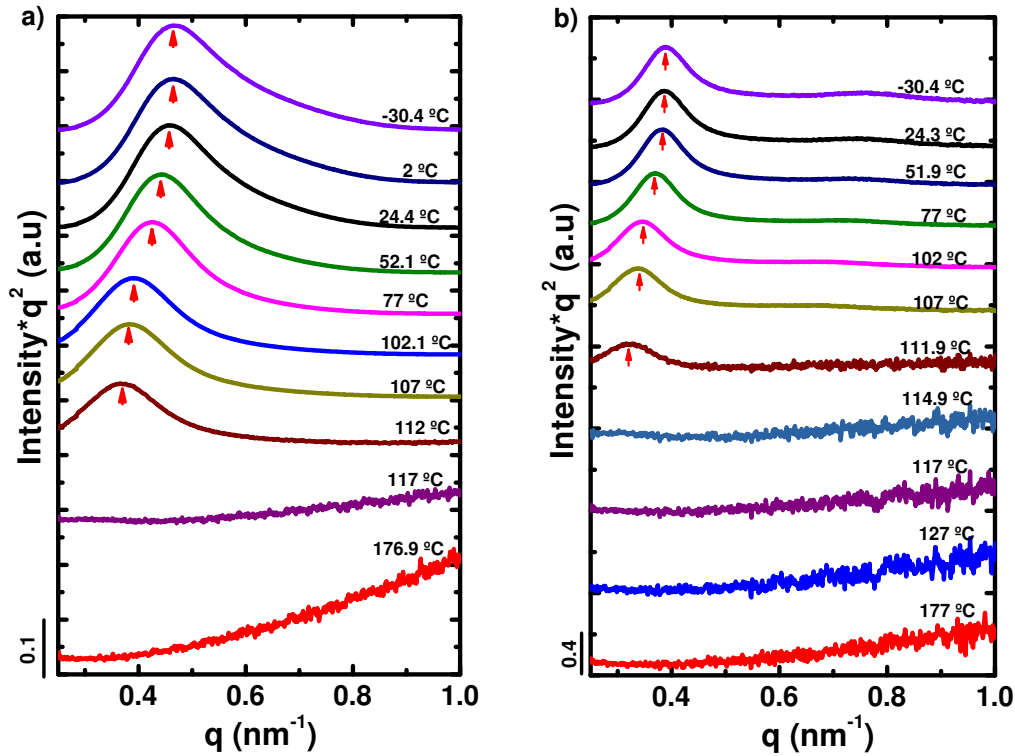


**Figure 7.11.** Lorentz-corrected SAXS profiles for (a) PHT and (b) PLLA<sub>51</sub>PHT<sub>49</sub>, with intensity as a function of scattering vector. Data taken of samples cooled from the 180 °C to -30 °C at 20 °C/min.

The segregation strength that could exist between PHT and PLLA was calculated ( $\chi N$ ). First, the Flory-Huggins interaction parameter ( $\chi$ ) between PHT and PLLA was determined using the following equation:<sup>26</sup>

$$\chi = \frac{V_1}{RT} (\delta_1 - \delta_2)^2 \quad (7.1)$$

where  $V_1$  is the molar volume of the solvent ( $\text{m}^3/\text{mol}$ ),  $R$  is the gas constant (8.314 J/K\* $\text{mol}$ ),  $T$  is the temperature (298.15 K) and  $\delta_1, \delta_2$  are the solubility

parameters of solvent and solute respectively  $(\text{J}/\text{m}^3)^{1/2}$ . To apply this equation to PHT-PLLA system, it is necessary to consider the PHT as the solute and the PLLA as the solvent. The value of  $\delta_1$  was calculated by the Method of Hoftyzer and Van Krevelen using the data and the procedure reported in the literature  $(20 (\text{MJ}/\text{m}^3)^{1/2})$ .<sup>27</sup> The same procedure was applied to calculate  $\delta_2$  (PHT), the value obtained was 21.9  $(\text{MJ}/\text{m}^3)^{1/2}$ .<sup>27</sup> On the other hand  $V_1$  for PLLA was calculated from  $V_1 = m/\rho$  (5.95E-05  $\text{m}^3/\text{mol}$ ). Considering all the parameters previously describe, the interaction parameter  $\chi$  was calculated and value of  $\chi=0.09$  was obtained. The book of Hiemenz and Lodge reports that when the value predicted by Equation 7.1 is less than 0.3, Equation 7.2 is much more reliable for estimating the value of  $\chi$ .<sup>26</sup>

$$\chi = \frac{V_1}{RT} (\delta_1 - \delta_2)^2 + 0.34 \quad (7.2)$$

Because the value of  $\chi$  calculated with the Eq. 7.1 was less than 0.3, the value considered for  $\chi$  was determined with the Eq. 7.2, the new value obtained was  $\chi=0.43$ .

The value of  $N$  (total degree of polymerization) was calculated by equation 7.3:

$$N = \frac{(Mn_A * \Phi_A) + (Mn_B * \Phi_B)}{(Mnr_A * \Phi_A) + (Mnr_B * \Phi_B)} \quad (7.3)$$

where  $Mn_A$  is the molecular weight of the PHT block (calculated by  $Mn = L_{\text{PHT}}$  from Table 7.1\*248 g/mol),  $Mn_B$  is the molecular weight of the PLLA block (calculated by  $Mn = L_{\text{PLLA}}$  from Table 7.1\*72 g/mol),  $\Phi_A$  and  $\Phi_B$  are the molar fractions of PHT and PLLA (this molar fraction is calculated considering the block of PHT bound to only one block of PLLA, that is, an AB link.) respectively, present in the copolymer.  $Mnr_A$  is the molecular weight of the repetitive unit of PHT (248 g/mol) and  $Mnr_B$  is the molecular weight of the repetitive unit of PLLA (72 g/mol). The values of  $N$  were calculated for every copolymer and the results are shown in Table 7.5.

**Table 7.5**  $N$  and  $\chi N$  of PLLA-*b*-PHT-*b*-PLLA.

Sample	$N$	$\chi N$
PLLA <sub>51</sub> PHT <sub>49</sub>	13	6
PLLA <sub>66</sub> PHT <sub>34</sub>	14	6
PLLA <sub>80</sub> PHT <sub>20</sub>	19	8
PLLA <sub>94</sub> PHT <sub>06</sub>	81	35

The segregation strength ( $\chi N$ ) between PLLA and PHT was calculated multiplying  $\chi$  by  $N$ . The results are appreciated in Table 7.5. In a diblock copolymer, ( $\chi N$ ) is the parameter that controls the segregation between blocks A and B. Generally segregation is classified into three regimes: weak, intermediate and strong. There is no well-defined criterion to separate these regimes, however there are works that discuss this issue, the articles reported by Matsen and Bates, indicate that  $\chi N \leq 10$  represents a copolymer without phase segregation, when  $\chi N \approx 12$  indicates the beginning of a weak to intermediate segregation and a value of  $\chi N \approx 50$  indicates the beginning of a segregation from intermediate to strong.<sup>28,29</sup>

In this case, the copolymers are triblock of the ABA form; therefore the parameter  $\chi N$  is calculated for the interaction between one block A and one block B, that is, one side AB, considering that the other side BA has the same interaction  $\chi N$ . In all copolymers, the  $\chi N$  values are below 50 which indicate a weak to intermediate segregation strength in these systems. For copolymers with less than or equal to 80% PLLA, the value of  $\chi N$  is less than 10, suggesting no segregation in these copolymers. On the other hand, a value of 35 for  $\chi N$  is appreciated when the copolymer has a 94% PLLA which indicates that in this composition segregation between the components of the copolymer (PHT and PLLA) is more likely to occur. This corroborates the results of SAXS for this composition.

For every sample, the long periods ( $d^*$ ) at different temperatures were estimated by Eq. (7.4) from  $q_{max}$  values taken from the Lorentz corrected plots ( $I^*q^2$  versus  $q$ ).

$$d^* = \frac{2\pi}{q_{max}} \quad (7.4)$$

Figure 7.12 shows that the value of  $d^*$  at low temperatures is a function of composition. The long period also increased with temperature, as the amorphous content increases, especially above 80 °C, where melting can start in some of the samples.

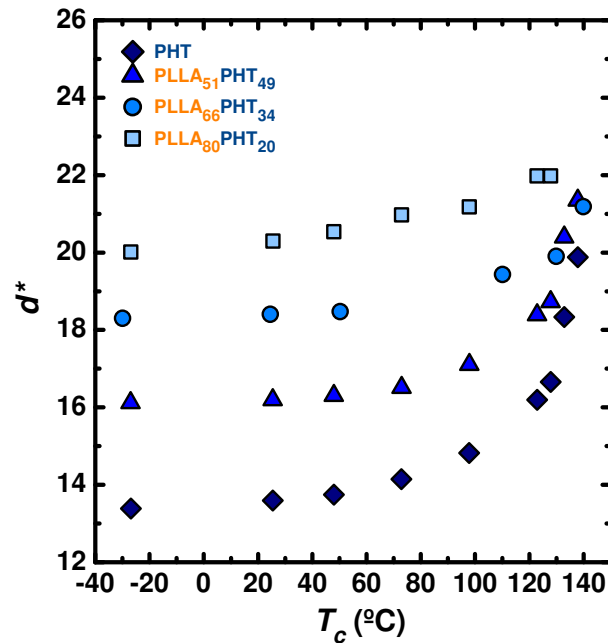


**Figure 7.12.** Long periods ( $d^*$ ) calculated from SAXS data as a function of temperature for PLLA-*b*-PHT-*b*-PLLA.

Parameters such as the degree of crystallinity of each phase and the lamellar thickness ( $l$ ), can be calculated from the analysis of data obtained from WAXS, SAXS and DSC. For the calculation of an average lamellar thickness ( $l$ ) the following approximation was employed:

$$l = d^* \cdot X_c \quad (7.5)$$

**Table 7.6** For PLLA-*b*-PHT-*b*-PLLA: Long Period ( $d^*$ ), Crystalline Fraction ( $X_c$ ) and Lamellar Thickness ( $l$ ).

Sample	$d^*$	$X_c$		$l$ (nm)	
		WAXS	DSC	WAXS	DSC
PHT	13.597	0.18	0.32	2.45	4.35
PLLA <sub>51</sub> PHT <sub>49</sub>	16.197	0.20	0.34	3.23	5.50
PLLA <sub>66</sub> PHT <sub>34</sub>	18.404	0.27	0.33	4.96	6.07
PLLA <sub>80</sub> PHT <sub>20</sub>	20.294	---	0.35	---	7.10
PLLA <sub>94</sub> PHT <sub>06</sub>	---	---	0.08	---	---

- Values of  $X_c$  and  $d^*$  calculated with data from WAXS and SAXS respectively at 25 °C.

Table 7.6 shows the values of  $X_c$  determined by DSC. Using these values the lamellar thickness ( $l$ ) was calculated (Table 7.6). As the lamellar thickness values depend on the crystallinity degree according to equation 7.5, the degree of crystallinity by also estimated by WAXS (an example is provided in Figure E.12, Annex E). Table 7.6 lists the lamellar thickness calculated with crystallinity values derived from both DSC and WAXS.

The WAXS results indicate that the PLLA does not crystallize and that the only block capable of crystallizing is the PHT, this corroborates what is shown in the DSC scans, where only peaks corresponding to PHT are appreciated (Figure 7.6). The degree of crystallinity ( $X_c$ ) in the copolymers does not seem to vary much when the amount of PLLA is increased, this behavior is observed below 80% PLLA, above this composition (94% PLLA), the degree of crystallinity decreases remarkably (Table 7.6 and Figure 7.7 (b)).

The SAXS technique reflects only the diffraction caused by the PHT lamellae, where as the PLLA content increases in the copolymer, these lamellae are more separated from each other and therefore the value of long period ( $d^*$ ) increases. The above is related to the fact that when increasing the amount of PLLA the amorphous region increases generating more separation between the lamellae present in the system.

From the above, the values of lamellar thickness ( $l$ ) correspond only to PHT, in Table 7.6 it can be seen that the value of  $l$  changes slightly, this is due to the molecular weight of the PHT block in all the copolymers is the same, therefore this parameter should not vary significantly. This is also related to the fact that values of  $T_m$  and  $T_c$  that are due solely to PHT do not vary significantly in the copolymers; this behavior is only appreciated for compositions of up to 80% of PLLA. When the copolymer has more than this amount of PLLA, for example 94%, the properties and parameters related to the crystalline phase (PHT) show a marked decrease.

### 7.3.3.2 PLLA-*b*-PHF-*b*-PLLA Copolymers

On the other hand the copolymers made of PHF and PLLA were also characterized by WAXS. The crystal type of the PHF is triclinic  $\beta$ -form and its crystalline

parameters are reported in the Table 7.7 and are consistent with those reported in the literature.<sup>13</sup> In Figure 7.13(a), the characteristic peaks of the PHF are shown and are consistent with those reported in the literature.<sup>13</sup>

**Table 7.7** Values of  $q$ ,  $2\theta$ , Crystalline Planes and  $d_{hkl}$  of PHF.

$q(\text{nm}^{-1})$	$2\theta$	Planes	$d_{hkl}(\text{nm})$
9.77	9.19	002	0.643
12.13	11.41	011	0.518
17.69	16.67	100	0.355

The neat PHF and copolymer PLLA<sub>57</sub>PHF<sub>43</sub>, respectively, are shown in Figure 7.13 (a, b) it is observed that PLLA causes an effect in the crystallization of PHF, for example at 25 °C the intensity of the peaks seems to decrease in the copolymer versus the homopolymer. On the other hand, the temperature at which the materials started to crystallize from the melt also decreases when PLLA is present in the copolymer. In the case of the copolymer with 94 mol% of PLLA, no crystallization peak in the diffractogram was obtained. The diffractograms of the rest of copolymers are shown in the Annex E.

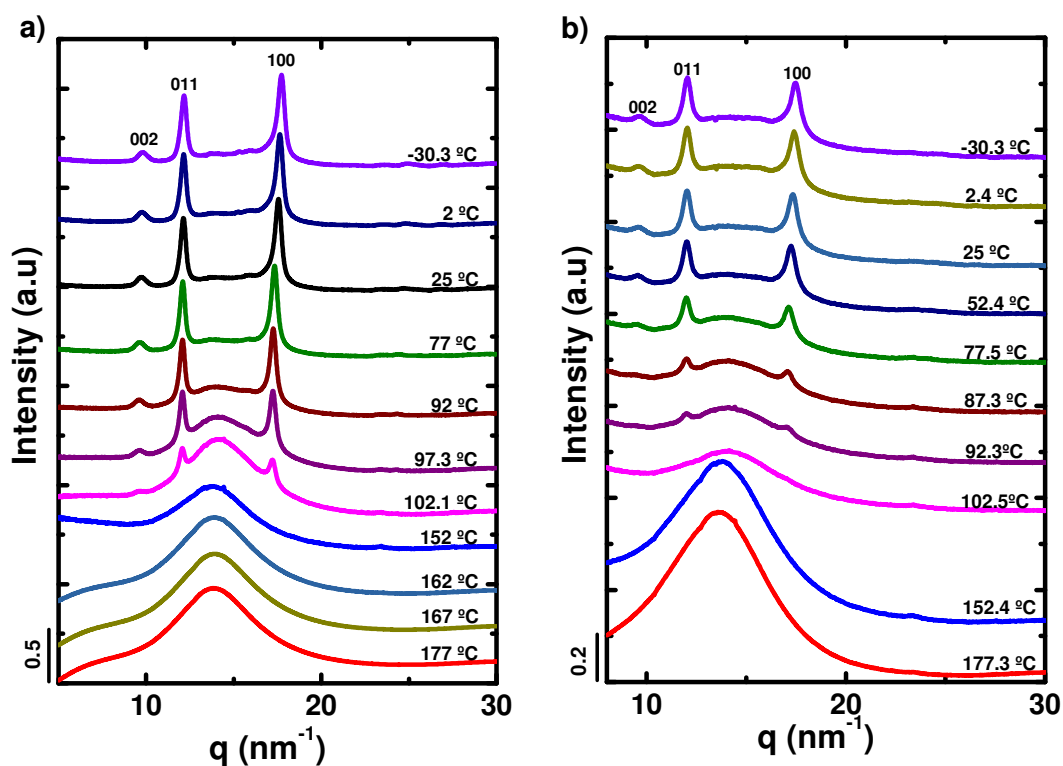


**Figure 7.13.** Real time synchrotron WAXS diffraction patterns for samples (a) PHF and (b) PLLA<sub>57</sub>PHF<sub>43</sub>, cooled from the 180 °C to -30 °C at 20 °C/min.

For this series of copolymers made with PLLA and PHF, SAXS experiments were also carried out, Figure 7.14 shows the SAXS results at different temperatures for (a) PHF and (b) PLLA<sub>57</sub>PHF<sub>43</sub> samples, where the intensity is plotted as a function of the scattering vector  $q$ .

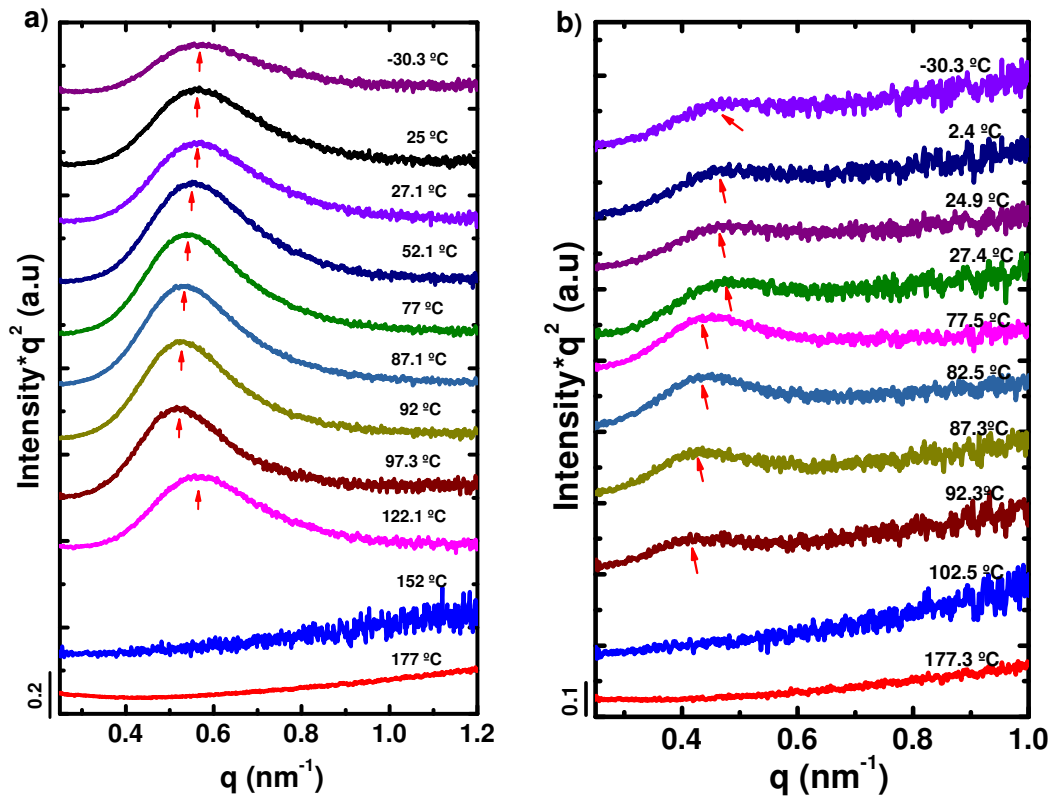


**Figure 7.14.** Lorentz-corrected SAXS profiles for (a) PHF and (b) PLLA<sub>57</sub>PHF<sub>43</sub>, with intensity as a function of scattering vector. Data taken of samples cooled from the 180 °C to -30 °C at 20 °C/min.

The copolymers showed a clear intense maximum due to the scattering caused by the periodic lamellar stacks (i.e., long period). The intensity of this maximum decreased as the amount of PLLA increased in the copolymers. In the melt state, all copolymers do not exhibit any signal, this means that there is no phase segregation and there is a mixed phase in the melt (Annex E).

The segregation strength that could exist between PHT and PLLA was calculated ( $\chi N$ ), following the procedure described for the copolymers of PLLA/PHT. The value of  $\delta_2$  (PHF) was calculated by the Method of Hoftzyer and Van Krevelen using the data and the procedure reported in the literature (20.3 (MJ/m<sup>3</sup>)<sup>1/2</sup>).<sup>27</sup> The interaction parameter  $\chi$  was calculated and value of  $\chi=0.002$  was obtained (with Eq. 7.1), the value

was less than 0.3, therefore the equation 7.2 was applied and the new value of  $\chi$  was 0.34.

The value of  $N$  (total degree of polymerization) was calculated by equation 7.3, where  $Mn_A$  is the molecular weight of the PHF block (calculated by  $Mn = L_{PHF}$  from Table 7.1\*238 g/mol) and  $Mnr_A$  is the molecular weight of the repetitive unit of PHF (238 g/mol). The values of  $N$  were calculated for every copolymer and the results are shown in Table 7.8.

**Table 7.8**  $N$  and  $\chi N$  of PLLA-*b*-PHF-*b*-PLLA.

Sample	$N$	$\chi N$
PLLA <sub>57</sub> PHF <sub>43</sub>	15	5
PLLA <sub>67</sub> PHF <sub>33</sub>	16	5
PLLA <sub>78</sub> PHF <sub>22</sub>	22	7
PLLA <sub>94</sub> PHF <sub>06</sub>	87	30

The segregation strength ( $\chi N$ ) between PLLA and PHT was calculated multiplying  $\chi$  by  $N$ . In all copolymers, the  $\chi N$  values are below 50 which indicate a weak to intermediate segregation strength in these systems. For copolymers with less than or equal to 78% PLLA, the value of  $\chi N$  is less than 10, suggesting no segregation in these copolymers. On the other hand, a value of 30 for  $\chi N$  is appreciated when the copolymer has a 94% PLLA which indicates that in this composition an intermediate segregation between the components of the copolymer (PHF and PLLA) can happen. By the SAXS technique no segregation was observed in the molten state, suggesting that the system tends more to weak segregation (not appreciated) or no segregation.

The long periods ( $d^*$ ) at different temperatures for each sample were estimated by Eq. (7.4) from  $q_{max}$  values taken from the Lorentz corrected plots ( $I \cdot q^2$  versus  $q$ ). Figure 7.15 shows that the value of  $d^*$  at low temperatures is a function of composition. The long period increased with temperature, as the amorphous content increases, especially above 80 °C, where melting can start in some of the samples.

With compositions above 67% of PLLA the intensities in SAXS are in some temperatures so small that it was not possible to measure the value, however in Figure 7.15, the data of some temperatures are appreciated where it was possible to obtain a value.

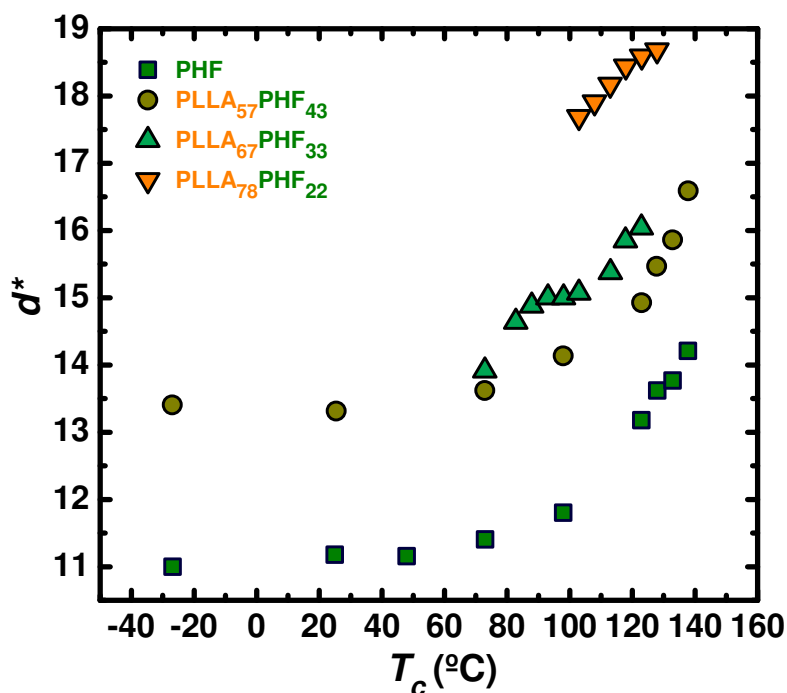


**Figure 7.15.** Long periods ( $d^*$ ) calculated from SAXS data as a function of temperature for PLLA-*b*-PHF-*b*-PLLA.

Table 7.9 shows the values of  $X_c$  determined by DSC (calculus described in previous paragraphs) and values of  $X_c$  determined by WAXS. The lamellar thickness ( $l$ ) was calculated (Table 7.9) using values of  $X_c$  determined from DSC and WAXS.

**Table 7.9** For PLLA-*b*-PHF-*b*-PLLA: Long Period ( $d^*$ ), Crystalline Fraction ( $X_c$ ) and Lamellar Thickness ( $l$ ).

Sample	$d^*$	$X_c$		$l$ (nm)	
		WAXS	DSC	WAXS	DSC
PHT	11.178	0.35	0.40	3.91	4.47
PLLA <sub>57</sub> PHF <sub>43</sub>	13.311	0.40	0.43	5.32	5.72
PLLA <sub>67</sub> PHF <sub>33</sub>	---	0.18	0.09	---	---
PLLA <sub>78</sub> PHF <sub>22</sub>	---	0.04	0.07	---	---
PLLA <sub>94</sub> PHF <sub>06</sub>	---	---	---	---	---

- Values of  $X_c$  and  $d^*$  calculated with data from WAXS and SAXS respectively at 25 °C.

The Table 7.9 clearly shows how the crystallinity decreases with the PLLA content in the sample when the amount of PLLA is above the 67% in the copolymer, the lamellar thickness value ( $l$ ), seems to change slightly in the composition with 57% PLLA versus the homopolymer, this is expected since the PHF block has the same

molecular weight in all the copolymers. For the rest of the compositions the signals of  $d^*$  were not determined by the low intensity presented in the measurements.

The results by WAXS and DSC confirm that the only block that crystallizes in the copolymers is the PHF. SAXS showed the diffraction corresponding to the crystalline phase (PHF) and it is expected that the long period increases with the PLLA content, which can be attributed to the fact that an increase in PLLA generates a greater amorphous zone, which translates into greater separation between the lamella formed.

Comparing the block of PHT versus the block of PHF, in the block of PHT the properties decrease markedly above 80% of PLLA, while the properties of the PHF begin to have changes above 57% of PLLA. These results could suggest that the PHT compared to the PHF seems to be less affected in their properties when the amount of PLLA is increased in the copolymers.

## 7.4 Conclusions

Triblock copolymers made from PLLA with PHT or PHF were obtained, where the triblock structure was checked by NMR and the absence of racemization was observed. Each copolymer formed has a different PLLA block length. In addition, both series of copolymers have in their structure blocks that may be susceptible to degradation (PLLA), but also the polymer of the central block, PHT or PHF, is made from monomers derived from plastic waste or renewable sources, respectively. Therefore, these triblock copolymers follow the sustainability line in their synthesis route.

The behavior shown by the copolymers indicated that the PLLA is unable to crystallize in both series, i.e. in PLLA-*b*-PHT-*b*-PLLA or PLLA-*b*-PHF-*b*-PLLA copolymers. From the above, the PHT and PHF are the crystalline phases appreciated in the triblock copolymers. The amount of PLLA present in the copolymers appears to slightly affect the properties of the copolymers up to a maximum amount, above which the properties decrease markedly.

Even though the properties and behavior shown by both families of copolymers to be linked with PLLA appear to be similar to each other, it is noteworthy that copolymers made with PHT tolerate a greater amount of PLLA before showing significant impact on their properties, in comparison with the copolymers made with PHF.

## 7.5 References

- (1) Nakajima, H.; Dijkstra, P.; Loos, K. The Recent Developments in Biobased Polymers toward General and Engineering Applications: Polymers That Are Upgraded from Biodegradable Polymers, Analogous to Petroleum-Derived Polymers, and Newly Developed. *Polymers* **2017**, *9* (12), 523. <https://doi.org/10.3390/polym9100523>.
- (2) Genovese, L.; Soccio, M.; Lotti, N.; Gazzano, M.; Siracusa, V.; Salatelli, E.; Balestra, F.; Munari, A. Design of Biobased PLLA Triblock Copolymers for Sustainable Food Packaging: Thermo-Mechanical Properties, Gas Barrier Ability and Compostability. *European Polymer Journal* **2017**, *95*, 289–303. <https://doi.org/10.1016/j.eurpolymj.2017.08.001>.
- (3) Shi, S. X.; Xia, Y. Z.; Ma, X. Y.; Jiao, S. K.; Li, X. Y. Synthesis and Properties of Biodegradable ABA Triblock Copolymers of Polylactide (A) and Polyethylene Glycol (B). *Advanced Materials Research* **2006**, *11–12*, 469–472. <https://doi.org/10.4028/www.scientific.net/AMR.11-12.469>.
- (4) Xiao, L.; Wang, B.; Yang, G.; Gauthier, M. Poly(Lactic Acid)-Based Biomaterials: Synthesis, Modification and Applications. In *Biomedical Science, Engineering and Technology*; Ghista, D. N., Ed.; InTech, 2012. <https://doi.org/10.5772/23927>.
- (5) Ding, Y.; Lu, B.; Wang, P.; Wang, G.; Ji, J. PLA-PBAT-PLA Tri-Block Copolymers: Effective Compatibilizers for Promotion of the Mechanical and Rheological Properties of PLA/PBAT Blends. *Polymer Degradation and Stability* **2018**, *147*, 41–48. <https://doi.org/10.1016/j.polymdegradstab.2017.11.012>.
- (6) Ding, Y.; Feng, W.; Lu, B.; Wang, P.; Wang, G.; Ji, J. PLA-PEG-PLA Tri-Block Copolymers: Effective Compatibilizers for Promotion of the Interfacial Structure and Mechanical Properties of PLA/PBAT Blends. *Polymer* **2018**, *146*, 179–187. <https://doi.org/10.1016/j.polymer.2018.05.037>.
- (7) Sun, Z.; Zhang, B.; Bian, X.; Feng, L.; Zhang, H.; Duan, R.; Sun, J.; Pang, X.; Chen, W.; Chen, X. Synergistic Effect of PLA–PBAT–PLA Tri-Block Copolymers with Two Molecular Weights as Compatibilizers on the Mechanical and Rheological Properties of PLA/PBAT Blends. *RSC Advances* **2015**, *5* (90), 73842–73849. <https://doi.org/10.1039/C5RA11019J>.

- (8) Lefèvre, C.; Villers, D.; Koch, M. H. J.; David, C. Synthesis and Thermal Characterization of Crystallizable Poly(Caprolactone)/Poly(Hexamethylene Terephthalate) Block Copolymer. *Polymer* **2001**, *42* (21), 8769–8777. [https://doi.org/10.1016/S0032-3861\(01\)00362-7](https://doi.org/10.1016/S0032-3861(01)00362-7).
- (9) Wu, M. C.; Woo, E. M.; Yoshioka, T.; Tsuji, M. Thermal Analysis, X-Ray and Electron Diffraction Studies on Crystalline Phase Transitions in Solvent-Treated Poly(Hexamethylene Terephthalate). *Polymer* **2006**, *47* (15), 5523–5530. <https://doi.org/10.1016/j.polymer.2005.05.161>.
- (10) González-Vidal, N.; de Ilarduya, A. M.; Muñoz-Guerra, S.; Castell, P.; Martínez, M. T. Synthesis and Properties of Poly(Hexamethylene Terephthalate)/Multiwall Carbon Nanotubes Nanocomposites. *Composites Science and Technology* **2010**, *70* (5), 789–796. <https://doi.org/10.1016/j.compscitech.2010.01.014>.
- (11) Jiang, M.; Liu, Q.; Zhang, Q.; Ye, C.; Zhou, G. A Series of Furan-Aromatic Polyesters Synthesized via Direct Esterification Method Based on Renewable Resources. *Journal of Polymer Science Part A: Polymer Chemistry* **2012**, *50* (5), 1026–1036. <https://doi.org/10.1002/pola.25859>.
- (12) Papageorgiou, G. Z.; Tsanaktsis, V.; Papageorgiou, D. G.; Chrissafis, K.; Exarhopoulos, S.; Bikiaris, D. N. Furan-Based Polyesters from Renewable Resources: Crystallization and Thermal Degradation Behavior of Poly(Hexamethylene 2,5-Furan-Dicarboxylate). *European Polymer Journal* **2015**, *67*, 383–396. <https://doi.org/10.1016/j.eurpolymj.2014.08.031>.
- (13) Jiang, Y.; Woortman, A. J. J.; Alberda van Ekenstein, G. O. R.; Loos, K. A Biocatalytic Approach towards Sustainable 2,5-Furandicarboxylic Acid Based Furanic-Aliphatic Polyesters. *Polym. Chem.* **2015**, *6*, 5198–5211. <https://doi.org/10.1039/C5PY00629E>.
- (14) Zakharova, E.; León, S.; de Ilarduya, A. M.; Muñoz-Guerra, S. Triblock Copolyesters Derived from Lactic Acid and Glucose: Synthesis, Nanoparticle Formation and Simulation. *European Polymer Journal* **2017**, *92*, 1–12. <https://doi.org/10.1016/j.eurpolymj.2017.04.033>.
- (15) Zakharova, E.; Martínez de Ilarduya, A.; León, S.; Muñoz-Guerra, S. Hydroxyl-Functionalized Amphiphilic Triblock Copolyesters Made of Tartaric and Lactic

- Acids: Synthesis and Nanoparticle Formation. *Reactive and Functional Polymers* **2018**, *126*, 52–62. <https://doi.org/10.1016/j.reactfunctpolym.2018.03.007>.
- (16) de Ilarduya, A. M.; Muñoz-Guerra, S. Chemical Structure and Microstructure of Poly(Alkylene Terephthalate)s, Their Copolyesters, and Their Blends as Studied by NMR. *Macromolecular Chemistry and Physics* **2014**, *215* (22), 2138–2160. <https://doi.org/10.1002/macp.201400239>.
- (17) Liu, T.-Y.; Lin, W.-C.; Yang, M.-C.; Chen, S.-Y. Miscibility, Thermal Characterization and Crystallization of Poly(l-Lactide) and Poly(Tetramethylene Adipate-Co-Terephthalate) Blend Membranes. *Polymer* **2005**, *46* (26), 12586–12594. <https://doi.org/10.1016/j.polymer.2005.10.100>.
- (18) Woo, E.; Wu, P.-L.; Chiang, C.-P.; Liu, H.-L. Analysis of Polymorphism and Dual Crystalline Morphologies in Poly(Hexamethylene Terephthalate). *Macromolecular Rapid Communications* **2004**, *25* (9), 942–948. <https://doi.org/10.1002/marc.200300307>.
- (19) Ghosh, A. K.; Woo, E. M.; Sun, Y.-S.; Lee, L.-T.; Wu, M.-C. Characterization and Analyses on Complex Melting, Polymorphism, and Crystal Phases in Melt-Crystallized Poly(Hexamethylene Terephthalate). *Macromolecules* **2005**, *38* (11), 4780–4790. <https://doi.org/10.1021/ma0473667>.
- (20) Inomata, K.; Sasaki, S. Crystal Structure and Conformational Disorder of Poly(Hexamethylene Terephthalate). *Journal of Polymer Science Part B: Polymer Physics* **1996**, *34* (1), 83–92. [https://doi.org/10.1002/\(SICI\)1099-0488\(19960115\)34:1<83::AID-POLB6>3.0.CO;2-X](https://doi.org/10.1002/(SICI)1099-0488(19960115)34:1<83::AID-POLB6>3.0.CO;2-X).
- (21) Sun, Y.-S. Temperature-Resolved SAXS Studies of Morphological Changes in Melt-Crystallized Poly(Hexamethylene Terephthalate) and Its Melting upon Heating. *Polymer* **2006**, *47* (23), 8032–8043. <https://doi.org/10.1016/j.polymer.2006.09.003>.
- (22) Hall, I. H.; Ibrahim, B. A. The Structure and Properties of Poly(Hexamethylene Terephthalate): 1. The Preparation, Morphology and Unit Cells of Three Allomorphs. *Polymer* **1982**, *23* (6), 805–816. [https://doi.org/10.1016/0032-3861\(82\)90138-0](https://doi.org/10.1016/0032-3861(82)90138-0).

- 
- (23) Van Krevelen, D. W.; Te Nijenhuis, K. Calorimetric Properties. In *Properties of Polymers*; Elsevier, 2009; pp 109–128. <https://doi.org/10.1016/B978-0-08-054819-7.00005-4>.
- (24) Lefèvre, X.; Koch, M. H. J.; Reynaers, H.; David, C. Thermal Behavior of Poly(Hexamethylene Terephthalate) Oligomers. I. Melting Behavior and Morphology of the Crystalline Phase. *Journal of Polymer Science Part B: Polymer Physics* **1999**, *37* (1), 1–18. [https://doi.org/10.1002/\(SICI\)1099-0488\(19990101\)37:1<1::AID-POLB1>3.0.CO;2-B](https://doi.org/10.1002/(SICI)1099-0488(19990101)37:1<1::AID-POLB1>3.0.CO;2-B).
- (25) Palmer, A.; Poulin-Dandurand, S.; Revol, J.-F.; Brisse, F. Poly(Hexamethylene Terephthalate)—I. Interpretation of Its Diffraction Patterns. *European Polymer Journal* **1984**, *20* (8), 783–789. [https://doi.org/10.1016/0014-3057\(84\)90114-9](https://doi.org/10.1016/0014-3057(84)90114-9).
- (26) Hiemenz, P. C.; Lodge, T. P. *Polymer Chemistry*, second.; CRC press, 2007.
- (27) Krevelen, D. W. van; Nijenhuis, K. te. *Properties of Polymers: Their Correlation with Chemical Structure: Their Numerical Estimation and Prediction from Additive Group Contributions*, 4th, completely rev. ed ed.; Elsevier: Amsterdam, 2009.
- (28) Matsen, M. W.; Bates, F. S. Block Copolymer Microstructures in the Intermediate-Segregation Regime. *The Journal of Chemical Physics* **1997**, *106* (6), 2436–2448. <https://doi.org/10.1063/1.473153>.
- (29) Matsen, M. W.; Bates, F. S. Unifying Weak- and Strong-Segregation Block Copolymer Theories. *Macromolecules* **1996**, *29* (4), 1091–1098. <https://doi.org/10.1021/ma951138i>.

# *Chapter 8*

---

---

## *Conclusions*

## Conclusions

The application of different approaches to obtain polymers derived from DMT allowed the development of various synthetic routes that through metal-free catalysts generated a variety of polymers and copolymers with different properties.

The data obtained in the Chapter 3 reveal that organic ionic compounds have potential for synthesizing metal free PET due to their thermal stability and catalytic activity. The protic ionic salt diazabicyclo-[5.4.0]undec-7-ene (DBU): benzoic acid (BA) has proven to be an efficient organocatalyst to produce PET of molecular weights comparable to those produced with organometallic catalyst.

New PET materials potentially susceptible to hydrolytic degradation were synthesized using organocatalysis, following a sustainable synthetic route, where PET was copolymerized with bio-based PLA (Chapter 4). Different PET-*ran*-PLA copolymers were prepared and the structure, morphology and crystallization of the PET component were studied. An interesting result found, was the radical change from nucleation to diffusion control, in the temperature dependence of the overall isothermal crystallization rate, when the PLA content approached the maximum tolerable limit for PET crystallization. It was found that the morphology of PET crystals could change from micron size spherulites to axialites when increasing the PLA content, as the nucleation rate also increased considerably by PLA incorporation.

PET-*mb*-Polyether copolymers with different ratios PET/Polyether were obtained in Chapter 5. The materials showed that both components in the copolymer (PET and Polyether) are able to crystallize at their respective crystallization temperatures giving rise to a double crystalline polymeric material. The thermal properties of the copolymers were affected by the PET/Polyether composition. Therefore, modifying the PET/Polyether composition a library of new materials adapted to various applications can be obtained. These copolymers appear to have a very low segregation in the melt state because they exhibit a single phase in the melt. However, phase segregation occurs within the amorphous phases in the copolymer, as evidenced by the presence of two  $T_{gs}$ . It should be noted that a micro-spherulitic morphology was found for all copolymer samples regardless polyether content present in the copolymers.

In Chapter 6, cyclic oligoesters derived from dimethyl terephthalate and dimethyl furanoate and 1,6-hexanediol were obtained in high yields by enzymatic cyclization. The successful polymerization of these cycles by enzymes has been proven, and even more interestingly, the cyclodepolymerization that converts the polyester into cyclic oligoesters has been also demonstrated. The approach described can be extrapolated to the synthesis of other cycles of higher industrial interest, such as those derived from ethylene glycol or 1,4-butanediol and aromatic diesters, which are usually obtained by HDC or CDP.

The obtaining of triblock copolymers made from PLLA with PHT or PHF has been demonstrated in chapter 7. Copolymers formed have a different PLLA block length. The behavior shown by the copolymers indicated that the PLLA is unable to crystallize in both series, i.e. in PLLA-*b*-PHT-*b*-PLLA or PLLA-*b*-PHF-*b*-PLLA copolymers. From the above, the PHT and PHF are the crystalline phases appreciated in the triblock copolymers. The amount of PLLA present in the copolymers appears to slightly affect the properties of the copolymers up to a maximum amount, above which the properties decrease markedly. It is noteworthy that copolymers made with PHT tolerate a greater amount of PLLA before showing significant impact on their properties, in comparison with the copolymers made with PHF.

It is important to highlight that this work is a base study for future research that follows the line of synthesizing polymers with metal-free catalysts, using monomers from renewable sources and additional features that reduce the ecological footprint that plastics manufacturing processes leave in the environment.

# Annexes

---

---

Annex A .....	198
Support Information of Chapter 03	
Annex B .....	203
Support Information of Chapter 04	
Annex C .....	212
Support Information of Chapter 05	
Annex D.....	221
Support Information of Chapter 06	
Annex E.....	231
Support Information of Chapter 07	

## Annexes

## Annex A

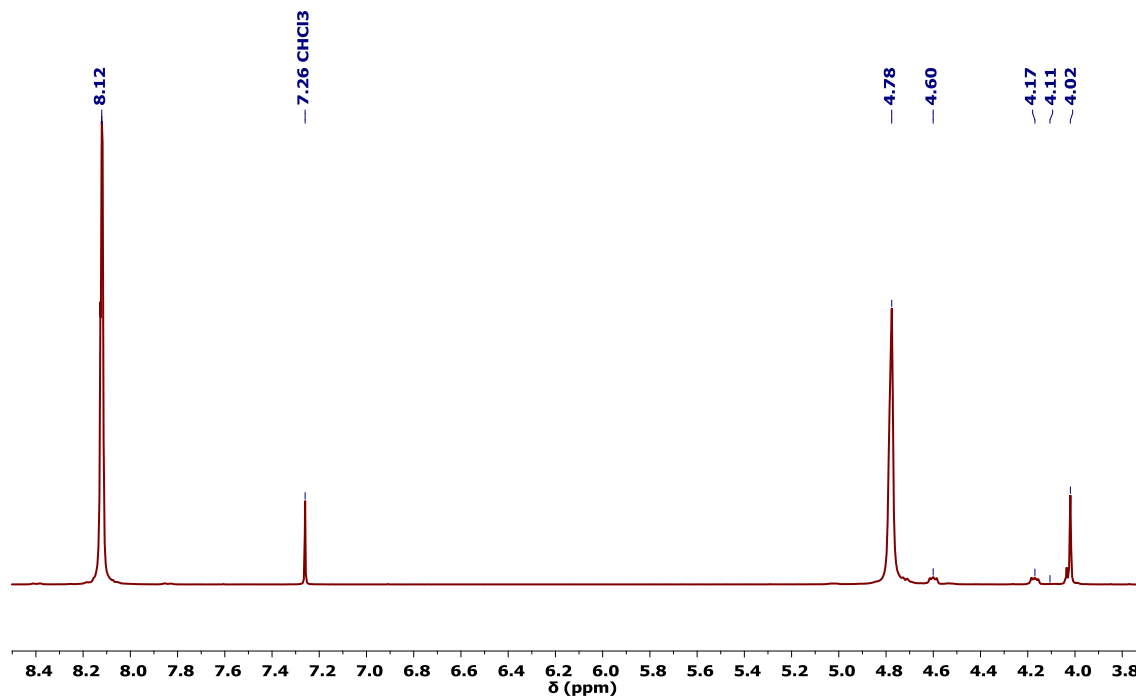


Figure A.1 <sup>1</sup>H NMR in CDCl<sub>3</sub>/TFA of PET synthesized without catalyst at 200 °C.

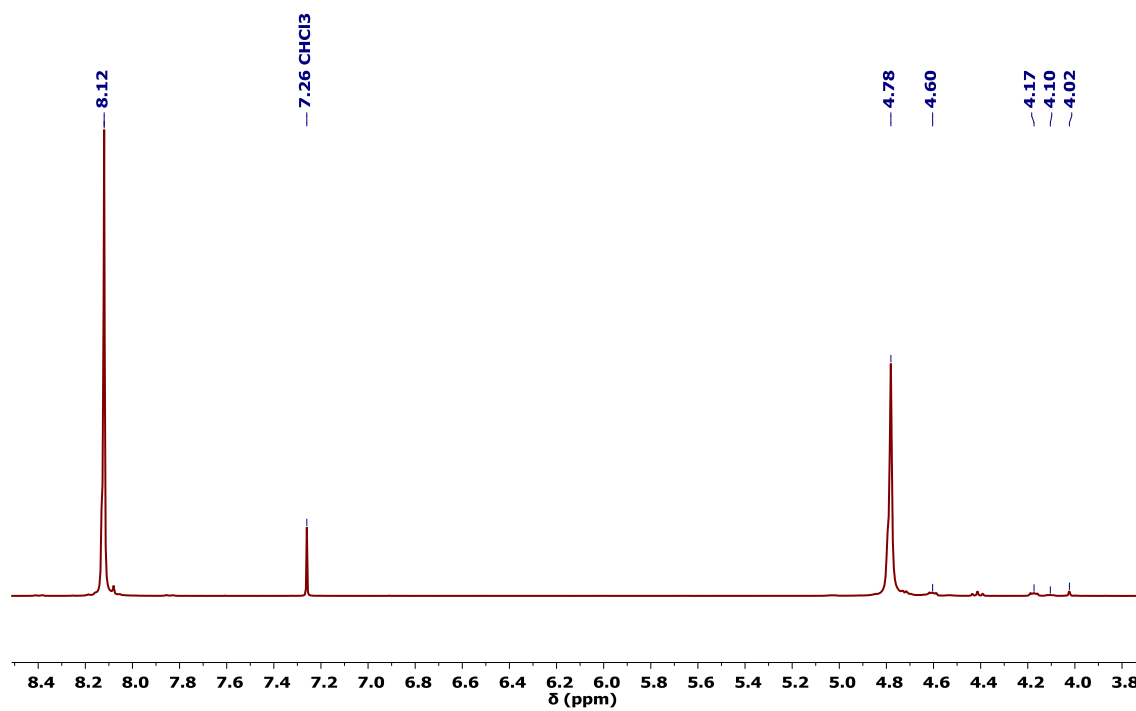
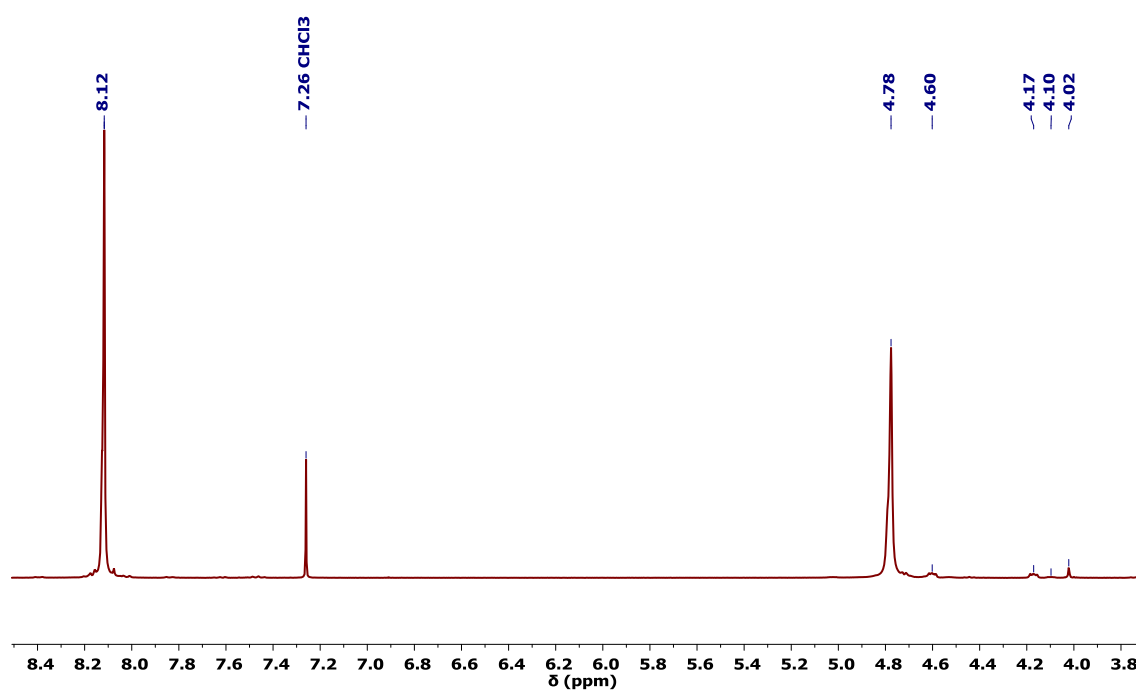
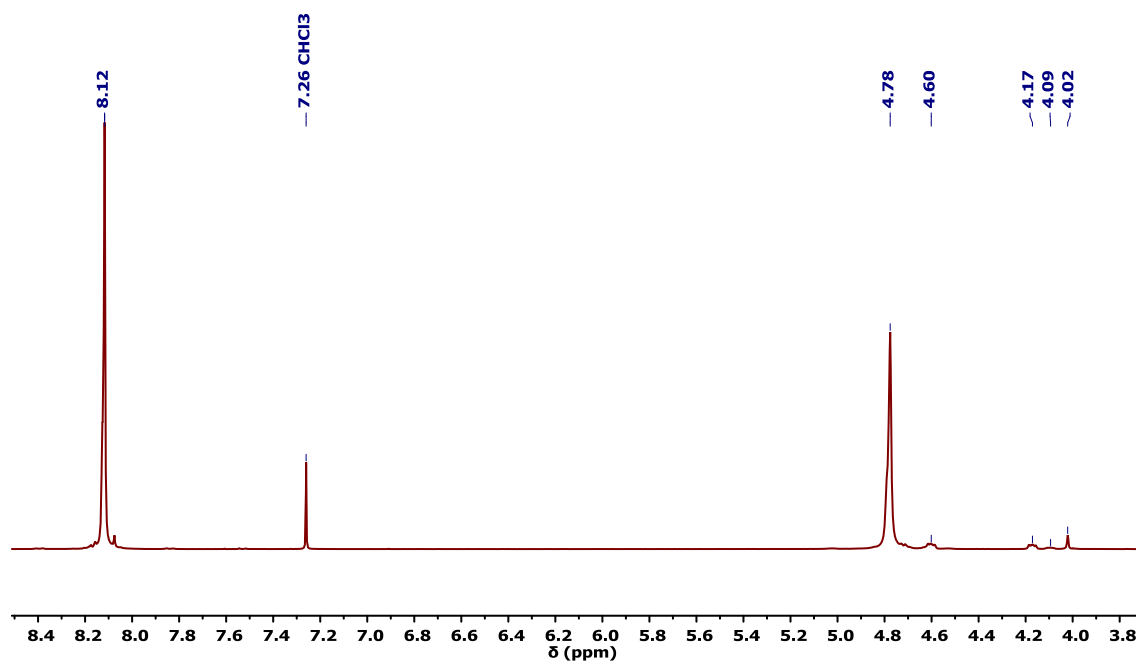


Figure A.2. <sup>1</sup>H NMR in CDCl<sub>3</sub>/TFA of PET synthesized with TiBut as catalyst at 200 °C.



**Figure A.3.** <sup>1</sup>H NMR in CDCl<sub>3</sub>/TFA of PET synthesized with DBU:BA(1:1) as catalyst at 200 °C.



**Figure A.4.** <sup>1</sup>H NMR in CDCl<sub>3</sub>/TFA of PET synthesized with DMAP as catalyst at 200 °C.

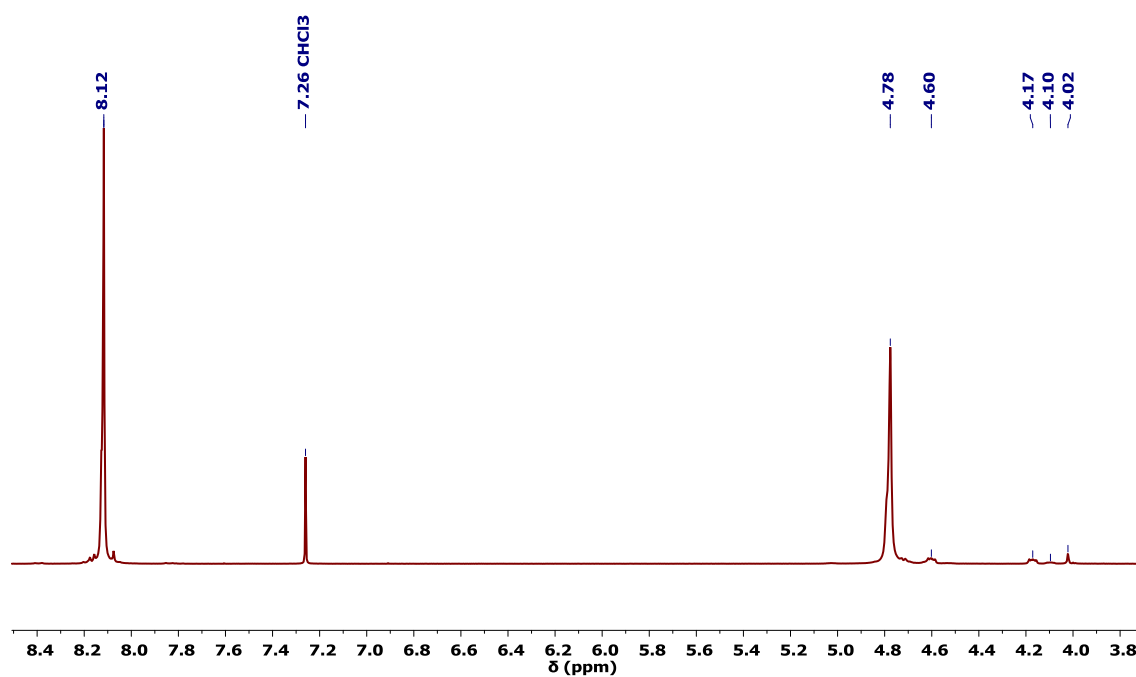


Figure A.5.  $^1\text{H}$  NMR in  $\text{CDCl}_3/\text{TFA}$  of PET synthesized with TBD as catalyst at 200 °C.

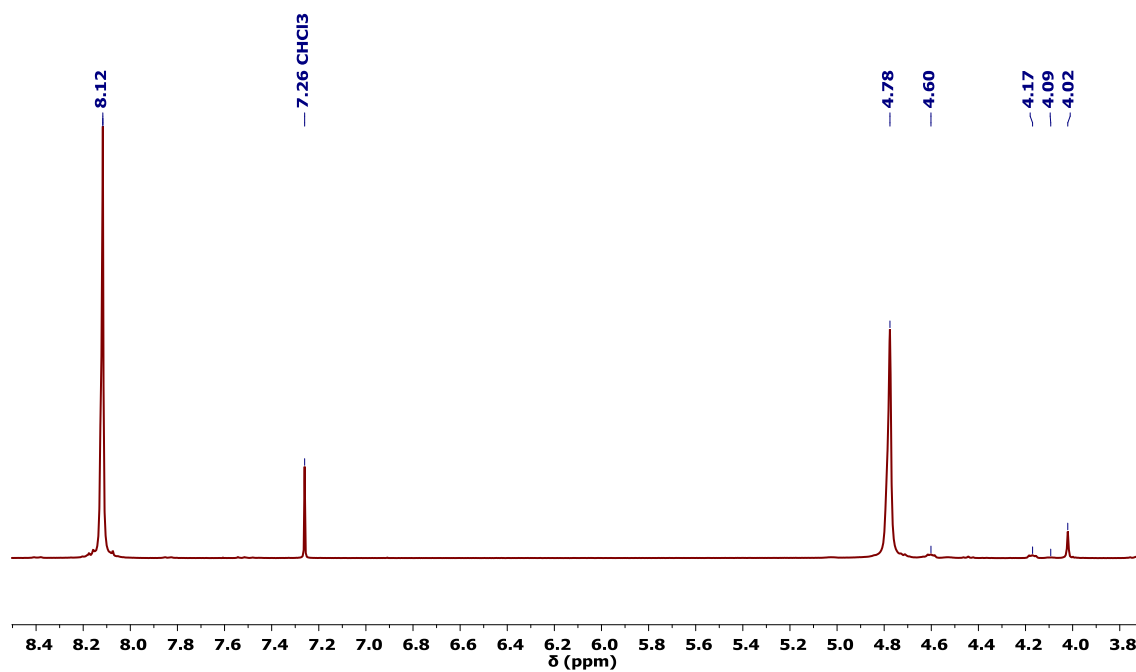


Figure A.6.  $^1\text{H}$  NMR in  $\text{CDCl}_3/\text{TFA}$  of PET synthesized with DBU as catalyst at 200 °C.

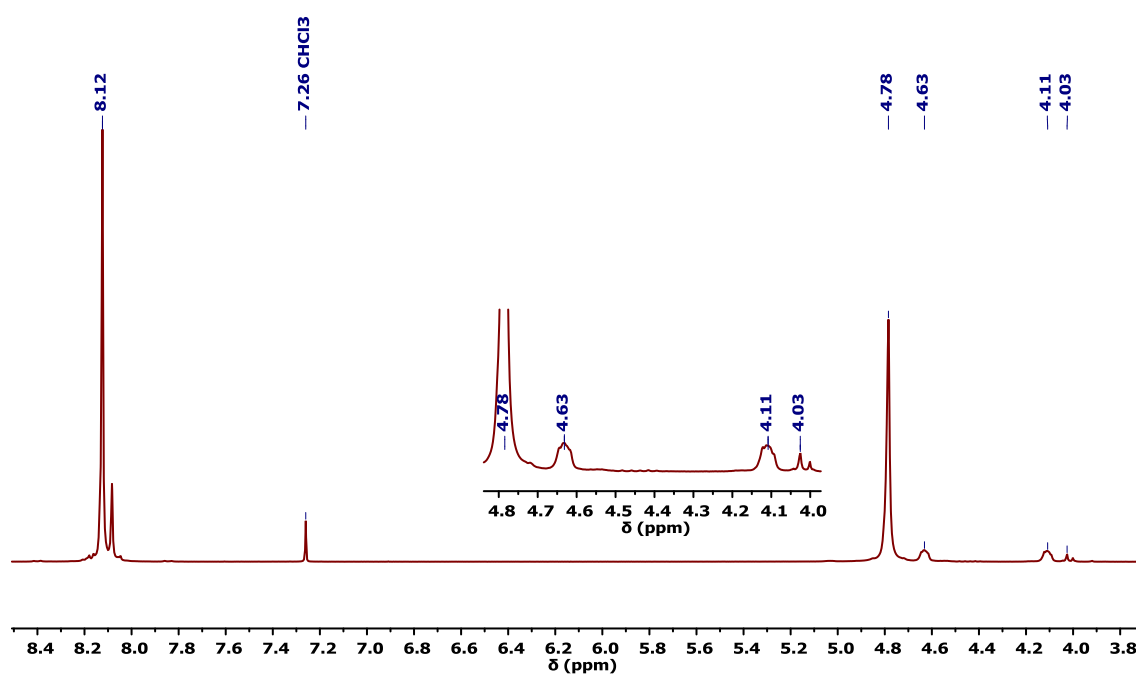


Figure A.7.  $^1\text{H}$  NMR in  $\text{CDCl}_3/\text{TFA}$  of PET synthesized with TiBut as catalyst at 250 °C.

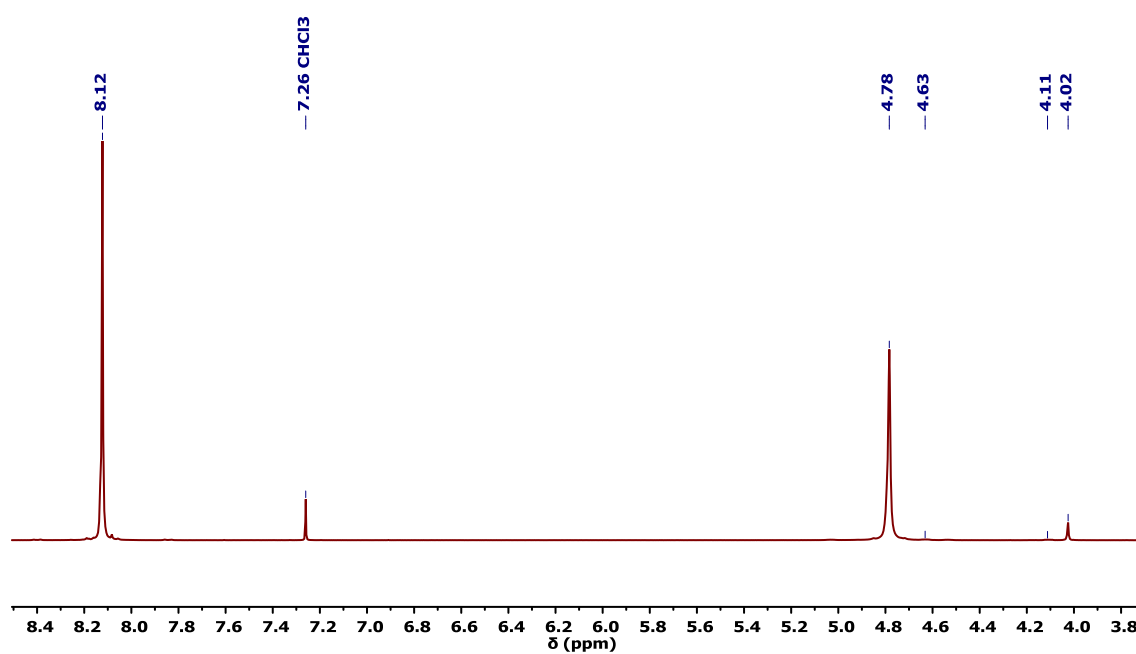
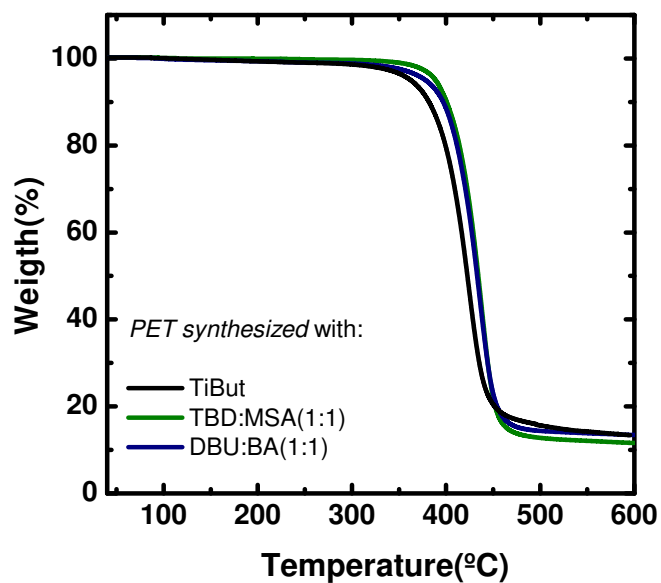


Figure A.8.  $^1\text{H}$  NMR in  $\text{CDCl}_3/\text{TFA}$  of PET synthesized with TBD:MSA (1:1) as catalyst at 250 °C.

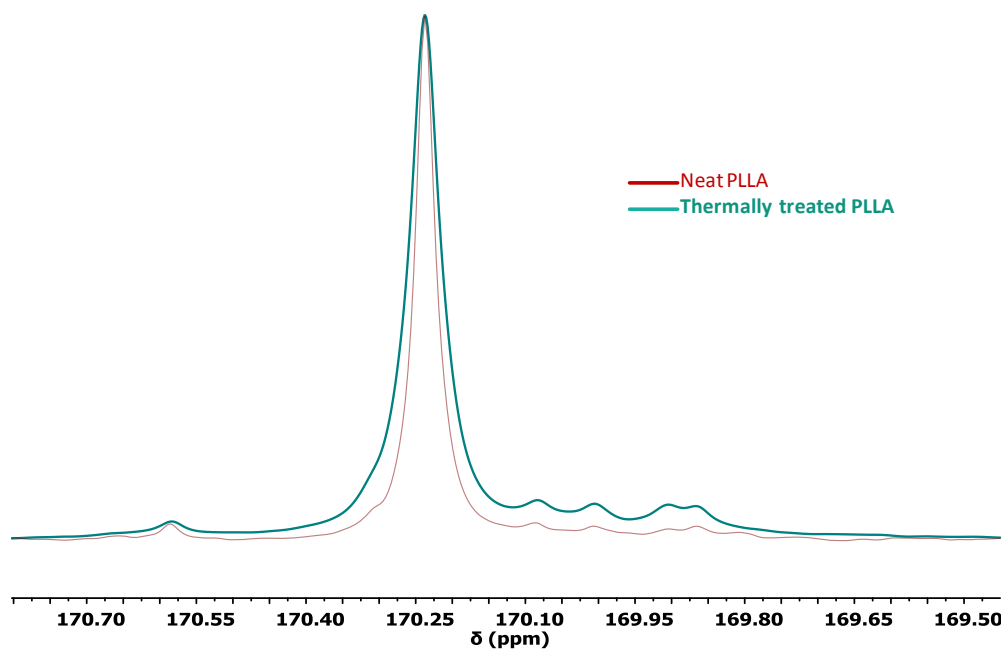
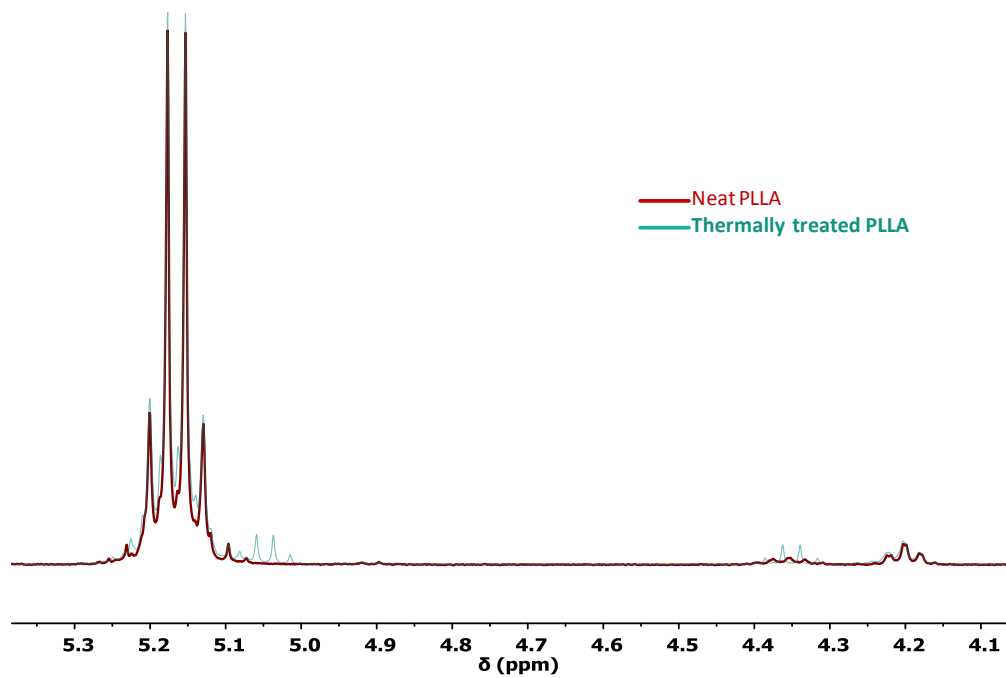


**Figure A.9.** Thermogravimetric analysis of PET synthesized (at 250 °C) with different catalysts.

**Table A.1** Molecular weights synthesized PET with 0.05 mol% calculated by  $^1\text{H}$  NMR.

Catalyst	$M_n$ (by NMR) kDa
TiBut	3.0
TBD:MSA (1:1)	3.6
DBU:BA (1:1)	2.4

## Annex B

Figure B.1.  $^{13}\text{C}$  NMR Spectrum of PLLA vs. PLA.Figure B.2.  $^1\text{H}$  NMR Spectrum of PLLA vs. PLA.

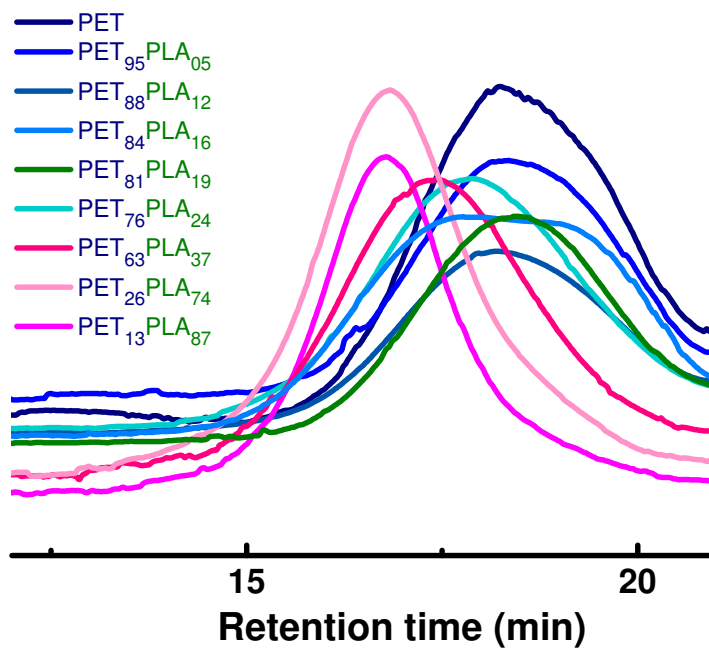


Figure B.3. Curves of GPC for polymers samples

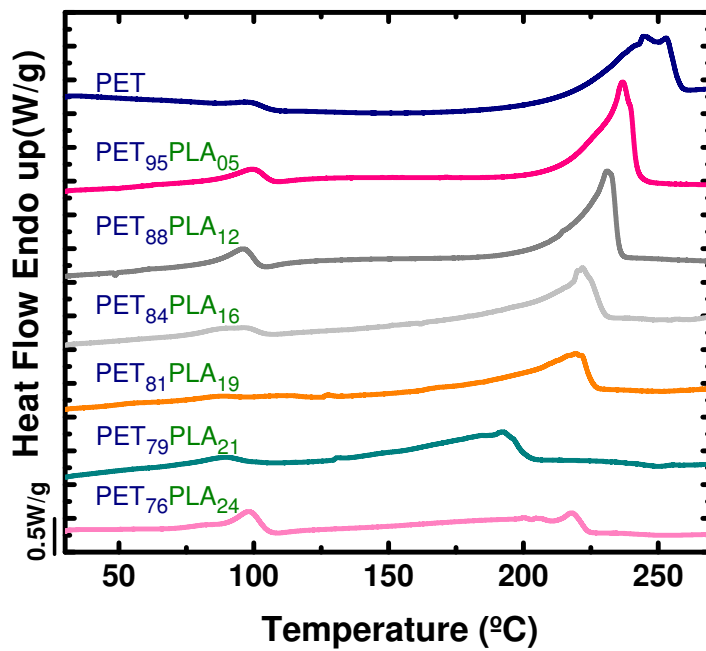


Figure B.4. DSC first heating scans for polymers samples.

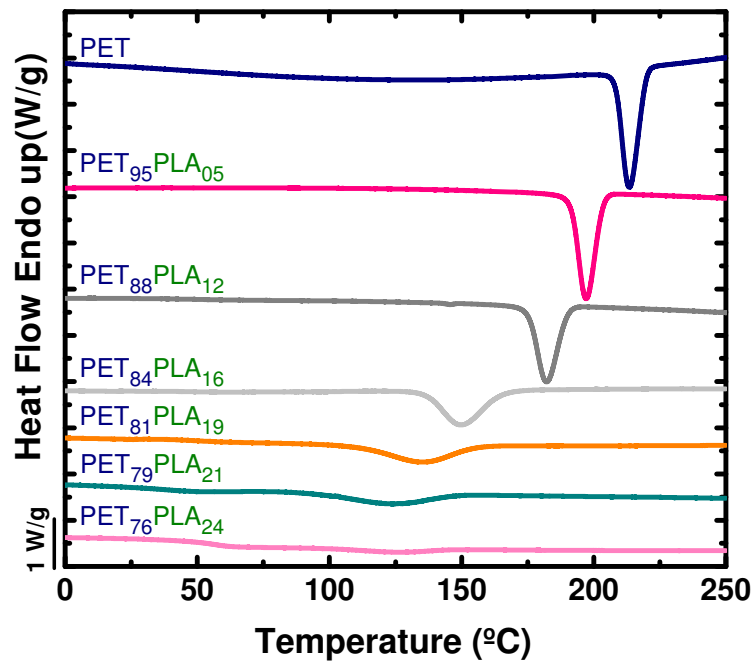


Figure B.5. DSC cooling scans for polymers samples.

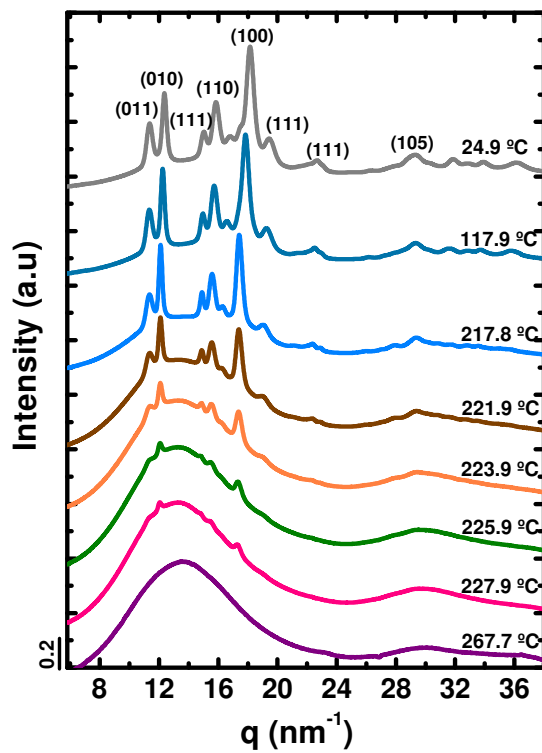


Figure B.6. WAXS diffraction patterns of PET cooled from the 270 °C to 25 °C at 20 °C/min.

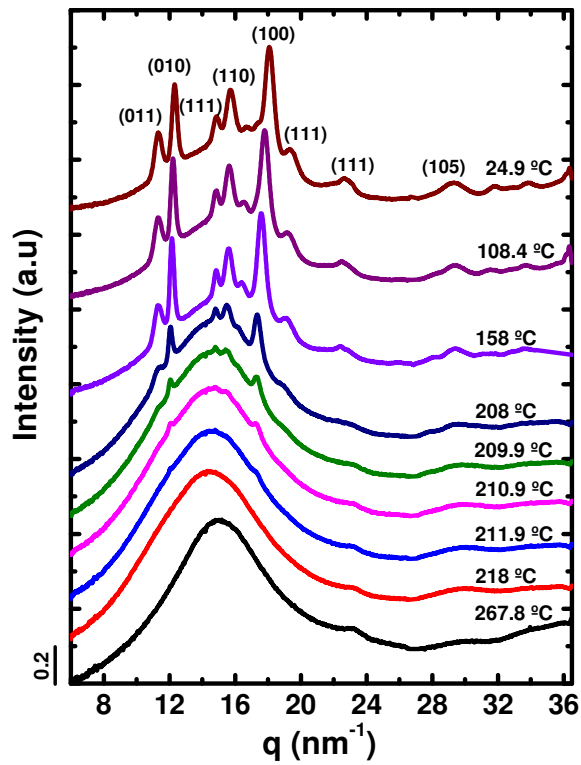


Figure B.7. WAXS diffraction patterns of PET<sub>95</sub>PLA<sub>05</sub> cooled from the 270 °C to 25 °C at 20 °C/min.

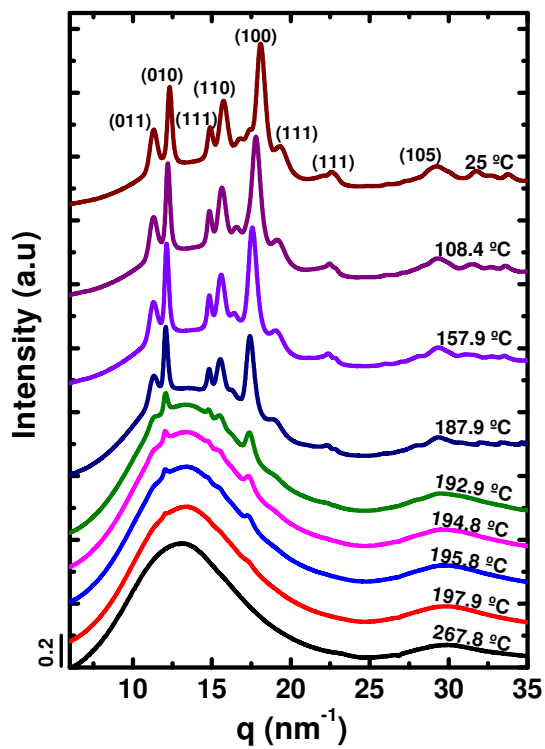


Figure B.8. WAXS diffraction patterns of PET<sub>88</sub>PLA<sub>12</sub> cooled from the 270 °C to 25 °C at 20 °C/min.

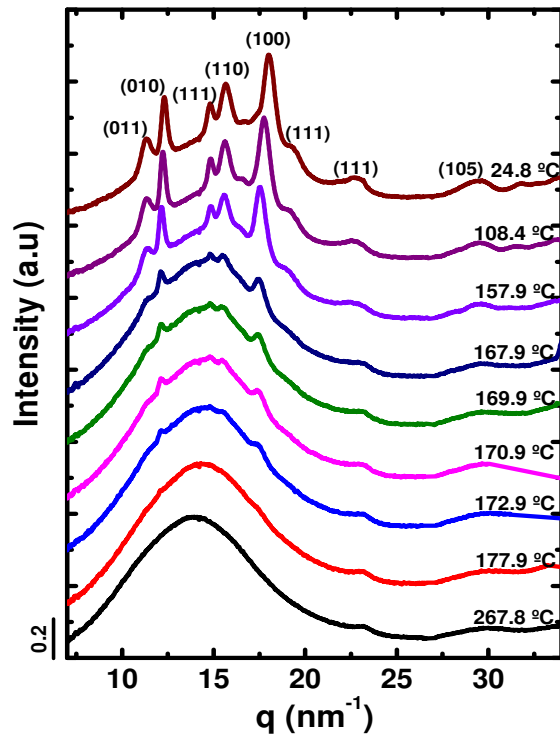


Figure B.9. WAXS diffraction patterns of PET<sub>84</sub>PLA<sub>16</sub> cooled from the 270 °C to 25 °C at 20 °C/min.

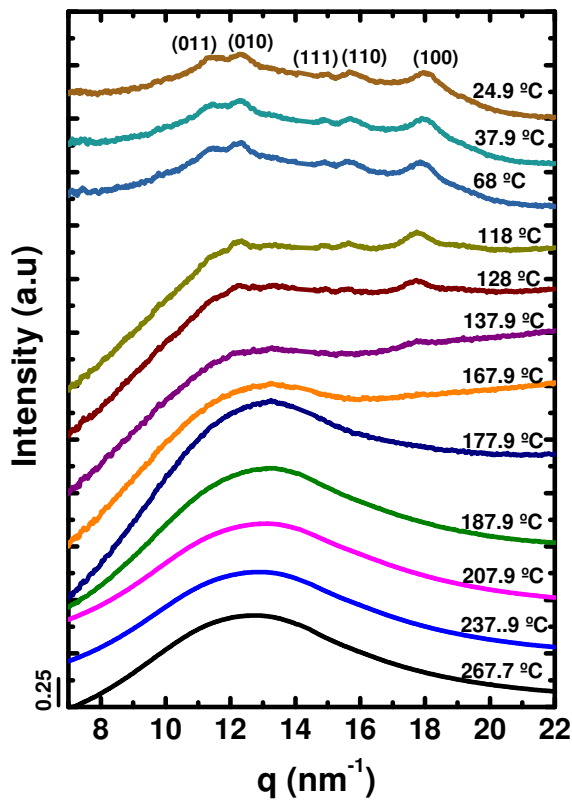


Figure B.10. WAXS diffraction patterns of PET<sub>76</sub>PLA<sub>24</sub> cooled from the 270 °C to 25 °C at 20 °C/min.

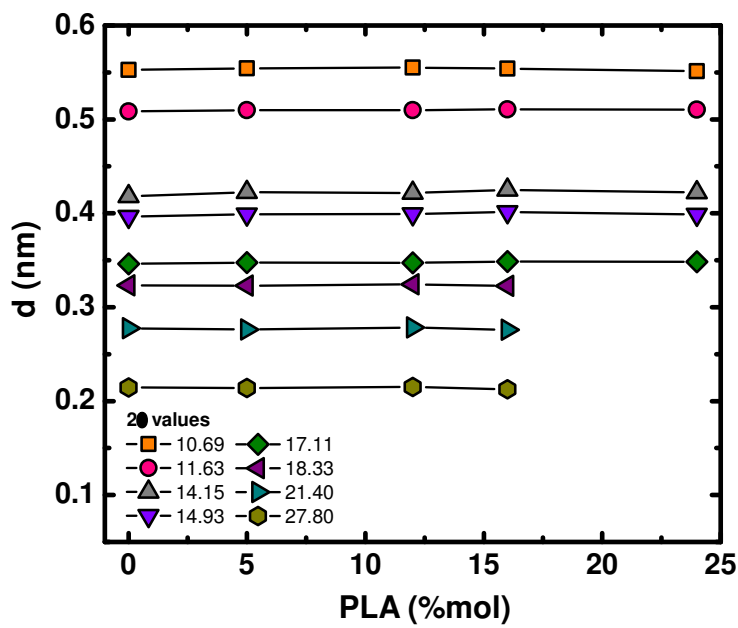


Figure B.11. Interplanar distance ( $d_{hkl}$ ) for all reflections at 25 °C.

Measurements at different temperatures in WAXS were made for each of the polymers. The average interplanar distance ( $d_{hkl}$ ) for all reflections was calculated using Bragg's law. The values of  $d_{hkl}$  taken at constant temperature were not affected by copolymer composition (Figure B.11). The invariance of  $d_{hkl}$  values corroborates the total exclusion of the PLA comonomer units from the crystallites formed by PET.

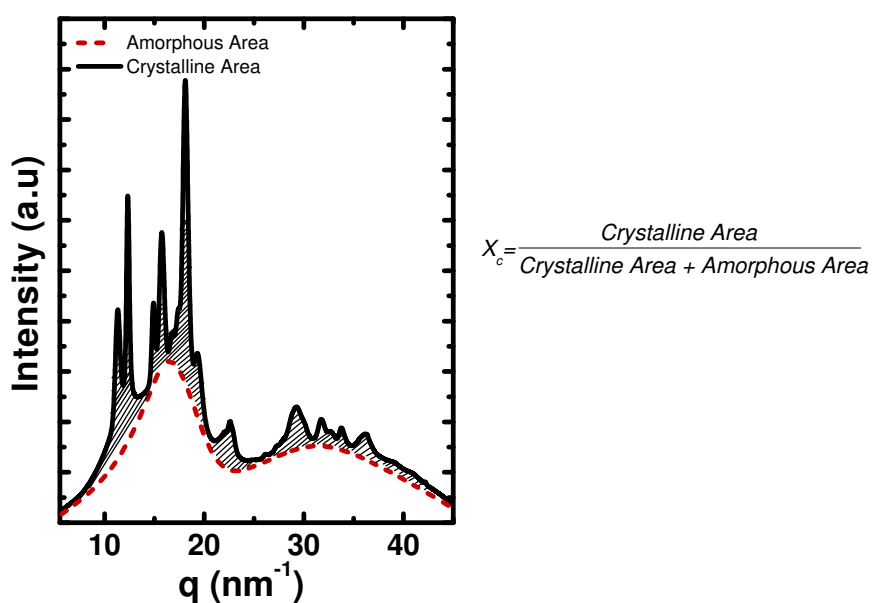
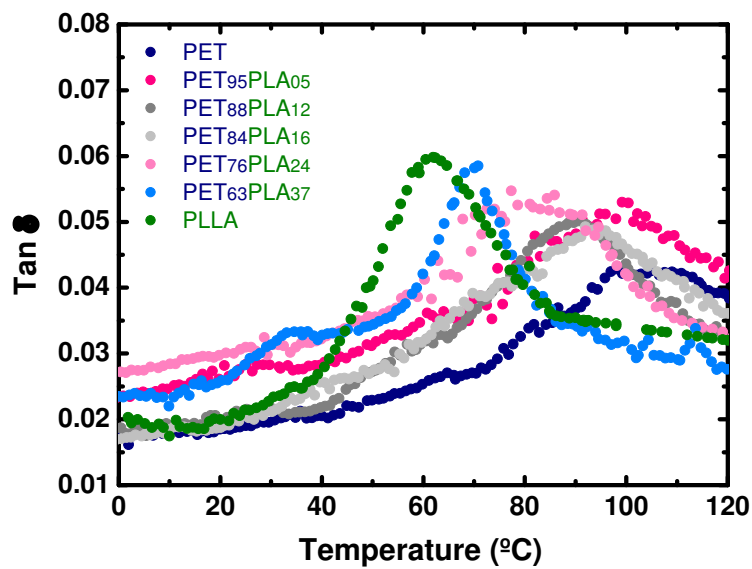
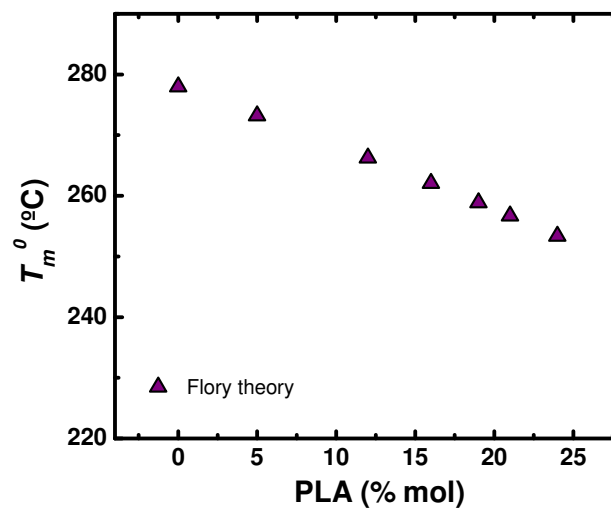


Figure B.12. Degree of crystallinity ( $X_c$ ) for PET-co-PLA copolymers.



**Figure B.13.** DMTA of Copolymers synthesized at different compositions (PET-co-PLA).

$T_g$  values for copolymers with amounts larger than 37 mol% PLA are very close to one another, and their  $\tan \delta$  plots tend to overlap. For this reason, Figure S15 shows only data for copolymer samples with PLA contents of 37 mol % and lower.



**Figure B.14.** Values of  $T_m^0$  versus PLA content.

Values of  $T_m^0$  for each one copolymer were calculated using the Flory theory, where Flory developed an equation to find the equilibrium melting temperature of random copolymers, assuming the complete exclusion of B counits (noncrystallizable

counit) from the crystalline lattice of the cryztallizable unit (A). <sup>1</sup> The equilibrium melting point of the copolymer [ $T_m(X_B)$ ] expressed as:

$$\frac{1}{T_m^0} - \frac{1}{T_m(X_B)} = \left( \frac{R}{\Delta H_m^0} \right) \ln(1 - X_B) \quad (B - 1)$$

where  $T_m^0$  is the homopolymer equilibrium melting temperature,  $\Delta H_m^0$  is the homopolymer heat of fusion,  $R$  is the universal gas constant and  $X_B$  is the mole fraction of the noncrystallizable B counit.

**Equation B-2.** Calculation of the Degree of Randomness.

$$\eta = \frac{2(LT)}{2(L) * (T)} \quad (B - 2)$$

where ( $T$ ) is the mole fraction of the terephthalate in the copolymer, ( $L$ ) is the mole fraction of lactyl o LA in the copolymer and ( $LT$ ) is the molar fraction of the exchange dyad in the copolymer (unit where lactyl or LA is attached to the terephthalate unit), these parameters were obtained by NMR.

**Table B.1** Composition of PET/PLA in different solvents.

Copolymer diluted in CHCl <sub>3</sub> /TFA		Copolymer diluted in CHCl <sub>3</sub>	
% mol of Copolymer		% mol of Copolymer	
PET	PLA	PET	PLA
95	05	76	24
88	12	75	25
84	16	77	23
81	19	74	26
79	21	75	25
76	24	73	27
63	37	61	39
26	74	25	75
13	87	12	88

## References

- (1) Flory, P. Theory of Crystallization in Copolymers. *Transactions of the Faraday Society* **1955**, *51*, 848–857.

**Annex C**

**Equation C-1.** Calculation of the EG-Polyether molar relation.

The molar fraction between both dyols has been calculated from  $^1\text{H}$  NMR using the intensities ( $A_i$ ) of signals at 4.78 and 4.40 ppm for EG and polyether units, respectively, using:

$$(\text{EG}) = \frac{A_{4.78}}{A_{4.78} + A_{4.40}} \quad (\text{C} - 1)$$

**Equation C-2.** Calculation of the Degree of Randomness.

$$\eta = \frac{2(\text{PE-EG})}{2(\text{EG}) * (\text{PE})} \quad (\text{C} - 2)$$

where (EG) and (PE) are the mole fractions of the EG and PE units, respectively. (PE-EG) is the mole fraction of the so-called interchange dyad unit: PE-EG. (PE-EG) has been calculated from the aromatic quaternary carbon of the terephthalic unit.

**Equation C-3.** Number Average Sequential Length

The experimental values of the number of ethylene terephthalate units ( $L_{\text{EG}}$ ) and polyether terephthalate units ( $L_{\text{PE}}$ ) were determined using the equation below:<sup>1</sup>

$$L_{\text{EG}} = \frac{2(\text{EG})}{(\text{PE-EG})}; L_{\text{PE}} = \frac{2(\text{PE})}{(\text{PE-EG})} \quad (\text{C} - 3)$$

Equations (C-3) have used to determine  $L_i$  values in copolymers where interchange signal gives a reliable intensity: 9-81 molar % of polyether.

In random copolymers these equations can written in this way:

$$L_{\text{EG}} = \frac{1}{(\text{PE})}; L_{\text{PE}} = \frac{1}{(\text{EG})} \quad (\text{C} - 4)$$

Assuming their random character, equations (C-4) have used to calculate theoretical  $L_i$  values in copolymers with low contents of polyether: 0-9 molar % of polyether.<sup>1</sup>

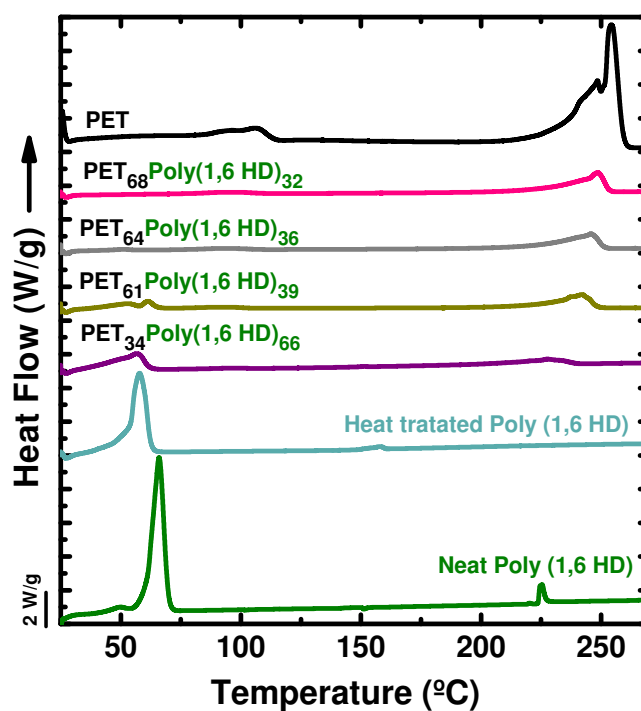


Figure C.1. DSC first heating scans for PET-*b*-Poly(1,6 HD) copolymers.

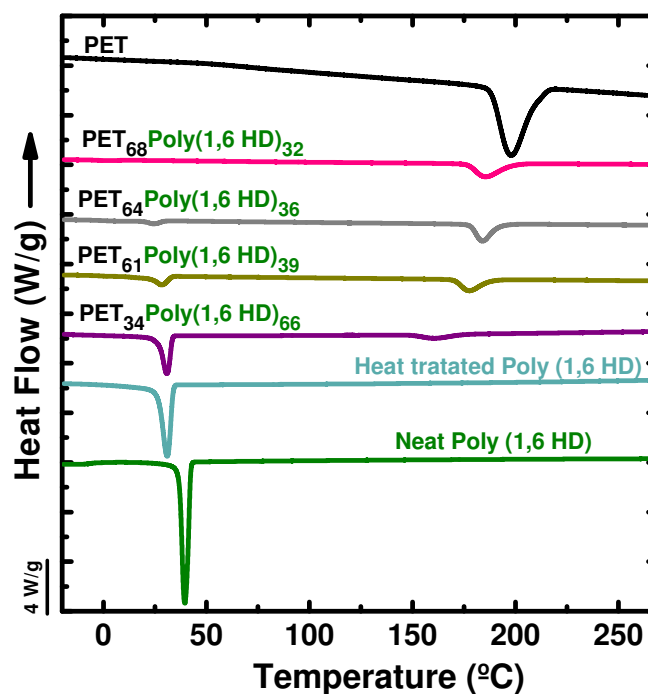


Figure C.2. DSC cooling scans for PET-*b*-Poly(1,6 HD) copolymers.

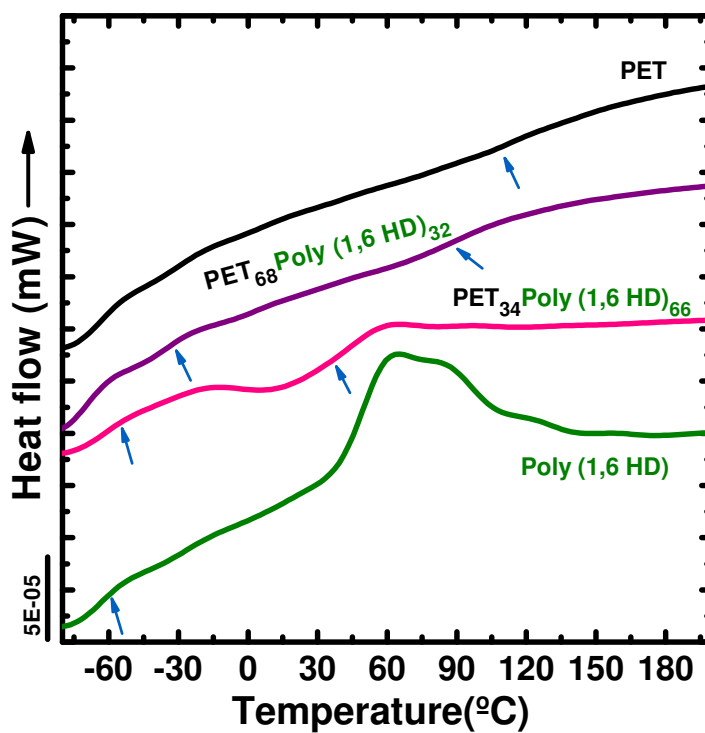


Figure C.3. flashDSC heating scans for PET-*b*-Poly (1,6 HD) copolymers.

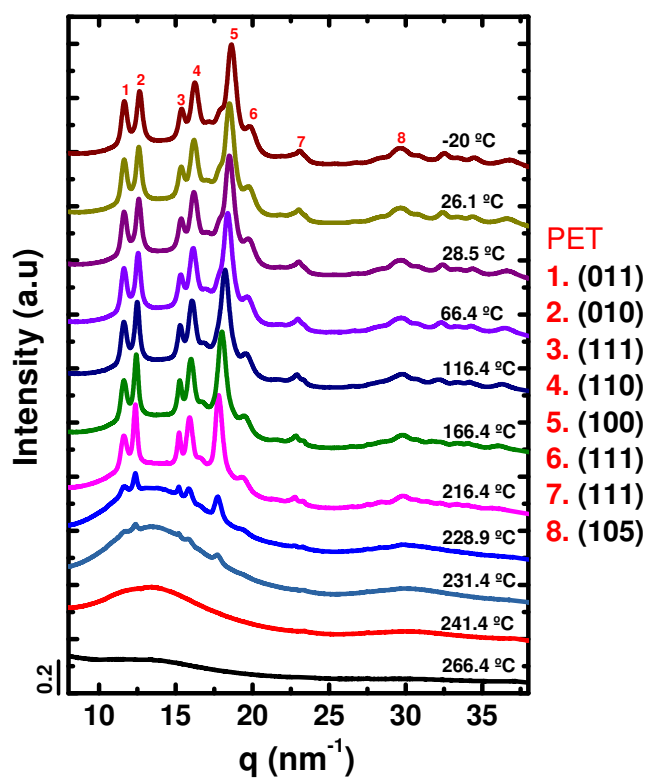
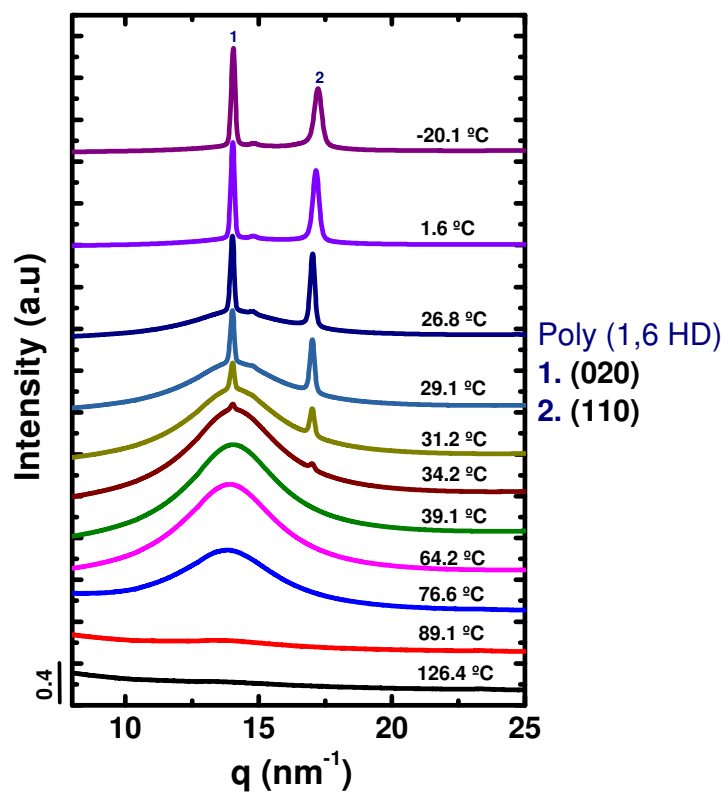
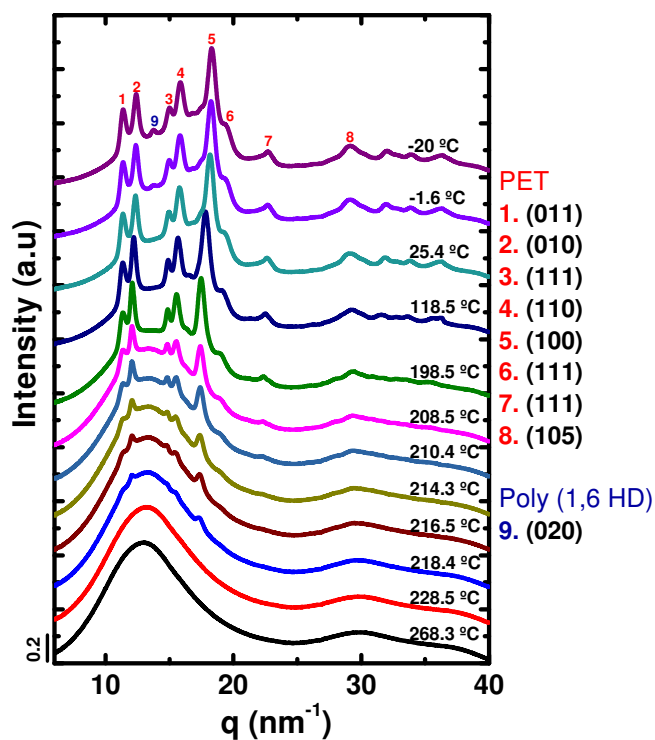


Figure C.4. WAXS diffraction patterns of PET cooled from the 270 °C to -20 °C at 20 °C/min.



**Figure C.5.** WAXS diffraction patterns of Poly (1,6 HD) cooled from the 130 °C to -20 °C at 20 °C/min.



**Figure C.6.** WAXS diffraction patterns of PET<sub>68</sub>Poly(1,6 HD)<sub>32</sub> cooled from the 270 °C to -20 °C at 20 °C/min.

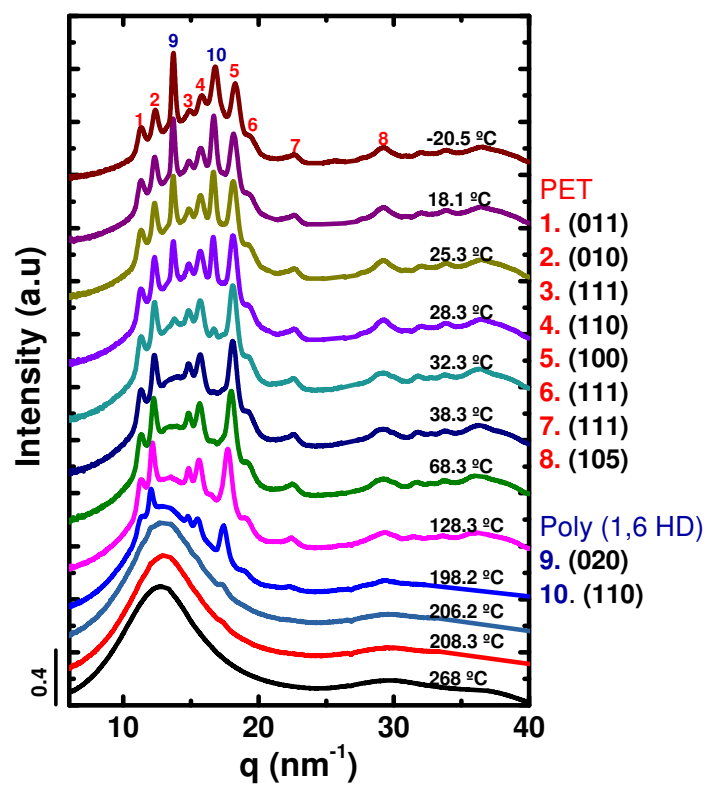


**Figure C.7.** WAXS diffraction patterns of PET<sub>61</sub>Poly(1,6 HD)<sub>39</sub> cooled from the 270 °C to -20 °C at 20 °C/min.

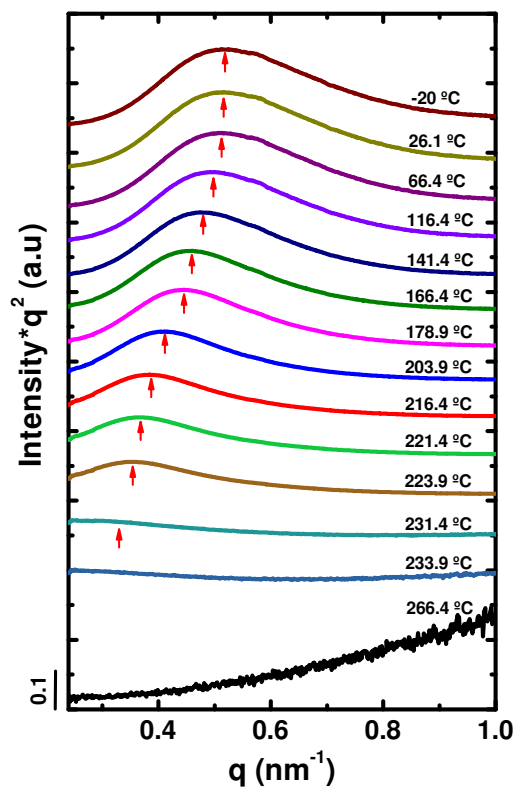


**Figure C.8.** SAXS diffraction patterns of PET cooled from the 270 °C to -20 °C at 20 °C/min.

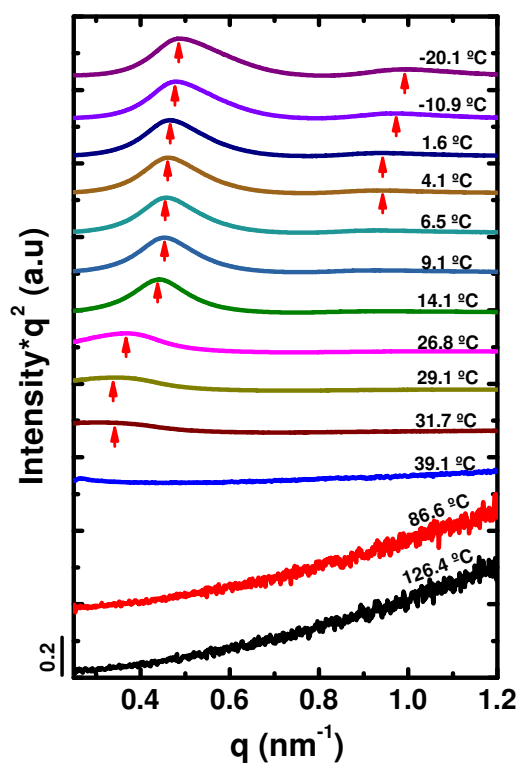


**Figure C.9.** SAXS diffraction patterns of Poly(1,6 HD) cooled from the 130 °C to -20 °C at 20 °C/min.

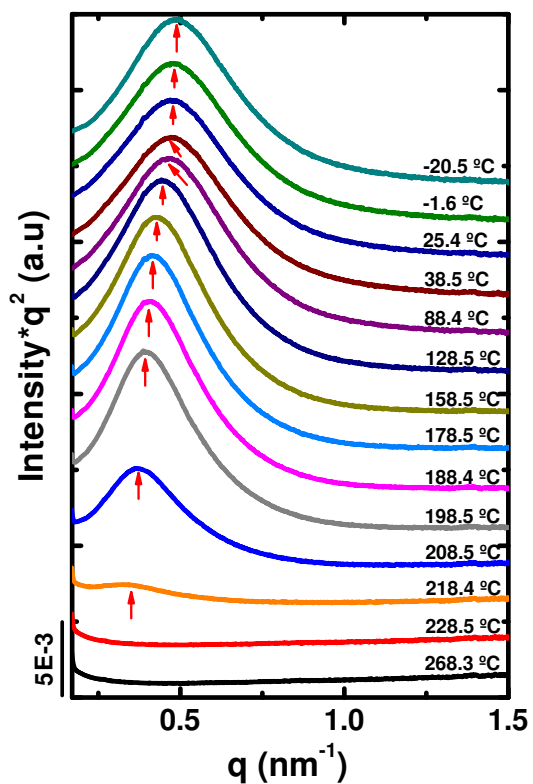


**Figure C.10.** SAXS diffraction patterns of PET<sub>68</sub>Poly(1,6 HD)<sub>32</sub> cooled from the 270 °C to -20 °C at 20 °C/min.

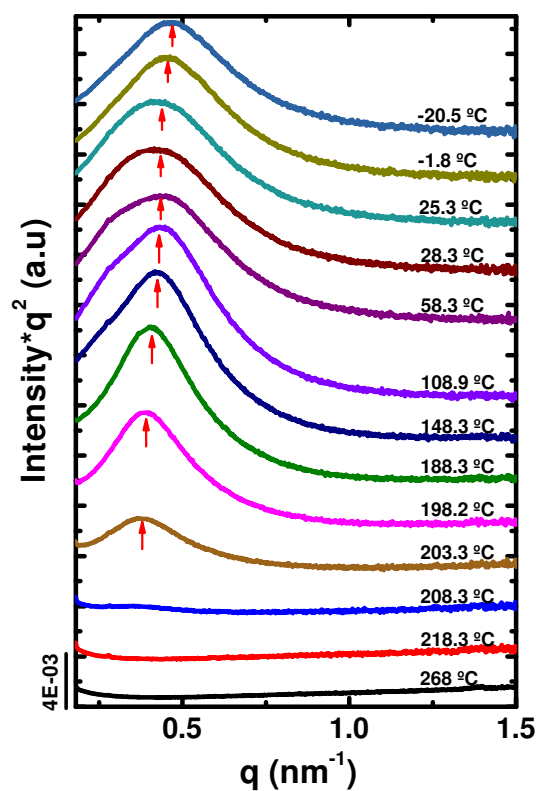


Figure C.11. SAXS diffraction patterns of PET<sub>61</sub>Poly(1,6 HD)<sub>39</sub> cooled from the 270 °C to -20 °C at 20 °C/min.

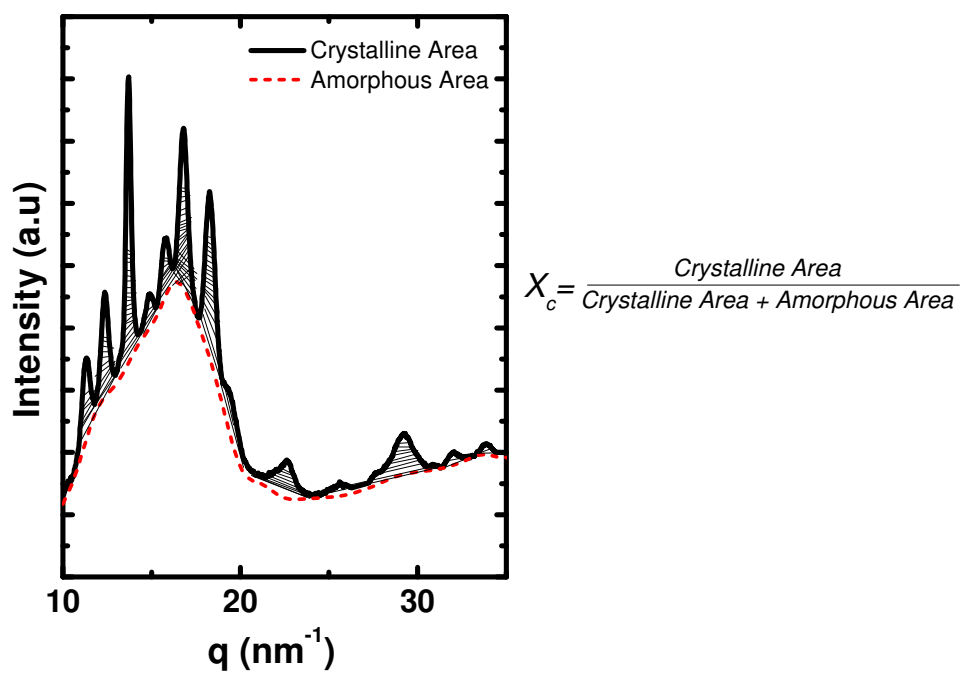


Figure C.12. Degree of crystallinity ( $X_c$ ) by WAXS for PET-*b*-Polyether.

**Table C.1** Number average sequential length ( $L_i$ ) and randomness ( $\eta$ ).

Sample	PET / Polyether		Number average sequential length <sup>a</sup>		$\eta^a$
	% mass ratio <sup>a</sup>	% mol ratio <sup>a</sup>	$L_{EG}$ (PET)	$L_{PE}$ (Polyether)	
PET <sub>34</sub> Poly(1,6 HD) <sub>66</sub>	34/66	90/10	10.4	1.11	0.99
PET <sub>03</sub> Poly(1,6 HD) <sub>97</sub>	03/97	38/62	1.4	2.32	1.13
PET <sub>01</sub> Poly(1,6 HD) <sub>99</sub>	01/99	18/82	1.1	4.95	1.13

## References

- (1) Ibbett, R. N. *NMR Spectroscopy of Polymers*, First edition.; Chapman & Hall: Great Britain, 1993.

## Annex D

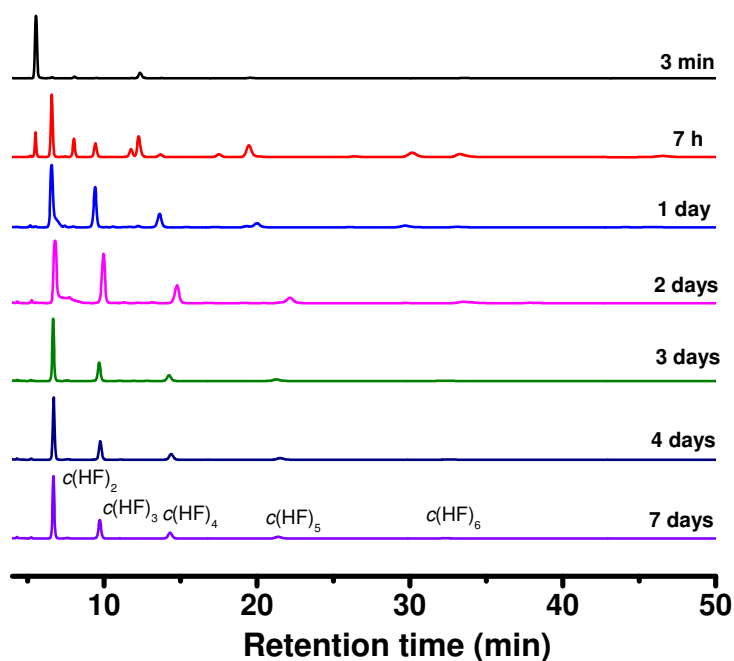


**Figure D.1.** HPLC chromatograms of crude reaction product of enzymatic reaction of 1,6-hexanediol and dimethyl furanoate at different reaction times.

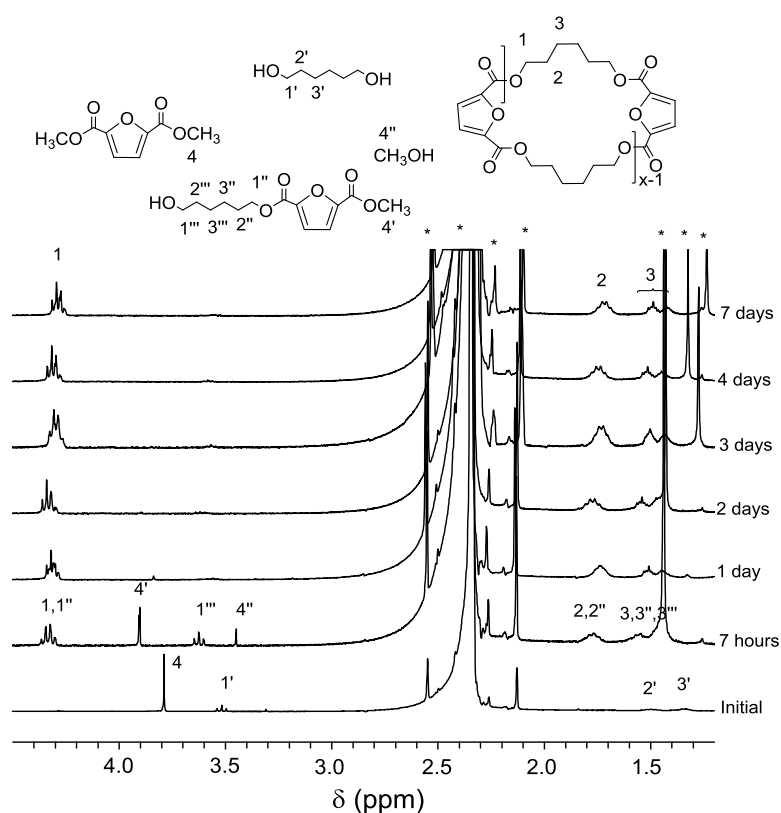


**Figure D.2.**  $^1\text{H}$  NMR spectra of crude reaction product of enzymatic reaction of 1,6-hexanediol and dimethyl furanoate at different reaction times. (\*) Signals from solvent used in the reaction and water from deuterated chloroform.

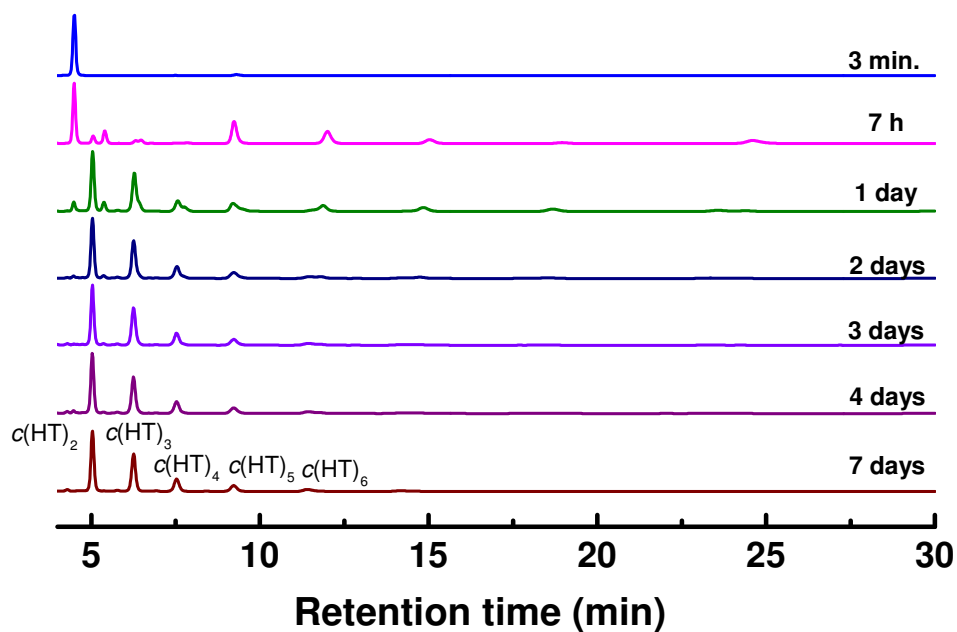


**Figure D.3.** HPLC chromatograms of crude reaction product of enzymatic reaction of 1,6-hexanediol and dimethyl terephthalate at different reaction times.

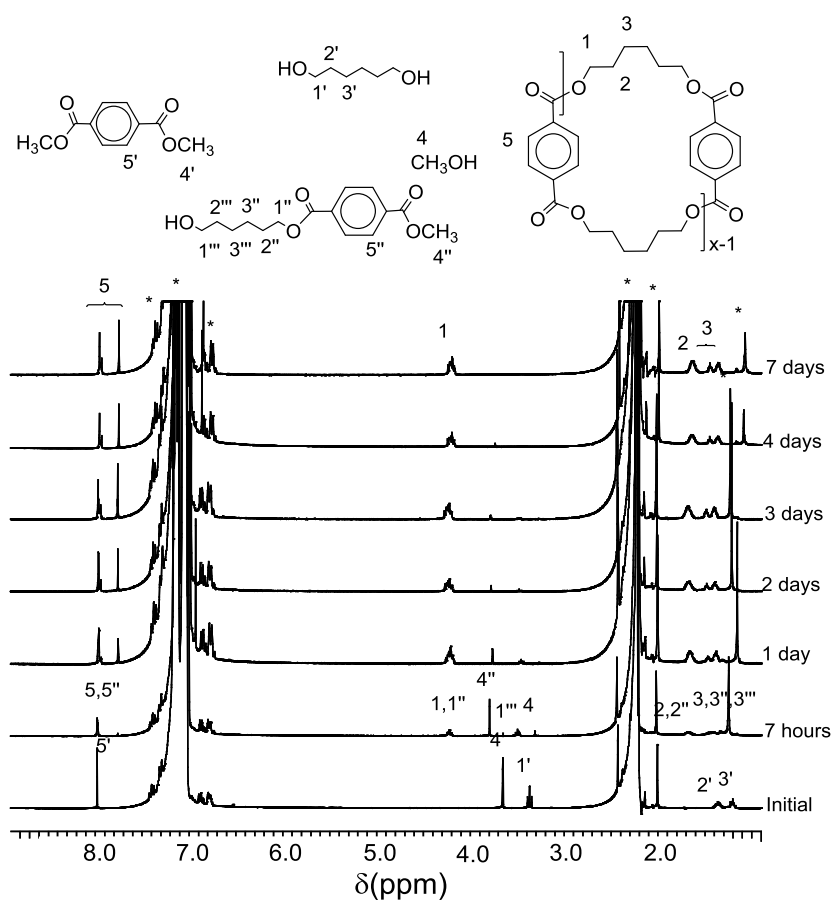


**Figure D.4.**  $^1\text{H}$  NMR spectra of crude reaction product of enzymatic reaction of 1,6-hexanediol and dimethyl terephthalate at different reaction times. (\*) Signals from solvent used in the reaction and water from deuterated chloroform.

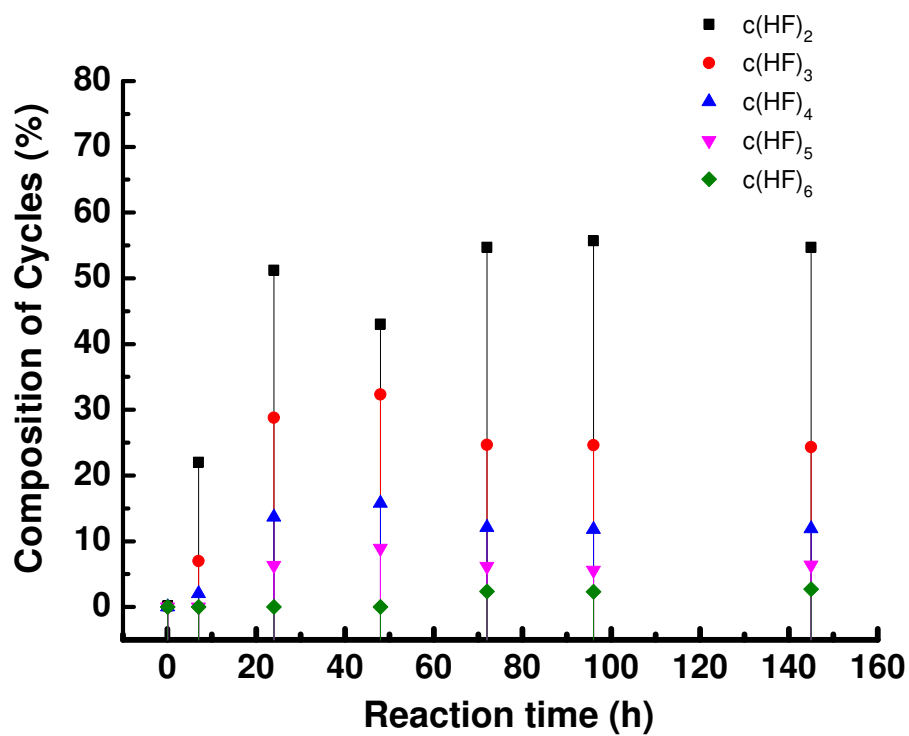


Figure D.5. Evolution of  $c(\text{HF})_x$  content with reaction time determined from HPLC chromatograms.

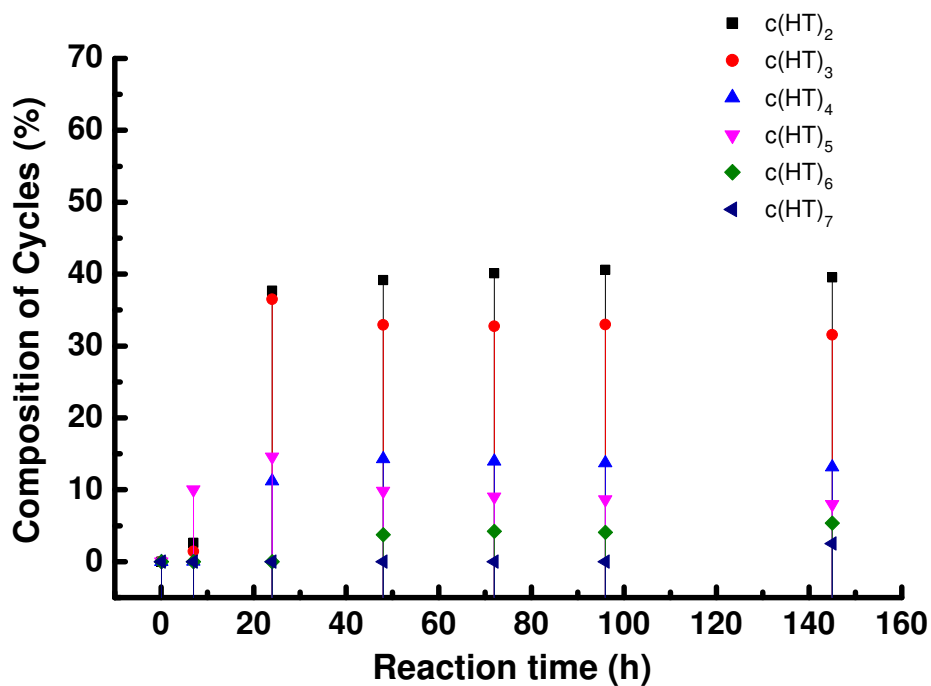
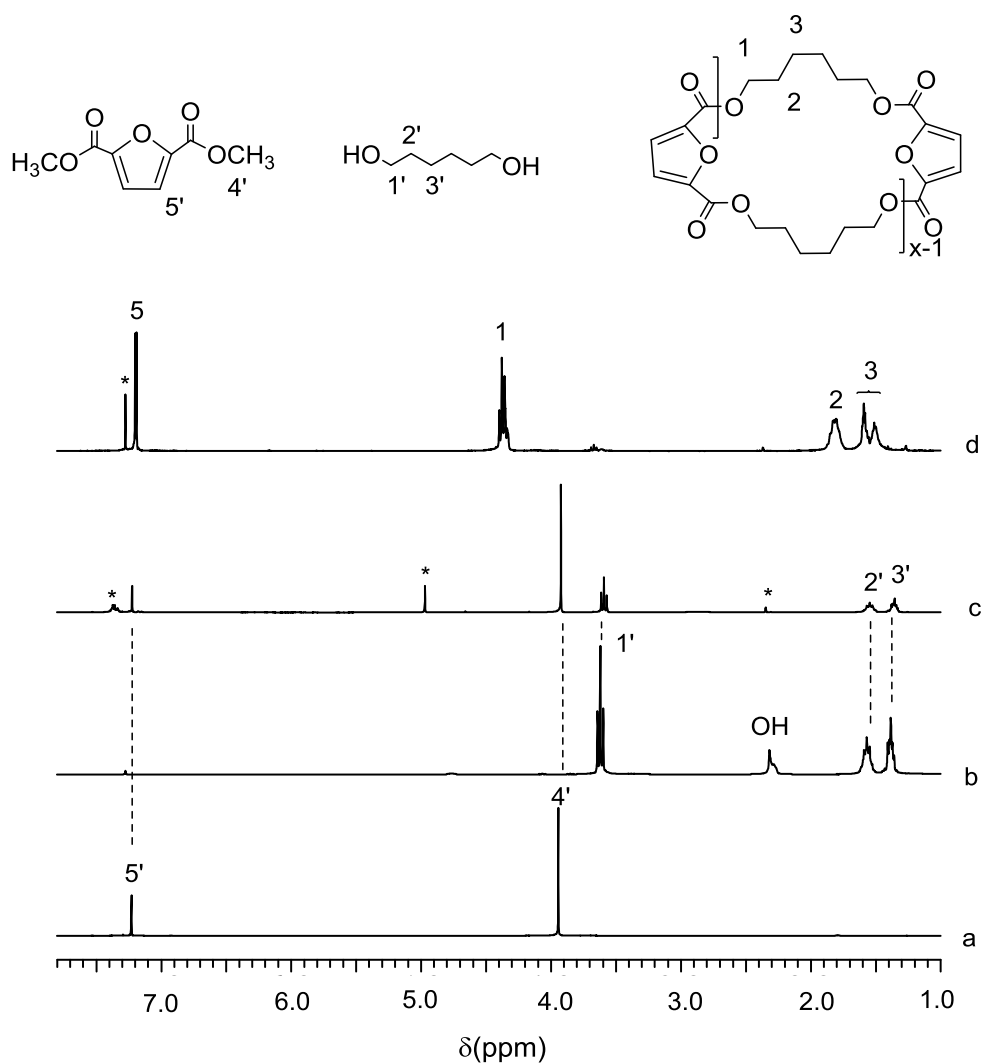
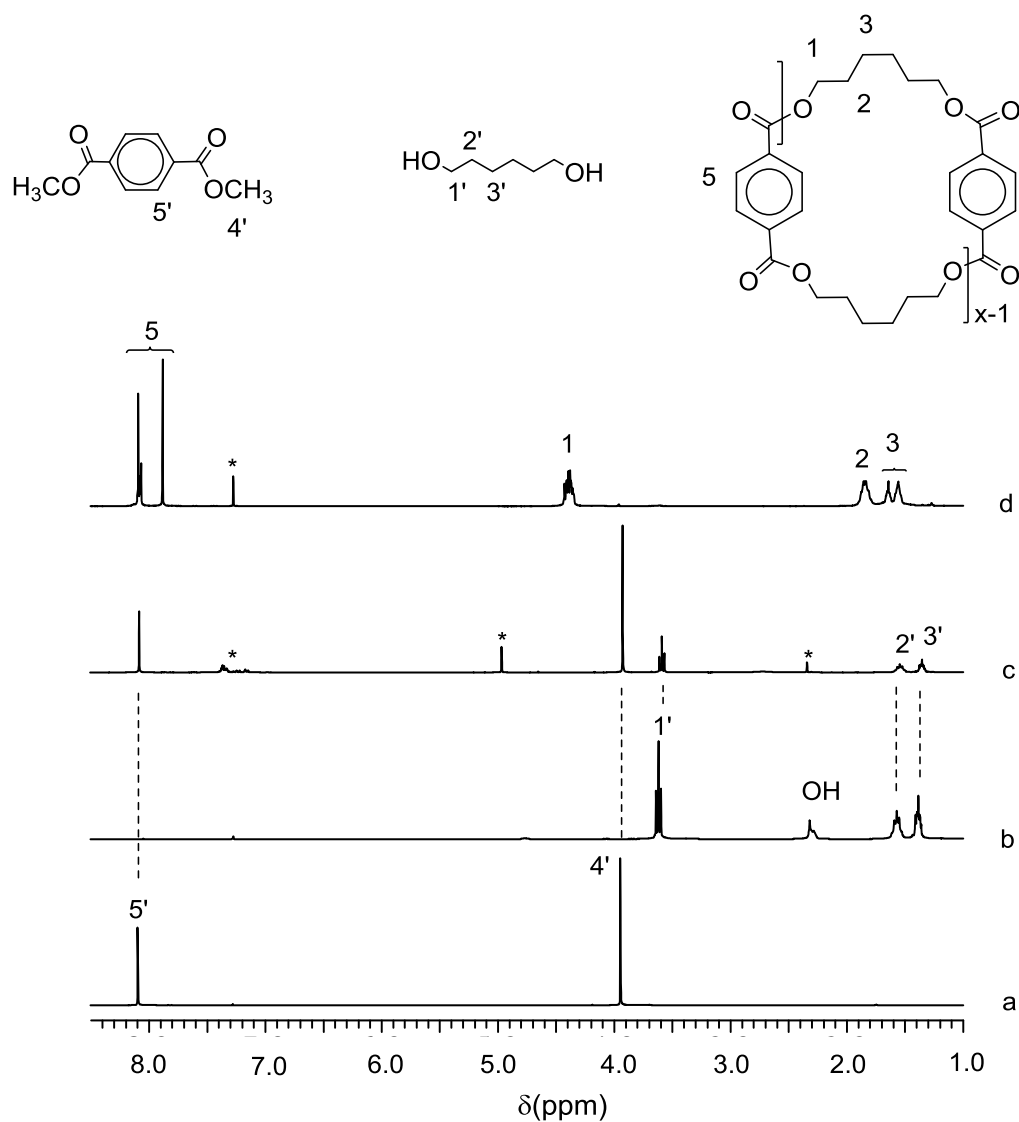


Figure D.6. Evolution of  $c(\text{HT})_x$  content with reaction time determined from HPLC chromatograms.



**Figure D.7.**  $^1\text{H}$  NMR spectra of DMF (a), HD (b), and crude reaction product of enzymatic reaction of 1,6-hexanediol and dimethyl furanoate after 7 days of reaction in absence (c) and presence (d) of CALB enzyme. (\*) Signals from impurities, solvent used in the reaction and residual signal from deuterated chloroform.



**Figure D.8.**  $^1\text{H}$  NMR spectra of DMT (a), HD (b), and crude reaction product of enzymatic reaction of 1,6-hexanediol and dimethyl terephthalate after 7 days of reaction in absence (c) and presence (d) of CALB enzyme. (\*) Signals from impurities, solvent used in the reaction and residual signal from deuterated chloroform.

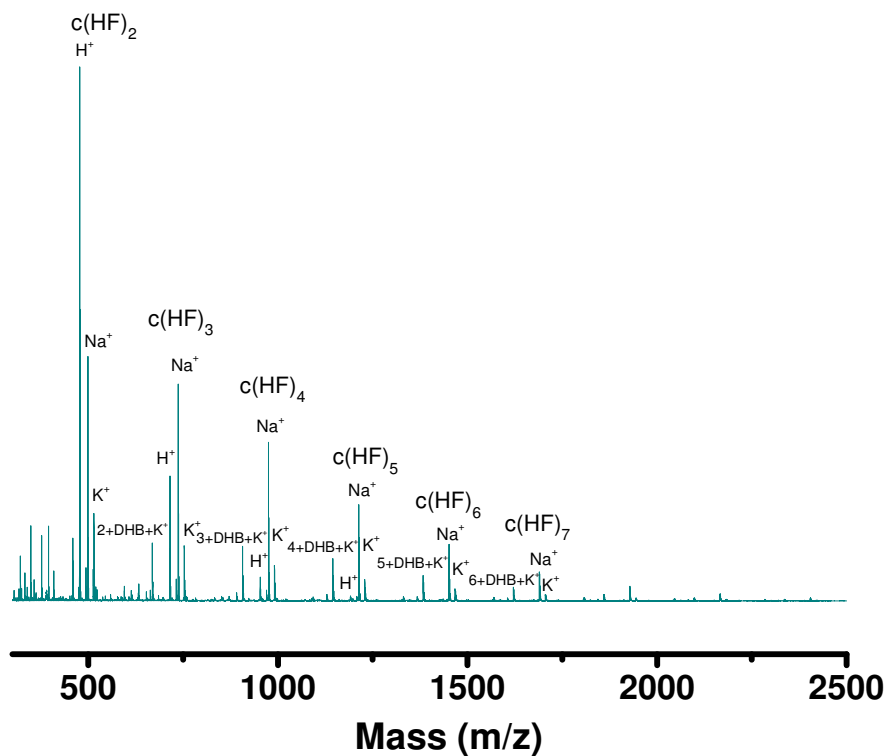


Figure D.9. MALDI-TOF MS spectra of  $c(\text{HF})_x$  cycles recovered the day 7 of reaction.

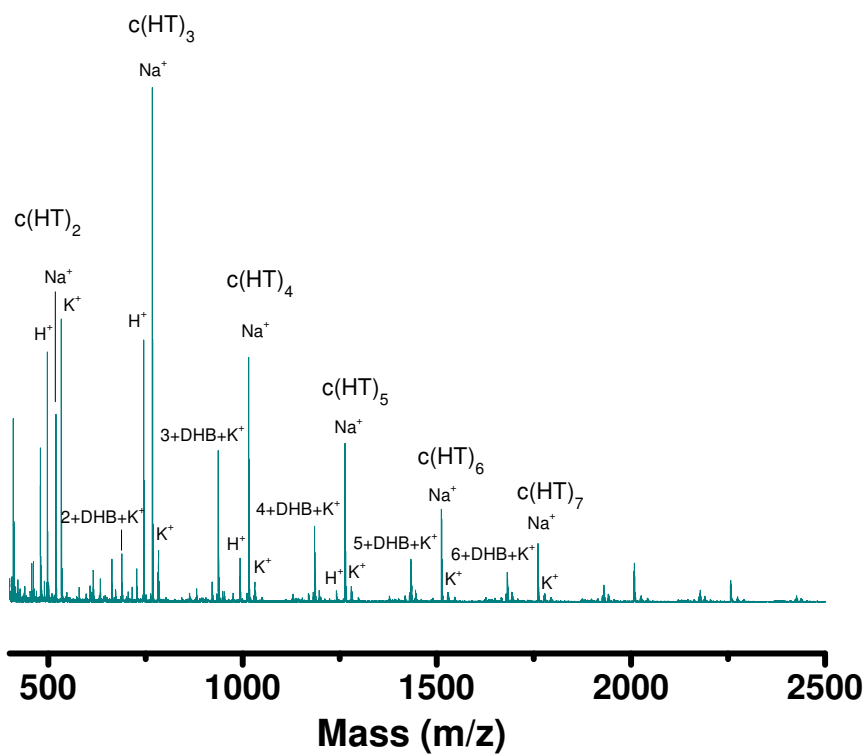
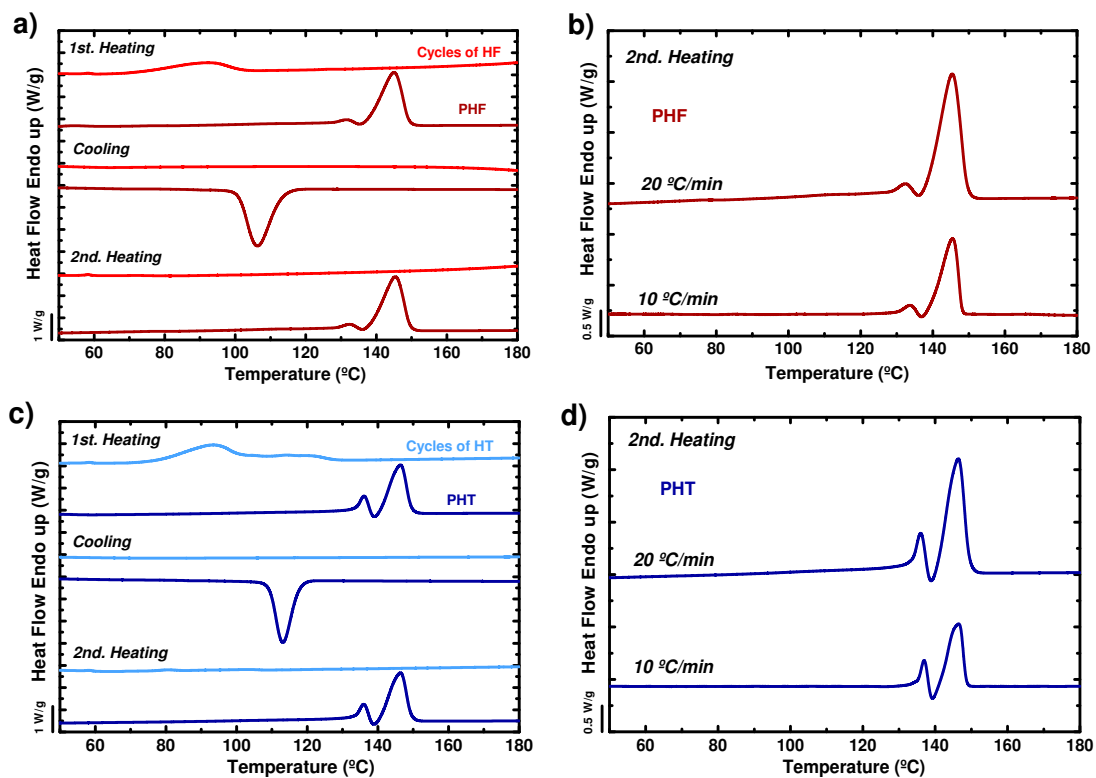
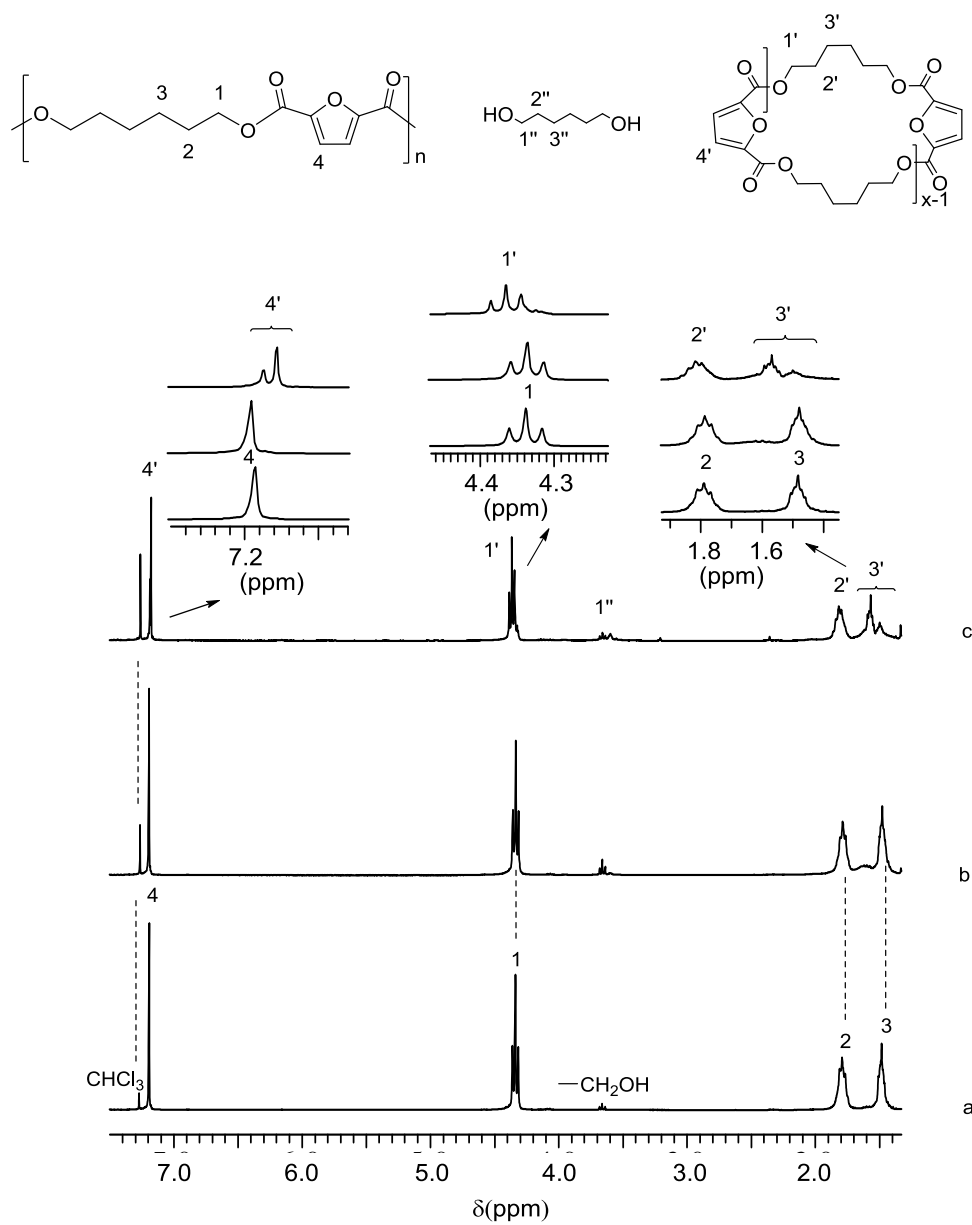


Figure D.10. MALDI-TOF MS spectra of  $c(\text{HT})_x$  cycles recovered the day 7 of reaction.



**Figure D.11.** DSC heating-cooling-heating thermograms of a)  $c(\text{HF})_x$  and PHF and c)  $c(\text{HT})_x$  and PHT. DSC heating scans at different heating rates of b) PHF and d) PHT.



**Figure D.12.**  $^1\text{H}$  NMR spectra of a) PHF and crude reaction products obtained after 3 days of CDP b) without CALB enzyme added and c) with CALB enzyme added.

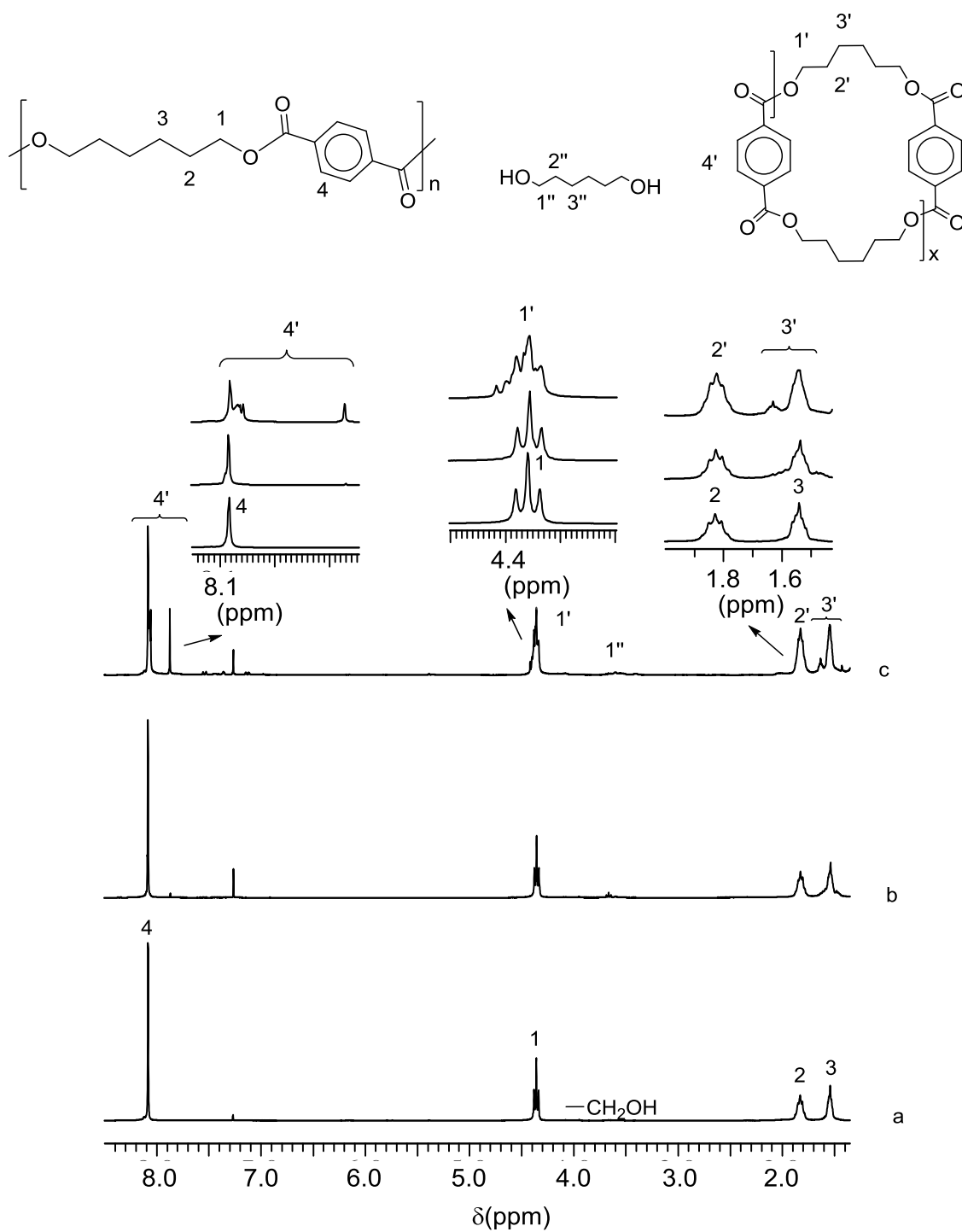


**Figure D.13.**  $^1\text{H}$  NMR spectra of a) PHT and crude reaction products obtained after 3 days of CDP b) without CALB enzyme added and c) with CALB enzyme added.

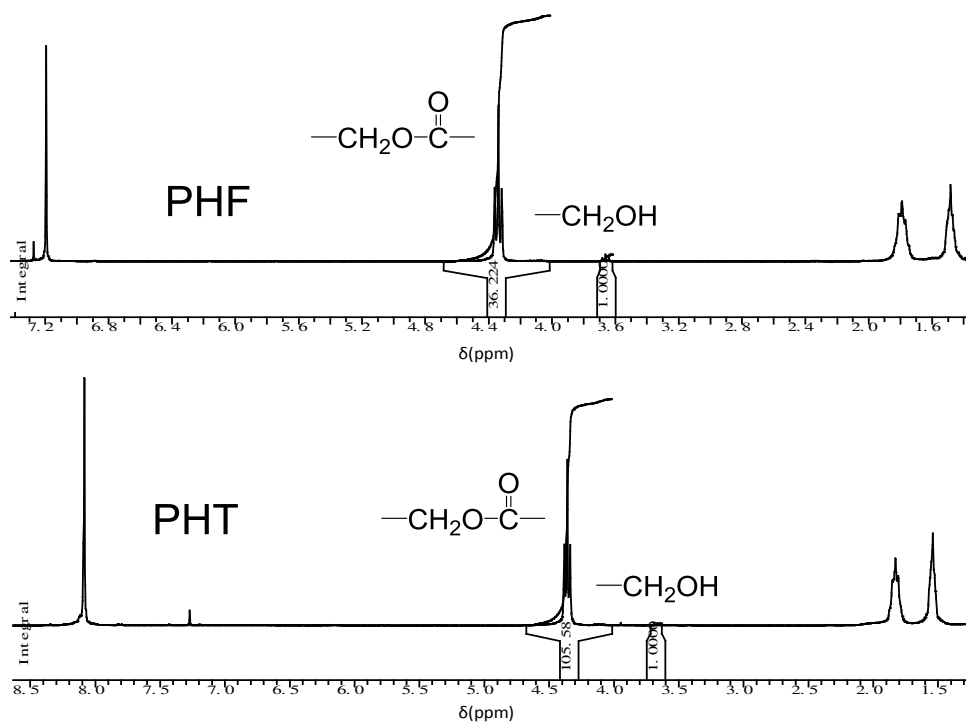


**Figure D.14.** NMR spectra of PHT (bottom) and PHF (top) with integrals for  $M_n$  determination by end group analysis (hydroxyl end groups).

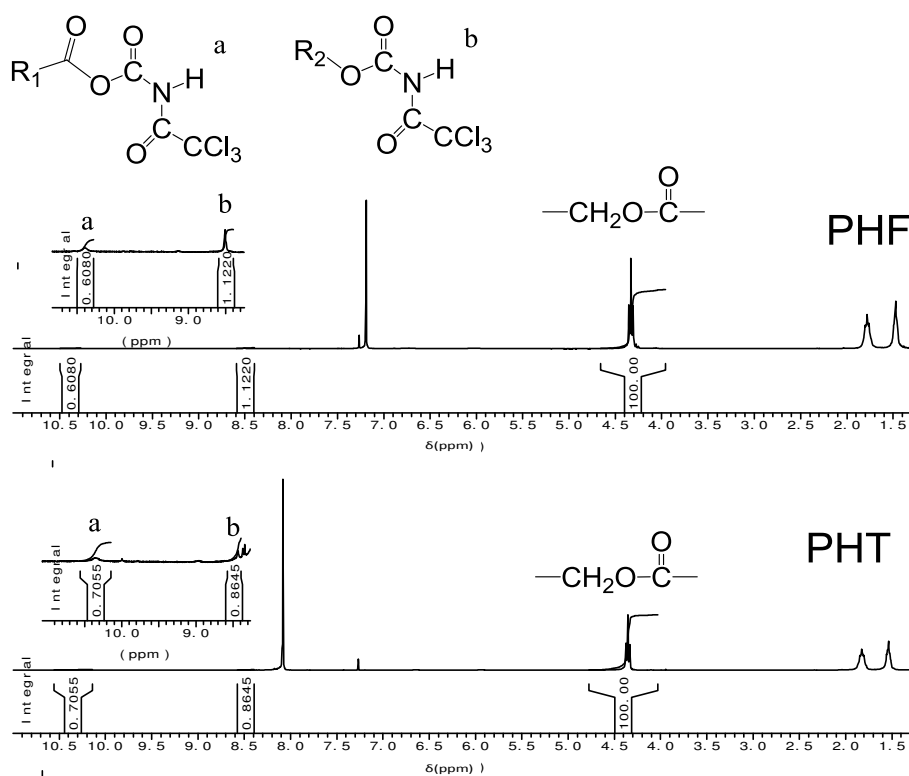


**Figure D.15.** NMR spectra of PHT (bottom) and PHF (top) with integrals for  $M_n$  determination by end group analysis (carboxyl end groups). a and b, signals of NH imide groups that emerged by reaction of carboxyl ( $R_1COOH$ ) and hydroxyl ( $R_2OH$ ) end groups, respectively, with TAI.

## Annex E

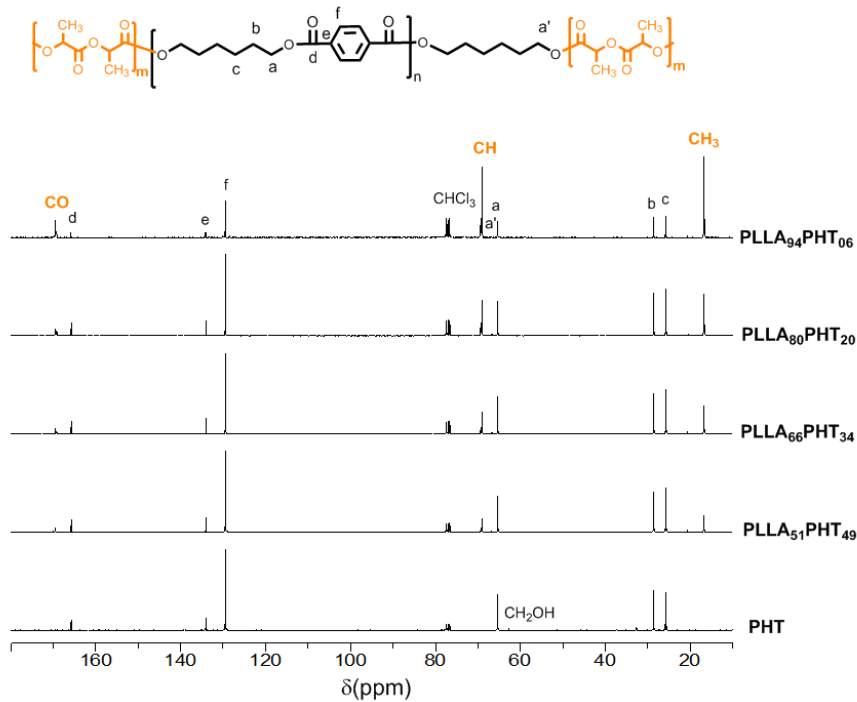


**Figure E.1.**  $^{13}\text{C}$  NMR spectra of PHT and PLLA-*b*-PHT-*b*-PLLA copolyesters with peak assignments.

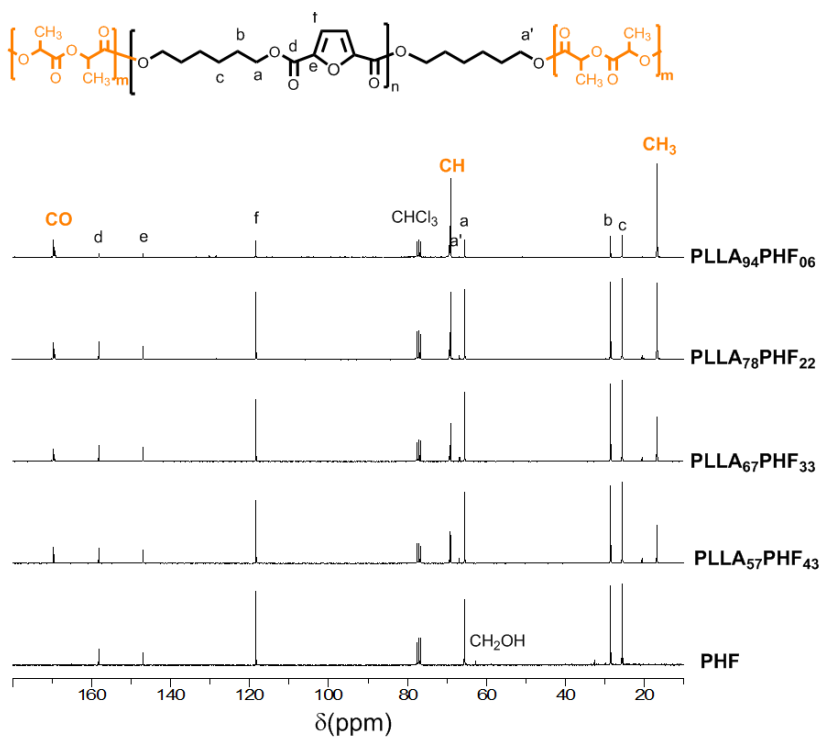


**Figure E.2.**  $^{13}\text{C}$  NMR spectra of PHF and PLLA-*b*-PHF-*b*-PLLA copolyesters with peak assignments.

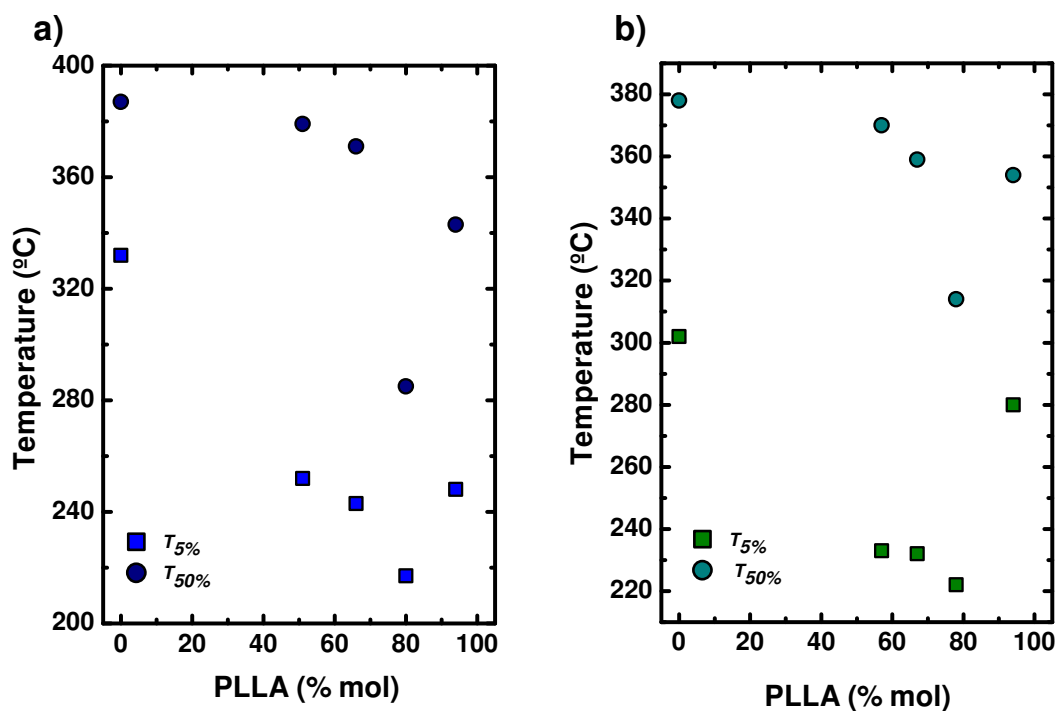


**Figure E.3.** Temperature at which the copolymers lose 5 and 50% of their weight. (a) PLLA-*b*-PHT-*b*-PLLA and (b) PLLA-*b*-PHF-*b*-PLLA.

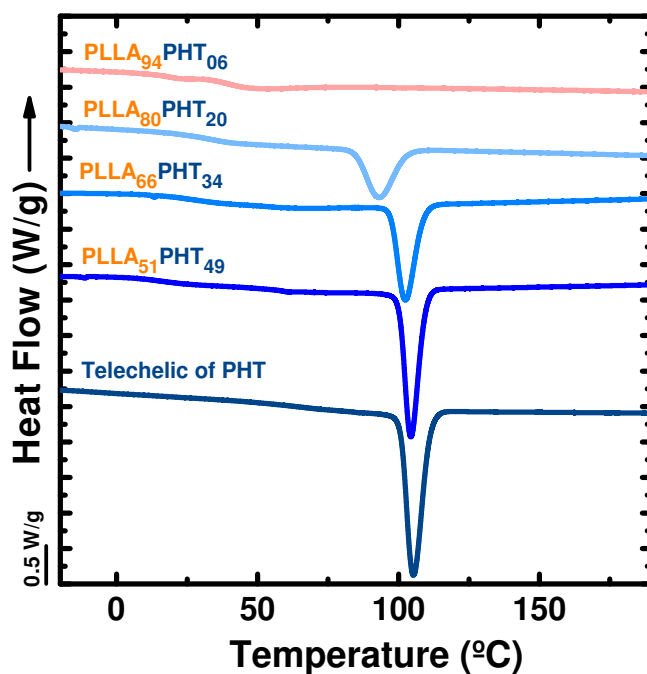


**Figure E.4.** DSC cooling scans for PHT and copolymers.

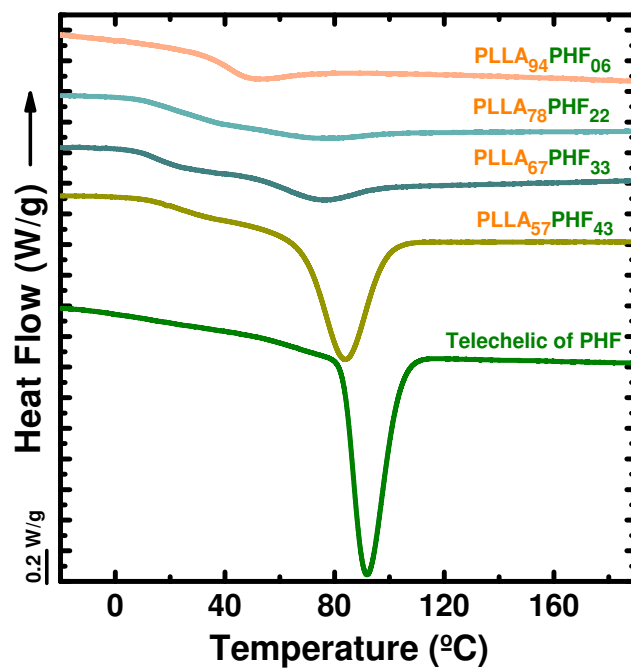


Figure E.5. DSC cooling scans for PHF and copolymers.

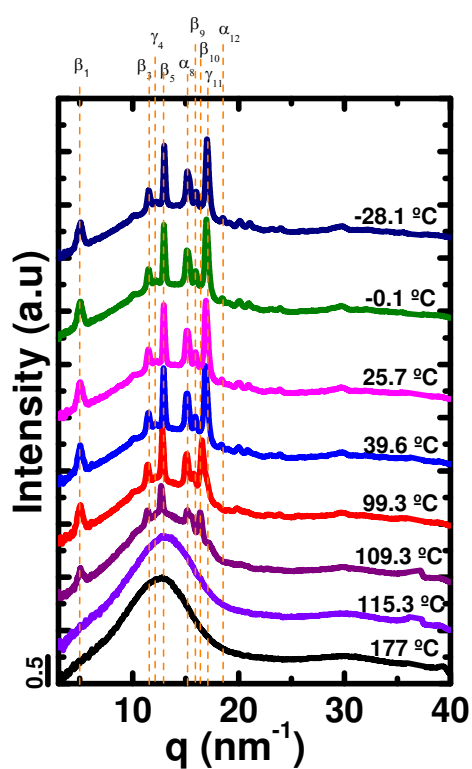
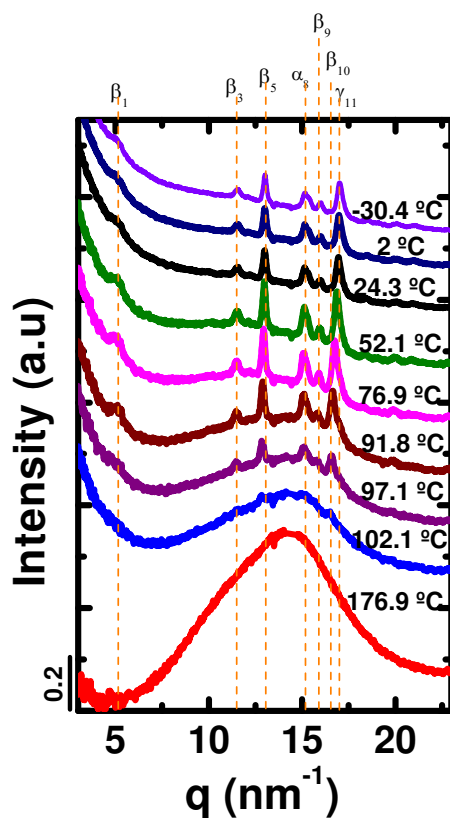
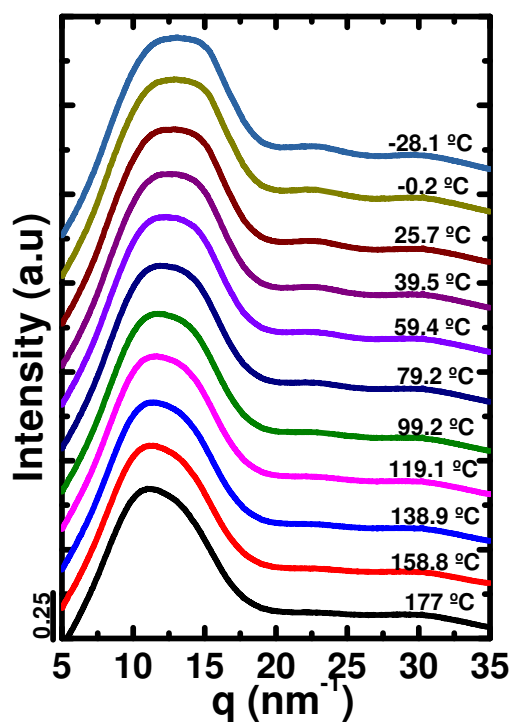


Figure E.6. WAXS diffraction patterns of PLLA<sub>66</sub>PHT<sub>34</sub> cooled from the 180 °C to -30 °C at 20 °C/min.



**Figure E.7.** WAXS diffraction patterns of PLLA<sub>80</sub>PHT<sub>20</sub> cooled from the 180 °C to -30 °C at 20 °C/min.



**Figure E.8.** WAXS diffraction patterns of PLLA<sub>94</sub>PHT<sub>06</sub> cooled from the 180 °C to -30 °C at 20 °C/min.

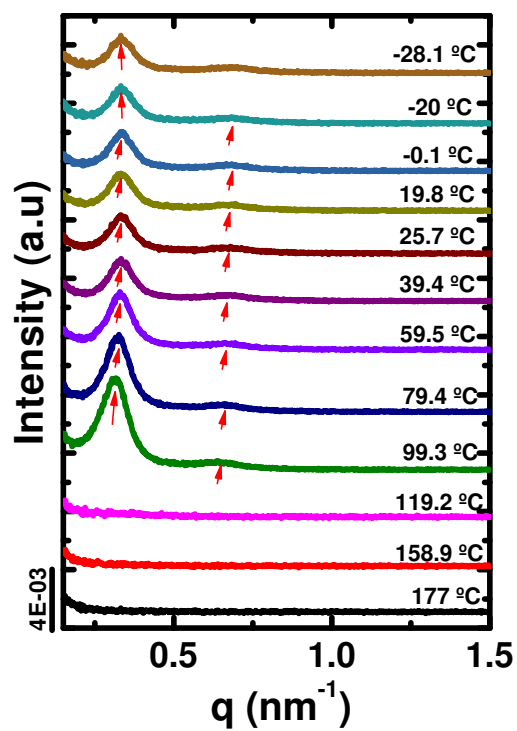


**Figure E.9.** SAXS diffraction patterns of PLLA<sub>66</sub>PHT<sub>34</sub> cooled from the 180 °C to -30 °C at 20 °C/min.

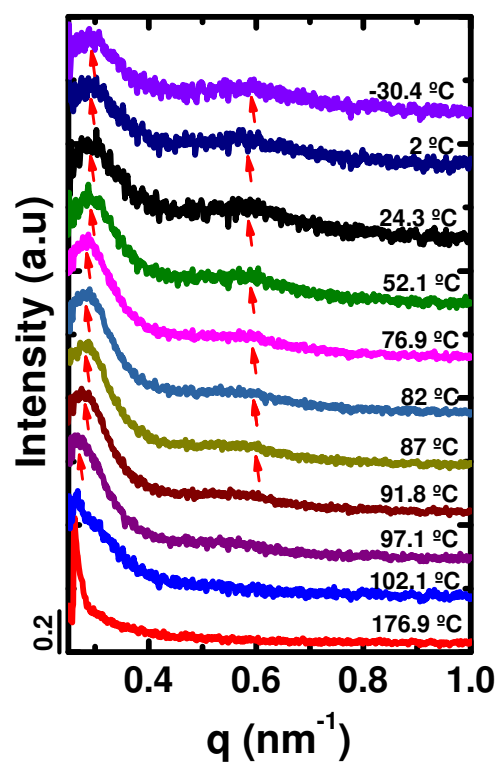


**Figure E.10.** SAXS diffraction patterns of PLLA<sub>80</sub>PHT<sub>20</sub> cooled from the 180 °C to -30 °C at 20 °C/min.

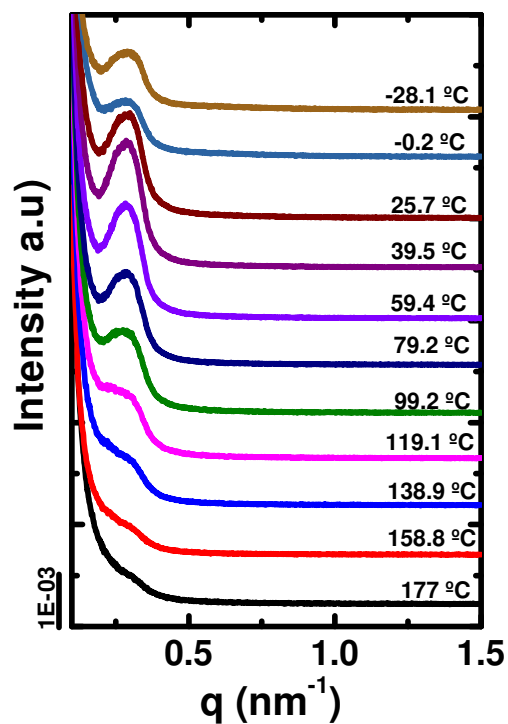


**Figure E.11.** SAXS diffraction patterns of PLLA<sub>94</sub>PHT<sub>06</sub> cooled from the 180 °C to -30 °C at 20 °C/min.

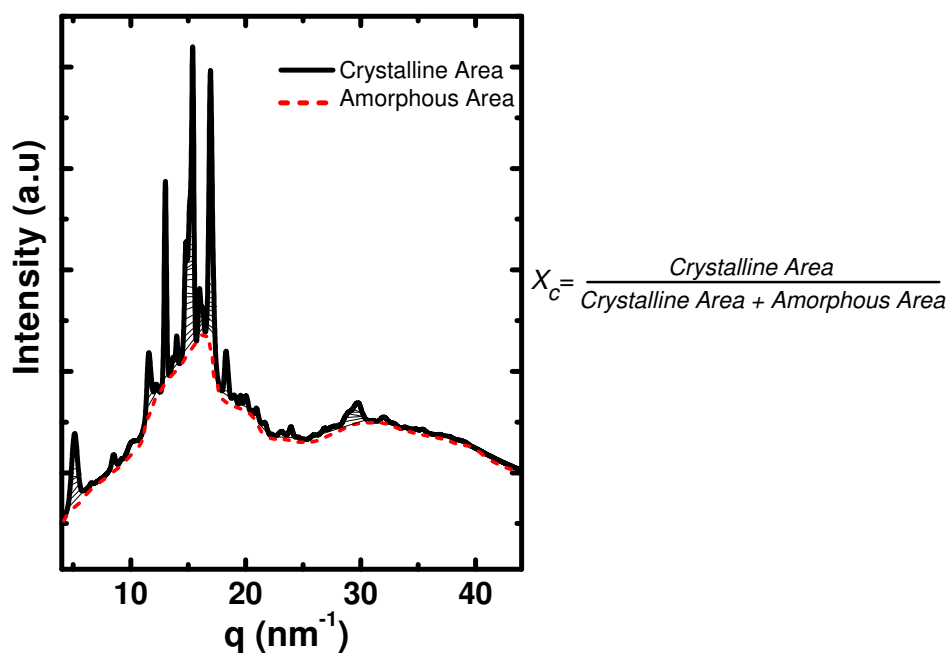


**Figure E.12.** Degree of crystallinity ( $X_c$ ) by WAXS.

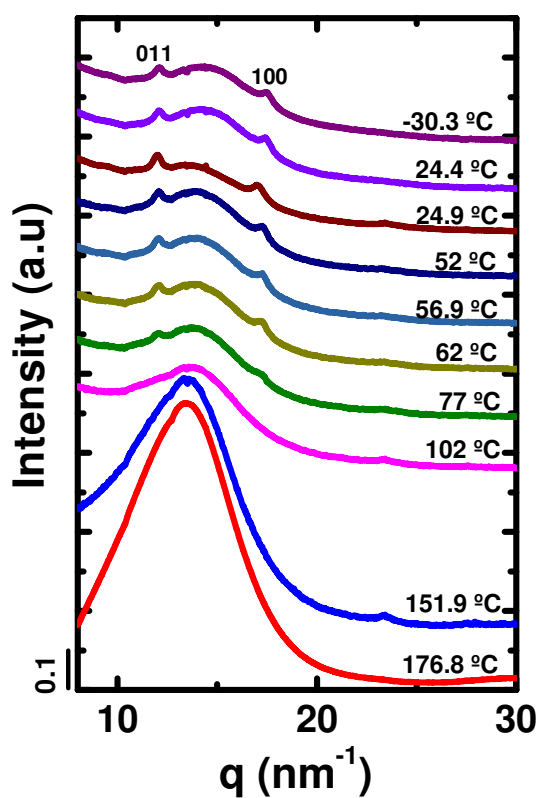


**Figure E.13.** WAXS diffraction patterns of PLLA<sub>67</sub>PHF<sub>33</sub> cooled from the 180 °C to -30 °C at 20 °C/min.

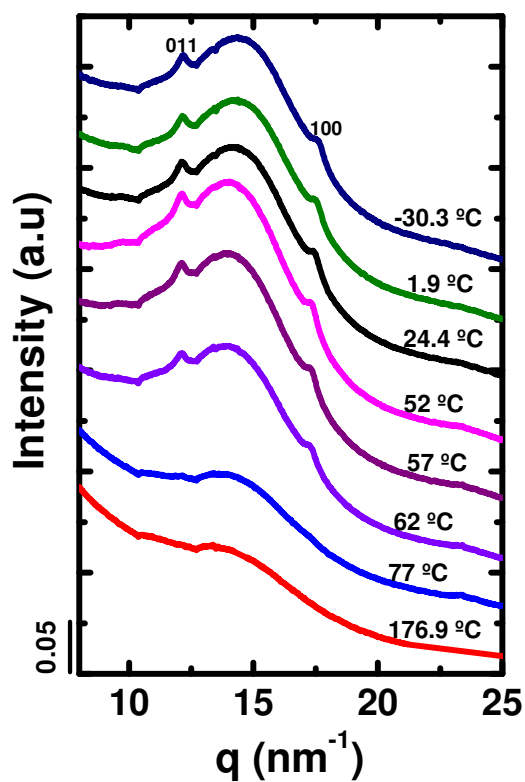


**Figure E.14.** WAXS diffraction patterns of PLLA<sub>78</sub>PHF<sub>22</sub> cooled from the 180 °C to -30 °C at 20 °C/min.

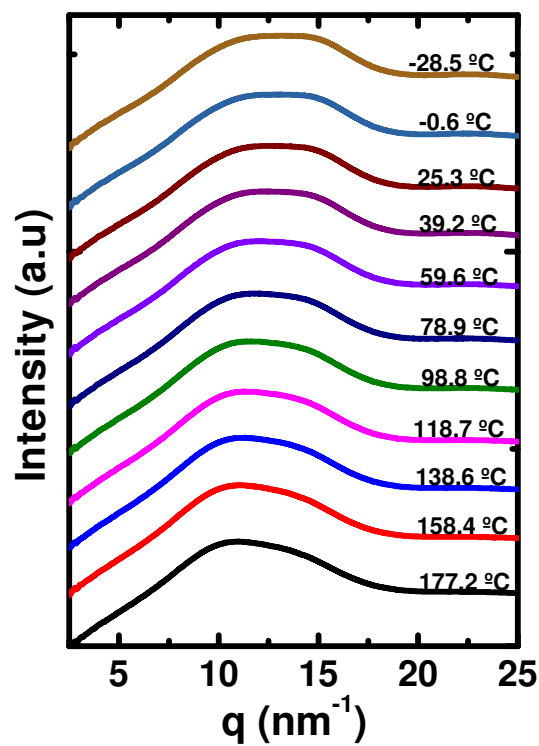


**Figure E.15.** WAXS diffraction patterns of PLLA<sub>94</sub>PHF<sub>06</sub> cooled from the 180 °C to -30 °C at 20 °C/min.

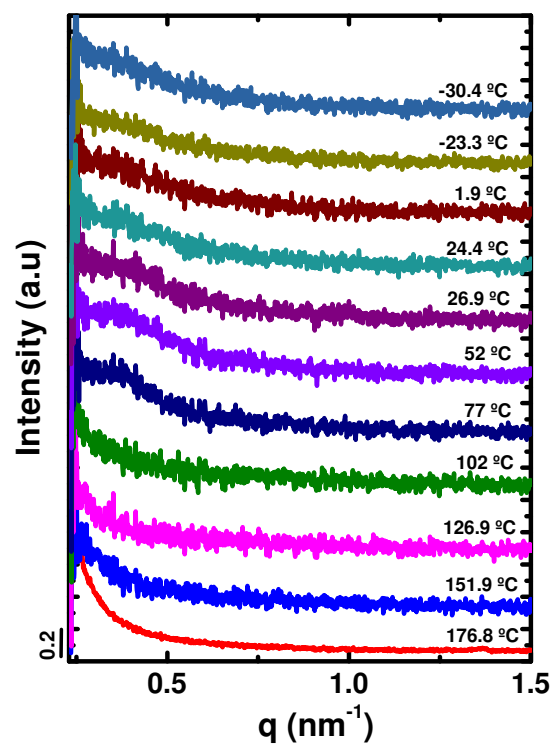


**Figure E.16.** SAXS diffraction patterns of PLLA<sub>66</sub>PHT<sub>34</sub> cooled from the 180 °C to -30 °C at 20 °C/min.

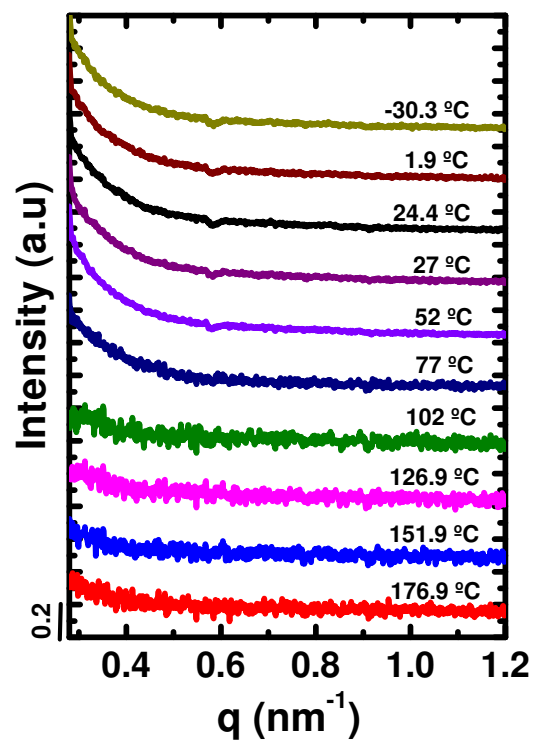


**Figure E.17.** SAXS diffraction patterns of PLLA<sub>78</sub>PHF<sub>22</sub> cooled from the 180 °C to -30 °C at 20 °C/min.

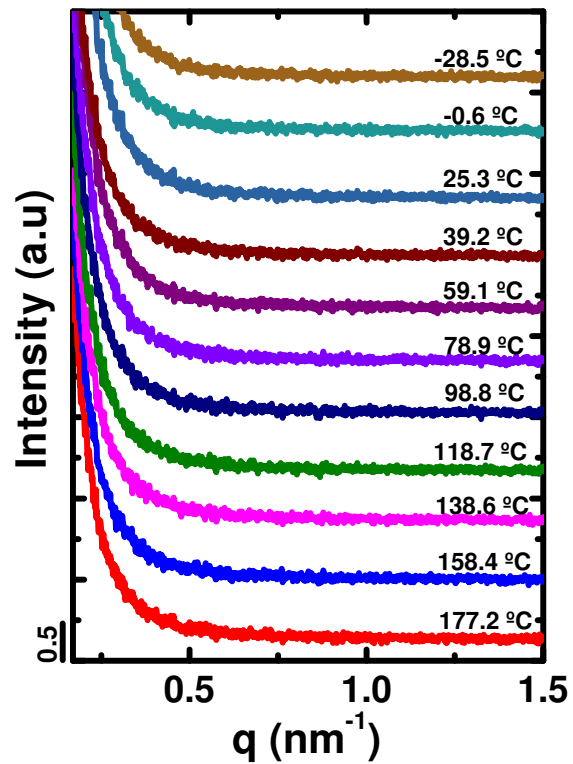


**Figure E.18.** SAXS diffraction patterns of PLLA<sub>94</sub>PHF<sub>06</sub> cooled from the 180 °C to -30 °C at 20 °C/min.

## Publications

- (1) Flores, I.; Demarteau, J.; Müller, A. J.; Etxeberria, A.; Irusta, L.; Bergman, F.; Koning, C.; Sardon, H. Screening of Different Organocatalysts for the Sustainable Synthesis of PET. *European Polymer Journal* **2018**, *104*, 170–176. <https://doi.org/10.1016/j.eurpolymj.2018.04.040>.
- (2) Jehanno, C.; Flores, I.; Dove, A. P.; Müller, A. J.; Ruipérez, F.; Sardon, H. Organocatalysed Depolymerisation of PET in a Fully Sustainable Cycle Using Thermally Stable Protic Ionic Salt. *Green Chemistry* **2018**, *20* (6), 1205–1212. <https://doi.org/10.1039/C7GC03396F>.
- (3) Flores, I.; Martínez de Ilarduya, A.; Sardon, H.; Müller, A. J.; Muñoz-Guerra, S. Synthesis of Aromatic–Aliphatic Polyesters by Enzymatic Ring Opening Polymerization of Cyclic Oligoesters and Their Cyclodepolymerization for a Circular Economy. *ACS Applied Polymer Materials* **2019**, *1* (3), 321–325. <https://doi.org/10.1021/acsapm.8b00265>.
- (4) Basterretxea, A.; Gabirondo, E.; Jehanno, C.; Zhu, H.; Flores, I.; Müller, A. J.; Etxeberria, A.; Mecerreyes, D.; Coulembier, O.; Sardon, H. Polyether Synthesis by Bulk Self-Condensation of Diols Catalyzed by Non-Eutectic Acid–Base Organocatalysts. *ACS Sustainable Chemistry & Engineering* **2019**, *7* (4), 4103–4111. <https://doi.org/10.1021/acssuschemeng.8b05609>.
- (5) Flores, I.; Etxeberria, A.; Irusta, L.; Calafel, I.; Vega, J.F.; Martínez-Salazar, J.; Sardon, H.; Müller, A. J. PET-ran-PLA partially degradable random copolymers prepared by organocatalysis: Effect of PLA incorporation on crystallization and morphology. *ACS Sustainable Chemistry & Engineering* **2019**, (Accepted).
- (6) Basterretxea, A.; Gabirondo, E.; Flores, I.; Etxeberria, A.; González, A.; Müller, A.J.; Mecerreyes, D.; Coulembier, O.; Sardon, H. Isomorphic polyoxyalkylenes copolyethers obtained by copolymerization of aliphatic diols. *Macromolecules* **2019**, (Accepted).

## Resumen

A lo largo de estos últimos años muchas investigaciones se han enfocado en intentar hacer síntesis de polímeros de forma más sostenible, ya sea usando diversos monómeros provenientes de fuentes renovables o incluso de residuos plásticos; así como también evitando el uso de solventes de alta toxicidad y reemplazando los catalizadores comunes por catalizadores no metálicos que son más amigables con el medio ambiente.

Siguiendo la línea del desarrollo sustentable, diversos trabajos muestran el reciclado de polímeros (mecánico, químico o la recuperación de energía) como una alternativa para reutilizar los plásticos al final de su ciclo de vida y disminuir la cantidad de residuos dispuestos en vertederos. En este sentido, algunos investigadores han encontrado en el reciclado químico de polímeros una fuente de materia prima (monómeros), la cuál puede ser usada posteriormente para obtener nuevos materiales. Algunos trabajos incluso, han intentado hacer lo más sostenible posible el propio proceso de reciclado, reduciendo o evitando el uso de solventes, recuperando los catalizadores para el reciclado, entre otras cosas.

Otra línea de investigación que ha emergido como necesidad para solucionar problemas ambientales generados en el proceso de síntesis de materiales, es el estudio de catalizadores que sean menos contaminantes que los catalizadores metálicos usados actualmente. Aquí, el término organocatalisis ha sido usado para indicar el uso de catalizadores orgánicos en la síntesis de un polímero. Una gran cantidad de autores han dedicado su tiempo a investigar y encontrar catalizadores orgánicos que sean capaces de sintetizar polímeros con la misma capacidad catalítica o incluso mejor que los catalizadores metálicos. Los catalizadores orgánicos han mostrado ser bastante efectivos para polimerizar y copolimerizar una gran cantidad de materiales, ofreciendo la ventaja de no dejar residuos en el producto final lo que se traduce por un lado en productos con una alta pureza y por otro lado en la ausencia de residuos tóxicos que podrían terminar en el ambiente. Estos catalizadores orgánicos versus los catalizadores metálicos parecen ser una opción que deja una menor huella ambiental.

En este sentido, este trabajo reporta la síntesis de polímeros implicando diversos elementos que otorgan a la ruta sintética de obtención de los materiales un alto grado de sostenibilidad.

El primer capítulo es una introducción que describe el origen del trabajo desarrollado y todo lo reportado en literatura en relación a los polímeros sintetizados en esta tesis, así como el contenido de la tesis de forma genérica

Un segundo capítulo muestra los materiales usados, el procedimiento de síntesis de cada polímero y las técnicas de caracterización para analizar todos los polímeros sintetizados, además en este mismo capítulo se incluyen conceptos empleados a lo largo del trabajo que son útiles para entender más fácilmente algunos temas y que ayudan a ampliar el panorama teórico.

Para obtener los diversos polímeros se han utilizado catalizadores orgánicos y enzimas, ambos libres de metal en su composición. Por otro lado se han usado dos monómeros sostenibles, por un lado el dimetil tereftalato (DMT) que puede ser obtenido como producto del reciclado químico de residuos de PET y por otro lado el dimetil furanoato (DMF) que es obtenido a partir de la biomasa. Todos estos elementos en conjunto son una alternativa para disminuir el impacto ambiental durante la síntesis de los materiales y al final del ciclo de vida de los polímeros.

En el tercer capítulo de la tesis se lleva a cabo un estudio para encontrar un catalizador orgánico que favorezca la formación de PET, para lo cual diversos catalizadores orgánicos son probados y comparados con un catalizador metálico. Diversas técnicas de caracterización fueron empleadas para el análisis, como son: resonancia magnética nuclear (NMR), espectroscopia infrarroja de transformada de Fourier (FTIR), análisis termogravimétrico (TGA), calorimetría diferencial de barrido (DSC), entre otras. Se evaluó la actividad catalítica de los catalizadores orgánicos, así como el grado de conversión para polimerizar PET. Con esta información en conjunto, se demostró que existen catalizadores orgánicos con una actividad catalítica similar o incluso mejor que un catalizador metálico para sintetizar PET. También se analizaron los pesos moleculares obtenidos con cada uno de los catalizadores evaluados empleando cromatografía por exclusión de tamaño (SEC), donde se observó que algunos catalizadores orgánicos producían PET con pesos moleculares similares o más altos que los del PET hecho con catalizadores metálicos. Un estudio de la estabilidad

térmica de los catalizadores fue también hecho y se encontró que algunos catalizadores orgánicos son estables térmicamente a altas temperaturas ( $\approx 250$  °C).

Con el objeto de darle cierto grado de degradabilidad al PET que es un polímero no biodegradable, en el capítulo 4 se sintetizaron copolímeros de PET con un poliéster biodegradable y biobasado (PLA) usando un catalizador orgánico (DBU:BA). La formación del copolímero PET-*ran*-PLA fue demostrada por  $^1\text{H}$  NMR y posteriormente los copolímeros fueron caracterizados por DSC para obtener sus propiedades térmicas ( $T_m$ ,  $T_c$  and  $\Delta H_m$ ). La cristalización y morfología de los copolímeros fueron también analizadas por DSC, microscopía de fuerza atómica (AFM) y microscopía óptica de luz polarizada (PLOM) y ambas características mostraron ser dependientes de la composición PET/PLA. Se observó que el PLA tiene un efecto sobre la cristalinidad del PET y a medida que la cantidad de PLA era mayor en el copolímero el espesor lamelar del PET tendía a disminuir. Se usó la técnica del análisis térmico dinámico-mecánico (DMTA) para medir la  $T_g$ , donde los copolímeros obtenidos mostraron una sola  $T_g$ , indicando la formación de un sistema miscible, por otro lado al ajustarse los valores de  $T_g$  a la ecuación de Gordon-Taylor se dedujo que eran copolímeros al azar. Estudios de rayos X de ángulo grande y ángulo pequeño (WAXS y SAXS), develaron que solamente el PET era capaz de cristalizar, también, que el PLA inhibía la cristalinidad del PET y que ambos componentes (PET y PLA) eran miscibles en el fundido. Se hicieron pruebas de degradación que mostraron que los copolímeros podrían ser parcialmente degradables bajo condiciones de hidrólisis.

Nuevamente con la intención de modificar las propiedades del PET y haciendo uso de catalizadores orgánicos, se sintetizaron copolímeros de PET-*b*-Polieter, donde el polieter empleado fue previamente sintetizado bajo una ruta química sostenible. Este estudio es desarrollado en el capítulo 5, donde por  $^{13}\text{C}$  NMR se verificó la unión del PET y el polieter formando un copolímero multibloque. La  $T_g$  de estos materiales fue medida por DMTA y para algunos casos se usó también la técnica de flash DSC con la intención de corroborar la miscibilidad en el estado amorfo de los componentes que formaban el copolímero (PET y polieter). Estos copolímeros mostraron dos picos cristalinos, uno correspondiente al PET y el otro al polieter. Las propiedades térmicas de cada uno de los componentes en el copolímero fueron analizadas y se encontró que el polieter tiene un efecto sobre las propiedades del PET y viceversa. Estudios

isotérmicos de estos materiales fueron llevados a cabo y revelaron también que la velocidad de cristalización del PET es afectada por el Polieter y viceversa. Los difractogramas de mediciones de WAXS/SAXS exhibieron que ambos componentes (PET y Polieter) son capaces de cristalizar en el copolímero, en sus rangos de temperatura de cristalización respectivos, además la miscibilidad en el fundido de los componentes fue observada. La morfología de estos copolímeros no pudo ser observada por PLOM debido a la formación de microesferulitas. Los materiales obtenidos son de gran importancia pues tienen propiedades diferentes a las mostradas por los homopolímeros que los forman.

En el capítulo 6, siguiendo con la idea de polimerizar el PLA con un polímero donde el DMT (monómero) fuese usado, se decidió sintetizar poli (hexametileno tereftalato) (PHT), donde debido a la condiciones de reacción se usó una enzima como catalizador. La síntesis empezó con la obtención de ciclos a partir de DMT y 1,6 hexanediol, una vez que los ciclos fueron formados se caracterizaron por NMR, cromatografía líquida de alta resolución (HPLC) y espectroscopia de masas MALDITOF para corroborar la existencia de ciclos y la ausencia de polímeros lineales. Posteriormente, se tomaron esos ciclos y se abrieron por ROP (Ring Opening Polymerization) para formar el poliéster PHT. El polímero fue caracterizado por NMR para verificar la desaparición de ciclos. Una vez en este punto de la síntesis y encontrando que el PHT no es biodegradable, pensamos que una forma sostenible de reutilizar este polímero era reciclarlo mediante ciclodepolimerización, una técnica que consiste en convertir los polímeros lineales en ciclos. De lo anterior se decidió ciclodepolimerizar el PHT y obtener ciclos. Nuevamente se caracterizó el producto por NMR, HPLC y MALDITOF para confirmar la obtención de ciclos y la desaparición de grupos terminales pertenecientes al polímero lineal. Las características térmicas de los materiales fueron analizadas por DSC y TGA, los resultados revelaron que las propiedades térmicas de los polímeros lineales eran superiores a las de los ciclos.

Durante el desarrollo de los materiales anteriores, surgió la pregunta de qué pasaría si el monómero DMT no estuviese disponible y si se podría sustituir por otro que diera polímeros de propiedades similares a las obtenidas cuando se usa el DMT, pero manteniendo la sostenibilidad de la fuente de origen del monómero. Con esta

información se encontró que el dimetil furanoato (DMF), es un monómero proveniente de la biomasa que podría sustituir al DMT. De lo anterior, se sintetizaron todos los polímeros anteriormente descritos (ciclos, polímeros lineales y ciclos provenientes de la ciclodepolimerización de polímeros lineales) usando el DMF como monómero, obteniendo ciclos de Hexametileno furanoato y poli (hexametileno furanoato) (PHF). Estos materiales, fueron también caracterizados por las técnicas descritas para los polímeros derivados de DMT. Las propiedades térmicas mostraron también ser mayores para los polímeros lineales que para los ciclos.

En el capítulo 7, se describe la síntesis de copolímeros tribloque usando L-lactida y PHT o PHF como materiales de partida. Para confirmar la formación de la estructura tribloque se usó  $^{13}\text{C}$  NMR. Se midieron los pesos moleculares por GPC de los copolímeros obtenidos. Por TGA se estudio la estabilidad térmica de los materiales y se observó que a medida que aumenta la cantidad de L-Lactida en el copolímero disminuye la estabilidad. Las propiedades térmicas fueron obtenidas por DSC, los resultados indicaron que los valores de las propiedades térmicas de los homopolímeros (PHT o PHF) versus las propiedades de los copolímeros eran muy similares entre sí, a excepción de la  $T_g$ , cuyo valor depende de la composición y parece incrementar con el aumento de L-lactida presente en el copolímero, por otro lado la cristalinidad parece ser afectada cuando la cantidad de L-lactida presente en el copolímero incrementa. Lo anterior es también corroborado en los difractogramas de WAXS/SAXS, donde es apreciado claramente que la cristalinidad en el copolímero parece disminuir en composiciones con una gran cantidad de L-lactida, además es observado la ausencia de cristales de PLLA y solo se aprecian picos cristalinos correspondientes al PHT o PHF. En el caso del PHT puro y sus copolímeros se puede apreciar el polimorfismo de este homopolímero y cómo dependiendo de la composición en el copolímero unas fases cristalinas ( $\alpha$ ,  $\beta$  y  $\gamma$  provenientes del PHT) son más estables que otras. Una  $T_g$  fue exhibida por todos los copolímeros lo que sugiere que los componentes del copolímero (PLLA con PHT o PHF) son miscibles en el estado amorfo; por otro lado a ciertas composiciones una sola fase en el fundido fue observada lo que indica la existencia de miscibilidad entre los componentes del copolímero en el estado fundido. Únicamente las composiciones con un alto contenido de PLLA parecen tener una tendencia a presentar de una débil a moderada

segregación en el estado fundido. Estos copolímeros tribloque presentan una gran versatilidad para modificar sus propiedades en función de la composición y podrían ser probados para compatibilizar mezclas de tereftalatos con PLLA.

Los resultados más relevantes de este trabajo son descritos en el capítulo 8.

Todos los resultados mostrados en los capítulos anteriores son complementados con gráficos, tablas y ecuaciones que están en la sección de Anexos.

Previo a este resumen, una lista de publicaciones hechas durante el periodo de doctorado ha sido incluida.